

AN INVESTIGATION OF LANDSLIDE AT KM: 12+200 OF ARTVIN-SAVSAT
JUNCTION-MEYDANCIK PROVINCIAL ROAD

A THESIS SUBMITTED TO
THE GRADUATE SCHOOL OF NATURAL AND APPLIED SCIENCES
OF
MIDDLE EAST TECHNICAL UNIVERSITY

BY

EBRU TOPSAKAL

IN PARTIAL FULFILLMENT OF THE REQUIREMENTS
FOR
THE DEGREE OF MASTER OF SCIENCE
IN
GEOLOGICAL ENGINEERING

SEPTEMBER 2012

Approval of the thesis:

**AN INVESTIGATION OF LANDSLIDE AT KM: 12+200 OF ARTVIN-SAVSAT
JUNCTION-MEYDANCIK PROVINCIAL ROAD**

Submitted by **EBRU TOPSAKAL** in partial fulfillment of the requirements for the degree of **Master of Science in Geological Engineering Department, Middle East Technical University** by,

Prof. Dr. Canan Özgen
Dean, Graduate School of **Natural and Applied Sciences**

Prof. Dr. Erdin Bozkurt
Head of Department, **Geological Engineering**

Prof. Dr. Tamer Topal
Supervisor, **Geological Engineering Dept., METU**

Examining Committee Members:

Prof. Dr. Nurkan Karahanoğlu
Geological Engineering Dept., METU

Prof. Dr. Tamer Topal
Geological Engineering Dept., METU

Serdar Aker (Msc.)
PETRA Müh. Müş. İnş. Ltd. Şti.

Prof. Dr. Erdal Çokça
Civil Engineering Dept., METU

Asst. Prof. Dr. Nejan Huvaj Sarıhan
Civil Engineering Dept., METU

Date: 10.09.2012

I hereby declare that all information in this document has been obtained and presented in accordance with academic rules and ethical conduct. I also declare that, as required by these rules and conduct, I have fully cited and referenced all material and results that are not original to this work.

Name, Last Name : Ebru TOPSAKAL

Signature :

ABSTRACT

AN INVESTIGATION OF LANDSLIDE AT KM: 12+200 OF ARTVIN-SAVSAT JUNCTION-MEYDANCIK PROVINCIAL ROAD

TOPSAKAL, Ebru

M.S., Department of Geological Engineering

Supervisor: Prof. Dr. Tamer TOPAL

September 2012, 159 pages

The purpose of this study is to determine the most suitable remediation techniques via engineering geological assessment of the landslide that occurred during the construction of Artvin-Şavşat Junction - Meydancık Provincial Road at Km: 12+200 in an active landslide area. For this purpose, the geotechnical parameters of the mobilized geological material which is colluvium along the sliding surface were determined by back analyses of the landslide at three geological sections.

The landslide were then modeled along the most representative section of the study area by considering the landslide mechanism, the parameters determined from the geotechnical investigations, the size of the landslide and the location of the slip circle. In addition, pseudostatic stability analyses were performed comprising the earthquake potential of the site.

The most suitable slope remediation technique was determined to be a combination of surface and subsurface conditions. A static analysis of the landslide shall also be performed through utilizing finite element analyses. The static analyses were compared with the inclinometer readings in the field to verify the direction of the movement. Consequently, shear strength parameters were specified as $c = 0$ kPa and $\phi = 10^\circ$ for the landslide material and pre-stressed anchoring and rock buttressing were considered as a remediation method.

Keywords: Colluvium, Back analysis, Finite element, Landslide, Remediation, Artvin

ÖZ

ARTVİN-ŞAVŞAT AYRIMI - MEYDANCIK İL YOLU KM: 12+200 DE MEYDANA GELEN HEYELANIN İNCELENMESİ

TOPSAKAL, Ebru

Yüksek Lisans, Jeoloji Mühendisliği Bölümü

Tez Yöneticisi: Prof. Dr. Tamer TOPAL

Eylül 2012, 159 sayfa

Bu çalışmanın amacı, Artvin-Şavşat Ayrımı - Meydancık İl Yolu inşaatı sırasında Km: 12+200 de meydana gelen heyelanın mühendislik jeolojisi açısından değerlendirilmesinin yapılarak en uygun iyileştirme tekniklerini belirlemektir. Bu amaçla, öncelikli olarak heyelan geometrisi 3 adet jeolojik kesit üzerinde geriye dönük analiz yöntemi ile incelenerek kayma yüzeyi boyunca mobilize olmuş Kolüvyon malzemesinin parametreleri bulunmuştur.

Çalışma sahasını en iyi şekilde temsil eden kesit üzerinde heyelanın mekanizması, jeoteknik değerlendirmelerden elde edilen parametreler, heyelanın büyüklüğü ve kayma dairesinin konumu göz önüne alınarak heyelan modellenmiştir. Ayrıca çalışma sahasının deprem durumu için psödo statik analizi yapılmıştır.

En uygun iyileştirme tekniği yüzey ve yeraltı durumları göz önünde bulundurularak belirlenmiştir. Heyelanın statik koşullardaki analizi sonlu eleman yöntemi kullanılarak yapılmıştır. Statik koşuldaki analiz, arazide yapılan inklinometre ölçümleri ile karşılaştırılmış ve hareket yönü doğrulanmıştır. Sonuç olarak, heyelan malzemesinin kayma dayanımı parametreleri $c = 0$ kPa and $\phi = 10^\circ$ olarak belirlenmiş ve öngermeli ankraj ve kaya destek dolgusu iyileştirme metodu olarak değerlendirilmiştir.

Anahtar Kelimeler: Geriye dönük analiz, Kolüvyon, Sonlu eleman, Heyelan, İyileştirme, Artvin

ACKNOWLEDGEMENTS

I am heartily thankful to my advisor, Prof. Dr. Tamer Topal, whose encouragement, guidance and support from the initial to the final level enabled me to develop an understanding of the subject. This thesis would not have been possible without his kind support.

Special thanks to my life, Can Barış Ağbay, who gave effortlessly his love, support and prayers throughout my academic career.

I would like to thank Mustafa Kaplan for his help, support and answering my questions in the progress of this thesis.

I am truly indebted and thankful to PETRA Company for providing landslide data.

Additional thanks are given to all my friends for their friendship and I wish the best of luck to everyone.

TABLE OF CONTENTS

ABSTRACT	iv
ÖZ	v
ACKNOWLEDGEMENTS	vi
TABLE OF CONTENTS.....	vii
LIST OF TABLES	x
LIST OF FIGURES	xii
CHAPTERS	
1. INTRODUCTION	1
1.1. Purpose and Scope	2
1.2. Location of the Study Area.....	2
1.3. Climate	3
1.4. Method of Study	5
1.5. Previous Studies.....	5
2. LITERATURE SURVEY ON LANDSLIDES.....	7
2.1. Landslide Analysis.....	7
2.1.1. Techniques of Landslide Analysis.....	7
2.1.1.1. Deterministic Analysis (Limit Equilibrium Method).....	8
2.1.1.2. Stress-Deformation Analysis (Finite Element Method).....	15
2.1.2. Seismic Techniques of Landslide Analysis	17
2.1.2.1. Pseudostatic Method	18
2.1.2.2. Newmark's Displacement Method	19
2.2. Methods of Slope Stabilization.....	20
2.2.1. Drainage.....	21

2.2.1.1.	Surface Drainage.....	22
2.2.1.2.	Subsurface Drainage.....	23
2.2.1.3.	Subsurface Drainage Blankets	23
2.2.1.4.	Trenches	24
2.2.1.5.	Cut-off Drains	25
2.2.1.6.	Horizontal Drains.....	26
2.2.1.7.	Relief Wells	27
2.2.1.8.	Drainage Tunnels or Galleries	28
2.2.2.	Excavations and Butress Fills.....	28
2.2.3.	Ground Anchors (Tiebacks).....	30
3.	GEOLOGICAL SETTING.....	33
3.1.	Regional Geology.....	33
3.1.1.	Stratigraphy	33
3.1.1.1.	Kızılkaya formation.....	34
3.1.1.2.	Çağlayan formation	35
3.1.1.3.	Ağıllar formation	35
3.1.1.4.	Kabaköy formation.....	36
3.1.1.4.1.	Kaçkar Granitoids.....	36
3.1.1.4.2.	Andesite	37
3.2.	Local Geology.....	37
3.3.	Structural Geology and Seismicity	40
3.4.	Hydrogeology	43
3.5.	Geomorphology	46
4.	SITE INVESTIGATION OF THE LANDSLIDE.....	48
4.1.	Field Studies.....	48
4.1.1.	Drilling	50

4.1.2.	Standard Penetration Test (SPT).....	53
4.1.3.	Inclinometers	53
4.2.	Laboratory Tests.....	57
4.3.	Assessment of Field Studies and Laboratory Tests	57
5.	GEOTECHNICAL ASSESSMENT OF THE LANDSLIDE.....	68
5.1.	Slope Failure Mechanism	68
5.2.	Shear Strength Characterization.....	70
5.2.1.	Back Analysis	70
5.2.2.	Shear Strength Characterization Considered In Stability of Slopes by Back Analysis	71
5.3.	Selection of the Landslide Model	79
5.4.	Pseudostatic Analysis of the Landslide.....	82
6.	STABILIZATION OF THE LANDSLIDE.....	86
7.	CONCLUSIONS AND RECOMMENDATIONS	96
	REFERENCES	98
APPENDICES		
A.	BOREHOLE LOGS	103
B.	CORE BOX PHOTOS	124
C.	SOIL LABORATORY TEST RESULTS	131
D.	INCLINOMETER RESULTS.....	135
E.	SUMMARY OF THE ABRAHAMSON AND SILVA (2008) GROUND-MOTION RELATIONS	153

LIST OF TABLES

TABLES

Table 1.1 Properties of the road.....	1
Table 2.1 Static equilibrium conditions satisfied by limit equilibrium methods (Abramson et al., 2002).	9
Table 2.2 Assumptions for interslice forces considered by limit equilibrium methods (Abramson et al., 2002).	11
Table 2.3 Equations and unknowns associated with the method of slices (Abramson et al., 2002).....	12
Table 2.4 Equations and unknowns associated with the method of slices (Abramson et al., 2002).....	14
Table 2.5 Typical seismic coefficients and FS in practice (Abramson et al., 2002)..	19
Table 2.6 Average ultimate bond stress for rocks (after Sabatini et al., 1999).....	32
Table 3.1 Measured groundwater levels in boreholes.	44
Table 3.2 Elevations of boreholes.....	46
Table 4.1 Summary of the borehole data.	51
Table 4.2 Summary of the inclinometer results.	55
Table 4.3 Ranges of the laboratory test results and SPT-N in landslide material. ..	60
Table 4.4 Range of total core recovery (TCR) and rock quality designation (RQD) of rocks present under the landslide material.....	60
Table 5.1 Material parameters used in limit equilibrium and finite element method analysis.	80

Table 5.2 Definition of parameters used in Abrahamson & Silva (2008) attenuation relationship.	84
Table 5.3 Values of all parameters used in the attenuation relationship.	85
Table 6.1 List of the factor of safeties for the rock buttressing technique.	91
Table 6.2 List of factor of safeties for the pre-stressed anchoring technique.	94
Table E.1 Coefficients for the median ground motion.....	158

LIST OF FIGURES

FIGURES

Figure 1.1 Location map of the study area.....	3
Figure 1.2 Average rainfall quantities for each month of the year (from 1970 to 2011) for the Artvin province (TSMS, 2012).....	4
Figure 1.3 Average temperature for each month of the year (from 1970 to 2011) for the Artvin province (TSMS, 2012).....	4
Figure 2.1 Division of sliding mass into slices (Abramson et al., 2002).	10
Figure 2.2 Forces acting on a typical slice (Abramson et al., 2002).	10
Figure 2.3 Definitions of terms used for finite element method (Abramson et al., 2002).	16
Figure 2.4 Surface drainage system (CANMET, 1977).	22
Figure 2.5 Placement of a drain blanket underneath embankments (Abramson et al., 2002).	24
Figure 2.6 Typical trench drain details: (a) free-draining soil at surface to capture surface runoff (b) (c) impervious seal to exclude surface water (two variations) (Cornforth, 2005).	25
Figure 2.7 Cut-off drain (Abramson et al., 2002).	26
Figure 2.8 Horizontal drains (Duncan and Wright, 2005).....	27
Figure 2.9 Drainage galleries (Duncan and Wright, 2005).....	28
Figure 2.10 Slope stabilization by excavation (Duncan and Wright, 2005).	29
Figure 2.11 Structural buttress (Duncan and Wright, 2005).	30

Figure 2.12 Slope stabilization by cut and fill (Duncan and Wright, 2005).	30
Figure 2.13 Ground anchor installed through a landslide (Cornforth, 2005).	31
Figure 2.14 Effect of anchor tensile load, T, on stability: (a) full load T acting at slip surface X (b) pullback load P and shear strength δS benefits (Cornforth, 2005).	32
Figure 3.1 Geological map of the study area (modified from MTA, 1998).....	33
Figure 3.2 Stratigraphic columnar section (modified from MTA, 1998).....	34
Figure 3.3 Local geological map of the study area.	38
Figure 3.4 Geological section of the study area along section line A-A'.	39
Figure 3.5 Seismic zonation map of city of Artvin and the study area (Earthquake Research Center, 2012).....	41
Figure 3.6 Seismic map of Turkey [EAFS: East Anatolian Fault System, NAFS: North Anatolian Fault System, EFZ: Erzurum Fault Zone] (Modified from Koçyiğit, 1991).	42
Figure 3.7 Epicentral distributions of earthquakes having a magnitude greater than 3.0 around the Şavşat District (Sayısal Grafik Ltd., 2012).....	43
Figure 3.8 Groundwater contour lines and movement directions.....	45
Figure 3.9 Digital elevation model of the study area.....	46
Figure 3.10 Slope map of the study area.	47
Figure 4.1 (a) General view of the landslide area, (b) tension cracks at crown.....	49
Figure 4.2 A close view from (a) tension cracks at crown, (b) failure surface at toe.	50
Figure 4.3 Borehole locations for the landslide investigation.....	52
Figure 4.4 Monitoring landslides with inclinometers and piezometers (Cornforth, 2005).	54
Figure 4.5 Inclinometer system: (a) probe and casing within borehole (b) measurement of tilt (Cornforth, 2005).	54

Figure 4.6 Movement direction of the landslide and section lines.....	56
Figure 4.7 Landslide boundary.....	58
Figure 4.8 Cross-section of the landslide along section 2-2'	59
Figure 4.9 SPT N values vs. depth graph for the landslide material.	61
Figure 4.10 LL values vs. depth graph for the landslide material.....	62
Figure 4.11 Particle size distribution of (a) SPT-15 sample taken from BH-4 (b) SPT-6 sample taken from BH-2.	63
Figure 4.12 Plasticity chart for the landslide material.	64
Figure 4.13 PI values vs. depth graph for the landslide material.	65
Figure 4.14 Wc-PL-LL values vs. depth graph for the landslide material.....	66
Figure 4.15 RQD value vs. depth graph for the basalt and limestone.....	67
Figure 5.1 Paleo-landslide boundary observed in the study area.	69
Figure 5.2 Cross-section of landslide along section line 1-1'	72
Figure 5.3 Cross-section of landslide along section line 2-2'.....	73
Figure 5.4 Cross-section of landslide along section line 3-3'.....	74
Figure 5.5 Normal stress vs. shear stress of the Çağlayan formation as calculated by RocLab 1.0.	75
Figure 5.6 Normal stress vs. shear stress of the Ağıllar formation as calculated by RocLab 1.0.	76
Figure 5.7 Back analysis results showing the $c'-\phi'$ pairs.....	77
Figure 5.8 Empirical information on fully softened strength and residual strength (data from Stark and Eid 1994; Eid 1996; and Stark and Eid 1997) (Mesri and Shahien, 2003).	78

Figure 5.9 Secant residual friction angle relationships with liquid limit, clay-size fraction, and effective normal stress (Stark et. al., 2005).....	79
Figure 5.10 Generated mesh of the landslide model.	81
Figure 5.11 Deformed mesh of the landslide model.	81
Figure 5.12 Contours of total displacement generated by Phase ² v.8.	81
Figure 6.1 Surface drainage canal layout in the landslide area.	87
Figure 6.2 Rock buttressing with static condition.....	89
Figure 6.3 Searching the most critical failure surface in rock buttressing with static condition.	89
Figure 6.4 Rock buttressing with pseudo-static condition.....	90
Figure 6.5 Searching the most critical failure surface in rock buttressing with pseudo-static condition.	91
Figure 6.6 Angle and capacity variations of pressure-grouted tieback for the landslide.	92
Figure 6.7 Pre-stressed anchors with static condition.	93
Figure 6.8 Pre-stressed anchors with pseudostatic condition.....	94
Figure A.1 Borehole No.1 (Page 1).....	103
Figure A.2 Borehole No.1 (Page 2).....	104
Figure A.3 Borehole No.1 (Page 3).....	105
Figure A.4 Borehole No.2 (Page 1).....	106
Figure A.5 Borehole No.2 (Page 2).....	107
Figure A.6 Borehole No.3 (Page 1).....	108
Figure A.7 Borehole No.3 (Page 2).....	109
Figure A.8 Borehole No.4 (Page 1).....	110

Figure A.9 Borehole No.4 (Page 2).....	111
Figure A.10 Borehole No.4 (Page 2).....	112
Figure A.11 Borehole No.5 (Page 1).....	113
Figure A.12 Borehole No.5 (Page 2).....	114
Figure A.13 Borehole No.6 (Page 1).....	115
Figure A.14 Borehole No.6 (Page 2).....	116
Figure A.15 Borehole No.6 (Page 3).....	117
Figure A.16 Borehole No.7 (Page 1).....	118
Figure A.17 Borehole No.7 (Page 2).....	119
Figure A.18 Borehole No.8 (Page 1).....	120
Figure A.19 Borehole No.8 (Page 2).....	121
Figure A.20 Borehole No.9 (Page 1).....	122
Figure A.21 Borehole No.9 (Page 2).....	123
Figure B.1 BH-1, core box no: 1/4.....	124
Figure B.2 BH-1, core box no: 2/4.....	124
Figure B.3 BH-1, core box no: 3/4.....	125
Figure B.4 BH-1, core box no: 4/4.....	125
Figure B.5 BH-2, core box no: 1/1.....	126
Figure B.6 BH-3, core box no: 1/1.....	126
Figure B.7 BH-4, core box no: 1/2.....	127
Figure B.8 BH-4 core box no: 2/2.....	127
Figure B.9 BH-5, core box no: 1/1.....	128

Figure B.10 BH-6, core box no: 1/1.....	128
Figure B.11 BH-7, core box no: 1/1.....	129
Figure B.12 BH-8, core box no: 1/1.....	129
Figure B.13 BH-9, core box no: 1/1.....	130
Figure C.1 Laboratory test results of BH-1 and BH-2.....	131
Figure C.2 Laboratory test results of BH-4 and BH-5.....	132
Figure C.3 Laboratory test results of BH-6 and BH-7.....	133
Figure C.4 Laboratory test results of BH-8 and BH-9.....	134
Figure D.1 Cumulative displacement of BH-1.....	135
Figure D.2 Incremental displacement of BH-1.....	136
Figure D.3 Cumulative displacement of BH-2.....	137
Figure D.4 Incremental displacement of BH-2.....	138
Figure D.5 Cumulative displacement of BH-3.....	139
Figure D.6 Incremental displacement of BH-3.....	140
Figure D.7 Cumulative displacement of BH-4.....	141
Figure D.8 Incremental displacement of BH-4.....	142
Figure D.9 Cumulative displacement of BH-5.....	143
Figure D.10 Incremental displacement of BH-5.....	144
Figure D.11 Cumulative displacement of BH-6.....	145
Figure D.12 Incremental displacement of BH-6.....	146
Figure D.13 Cumulative displacement of BH-7.....	147
Figure D.14 Incremental displacement of BH-7.....	148

Figure D.15 Cumulative displacement of BH-8	149
Figure D.16 Incremental displacement of BH-8.....	150
Figure D.17 Cumulative displacement of BH-9	151
Figure D.18 Incremental displacement of BH-9.....	152

CHAPTER 1

INTRODUCTION

Landslides and other slope failures are the natural result of decomposition of geologic materials, steepening of slopes by erosion, and alteration of inclinations by tectonic movements, earthquakes, rainfall, and snowmelt. The incidence of occurrence is related primarily to topography, geology, and climate (Hunt, 1986).

In Turkey, natural disasters such as earthquake, landslide, flood, etc. that cause loss of life and property are encountered frequently due to its geological, geomorphological structure and climatic features. Landslides are one of these natural disasters. Landslides are concentrated on Eastern, Middle and Western Black Sea Region, and along active faults and fault zones in Turkey. Total landslide occurrence are 13542 between the years of 1950-2011 and 3.5 % of them were observed in the Artvin province. Moreover, a lot of landslides occur in Şavşat, Ardanuç, Hopa and Arhavi Districts of the Artvin province (Gökçe et al., 2008).

In 2009, traffic of Artvin-Şavşat Junction - Meydancık Provincial Road was designed on the same road and it is planning to be completed at the end of year 2012. During road construction, landslide occurred at Km: 12+200. Therefore, it is required to investigate the causes of this landslide and suitable mitigation methods.

The properties of the road are given in Table 1.1.

Table 1.1 Properties of the road.

Road Type :	Provincial Road
Lane Number and Width :	2x1, 3.50 m
Platform Width :	8.00 m
Bench Width :	0.50 m

1.1. Purpose and Scope

The purpose of this study is to determine the most suitable remediation technique(s) via engineering geological assessment of the landslide that occurred during the construction of Artvin-Şavşat Junction - Meydancık Provincial Road Km: 12+200 in an active landslide area.

The scope of this thesis is to cover the landslide investigation methods and analysis to verify the remedial techniques. First of all, detailed literature review about geological information of the study area was conducted and suitable slope stabilization techniques were examined. Thereafter, available data concerning geology, results of inclinometer measurements and soil laboratory tests were utilized in order to get sense about slip surface of the landslide. The last stage included modeling of the landslide using back analysis and 2-D limit equilibrium slope stability analyses under both static and dynamic conditions to decide the most suitable remediation techniques of the landslide.

The thesis is divided into 7 Chapters. Chapter 2 includes background information of landslide analysis and remediation techniques. Chapter 3 gives an overview about geological setting of the study area. Chapter 4 introduces the geotechnical surveys and interpretation of their results. Chapter 5 includes geotechnical assessment of the landslide. Chapter 6 discusses the suitable stabilization techniques, and Chapter 7 gives conclusions and recommendations.

1.2. Location of the Study Area

The study area is located approximately 15 km away from the northwestern part of the Şavşat District of Artvin and 800 m away from the northeast of the Sebzeli village. The landslide area is located at 12.20 km of Artvin-Şavşat Junction - Meydancık Provincial Road which extends parallel to Meydancık Creek. Location map of the study area is shown in Figure 1.1.

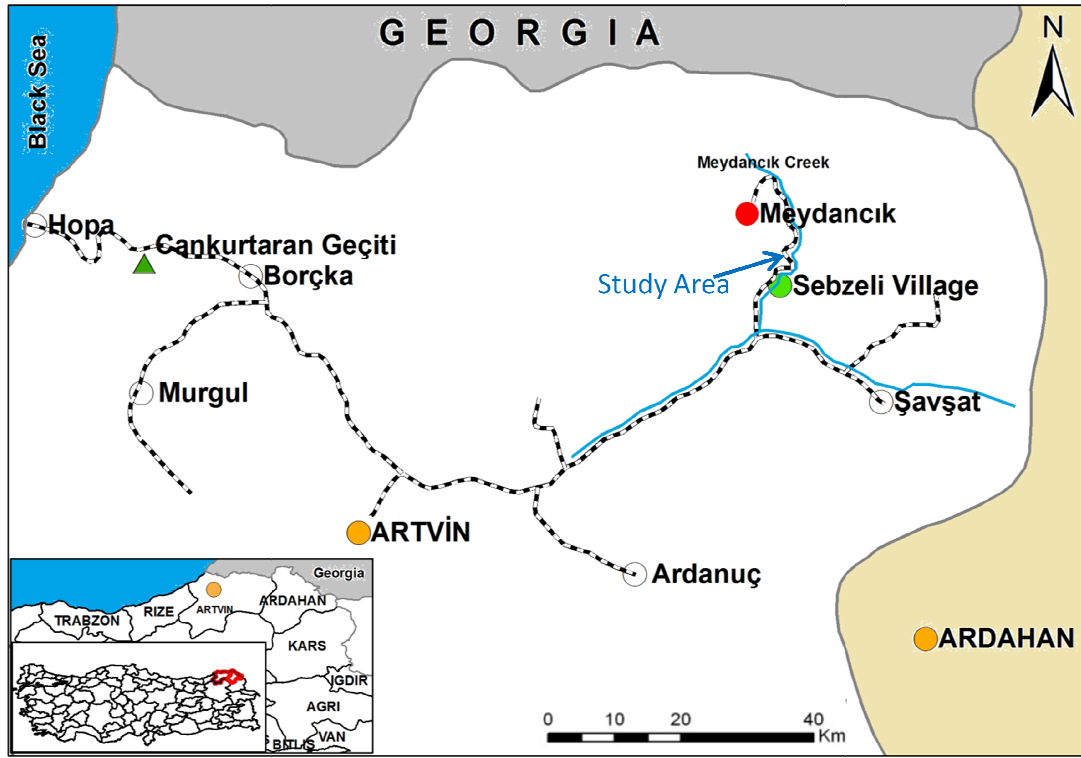


Figure 1.1 Location map of the study area.

1.3. Climate

Artvin is a city that shows the most variability regarding to climate in the East Black Sea region. All seasons rainy Black Sea climate are observed in the area between the coastal region and Cankurtaran Mountain range. From the Cankurtaran Mountain range until the Borçka District and the center of the Artvin Province, climate is in the form of the Black Sea climate which shows colder winters and less summer rains. These features are observed also in the Şavşat District and its surrounding. The Climate is the combination of partially continental climate and Mediterranean climate in Ardanuç and Yusufeli. Climate is hot and dry in summers; there is a warmer and less rainy climate than normal continental climate in winters. Further, in some parts of this area, climate approximates to Mediterranean climate (especially valley floor).

According to the Turkish State Meteorological Service (TSMS, 2012), the annual mean precipitation is 716.8 mm between the years of 1970-2011 and the annual mean temperature is 12.04°C in the period of 1970-2011. Furthermore, the

maximum and minimum precipitation is observed in May and August, respectively. The maximum and minimum temperature is observed in July and January, respectively. Figures 1.2 and 1.3 show the total rainfall quantities for each month of the year and the average temperatures for each month of the year between the years of 1970-2011.

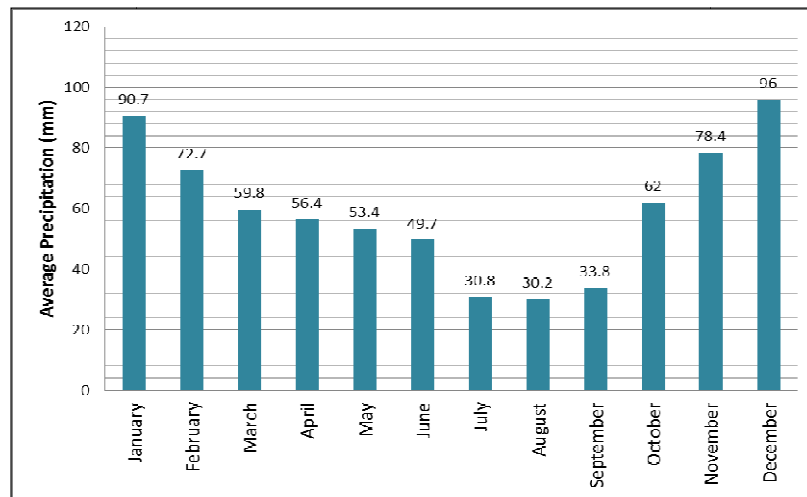


Figure 1.2 Average rainfall quantities for each month of the year (from 1970 to 2011) for the Artvin province (TSMS, 2012).

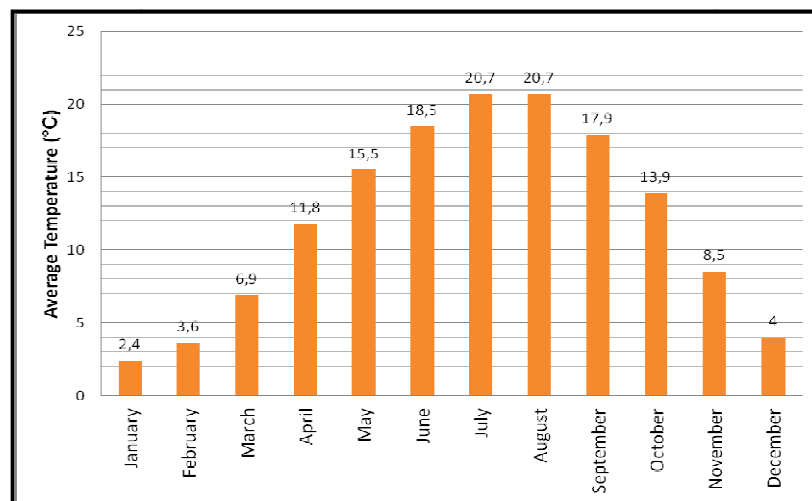


Figure 1.3 Average temperature for each month of the year (from 1970 to 2011) for the Artvin province (TSMS, 2012).

1.4. Method of Study

There are several steps in this study. In the first step a detailed literature survey was conducted. The literature survey was about the geological setting of the study area, landslide investigation methods and slope stability techniques.

Secondly, the field works have started. It covers the description and geotechnical assessment of the geological units present in the study area, drilling 9 boreholes to get laboratory samples, investigating hydrogeological conditions and installing an inclinometer to observe the location of slip surface of the landslide.

Thereafter, laboratory studies were carried out on the disturbed and undisturbed soil samples obtained from the boreholes. Sieve analysis, atterberg limits, unified soil classification, water contents, and unit weight of the soil samples were determined according to TS 1900-1 and 2 ICS 93.020 (2006) standards.

Landslide was analyzed by utilizing 2-D limit equilibrium methods. Non-circular failure analysis was selected in SLIDE version 6.0 software (Rocscience, 2012) to conduct a back analysis, since; the location of the slip surface was specified by utilizing inclinometer results. Then, PHASE² version 8.0 software (Rocscience, 2011) was used to confirm the direction of movement determined by evaluating inclinometer results, and to verify the factor of safety obtained from Slide 6.0 software.

Remedial slope stabilities such as dewatering, rock buttressing and anchoring were considered in the analyses.

1.5. Previous Studies

Artvin - Şavşat region was studied by few researchers, despite that there are many geological and geochemical studies in the Artvin province. There are three main geological units in the study area, namely; Çağlayan formation, Ağıllar formation and colluvium. Çağlayan formation which has the characteristics of alkaline volcano-sediment was observed at the southeast of the Zeytinlik town in the Artvin province. Maastrichtian - Paleocene aged sandy and reefal limestone which is lying concordantly on the Çağlayan formation was named by Güven et al. (1993) as Ağıllar formation since it was observed clearly around Ağıllar village. In the thesis

area –Şavşat/ Meydancık-, limestone which has the same lithological setting was also named as Ağıllar formation.

Yılmaz et al. (1998) studied the geology of the Artvin province and prepared the geological map and stratigraphy of the Artvin province and its districts. In the Artvin province, tholeitic and chalco-alkaline rocks which are belonging to three main geological eras -Paleozoic, Mesozoic and Cenozoic- are observed. Paleozoic aged rocks are composed of metamorphic, metagabbro –metadiabase and granite. Mesozoic era starts from Lias aged volcanics and continue with Upper Jurassic-Lower Cretaceous aged reefal limestones. In Upper Cretaceous period volcanic activity was observed. In the Late Paleocene granitoids were formed with orogenic activity. This activity has continued in Eocene period.

PETRA Engineering and Consulting Company (2009) carried out a geological and geotechnical study in the Artvin-Şavşat Junction - Meydancık Provincial Road Km: 12+200. Geological map of the study area and the geological profile for the area were prepared by this company. In 2009, PETRA Engineering and Consulting Company drilled nine boreholes for investigating the landslide. Then, data obtained from the field and laboratory tests were evaluated and engineering geological assessment of the landslide was also made by this company. However, the data are reevaluated and new landslide analyses are performed in this thesis.

CHAPTER 2

LITERATURE SURVEY ON LANDSLIDES

2.1. Landslide Analysis

For stability of natural slopes the objective is to determine the factor of safety (FS) against sliding for the existing slope angle in view of the occurrence of changing groundwater conditions and earthquake forces. Other transient conditions, such as increasing slope inclination from erosion or tectonic activity, or decreasing strength due to weathering, are long term effects that may be encountered for in critical situations. The approach is to evaluate the probability and effects of failure and if they are intolerable, to provide measures to achieve stability, or to avoid construction within the area possibly affected by a slope failure (Hunt, 1986). Geotechnical slope analysis should consider the basic concepts of geomechanics such as effective stress, shear strength, stability, and deformation and failure mechanisms. The primary purpose of geotechnical slope analysis in most engineering applications is to contribute to the safe and economic design of excavations, embankments, earth dams and spoil heaps (Chowdhury, 2010).

The main items required to evaluate the stability of a slope are shear strength of the soils, slope geometry, pore pressures or seepage forces, and loading and environmental conditions (Abramson et al., 2002).

2.1.1. Techniques of Landslide Analysis

Analyses of slopes can be divided into two categories: those used to evaluate the stability of slopes and those used to estimate slope movement. Stability of slopes is usually analyzed by methods of limit equilibrium, while movements of slopes are usually analyzed by the finite-element method (Duncan, 1996).

2.1.1.1. Deterministic Analysis (Limit Equilibrium Method)

For slope stability analysis, the limit equilibrium method (LEM) is widely used by engineers and researchers and this is a traditional and well established method (Cheng et al., 2006).

Once appropriate shear strength properties, pore water pressures, slope geometry and other soil and slope properties are established, slope stability calculations need to be performed to ensure that the resisting forces are sufficiently greater than the forces tending to cause a slope to fail. Calculations usually consist of computing a factor of safety using one of several limit equilibrium procedures of analysis. All of these procedures of analysis employ the same definition of the factor of safety and compute the factor of safety using the equations of static equilibrium (Duncan and Wright, 2005).

Two different approaches are used to satisfy static equilibrium in the limit equilibrium analysis procedures. Some procedures consider equilibrium for the entire mass of soil bounded beneath by an assumed slip surface and above by the surface of the slope. In these procedures, equilibrium equations are written and solved for a single free body. The infinite slope procedure and the Swedish slip circle method are examples of such single-free-body procedures. In other procedures the soil mass is divided into a number of vertical slices and equilibrium equations are written and solved for each slice. These procedures, termed procedures of slices, include such methods as the Ordinary Method of Slices, Bishop, Janbu's, Sarma's, Morgenstern-Price and Spencer's procedures (Duncan and Wright, 2005).

Three static equilibrium conditions are to be satisfied: (1) equilibrium of forces in the vertical direction, (2) equilibrium of forces in the horizontal direction, and (3) equilibrium of moments about any point. The limit equilibrium procedures all use at least some static equilibrium equations to compute the factor of safety (Duncan and Wright, 2005). Static equilibrium conditions satisfied by limit equilibrium methods are given in Table 2.1. All methods require both horizontal and vertical force equilibrium except Bishop's simplified method.

Table 2.1 Static equilibrium conditions satisfied by limit equilibrium methods (Abramson et al., 2002).

Methods	Developed by	$\Sigma \text{Moment} = 0$	$\Sigma \text{Force} = 0$
Ordinary	Fellenius (1927)	√	-
Bishop's simplified	Bishop (1955)	√	$\Sigma F_x = 0$
Janbu's simplified	Janbu (1968)		√
Bishop's rigorous	Bishop (1955)	√	√
Janbu's generalized	Janbu (1968)	-	√
Lowe and Karafiath	Lowe and Karafiath (1960)	-	√
Corps of Engineers	U.S. Army Corps of Engineers (1970)	-	√
Sarma's	Sarma (1973)	√	√
Spencer's	Spencer (1967)	√	√
Morgenstern-Price	Morgenstern and Price (1965)	√	√

Regardless of whether equilibrium is considered for a single free body or a series of individual vertical slices making up the total free body, there are more unknowns (forces, locations of forces, factor of safety, etc.) than the number of equilibrium equations; the problem of computing a factor of safety is statically indeterminate. Therefore, assumptions must be made to achieve a balance of equations and unknowns. Different procedures make different assumptions to satisfy static equilibrium. Two procedures may even satisfy the same equilibrium conditions but make different assumptions and therefore produce different values for the factor of safety (Duncan and Wright, 2005).

All limit equilibrium methods for slope stability analysis divide a slide-mass into “n” smaller slices (Figure 2.1). Each slice is affected by a general system of forces, as shown in Figure 2.2 (Abramson et al., 2002).

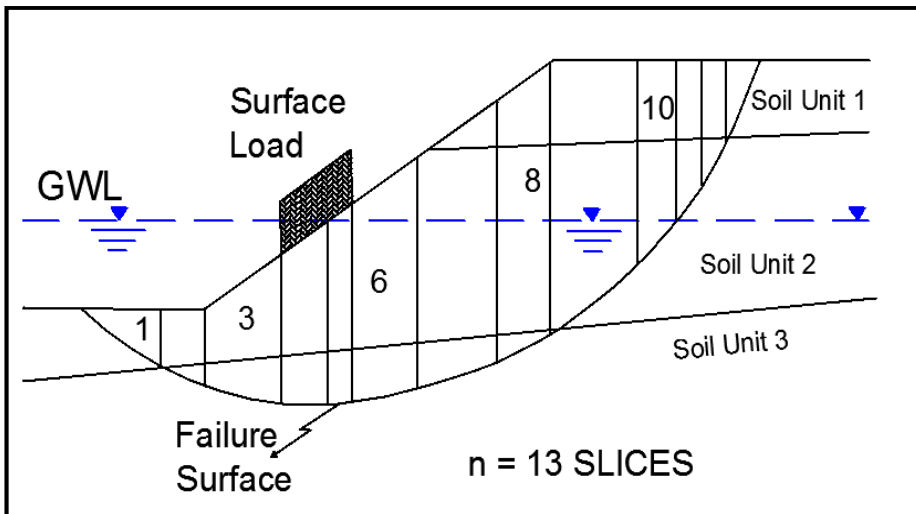


Figure 2.1 Division of sliding mass into slices (Abramson et al., 2002).

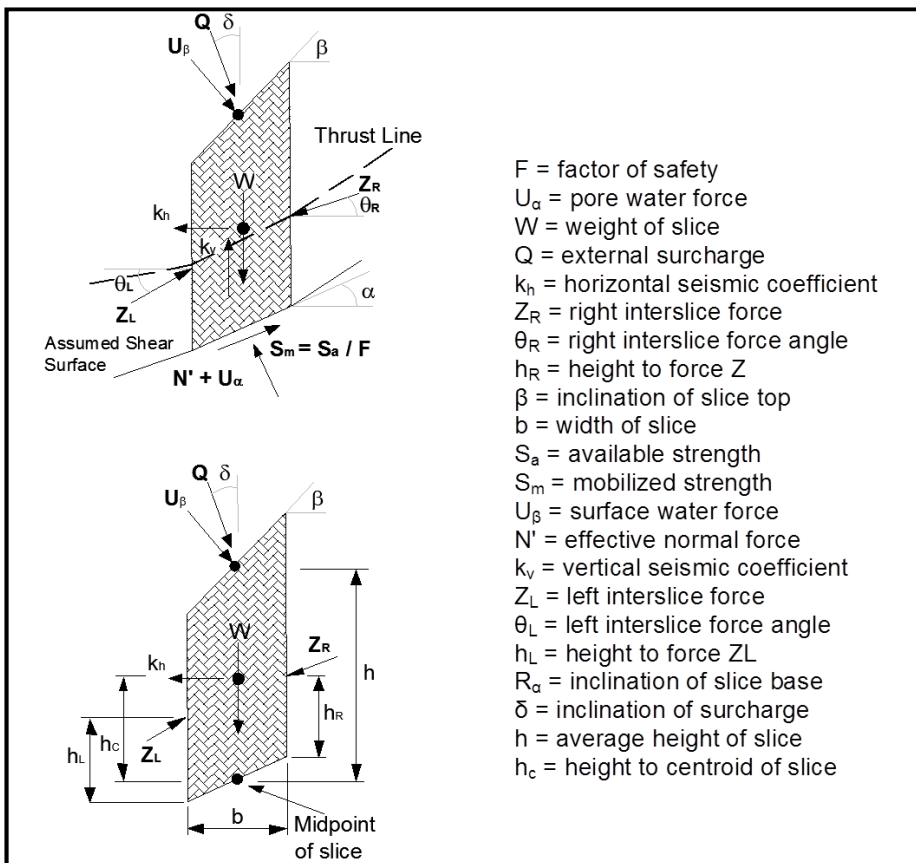


Figure 2.2 Forces acting on a typical slice (Abramson et al., 2002).

All limit equilibrium methods are based on certain assumptions for the interslice normal (N') and shear (S_m) forces, and the basic difference among the methods is how these forces are determined or assumed. In addition to this, the shape of the assumed slip surface and the equilibrium conditions for calculation of the factor of safety are among the others. A summary of selected limit equilibrium methods and their assumptions are presented in Table 2.2.

Table 2.2 Assumptions for interslice forces considered by limit equilibrium methods (Abramson et al., 2002).

Methods	Assumptions for Interslice Normal and Shear Forces
Ordinary	Neglects both N' and S_m
Bishop's simplified	Considers N' , but neglects S_m
Janbu's simplified	Considers N' , but neglects S_m
Bishop's rigorous	Assume distribution
Janbu's generalized	Considers both N' and S_m , act at thrust line
Lowe and Karafiath	Considers both N' and S_m
Corps of Engineers	Considers both N' and S_m
Sarma's	Interslice shear
Spencer's	Constant Inclination
Morgenstern-Price	Defined by $f(x)$, $S_m / N' = f(x)\lambda$

For this system there are $(6n-2)$ unknowns, as listed in Table 2.3. In addition, since only four equations can be written for the limit equilibrium of the system, the solution is statically indeterminate. However, a solution is possible provided that the number of unknowns can be reduced by making some simplifying assumptions. One of the common assumptions is that the normal force on the base of the slice acts at the midpoint thus reducing the number of unknowns to $(5n - 2)$. This then requires an additional $(n-2)$ assumption to make the problem determinate. It is these assumptions that generally categorize the available methods of analysis (Abramson et al., 2002).

Table 2.3 Equations and unknowns associated with the method of slices (Abramson et al., 2002).

Equations	Conditions
n	Moment equilibrium for each slice
2n	Force equilibrium in two directions (for each slice)
n	Mohr-Coulomb relationship between shear strength and normal effective stress
4n	Total number of equations
Unknowns	Variable
1	Factor of safety
n	Normal force at base of each slice, N'
n	Location of normal force, N'
n	Shear force at base of each slice, S _m
n-1	Interslice force, Z
n-1	Inclination of interslice force, θ
n-1	Location of interslice force (line of thrust)
6n-2	Total number of unknowns

The assumptions made by each of these methods, to render the problem determinate, are summarized below (Abramson et al., 2002).

Ordinary Method of Slices: This method neglects all interslice forces and fails to satisfy force equilibrium for the slide mass as well as for individual slices. However, this is one of the simplest procedures based on the method of slices.

Bishop's Simplified Method: Bishop assumes that all interslice shear forces are zero, reducing the number of unknowns by (n-1). This leaves (4n-1) unknowns, leaving the solution overdetermined as horizontal force equilibrium will not be satisfied for one slice.

Janbu's Simplified Method: Janbu also assumes zero interslice shear forces, reducing the number of unknowns to (4n -1). This leads to an overdetermined solution that will not completely satisfy moment equilibrium conditions. However, Janbu presented a correction factor, f_o , to account for this inadequacy.

Bishop's Rigorous Method: Bishop assumes $(n - 1)$ interslice shear forces to calculate a factor of safety. Since this assumption leaves $(4n - 1)$ unknowns, moment equilibrium cannot be directly satisfied for all slices. However, Bishop introduces an additional unknown by suggesting that there exists a unique distribution of the interslice resultant force, out of a possible infinite number, that will rigorously satisfy the equilibrium equations.

Janbu's Generalized Method: Janbu assumes a location of the thrust line, thereby reducing the number of unknowns to $(4n - 1)$. Similar to the rigorous Bishop method, Janbu's generalized method also suggests that the actual location of the thrust line is an additional unknown, and thus equilibrium can be satisfied rigorously if the assumption selects the correct thrust line.

Lowe and Karafiath's Method: Lowe and Karafiath assume that the interslice forces are inclined at an angle equal to the average of the ground surface and slice base angles, that is, $\theta = 0.5(\alpha + \beta)$, where θ is the assumed inclination of the interslice force on the right-hand side of the typical slice shown in Figure 2.2. This simplification leaves $(4n - 1)$ unknowns and fails to satisfy moment equilibrium.

Corps of Engineers Method: The Corps of Engineers approach considers the inclination of the interslice force as either parallel to ground surface or equal to the average slope angle between the left and right end points of the failure surface. The approach is similar to the one proposed by Lowe and Karafiath and presents an overdetermined system where moment equilibrium is not satisfied for all slices.

Sarma's Method: Sarma uses the method of slices to calculate the magnitude of a horizontal seismic coefficient needed to bring the failure mass into a state of limiting equilibrium. This allows the procedure to develop a relationship between the seismic coefficient and the presumed factor of safety (FS). The static FS will then correspond to the case of a zero seismic coefficient. Sarma uses an interslice force distribution function and the value of the seismic coefficient can be calculated directly for the presumed FS. All equilibrium conditions are satisfied by this method. However, it should be noted that the critical surface corresponding to the static FS will often be different than the surface determined using the more conventional approach where the FS is treated as an unknown.

Spencer's Method: In the Spencer method, it is assumed that the resultant interslice force has a constant, but an unknown inclination (Spencer, 1967). These (n-1) assumptions again reduce the number of unknowns to (4n-1), but the unknown inclination is an additional component that subsequently increases the number of unknowns to match the required 4n equations.

Morgenstern-Price Method: Morgenstern and Price method is similar to Spencer's method, except that the inclination of the interslice resultant force is assumed to vary according to a "portion" of an arbitrary function. This additional "portion" of a selected function introduces an additional unknown, leaving 4n unknowns and 4n equations (Morgenstern and Price, 1965).

A summary of the common limit equilibrium methods and their conditions are given in Table 2.4.

Table 2.4 Equations and unknowns associated with the method of slices (Abramson et al., 2002).

Methods	Circular	Non-circular	Assumptions for Interslice Normal and Shear Forces	Calculated by	
				Hand	Computer
Ordinary	√		Neglects both E and T	√	√
Bishop's simplified	√	√	Considers E, but neglects T	√	√
Janbu's simplified	√	√	Considers E, but neglects T	√	√
Bishop's rigorous	√	√	Assume distribution		√
Janbu's generalized	√	√	Considers both E and T, act at trust line		√
Sarma's	√	√	Interslice shear	√	√
Spencer's	√	√	Constant Inclination		√
Morgenstern-Price	√	√	Defined by $f(x)$, $T/E=f(x)\lambda$		√

2.1.1.2. Stress-Deformation Analysis (Finite Element Method)

Review of deformation analyses of slopes and embankments is focused primarily on the finite-element method. The finite-element method is the most generally applicable and the most widely used method of analyzing deformations (Duncan, 1996).

The finite element method (FEM) bypasses many of the deficiencies that are inherent with the limit equilibrium methods. It was first introduced to geotechnical engineering by Clough and Woodward (1967), but its use has been limited to the analysis of complex earth structures. For typical cases, the FEM can incorporate incremental construction for embankments and excavations in an attempt to simulate the stress history of the soil within the slope. However, the quality of the FEM is directly dependent on the ability of the selected constitutive model to realistically simulate the nonlinear behavior of the soil within the slope. For new embankment designs, the data may be collected from laboratory tests. For excavations and natural slopes, the constitutive model can only really be developed on the basis of high quality field tests that are further supported by field observations (Abramson et al., 2002).

The feature common to all finite element methods is that a continuum is divided into discrete parts called 'elements'. The elements are separated from each other by imaginary lines or surfaces and are assumed to be interconnected only at a finite number of nodal points situated on their boundaries (Figure 2.3). In geotechnical applications the most convenient and popular formulation is the one for a compatible model in which nodal point displacements are assumed to be the only unknowns. This is generally known as a displacement formulation. When displacements have been determined, the computer software proceeds to calculate respectively the element strains and the element stresses. Simple procedures can be devised to compute the nodal point stresses from the element stresses (Chowdhury, 2010).

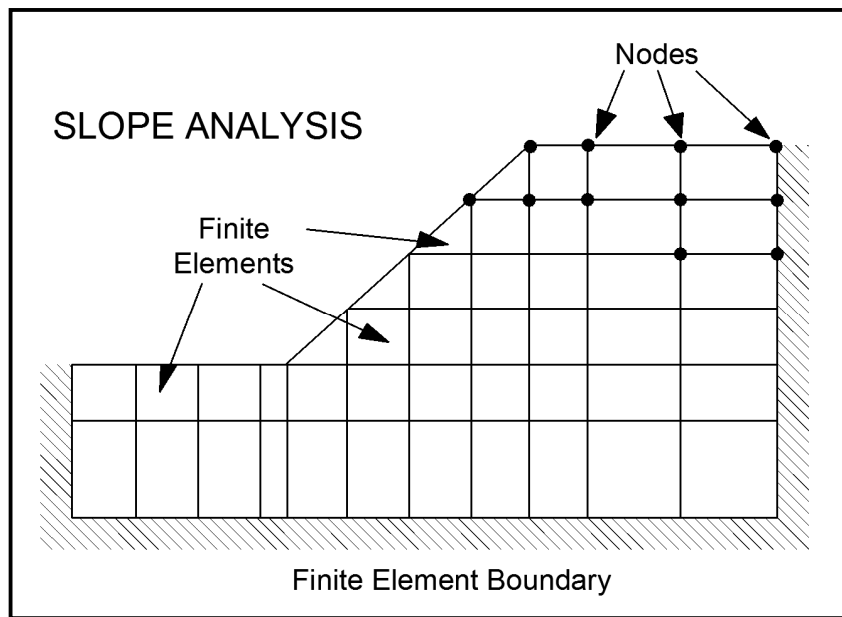


Figure 2.3 Definitions of terms used for finite element method (Abramson et al., 2002).

Finite-element analyses require definition of initial conditions, stress-strain, properties, and the construction or loading sequence. The initial stresses are needed for three reasons. First, in incremental analyses, the changes in stress calculated during each increment are added to the stresses at the beginning of the increment to evaluate the stresses at the end. To begin this process, it is necessary to know the initial stresses. Second, the stiffness of the soil depends on the stresses in the soil. Third, in analyses of excavation, the forces that are applied to simulate excavation of the soil are calculated using the before excavation stresses on the boundary of the excavation. To calculate these forces, it is necessary to know the initial stresses (Duncan, 1996). The stresses within the slopes are strongly influenced by K_0 , the ratio of lateral to vertical normal effective stresses, but conventional limit equilibrium procedures ignore this important feature (Chowdhury, 1981). In reality, the stress distributions within the slopes would be different and hence, would significantly influence their stability (Abramson et al., 2002).

The advantages of a finite element (FE) approach to slope stability analysis over traditional limit equilibrium methods can be summarized as: (a) No assumption needs to be made in advance about the shape or location of the failure surface.

Failure occurs 'naturally' through the zones within the soil mass in which the soil shear strength is unable to sustain the applied shear stresses, (b) Since there is no concept of slices in the FE approach, there is no need for assumptions about slice side forces. The FE method preserves global equilibrium until 'failure' is reached, (c) If realistic soil compressibility data are available, the FE solutions will give information about deformations at working stress levels, (d) The FE method is able to monitor progressive failure up to and including overall shear failure (Griffiths and Lane, 1999).

2.1.2. Seismic Techniques of Landslide Analysis

Seismic slope stability is one of the most important areas of geotechnical earthquake engineering. Seismically-triggered failures may be associated with reduction in factor of safety, large deformations and liquefaction phenomena (Chowdhury, 2010).

Earthquake ground motions are capable of inducing large destabilizing inertial forces of a cyclic nature, in slopes and embankments. Also, the shear strength of the soil may be reduced due to transient loads (i.e., cyclic strains) or due to the generation of excess pore water pressures. The combined effect of the seismic loads and the changes in shear strength will result in an overall decrease in the stability of the affected slope (Abramson et al., 2002).

Typically, cyclic loads will generate excess pore water pressures in loose, saturated cohesionless material (gravels, sands and non-plastic silts), which may liquefy with a considerable loss of pre-earthquake strength. However, cohesive soils and dry cohesionless materials are not generally affected by cyclic loads to the same extent. If the cohesive soil is not sensitive, in most cases it appears that at least 80 percent of the static shear strength will be retained during and after the cyclic loading (Makdisi and Seed, 1978).

In general, four methods of analysis have been proposed for the evaluation of the stability of slopes during earthquakes. In increasing order of complexity and expense, these are: (1) Pseudostatic Method; the earthquake's inertial forces are simulated by the inclusion of a static horizontal and vertical force in a limit equilibrium analysis, (2) Newmark's displacement Method; based on the concept

that the actual slope accelerations may exceed the static yield acceleration at the expense of generating permanent displacements, (3) Postearthquake Stability; calculated using laboratory undrained strengths, determined on representative soil samples that have been subjected to the cyclic loads comparable to the anticipated earthquake, (4) Dynamic Finite Element Analysis; a coupled two- (or three-) dimensional analysis using an appropriate constitutive soil model will provide details concerning stresses, strains, and permanent displacements (Abramson et al., 2002).

2.1.2.1. Pseudostatic Method

The pseudostatic method of analysis, like all limit equilibrium methods, provides an index of stability (factor of safety) but no information on deformations associated with slope failure. Since the serviceability of a slope after an earthquake is controlled by deformation, analyses that predict slope displacements provide a more useful indication of seismic slope stability. Since earthquake-induced accelerations vary with time, the pseudostatic factor of safety will vary throughout an earthquake. If the inertial forces acting on a potential failure mass become large enough that the total (static plus dynamic) driving forces exceed the available resisting forces, the factor of safety will drop below 1.0 (Kramer, 1996).

The pseudo-static method offers the simplest approach for evaluating the stability of a slope in an earthquake prone region. In its implementation, the limit equilibrium method is modified to include horizontal and vertical static seismic forces that are used to simulate the potential inertial forces due to ground accelerations in an earthquake. These seismic forces are assumed to be proportional to the weight of the potential sliding mass times seismic coefficients, k_h and k_v , expressed in terms of the acceleration of the underlying earth (in units of g). It is recommended that only the most critical surface, as identified by a static analysis, should be reanalyzed using pseudostatic seismic coefficients, as it will be the most stressed region within the slope (Abramson, et al., 2002).

Typically, the seismic force is presumed to act in the horizontal direction only, that is, $k_v=0$, inducing inertial force, $k_h W$, in the slope, where W is the weight of the potential sliding mass. A factor of safety is then calculated using conventional methods. The greatest difficulty with this procedure involves the selection of an

appropriate seismic coefficient and the value of an acceptable FS (Abramson, et al., 2002).

The magnitude of the seismic coefficient should effectively simulate the nature of the expected earthquake forces, which will depend on earthquake intensity, for example, peak ground acceleration (PGA), duration of shaking and frequency content. Of course as a very conservative assumption, one can select a seismic coefficient that is equal to the PGA expected at the slope. However, this conservatism will lead to a very uneconomic evaluation. The selection of such coefficients, therefore, must be rationalized if slopes are to be designed economically (Abramson et al., 2002). Some typical seismic coefficients that have been used for evaluating the seismic stability of slopes are given in Table 2.5.

Table 2.5 Typical seismic coefficients and FS in practice (Abramson et al., 2002).

Seismic Coefficient	Remarks
0.1	Major Earthquake, FS >1.0 (Corps of Engineers, 1982)
0.15	Great Earthquake, FS >1.0 (Corps of Engineers, 1982)
0.15-0.25	Japan, FS >1.0
0.05-0.15	State of California
0.15	Seed (1979), with FS>1.15 and a 20% strength reduction
$\frac{1}{3}PGA^a - \frac{1}{2}PGA^a$	Marcuson and Franklin (1983), FS>1.0
$\frac{1}{2}PGA^a$	Hynes-Graffin and Franklin (1984), FS>1.0 and a 20% strength reduction

PGA^a: peak ground acceleration, in units of g

2.1.2.2. Newmark's Displacement Method

The procedure proposed by Newmark (1965) extends the simple pseudo-static approach by directly considering the acceleration time history (accelerogram) of the slide mass within the slope. This accelerogram, selected to represent a realistic model of the ground motions expected at the site, is then compared with the yield acceleration to determine permanent displacements (Abramson et al., 2002).

Newmark's method assumes existence of a well-defined slip surface, a rigid, perfectly plastic slide material, a negligible loss of shear strength during shaking, and occurrence of permanent strains only if the dynamic stress exceeds the shear resistance. Also, the slope is only presumed to deform in the downslope direction,

thus implying infinite dynamic shear resistance in the upslope direction. The procedure requires that the value of a yield acceleration or critical seismic coefficient, k_y , be determined for the potential failure surface using conventional limit equilibrium methods. The main difficulty associated with this method is related to the selection of an appropriate accelerogram that simulates the motions of the slide mass. However, once this has been selected, the permanent displacements are calculated by double integration of the portions of the accelerogram that exceed the yield acceleration for the critical failure surface (Abramson et al., 2002).

The reported permanent displacements represent the motion of the center of gravity of the slide mass. For a planar slip-surface, the direction of this permanent displacement will be parallel to the slip surface. For the typical non-planar failure surface, the direction of the permanent displacements is not immediately obvious. In such cases, the initial direction of the block's motion may be determined by considering the free-body forces that exist along the boundary of the slide mass. This direction may be calculated first by the resultant of all the shear forces and all the normal forces acting along the failure surface boundary. This essentially amounts to a vertical summation of the shear and normal forces at the base of all slices, as determined in a limit equilibrium analysis. The permanent displacements are then assumed to act along the direction of the resultant of the cumulative shear and normal forces (Bromhead, 1992).

A typical ground response analysis consists of selecting an accelerogram to represent expected motions on bedrock, which should effectively simulate the intensity, duration and frequency content of the shaking motions. Then by using a numerical model, these bedrock motions are propagated through the overlying soil layers. Results from such an analysis can provide acceleration, stress and strain time histories within the geometric model of the slope (Abramson et al., 2002).

2.2. Methods of Slope Stabilization

Selection of a treatment to provide stability is based on an assessment of the degree of the hazard presented by the existing conditions and the proposed construction and the degree of risk involved with the occurrence of failure. The degree of hazard relates to the potential failure itself in terms of its possible magnitude, such as a small volume of material with small displacements or a large

volume of material with large displacements, and the probability of occurrence, such as unlikely, likely, or certain. The degree of risk relates to the consequences of failure on construction such as a relatively low risk from a small volume of material partially covering a roadway and not endangering lives to the high risk from the failure of an earth dam resulting in the loss of many lives and much destruction and damage. Safe but economical construction is the desired result, but the degree of safety acceptable varies with the degree of the hazard and the risk (Hunt, 1986).

Slope stabilization methods generally reduce driving forces, increase resisting forces, or both. Driving forces can be reduced by excavation of material from the appropriate part of the unstable ground and drainage of water to reduce the hydrostatic pressures acting on the unstable zone. Resisting forces can be increased by: (1) Drainage that increases the shear strength of the ground, (2) Elimination of weak strata or other potential failure zones, (3) Building of retaining structures or other supports, (4) Provision of in-situ reinforcement of the ground, (5) Chemical treatment (hardening of soils) to increase the shear strength of the ground (Abramson et al., 2002).

2.2.1.Drainage

Drainage is by far the most frequently used means of stabilizing slopes. Slope failures are very often precipitated by a rise in the groundwater level and increased pore pressures. Therefore, lowering groundwater levels and reducing pore pressures are logical means of improving stability. In addition, improving drainage is often less expensive than other methods of stabilization, and a large volume of ground can frequently be stabilized at a relatively low cost. As a result, drainage is an often-used method, either alone or in conjunction with other methods. Drainage improves slope stability in two important ways:

1. It reduces pore pressures within the soil, thereby increasing the effective stress and the shear strength; and
2. It reduces the driving forces of water pressures in cracks, thereby reducing the shear stress required for equilibrium.

Once a system of drainage has been established, it must be maintained to keep it functional. Erosion may disrupt surface drains and ditches, and underground drains

may become clogged by siltation or bacterial growth. Siltation can be minimized by constructing drains of materials that satisfy filter criteria, and bacterial clogging can be removed by flushing with chemical agents, such as bleach (Duncan et al., 2005).

2.2.1.1. Surface Drainage

Carefully planned surface drainage is essential for treatment of any slide or potential slide. Every effort should be made to ensure that surface runoff is carried away from and not seeping downwards into the slope. Such considerations should always be made and are extremely important when evaluating a failure. Temporary remedial measures usually considered after a landslide include: (1) using sandbags to divert water runoff away from the failure zone, (2) sealing cracks with surface coatings such as shotcrete, lean concrete, or bitumen to reduce water infiltration, (3) covering the ground surface temporarily with plastic sheets or the like to reduce the risk of movement during construction (Abramson et al., 2002).

Surface runoff is usually collected in permanent facilities such as V- or U- shaped concrete lined or semicircular corrugated steel pipe channels and diverted away from the slide mass (Figure 2.4). These channels should be placed strategically at the head of the slope and along berms. The detailing of surface water collection systems should provide for minimum maintenance and displacement due to future slide movement (Abramson et al., 2002).

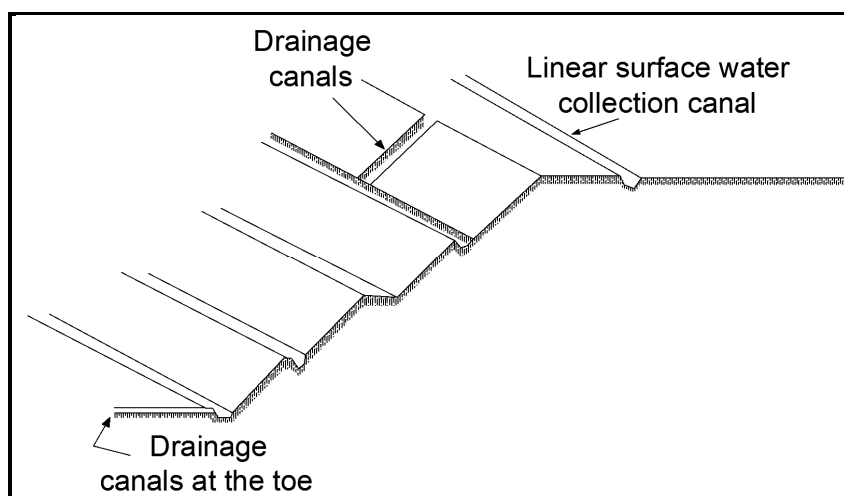


Figure 2.4 Surface drainage system (CANMET, 1977).

2.2.1.2. Subsurface Drainage

The factor of safety against failure on any potential slip surface that passes below the phreatic surface can be improved by subsurface drainage. Methods that can be used to accomplish subsurface drainage are:

- a) Drain blankets
- b) Trenches
- c) Cut-off drains
- d) Horizontal drains
- e) Relief drains
- f) Drainage tunnels or galleries (Abramson et al., 2002)

As compared to engineered embankment slopes, natural slopes are rarely homogenous enough to allow reliable subsurface drainage design according to simple principles of dewatering (Xanthakos et al., 1994). For a successful dewatering system, the designer must have a good understanding of geological structure and choose a drainage system layout that increases the probability of intersecting the major water-bearing layers (Hausmann, 1992).

2.2.1.3. Subsurface Drainage Blankets

When there is a thin layer of poor-quality saturated soil at a shallow depth, and when there are materials of better quality below that layer, it may be practical to remove the poor quality layer and replace it with a well-draining soil fill (Figure 2.5). The bottom of the excavation should be covered with a layer of filter fabric wrapping a 15-to 60-cm-thick filter stone layer with a perforated pipe embedded in it to capture flow. To avoid blockage of holes by vegetation, the first 152 cm of the outlet end of the perforated pipe should be installed to convey water flow from the outlet of the pipe to a suitable discharge point (Abramson et al., 2002).

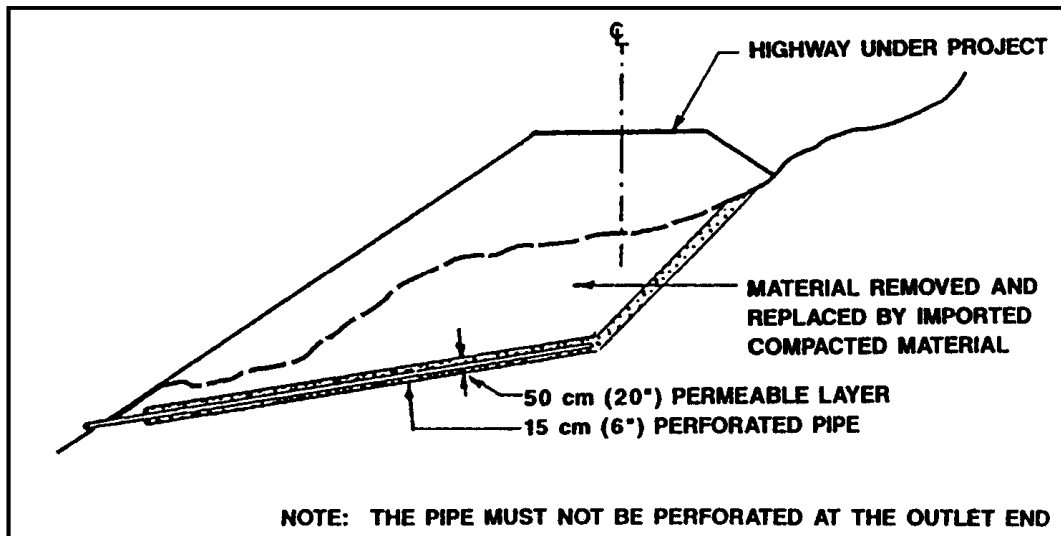


Figure 2.5 Placement of a drain blanket underneath embankments (Abramson et al., 2002).

2.2.1.4. Trenches

Deep trenches should be constructed when subsurface water or soils of questionable strength are found at such great depths that stripping of the soils is not practically feasible. Trenches usually are excavated at the steepest stable side slopes for the construction period. Shoring may be required. Any trench so excavated should extend below the water-bearing layer. The trench should be backfilled with a layer of pervious material encased in filter fabric that has an underdrain pipe running through it (Figure 2.6).

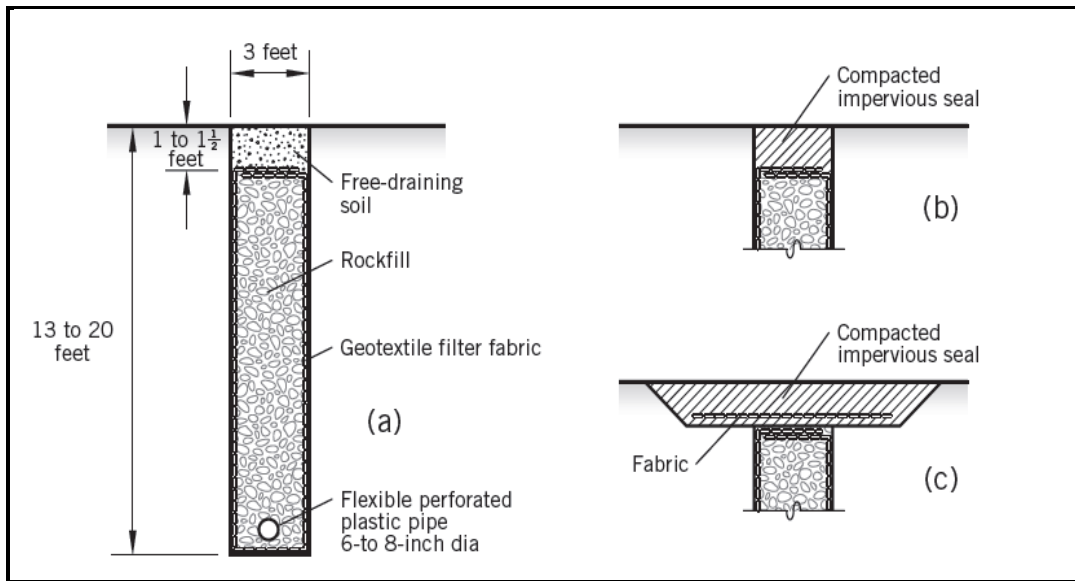


Figure 2.6 Typical trench drain details: (a) free-draining soil at surface to capture surface runoff (b) (c) impervious seal to exclude surface water (two variations) (Cornforth, 2005).

2.2.1.5. Cut-off Drains

At a site where shallow groundwater is encountered, cut-off drains can be used to intercept groundwater flow. A typical layout is shown in Figure 2.7. An impermeable zone or membrane is used as a cut-off downslope of the drain, and the top zone of the trench is backfilled with impermeable material. Runoff from the upper slopes should be collected in drainage channels. The free draining material used to backfill the trenches should be designed to conform to standard filter criteria. The size of perforations in pipes should be compatible with the grain size of the backfill filter material (Abramson et al., 2002).

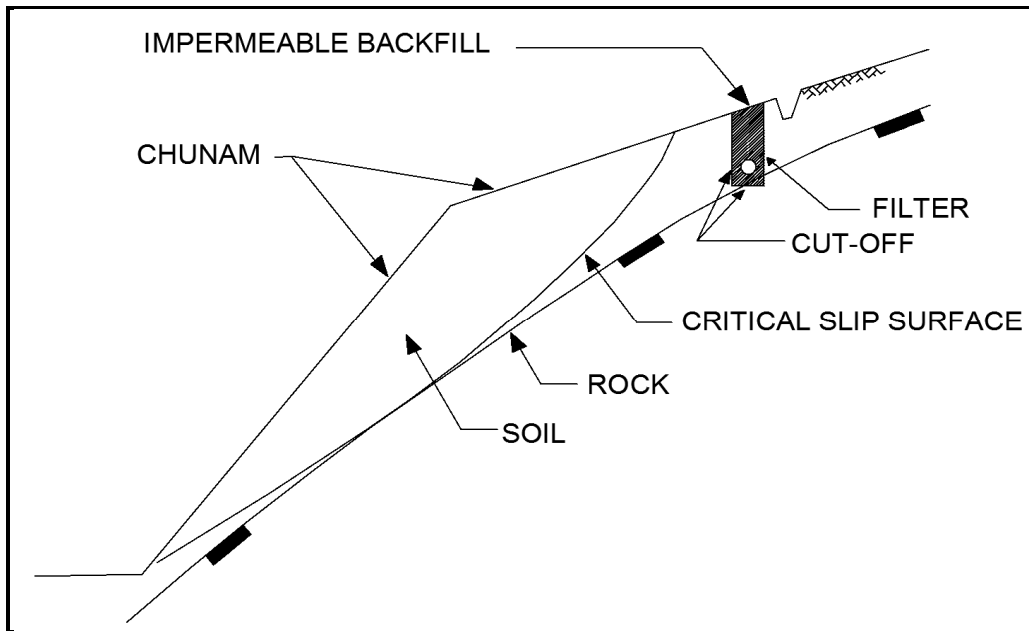


Figure 2.7 Cut-off drain (Abramson et al., 2002).

2.2.1.6. Horizontal Drains

Horizontal drains, sometime called Hydrauger drains, after the type of drill first used to install them, are perforated pipes inserted in drilled holes in a slope to provide underground drainage. As shown in Figure 2.8, they usually slope upward into the slope, to permit groundwater to drain by gravity. They are usually 30.5 to 91.5 m long, although longer drains have been used. The drain pipes are commonly perforated or slotted PVC pipe, although steel pipe was used for early applications. The drains are installed by drilling into the slope using a hollow-stem auger, inserting the drain pipe, and withdrawing the auger, leaving the drain in place. The hole is allowed to collapse around the drain pipe. There is no filter between the pipe and the soil (Duncan and Wright, 2005).

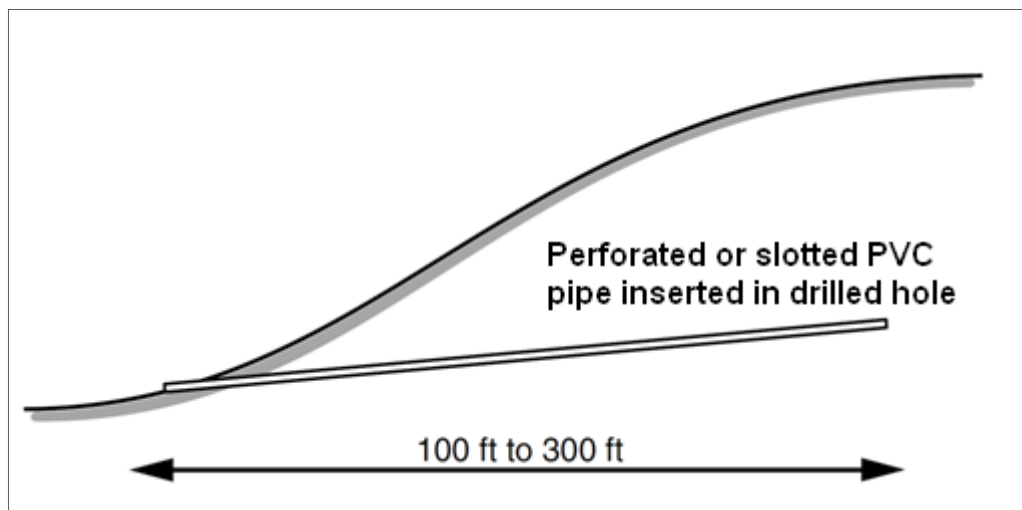


Figure 2.8 Horizontal drains (Duncan and Wright, 2005).

Horizontal drains are usually installed from points of convenient access for the drill rig. It is commonly found that some drains are very productive and others are nonproductive, but it is very difficult to predict in advance which drains will produce significant flow. Flows usually decline with time after installation and then fluctuate seasonally through wet and dry periods (Duncan and Wright, 2005). Rahardjo et al. (2003) found that horizontal drains are most effective when placed low angle in the slope, provided that the slope does not contain distinct layers of high permeability above the drains.

2.2.1.7. Relief Wells

The principal function of relief wells is to lower the water pressures in layers that are deep down in the subsoil, layers that cannot be reached by open excavation methods or horizontal drains because of cost or construction difficulties. Relief wells are vertical holes with a diameter of about 41 to 61 cm. A perforated pipe with a 10.2-to 20.3-cm diameter is placed inside the hole. The annular space between the borehole and the pipe should be filled with filter material. A water disposal system using a submersible pump or surface pumping and discharge channels is required to dispose of the water from the wells. Disposal of the water may be very costly, and an effective dewatering system will require frequent maintenance (Abramson et al., 2002).

2.2.1.8. Drainage Tunnels or Galleries

Where drainage is needed deep within a hillside, a drainage gallery (tunnel) can be used. As shown in Figure 2.9, drains can be drilled outward from the tunnel, extending the drainage through the slope. This technique was used to stabilize the hillside below the Getty Museum in Los Angeles, where improved stability was needed, but environmental considerations made it impossible to flatten the slopes or to construct access roads for the purpose of installing horizontal drains (Duncan and Wright, 2005).

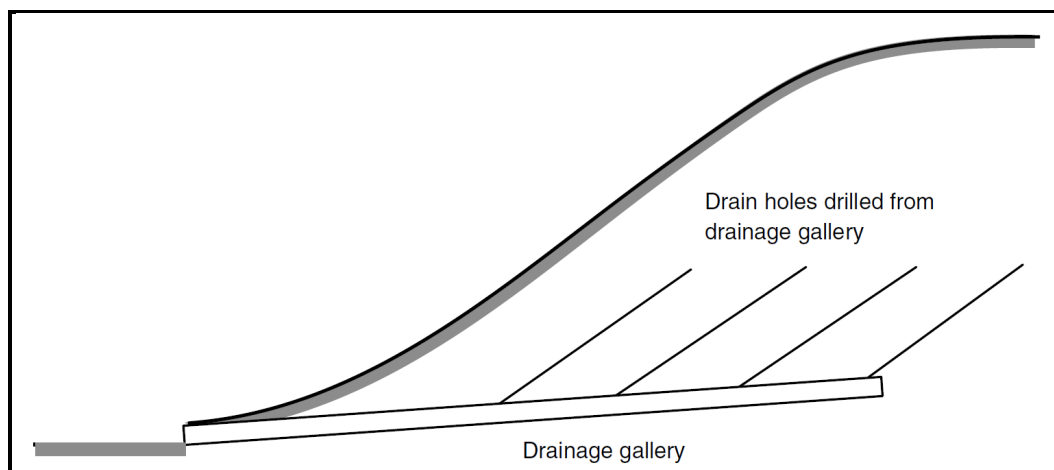


Figure 2.9 Drainage galleries (Duncan and Wright, 2005).

2.2.2. Excavations and Buttress Fills

A slope can be made more stable by excavation to reduce its height or make it less steep. Flattening a slope or reducing its height as shown in Figure 2.10 reduces the shear stresses along potential sliding surfaces and increases the factor of safety. As shown in Figure 2.10, any type of excavation results in a reduction of the useful area at the crest of the slope. Improving stability by excavation requires (1) that an area at the top of the slope can be sacrificed to improve stability, (2) that the site is accessible to construction equipment, and (3) that an area is available for disposal of the excavated material (Duncan and Wright, 2005).

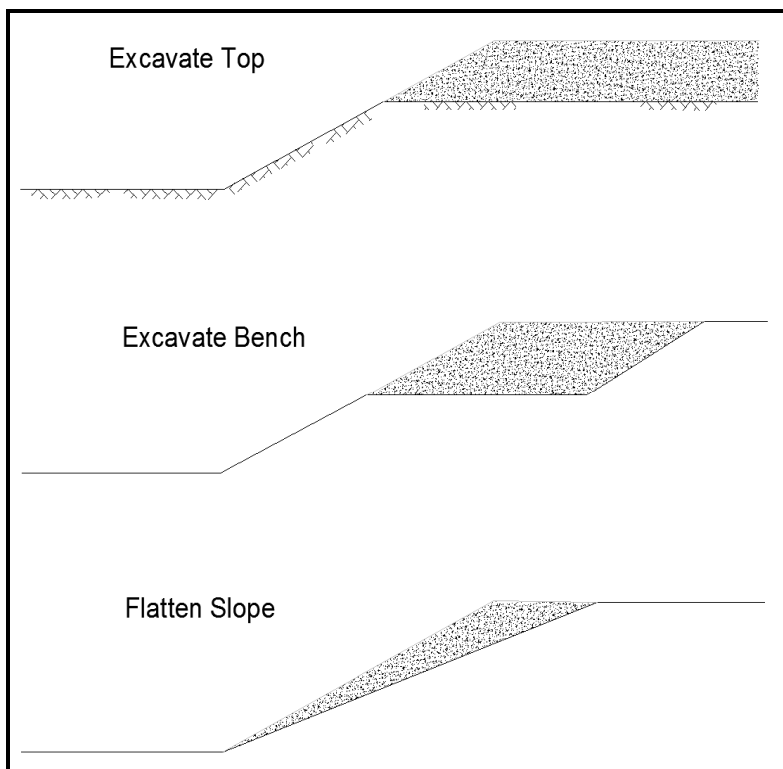


Figure 2.10 Slope stabilization by excavation (Duncan and Wright, 2005).

Buttress fills are of two types. A buttress of high strength well-compacted material (Figure 2.11) provides strength and weight, both of which improve stability. A berm of uncompact material at the bottom of a slope, sometimes called a gravity berm, provides weight and reduces the shear stresses in the slope, even if it consists of weak and compressible soil. The effectiveness of either type of berm is improved if it is placed on a layer of free-draining material that allows drainage of water from the soil beneath. An example involving both excavation and buttressing is shown in Figure 2.12. Balancing the volume of cut and fill makes it unnecessary to dispose of material off-site or to import soil for buttress construction. Even soil that has been involved in sliding can be improved and made suitable for berm construction by compaction to high density near optimum water content (Duncan and Wright, 2005).

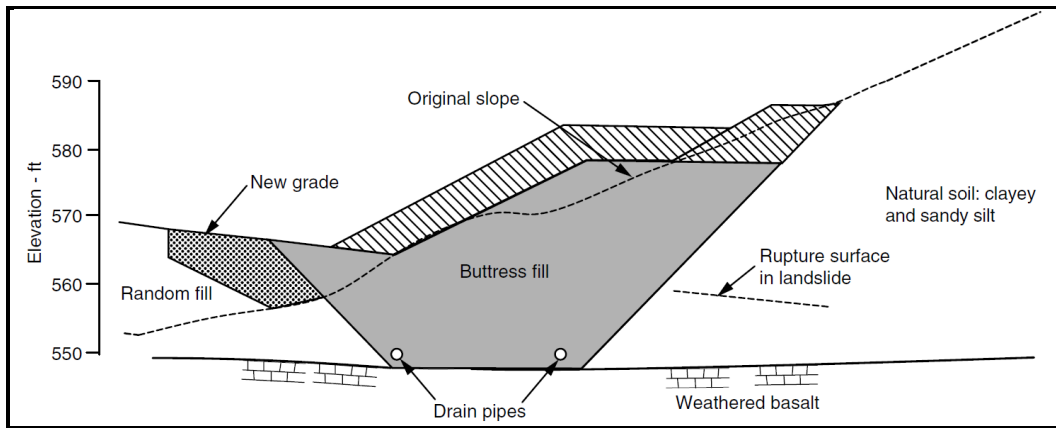


Figure 2.11 Structural buttress (Duncan and Wright, 2005).

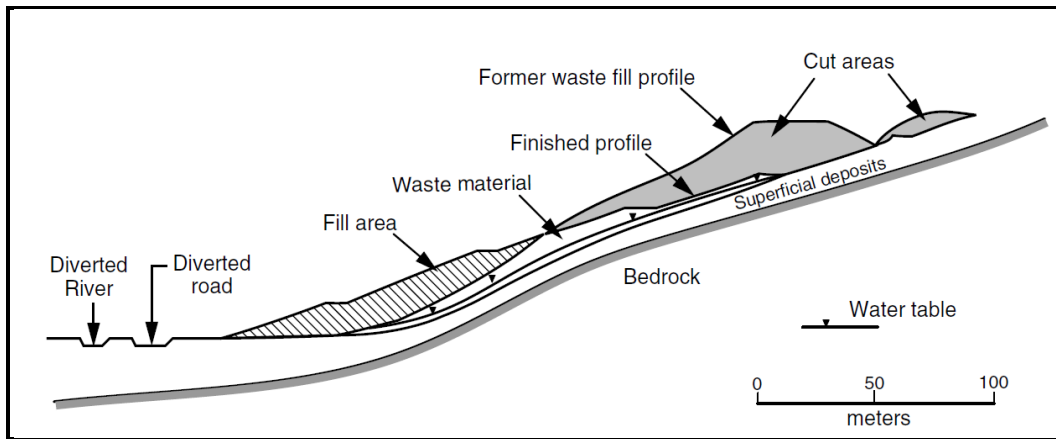


Figure 2.12 Slope stabilization by cut and fill (Duncan and Wright, 2005).

2.2.3. Ground Anchors (Tiebacks)

Anchors apply tensile loads to the face of a wall or slope. As a structural member, they prevent outward movements of the face. Anchors constructed on open face slopes restrain the outward movement of soil at the face, helping to provide stability against shallow slope failures. Finally, anchors passing through the slip surface of a landslide can create an uphill pull to resist the gravity forces and also increase the shear strength at the slip surface (Cornforth, 2005).

An anchor is drilled through overburden soils to an anchorage zone of bedrock or firm soils. For simple cut slopes, the anchorage is a short distance behind the active wedge or potential slip surface. In landslide analyses, the anchor has to be

constructed within the stable ground behind the slip surface (Figure 2.13). An additional contingency margin of at least 3 m should be provided between the slip surface and front edge of the anchor in soil landslides, but less when the anchor is within bedrock (Cornforth, 2005).

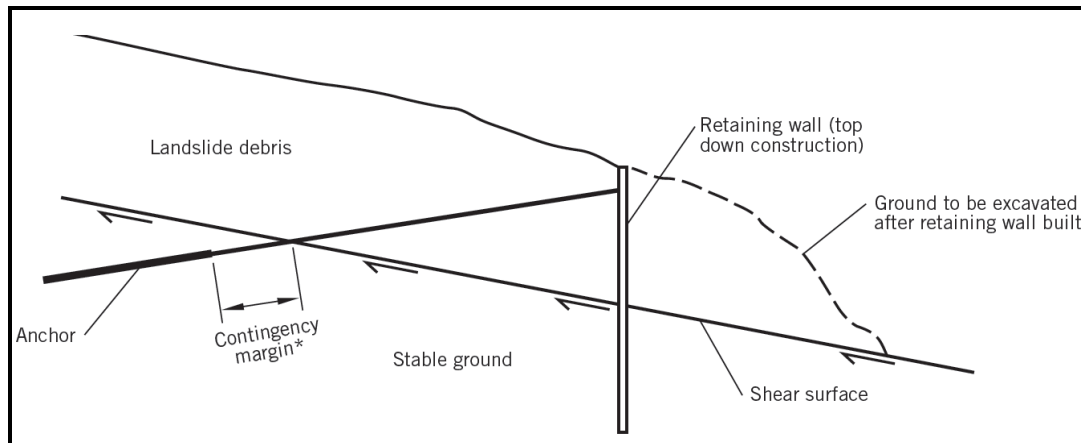


Figure 2.13 Ground anchor installed through a landslide (Cornforth, 2005).

An anchor is constructed by first drilling a deep angled hole into the ground. Next, a steel bar or stranded wire is inserted to the full depth of the hole and is grouted by a cement grout. There are four methods in use: gravity grouted, pressure grouted, post grouted, or under reamed (Cornforth, 2005).

Gravity grouted anchors allow the grout to be installed by tremie methods and require a down sloping drill hole. The technique is commonly used for rock or very stiff/hard clays. Casing is not usually needed but can be provided. Pressure grouted anchors are employed for cohesionless soils or weak fractured rock. The hole is cased. As the casing is withdrawn, the grout is injected under pressures higher than 345 kPa. The pressure may enlarge the whole diameter and produce higher normal stresses on the hole wall, both effects contributing to higher pullout resistance (Cornforth, 2005).

The unbonded length of the steel anchor passes through the landslide mass and applies the full anchor load T at the slip surface (Figure 2.14a). Because the anchor

usually crosses the slip surface at an oblique angle, the anchor provides: (i) a pullback component load P parallel to the slippage, and (ii) an increased normal load perpendicular to the slip surface, thereby increasing the shear resistance by an increment δS (Figure 2.14b). This dual function can produce a maximum total benefit to stability when the anchor is inclined at an optimum inclination to the horizontal (Cornforth, 2005).

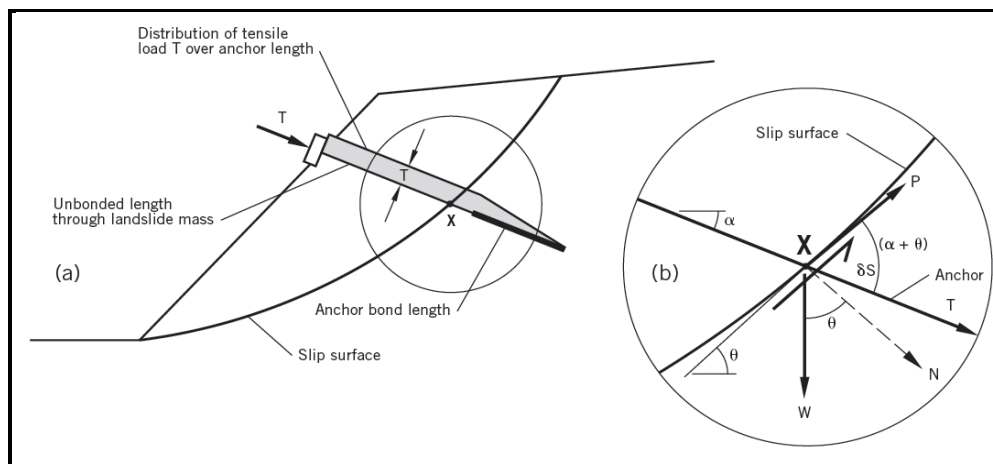


Figure 2.14 Effect of anchor tensile load, T , on stability: (a) full load T acting at slip surface X (b) pullback load P and shear strength δS benefits (Cornforth, 2005).

Some representative values of average ultimate bond stress for rocks (after Sabatini et al., 1999) are listed on Table 2.6.

Table 2.6 Average ultimate bond stress for rocks (after Sabatini et al., 1999).

Rock Type	Average Ultimate Bond Stress (kPa)	
Granite and basalt	1724	- 3103
Dolomitic limestone	1379	- 2069
Soft limestone	1034	- 1379
Slates and hard shales	827	- 1379
Soft shales	207	- 827
Sandstones	827	- 1724
Weathered sandstones	690	- 827
Chalk	207	- 1103
Weathered marl	152	- 248
Concrete	1379	- 2758

CHAPTER 3

GEOLOGICAL SETTING

3.1. Regional Geology

3.1.1. Stratigraphy

There are six main formations observed on the 1:100 000 scaled map of the study area (Figure 3.1). From older to younger, they are Kızılkaya formation, Çağlayan formation, Ağıllar formation, Kabaköy formation, Alluvium and Colluvium. Stratigraphic columnar section is given in Figure 3.2.

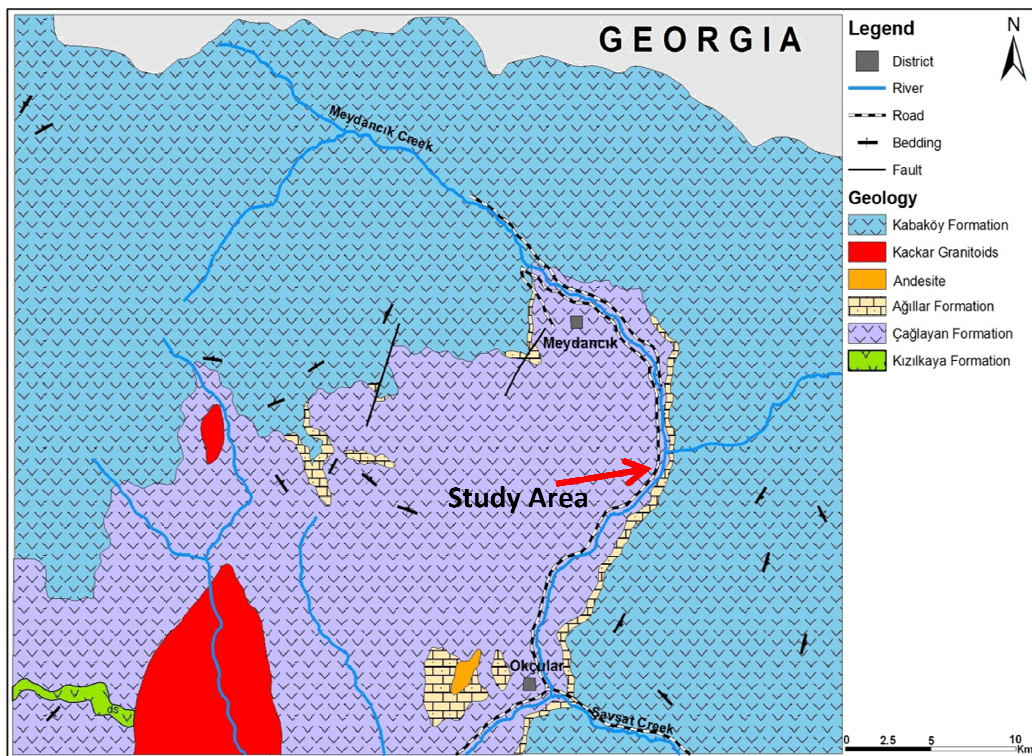


Figure 3.1 Geological map of the study area (modified from MTA, 1998).

ERA	PERIOD	EPOCH	AGE	FORMATION	SYMBOL	THICKNESS (m)	LITHOLOGY	EXPLANATIONS						
MESOZOIC	CRETACEOUS	UPPER CRETACEOUS	TERTIARY	QUATERNARY	Qa - Qc	5-10		Qa-Qc: Alluvium and Colluvium						
									Eocene	KABAKÖY	Ev	1000		Ev: Andesite-Basalt Lava and Pyroclastics Gk: Kaçkar Granitoid Ap: Andesite
									Campanian-Maastrichtian	ÇAĞLAYAN	Kr-2	1000		Kr-2: Basalt Lava and Pyroclastics

Figure 3.2 Stratigraphic columnar section (modified from MTA, 1998).

3.1.1.1. Kızılkaya formation

Rhyodacite-dacitic lava and pyroclastics typically outcropping in the Kızılkaya region located at south of the Espiye District in the Giresun Province are firstly named by Güven (1993) as Kızılkaya formation.

Kızılkaya formation is composed of grey-white rhyodacitic-dacitic lava and pyroclastics. In patches, columnar and flowing structures are observed in lavas. This formation has been observed in the southwest part of the study area shown in Figure 3.1.

Kızılkaya formation concordantly overlies the Çağlayan formation composed of alkaline volcano-sediment. Thickness of the formation is about 400 m. Sediment

level with fossil content in the formation are not found, therefore, age of the formation is determined relatively.

Kızılkaya formation overlies concordantly Turonian - Santonian aged Çatak formation and Campanian - Maastrichtian aged Çağlayan formation shown in Figure 3.2. Therefore, its age is suggested to be Santonian- Campanian.

3.1.1.2. Çağlayan formation

Typical outcropping of Campanian-Maastrichtian aged alkaline volcano-sediment imbrications is observed at Çağlayan town in the Trabzon Province and it was firstly named by Güven (1993) as Çağlayan formation. In the study area, alkaline volcano-sediment imbrications having the same lithostratigraphic feature calibrated with the Çağlayan formation and same formation name was used.

This formation was observed under the landslide material in the thesis area shown in Figure 3.1 and was evaluated as a slide contact at the crown of landslide during the stability analysis.

The formation is generally composed of red mudstone, grey marl and sandstones intercalated with grey-green andesitic basalt, basalt lava and pyroclastics. Undulated fold structures that enhanced the effect of thrust in the south contact are observed in layers inside the formation. Pillow lava structures are seen in basalt.

Çağlayan formation is found concordantly over the Kızılkaya formation composed of rhyodacite-dacite lava and pyroclastics shown in Figure 3.2. Thickness of the formation in the study area is about 1000 m. Its age is Campanian-Maastrichtian.

3.1.1.3. Ağıllar formation

Çağlayan formation which has the characteristics of alkaline volcano-sediment was observed at the southeast of the Zeytinlik town in the Artvin province. Maastrichtian - Paleocene aged sandy and reefal limestone which is lying concordantly on the Çağlayan formation was named by Güven (1993) as Ağıllar formation since it was observed clearly around Ağıllar village. In the thesis area, limestone which has the same lithological setting is also named as the Ağıllar formation.

This formation is also observed under the landslide material in the thesis area shown in Figure 3.1 and is evaluated as a slide contact at the toe of landslide during the stability analysis.

The formation consists of grey-white, sandy and reefal limestone. The thickness of the formation is about 200 m and its age is Upper Cretaceous (Maastrichtian-Paleocene transition).

3.1.1.4. Kabaköy formation

The formation is located around Kabaköy settlement area at the SE of the Gümüşhane Province. It is composed of andesite, basalt and pyroclastics. It is named by Güven (1993) as Kabaköy formation.

The Kabaköy formation comes as a transgressive discordant over the Ağıllar formation consisting of sandy and reefal limestone shown in Figure 3.2. The formation begins with coarse gravelly conglomerate that is hold together with red cement matrix. Gravels are generally composed of basalt, dacite and granite. Nummilitic limestone and sandstone overlap with conglomerate level. This base level with 20-30 m thickness consists of sandstone, sandy limestone and andesitic lava and pyroclastics with marl intercalations. This formation has been observed in the north-west-east part of the study area shown in Figure 3.1.

Thickness of the formation in the study area is about 1000 m. The age of this formation is Lower and Middle Eocene.

3.1.1.4.1. Kaçkar Granitoids

Kaçkar granitoids are observed typically around Kaçkar Mountains in the study area. For this reason this unit is identified as Kaçkar Granitoids (Güven, 19993). Granitoid observed in the study area has intruded in the Campanian-Maastrichtian aged Çağlayan formation and has been observed in the southwest part of the study area shown in Figure 3.1.

3.1.1.4.2. Andesite

In the study area, this unit outcrops in the northern east of the city center of the Artvin Province. Andesitic rocks are grey-white, highly jointed. Andesite observed in the study area has outcropped in the Upper Cretaceous aged Ağıllar formation and has been observed in the southwest part of the study area shown in Figure 3.1.

3.2. Local Geology

According to borehole data and field observations, the units from older to younger are basalt, limestone and colluvium, respectively (Figure 3.3 and Figure 3.4).

Basalt belonging to Çağlayan formation is dark grey, moderately weak-moderately strong, slightly weathered. There are discontinuities in this unit. It is determined that rough surfaced discontinuities have tight aperture, locally open aperture and clay filling. Basalt is located under locally limestone and colluvium.

Limestone (Ağıllar formation) observed in the study area has generally located over basalt. The unit is composed of grey-white, moderately weak-moderately strong, moderately weathered, locally highly weathered limestone. Limestone shows jointed structure. It is determined that discontinuities have rough surface and partially clay filling. The unit has narrow spacing joints with small aperture.

Colluvium is composed of multi-colored, very dense, clayey, blocky gravel, brown, fine-coarse grained, very dense, blocky, gravelly, clayey sand, reddish brown, hard, blocky, sandy, gravelly clay. Clay has low plasticity. Gravels are volcano-sediment origin. Sub angular-angular gravels are maximum 50 cm in size. This unit is 10-20 m in thickness determined by borehole and it overlies the limestone and basalt.

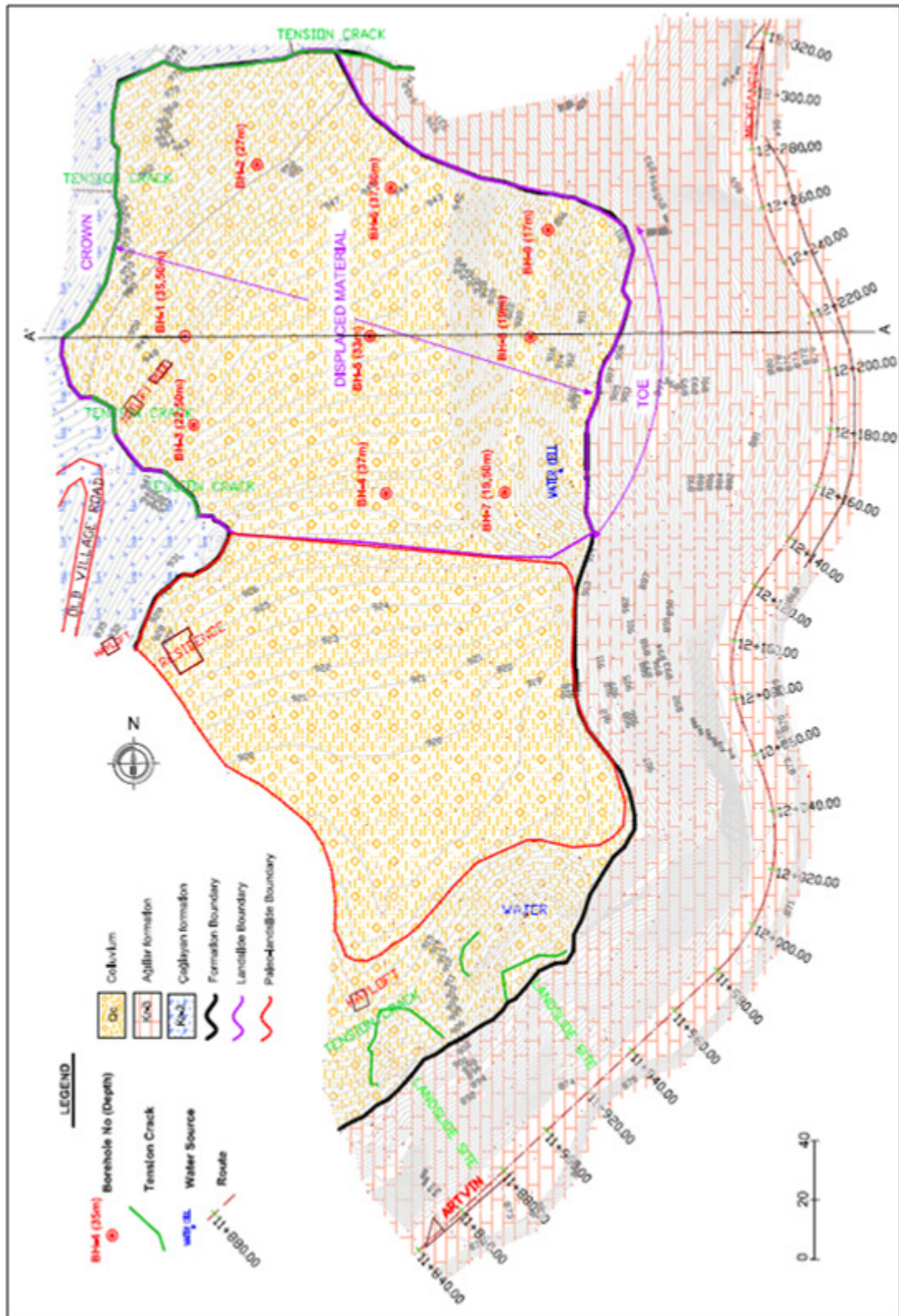


Figure 3.3 Local geological map of the study area.

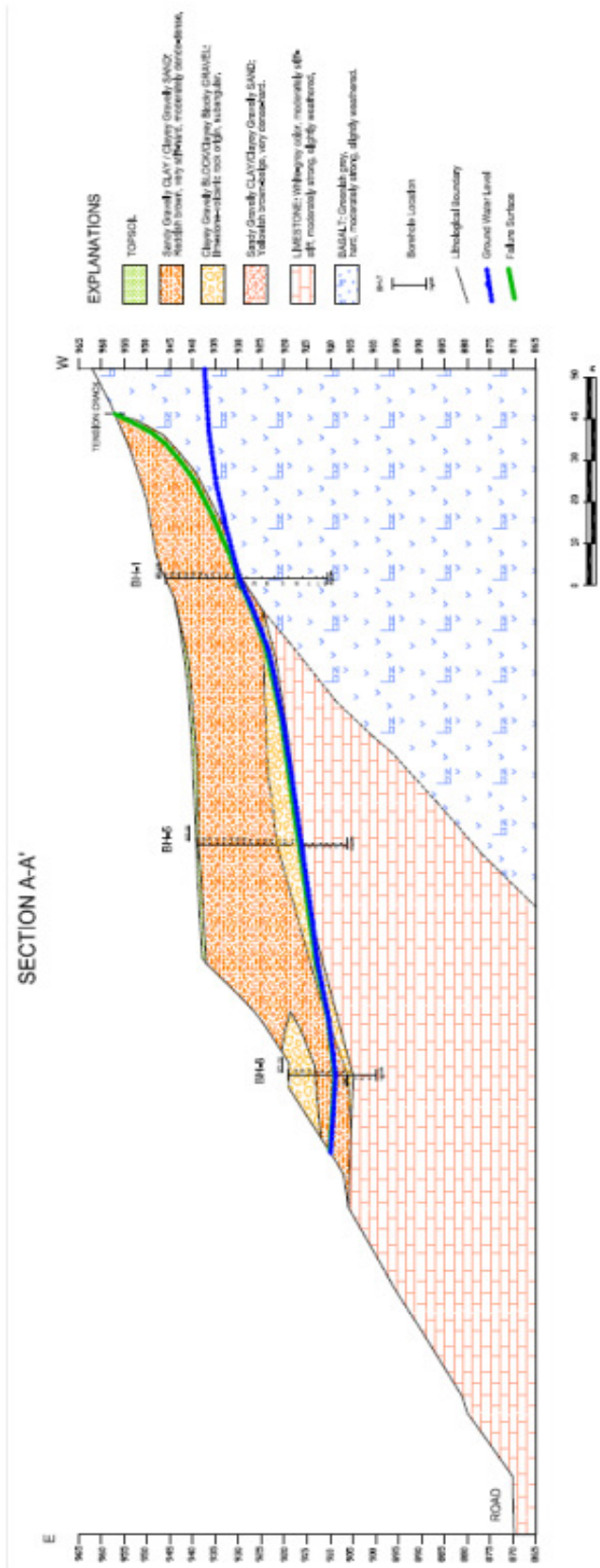


Figure 3.4 Geological section of the study area along section line A-A'.

3.3. Structural Geology and Seismicity

The study area is located inside the East Pontide tectonic block. Rock units in the area of investigation are under the influence of Alpien Orogenesis. This orogenic activity causes discordant, folded and fractured structures, complex faulting and overthrusts in the region. There are unconformities between Paleozoic and Jurassic, Jurassic and Cretaceous, Paleocene and Eocene, Eocene and Miocene, Miocene and Pliocene.

In the study area fold and fracture tectonic is enhanced due to effective Alpien orogenesis. Folded structures in the field are observed clearly in the Paleocene aged flysch and Eocene aged volcano-sediment rocks. Formations are fractured and faulted by the effect of same forces. Thrust faults observed in some regions in the study area show that the region is under the effect of normal forces.

Thrust faults observed in the study area and its surrounding are in the form of; the thrust passing the north and south of the Artvin Province and reaching from the east of the Yusufeli District to Morkaya, the thrust reaching from the Ardanuç District through SW to Yusufeli-Demirkent and Morkaya, the large thrust reaching from the Şavşat District through SW to the south of Yusufeli-Kılıçkaya and its strikes are generally NE-SW.

Beddings are distinct in the sedimentary units and especially flysch. They have various directions for the strike and dip. However, in general, strikes are in the NW-SE and NE-SW direction, dips are between 200° and 600° in the N and S direction.

The study area remains in the 3rd Degree Earthquake Zone according to the Earthquake Zoning Map of the Ministry of Public Works and Settlement of Turkish Republic, General Directorate of Disaster Affairs (Figure 3.5). Horizontal ground acceleration is recommended as 0.20 g for 3rd Degree Earthquake Zones. This information is given to provide general evaluation of the seismicity conditions. In the area remaining inside the Artvin provincial border, there are not any active fault capable of devastating earthquakes.

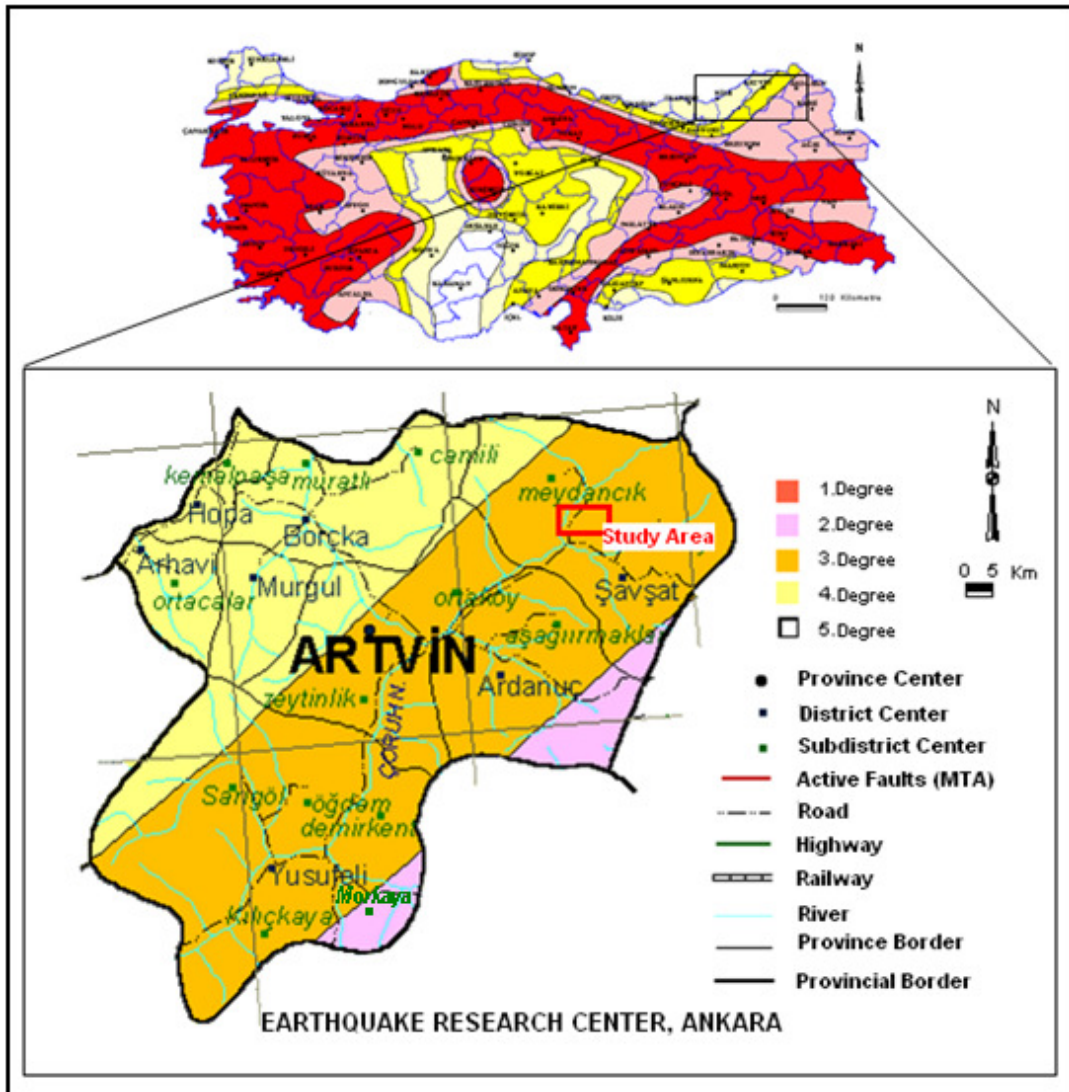


Figure 3.5 Seismic zonation map of city of Artvin and the study area (Earthquake Research Center, 2012).

Erzurum Fault Zone (EFZ) is the closest fault system to the Artvin Province and the map distance is 50-100 km. The other fault system is the North Anatolian Fault Zone (NAFZ) and its map distance is 100-160 km (Figure 3.6). Epicentral distributions of earthquakes having a magnitude greater than 3.0 around the Şavşat District are given in Figure 3.7.

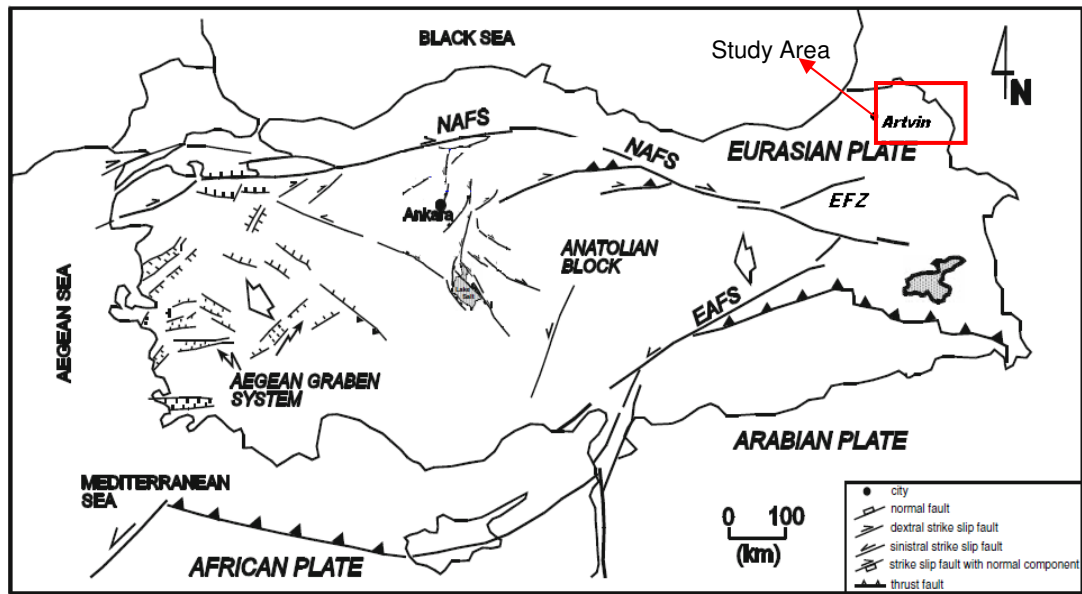


Figure 3.6 Seismic map of Turkey [EAFS: East Anatolian Fault System, NAFS: North Anatolian Fault System, EFZ: Erzurum Fault Zone] (Modified from Koçyiğit, 1991).

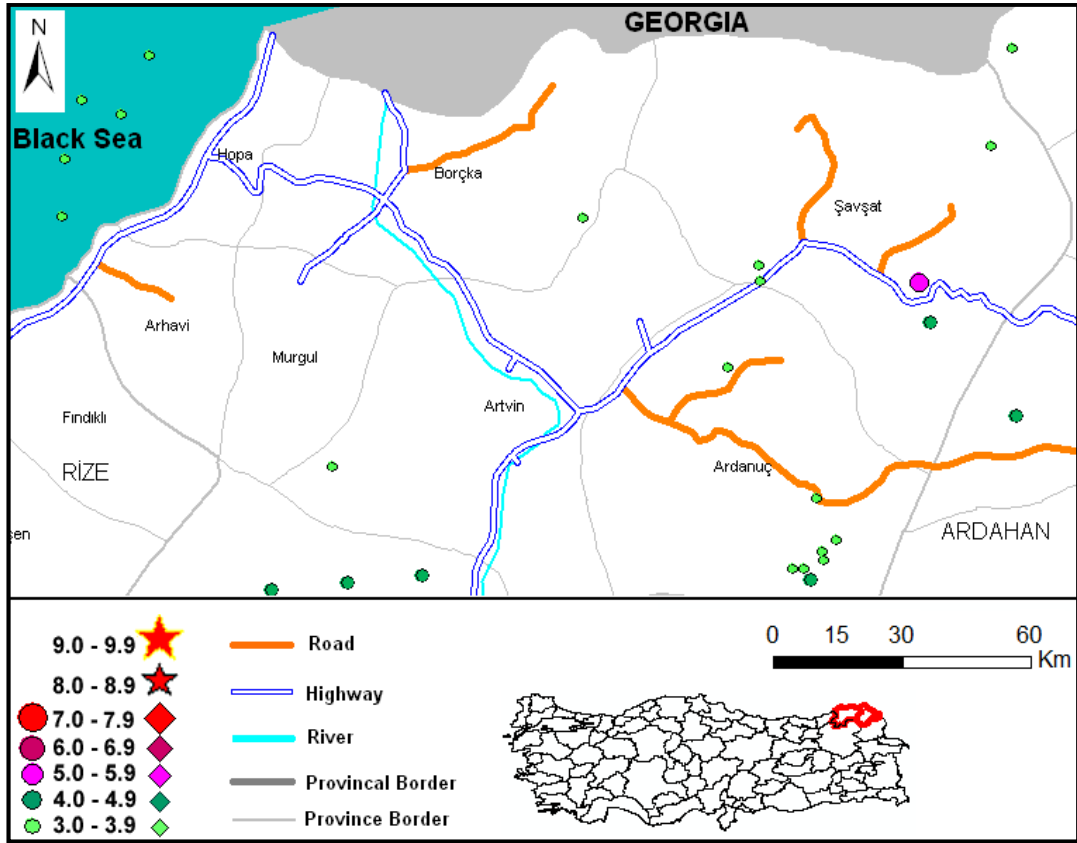


Figure 3.7 Epicentral distributions of earthquakes having a magnitude greater than 3.0 around the Şavşat District (Sayısal Grafik Ltd., 2012).

3.4. Hydrogeology

The units outcropping in the Artvin Province are generally volcanic origin like in the other region of the East Black sea Region. For this reason they are not show aquifer. The most important surface water located in the study area is Meydancık Creek that have at least 47.3 m³/s and at most 158.3 m³/s discharge. In the region there are seasonal creeks that arise after the heavy rain. It is observed that springs having low flow rate are in some places of the study area.

Moreover, groundwater was observed in all boreholes and recorded on the borehole logs given in Appendix A. Table 3.1 shows the groundwater levels measured at the time of the failure and corresponding boreholes.

Table 3.1 Measured groundwater levels in boreholes.

Borehole No.	Depth (m)	Groundwater Depth (m)
BH-1	35.5	16.2
BH-2	27.0	17.4
BH-3	22.5	14.0
BH-4	37.0	19.0
BH-5	33.0	23.0
BH-6	37.5	27.2
BH-7	19.5	11.0
BH-8	19.0	10.3
BH-9	17.0	6.2

Groundwater contour lines and its movement vectors were drawn on the topographic map to observe the variations through study area by using measured groundwater levels in boreholes. As it is seen from Figure 3.8, groundwater contour lines are not spread over the topographic map, since, there were not boreholes drilled at the south of the topographic map.

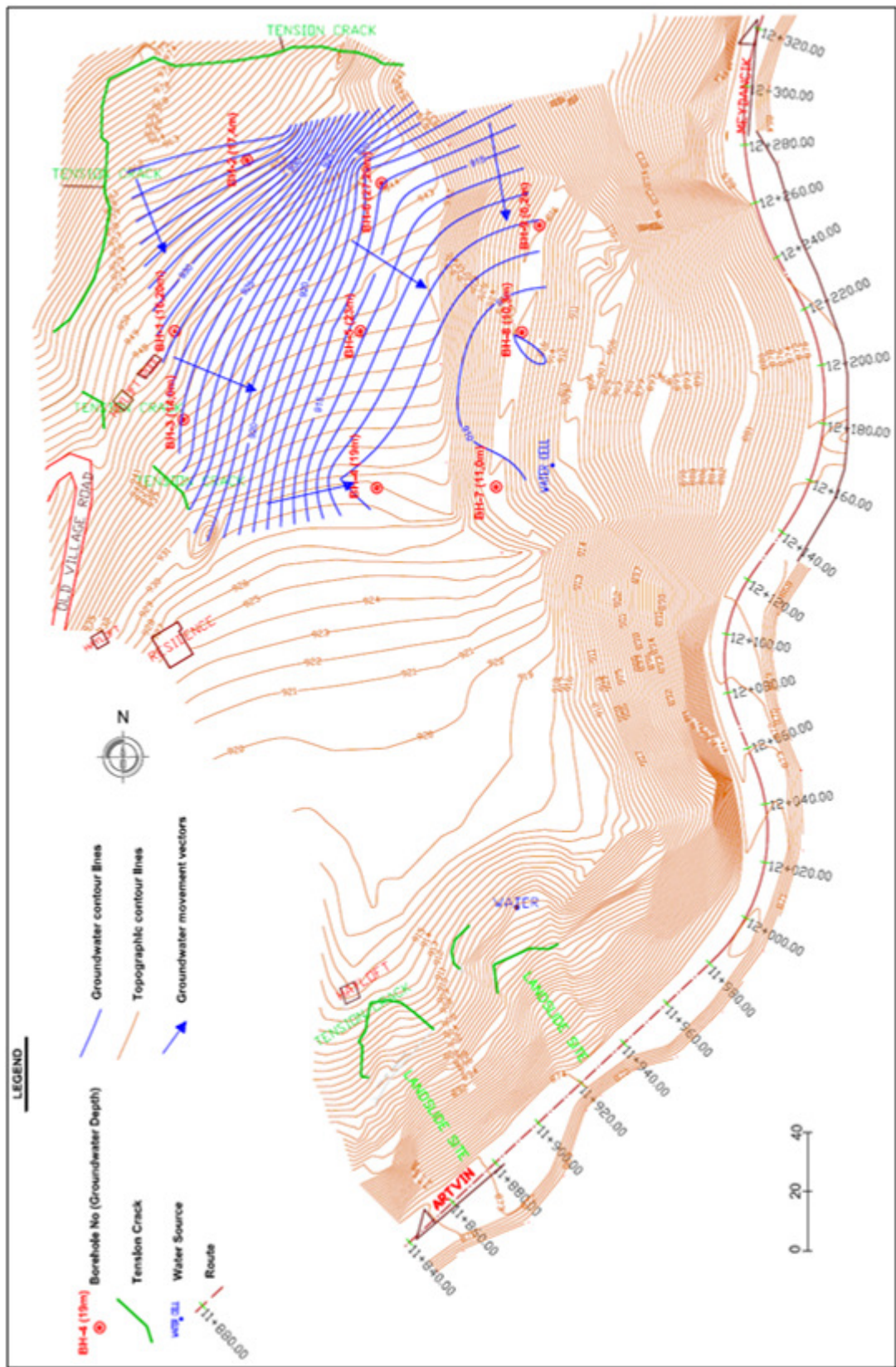


Figure 3.8 Groundwater contour lines and movement directions.

3.5. Geomorphology

The study area is located at the elevations between 980 and 864 meters. The elevations of boreholes are listed in Table 3.2.

Table 3.2 Elevations of boreholes.

Borehole No.	BH-1	BH-2	BH-3	BH-4	BH-5	BH-6	BH-7	BH-8	BH-9
Z (Elevation)	948.0	955.0	940.0	931.0	939.0	944.5	921.5	918.0	918.0

The digital elevation model of the study area and its close vicinity is shown in Figure 3.9.

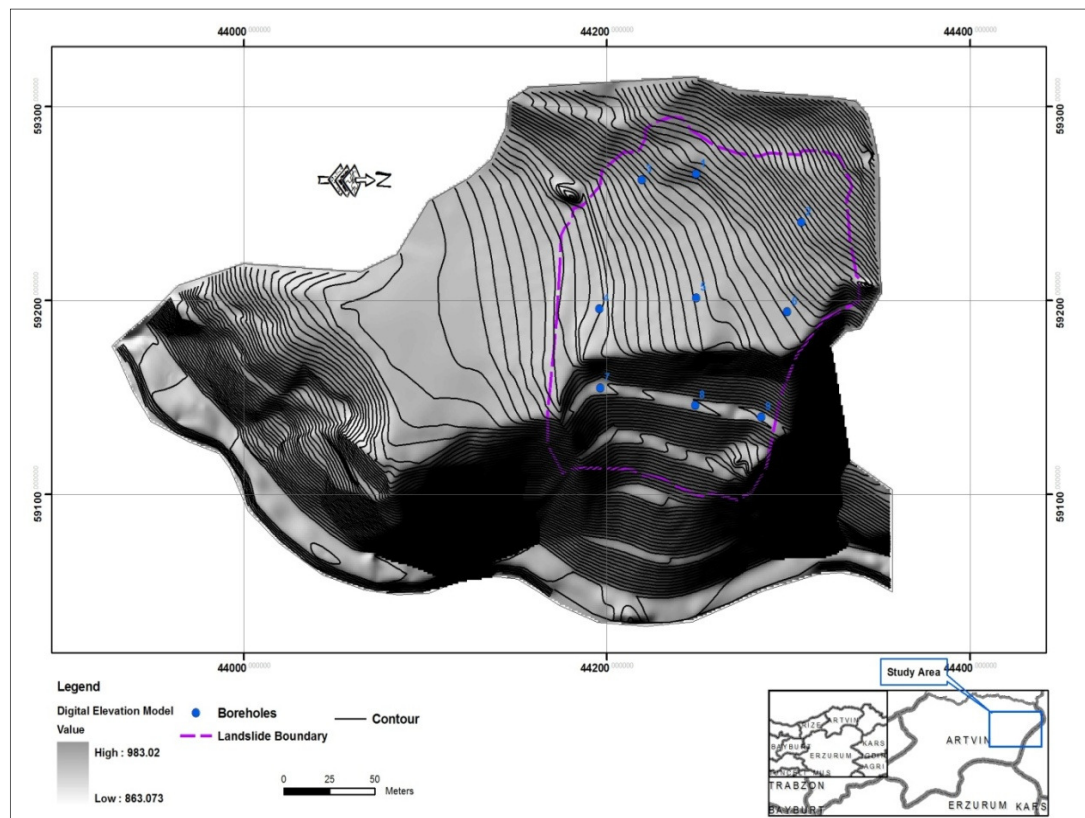


Figure 3.9 Digital elevation model of the study area.

As it is seen from Figure 3.9, slope is steep at the east part and gentle at the west part of the study area. Slope map of the study area was derived from digital elevation model and presented in Figure 3.10.

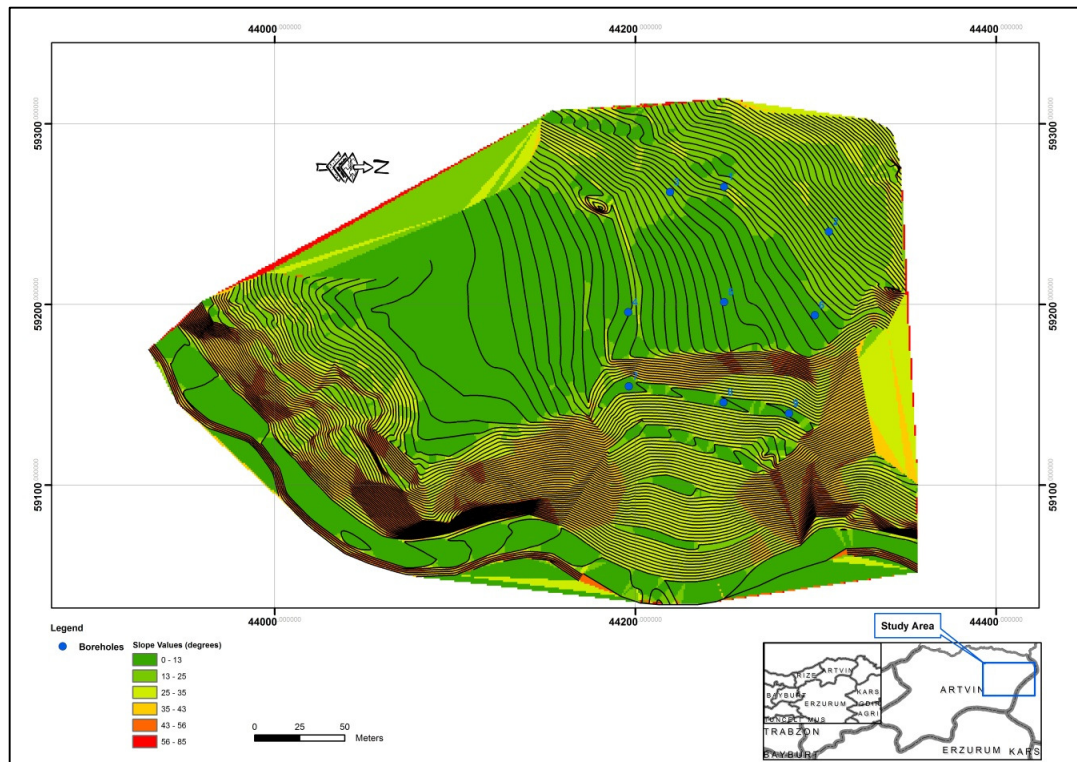


Figure 3.10 Slope map of the study area.

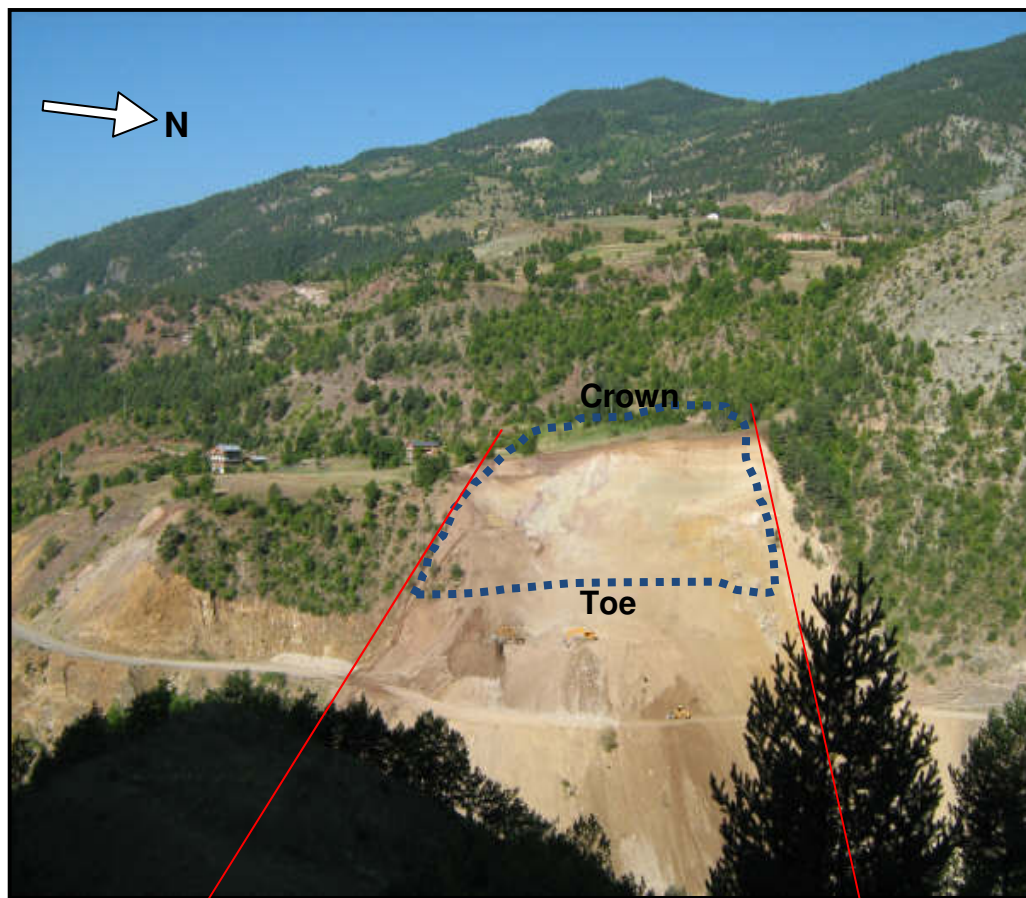
CHAPTER 4

SITE INVESTIGATION OF THE LANDSLIDE

Site investigation of the landslide at the Artvin-Şavşat Junction - Meydancık Provincial Road Km: 12+200 was initially conducted by PETRA Engineering and Consulting Company in 2009. These investigations included geological mapping of the area, borehole drillings, inclinometer placing, in-situ and laboratory tests to determine the physical and mechanical characteristics of the geological materials observed in the landslide area and to detect the failure surface and mechanism of the movement of the landslide material. Therefore, the geological map of the landslide area and geological cross sections has been prepared, boundary of the landslide material have been determined by the help of borehole data and mass movement measurements have been done. Geological and geotechnical properties of the landslide material are presented in this chapter.

4.1. Field Studies

Geological map of the landslide area has been prepared in detail to characterize the geological material observed in the study area, and to delineate the landslide boundary. During this process, the information about lithology has been recorded and transferred onto the topographic map of the study area. This information was the color, structure and boundary of the units. The landslide boundary has been delineated according to the field observations such as tension cracks and movement traces (Figure 4.1 and Figure 4.2). The local geological map and information about the formations were presented in Chapter 2.

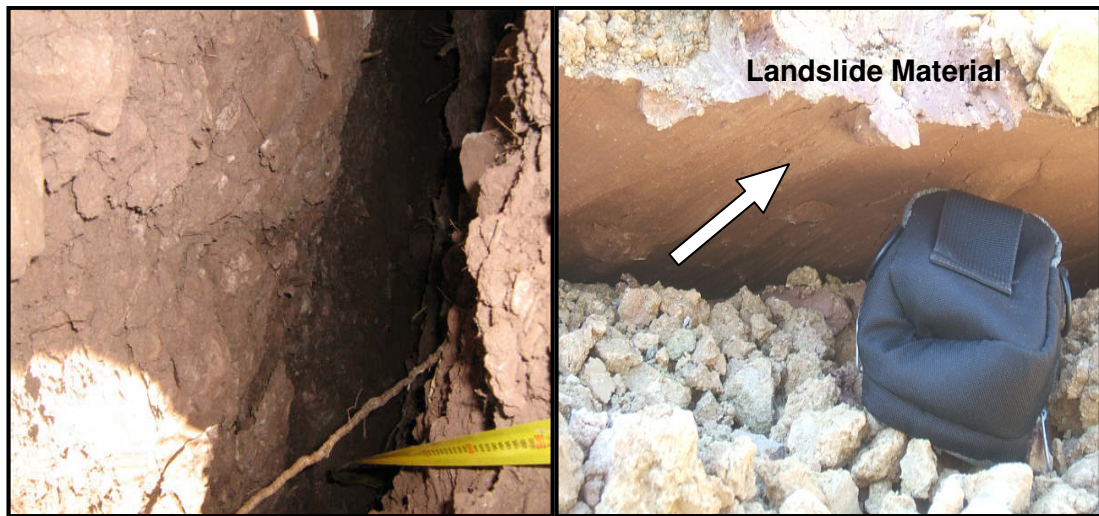


(a)



(b)

Figure 4.1 (a) General view of the landslide area, (b) tension cracks at crown.



(a)

(b)

Figure 4.2 A close view from (a) tension cracks at crown, (b) failure surface at toe.

As it is seen from Figure 4.1b long tension cracks were observed at the crown of the landslide and Figure 4.2a shows the close view of this crown crack which has a 30 to 40 cm wide and 180-240 cm deep. Failure surface have appeared at the toe of the slope and it is seen from Figure 4.2b.

4.1.1. Drilling

There were nine boreholes which have the length varying between 17.0 m and 37.50 m to investigate the slide mechanism of the landslide area (Figure 4.3). Boreholes (248.0 m in total) are drilled by PETRA Engineering and Consulting Company in between 27 October and 3 December 2008 by using Mobile Drill B-53 which is hydraulic machine and equipped with SPT (standard penetration test) automatic hammer. Borehole logs are given in the Appendix A.

Table 4.1 shows the borehole data including coordinates, depth, depth to the ground water and inclinometer pipe length. The coordinate system of the boreholes is European 1950 Transverse Mercator.

Table 4.1 Summary of the borehole data.

Borehole No.	Coordinate			Depth (m)	Groundwater Depth (m)	Inclinometer Casing (m)
	X (Easting)	Y (Northing)	Z (Elevation)			
BH-1	523875.0	4581001.0	948.0	35.5	16.2	18.0
BH-2	523921.0	4581047.0	955.0	27.0	17.4	22.0
BH-3	523865.0	4580945.0	940.0	22.5	14.0	21.7
BH-4	523917.0	4580927.0	931.0	37.0	19.0	32.1
BH-5	523924.0	4580977.0	939.0	33.0	23.0	23.5
BH-6	523944.0	4581028.0	944.5	37.5	27.2	32.0
BH-7	523969.0	4580915.0	921.5	19.5	11.0	16.0
BH-8	523984.0	4580964.0	918.0	19.0	10.3	16.5
BH-9	523998.0	4580998.0	918.0	17.0	6.2	14.5

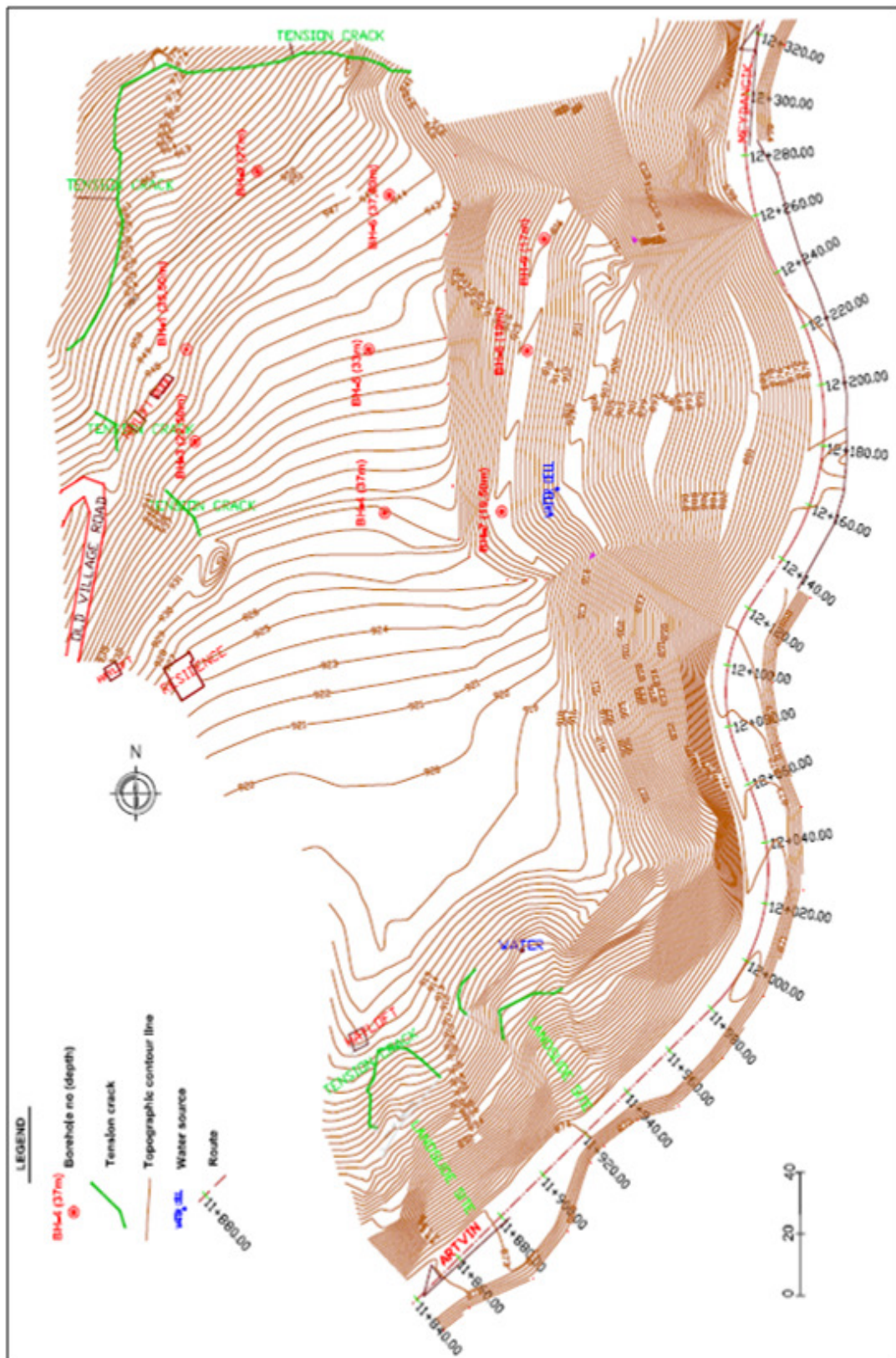


Figure 4.3 Borehole locations for the landslide investigation.

4.1.2. Standard Penetration Test (SPT)

Standard penetration test (SPT) was carried out in all boreholes in soil down to the full depth of boring at approximate 1.50 m intervals. The test was carried out according to ASTM (2000). The energy efficiency of the hammer was estimated as 73% consistent with the energy requirements of an automatic hammer. A number of 109 standard penetration tests were completed at preferred depths. Blow counts for the last 30 cm (SPT-N) vary between 13 and 60 and it generally increases with depth since unit become more compact with depth. Details of the SPT-N variations will be presented in section 4.3. Moreover, rock core photos of the units that are lying under the landslide material are presented in the Appendix B. Soil mechanical tests were performed on the samples obtained from the split barrel sampler of the SPT and the results of the laboratory tests performed by EFOL are given in the Appendix C.

4.1.3. Inclinerometers

Inclinometers are one of the most important field instruments in the modeling a landslide to determine the location of the slip surface (Figure 4.4). Lateral movements below the ground surface can be measured by an inclinometer system. First, a special casing is installed in a borehole (Figure 4.5). The inside of the casing has four longitudinal grooves at the four quadrants and the inclinometer probe has wheels that track along a diametrically opposite pair of grooves. An accelerometer within the probe, aligned in the plane of the wheels, measures the tilt of the probe and casing at any position along its length. By taking successive incremental readings as the probe is pulled up the casing, the in-ground shape of the casing is obtained. If landslide movements occur after the casing has been installed and initially read, the tilt of the casing in the shear zone of the landslide will change. The depth and amount of shear movement is obtained by subtracting the initial set of tilt readings from the subsequent readings. Inclinerometers provide information on the depth of landslide movements, thickness of the shear zone, amount of movements, rate of movements and direction of movements (Cornforth, 2005).

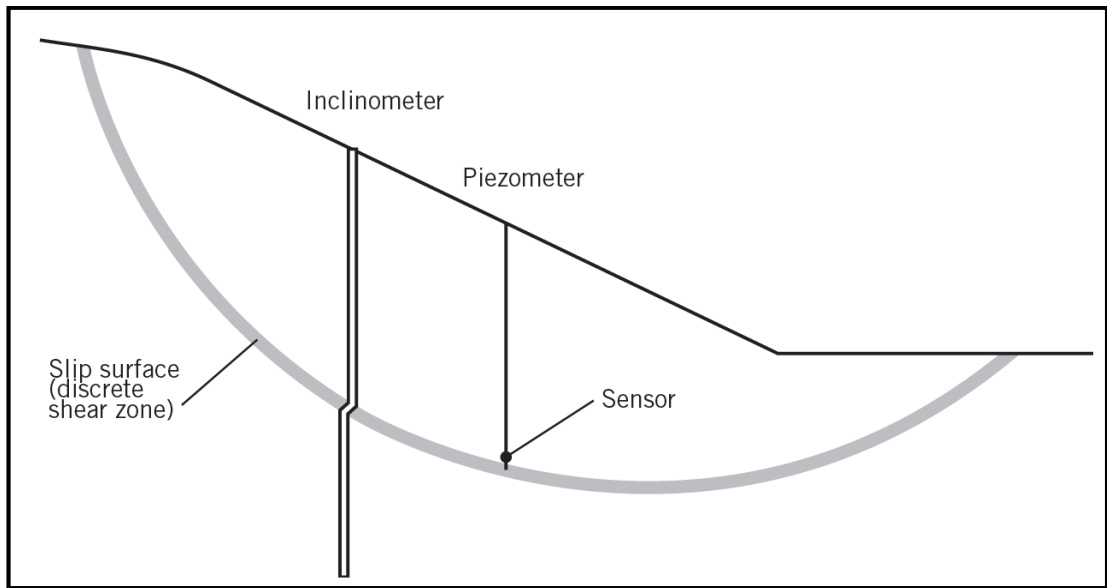


Figure 4.4 Monitoring landslides with inclinometers and piezometers (Cornforth, 2005).

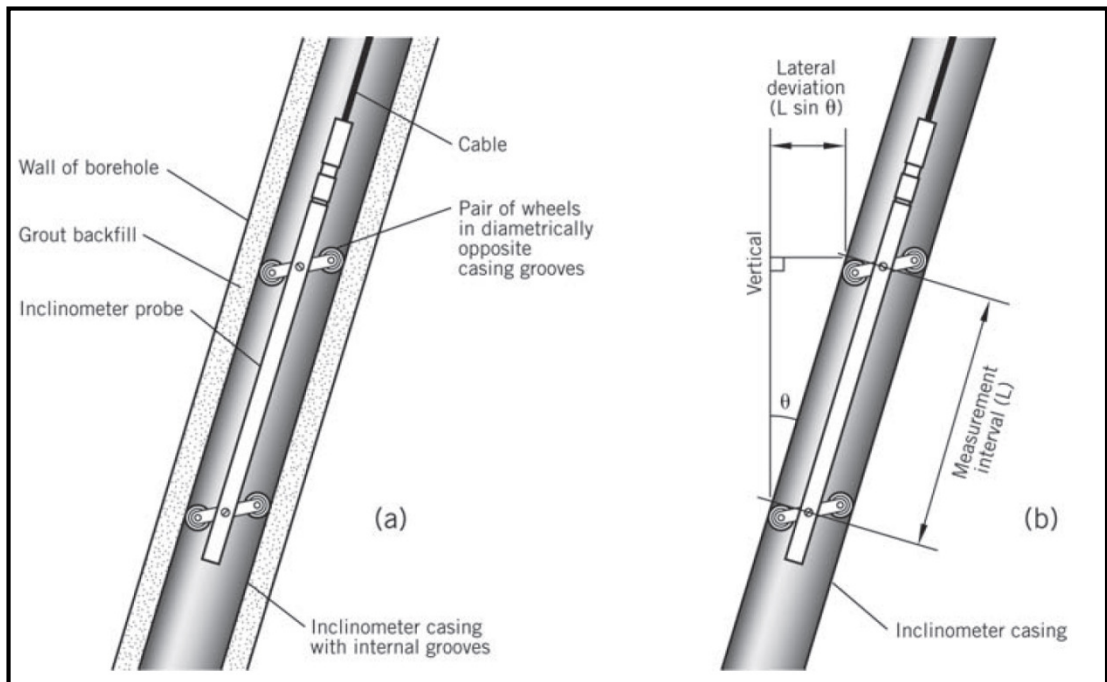


Figure 4.5 Inclinometer system: (a) probe and casing within borehole (b) measurement of tilt (Cornforth, 2005).

The landslide at the Artvin-Şavşat Junction - Meydancık Provincial Road Km: 12+200 was investigated by nine boreholes (BH-1 to BH-9) equipped with inclinometers which have the model of RST Digital MEMS Inclinometer system (Figure 4.3). Movement direction of the slide has been obtained by the help of movement vectors derived from inclinometer results which obtained at every 0.5 m interval (Figure 4.6). Inclinometer measurements revealed some slip surfaces at depths between 3.0 and 27 meters. The inclinometer measurements were reported and plotted as depth vs. cumulative displacement and depth vs. incremental displacement graphs that are presented in Appendix D. The results of the inclinometer measurements are summarized in Table 4.2. It can be concluded that average rate of the slip movement is 0.6 mm/day for the time interval of the site investigation.

Table 4.2 Summary of the inclinometer results.

Borehole No.	Depth (m)	Inclinometer Casing (m)	Slip Surface (m)	Measurement Duration (days)	Displacement Amount (mm)	Rate (mm/day)
BH-1	35,5	18,0	16,0	160,0	214,2	1,34
BH-2	27,0	22,0	17,0	154,0	81,1	0,53
BH-3	22,5	21,7	3,0	156,0	57,5	0,37
BH-4	37,0	32,1	18,5	167,0	180,5	1,08
BH-5	33,0	23,5	22,5	171,0	17,5	0,10
BH-6	37,5	32,0	27,0	160,0	76,8	0,48
BH-7	19,5	16,0	11,0	146,0	38,9	0,27
BH-8	19,0	16,5	10,0	143,0	96,5	0,67
BH-9	17,0	14,5	6,0	148,0	86,1	0,58

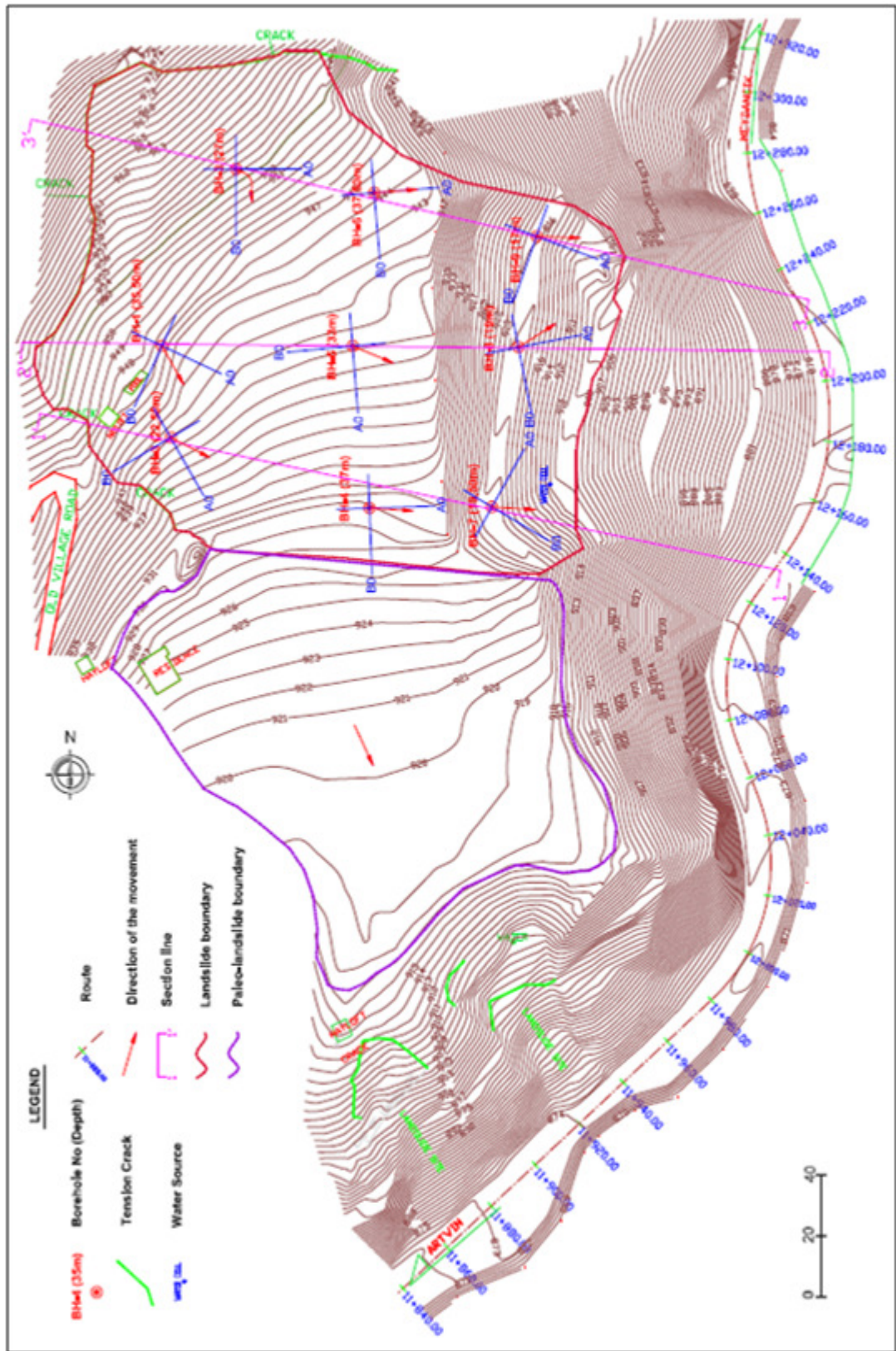


Figure 4.6 Movement direction of the landslide and section lines.

4.2. Laboratory Tests

Soil laboratory tests were conducted on undisturbed samples taken by in-situ test (SPT) to determine the physical and index properties of the geological material, namely; natural unit weight, moisture content, sieve and atterberg tests. Laboratory test results are given in Appendix C. However, shear strength parameters of landslide material was obtained by the aid of adoption of the natural modeling and back analysis of the active slides.

4.3. Assessment of Field Studies and Laboratory Tests

BH-1, BH-2 and BH-3 at the upper part of the landslide, BH-4, BH-5 and BH-6 at the middle part of the landslide and BH-8 and BH-9 near the toe of the landslide were drilled. In the study area slip surface intersects lower parts of the colluvium which has a various thickness between 3.0 and 27.0 m and is composed of gravelly sandy clay, clayey gravelly sand, clayey gravel, and clayey gravelly block. Limestone that is hard, moderately strong-moderately weak, moderately weathered, highly weathered locally, and basalt that is moderately weak are located under this colluvium unit. According to the inclinometer readings and field investigations it is concluded that the rupture surface is placed between the lower parts of the colluvium and bedrock.

Landslide and paleo-landslide boundaries have been defined by field observation such as tension cracks and interpretation of the topographical contours (Figure 4.7). When a slope fails, it is usually not possible to pinpoint a single cause that acted alone and resulted in instability (Duncan and Wright, 2005). The landslide has been probably triggered due to weak geomechanical strength, permeability of the landslide material and slope geometry (PETRA, 2009). Landslide has a complex type of movement which is combination of rotational and translational movements (Figure 4.8). Landslide failure mechanism will be explained in detail in Chapter 5.

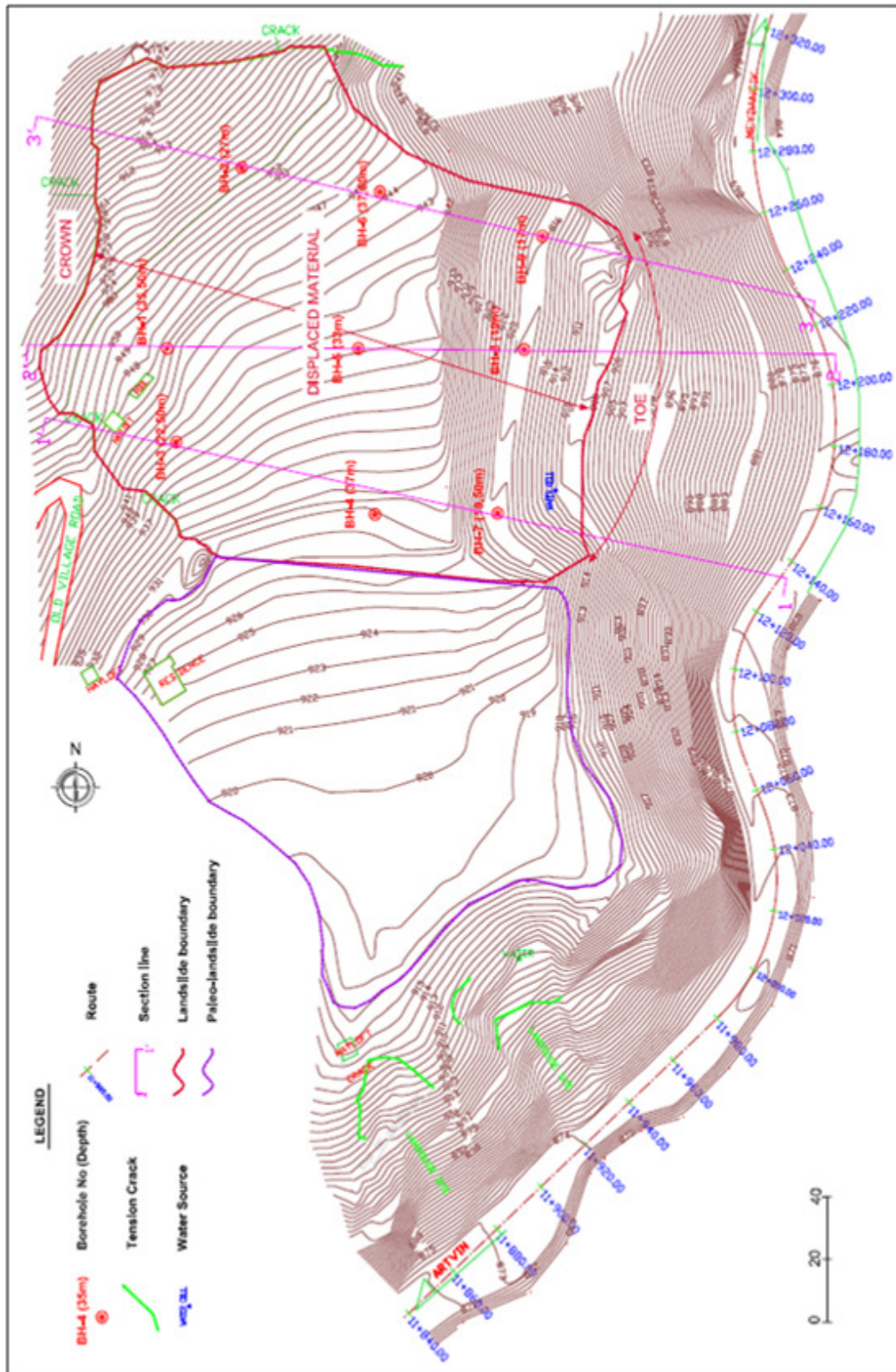


Figure 4.7 Landslide boundary.

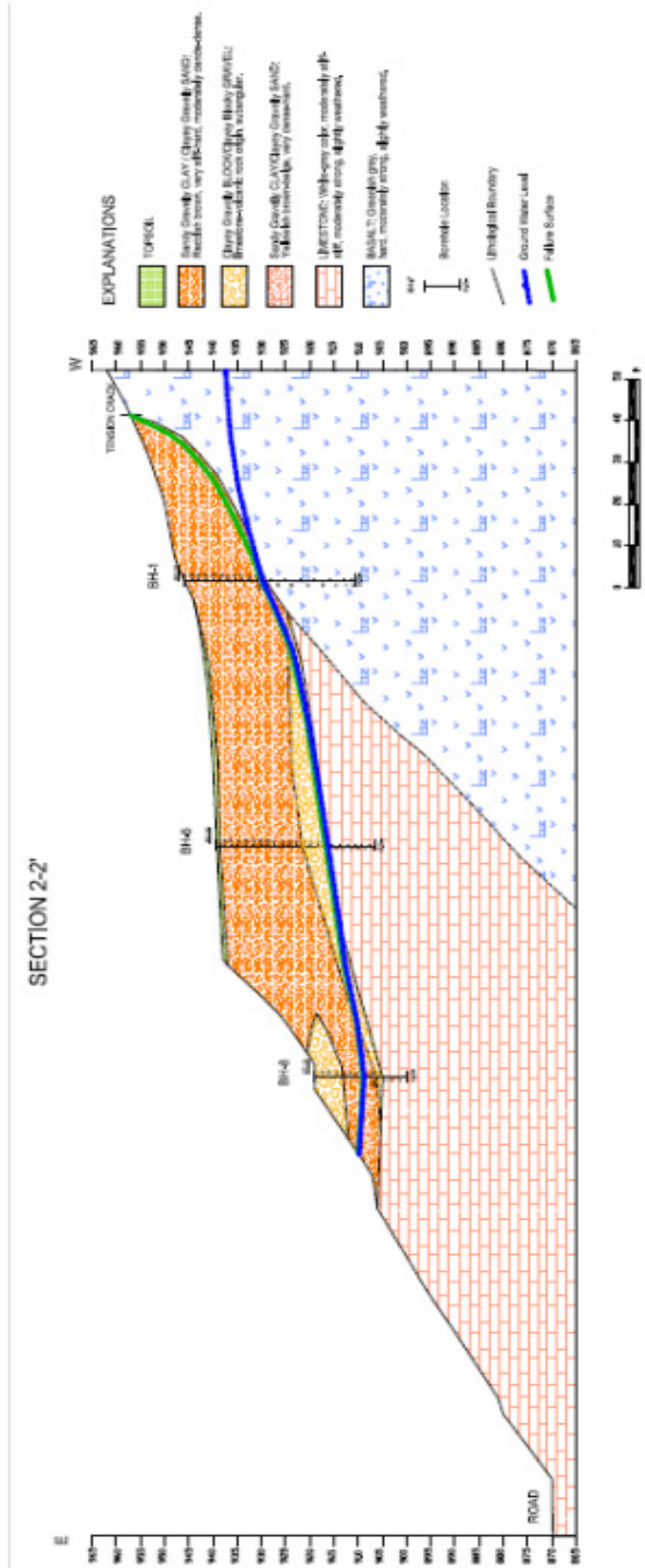


Figure 4.8 Cross-section of the landslide along section 2-2'

The ranges of the laboratory test results of the samples obtained from the SPT conducted within the landslide material are given in Table 4.3. Soil classification has verified the field observations of the colluvium which is a mixture of the coarse and fine soil particles.

Table 4.3 Ranges of the laboratory test results and SPT-N in landslide material.

Soil class (USCS)	CL, SC, GC
SPT (N)	N \approx 13 - R
Water content (W_n)	w _n (%) \approx 8 - 23
Liquid limit (LL)	LL (%) \approx 25 - 47
Plastic Limit (PL)	PL (%) \approx 14 - 17
Plasticity Index (PI)	PI (%) \approx 11 - 30
Fine Content	F (%) \approx 48 - 65

Since there is a rock unit under the landslide material, rock core has been taken and evaluated in the sense of rock quality. Rock quality is based indirectly on the number of fractures and amount of softening or alteration in the rock mass as observed in the rock cores from a drill hole. The range of total core recovery (TCR), rock quality designation (RQD) of the limestone and basalt are summarized in Table 4.4.

Table 4.4 Range of total core recovery (TCR) and rock quality designation (RQD) of rocks present under the landslide material.

Total Core Recovery (TCR)	7% \leq TCR \leq 100%
Rock Quality Designation (RQD)	0% \leq RQD \leq 73%

SPT N values vs. depth graph for the landslide material is shown in Figure 4.9.

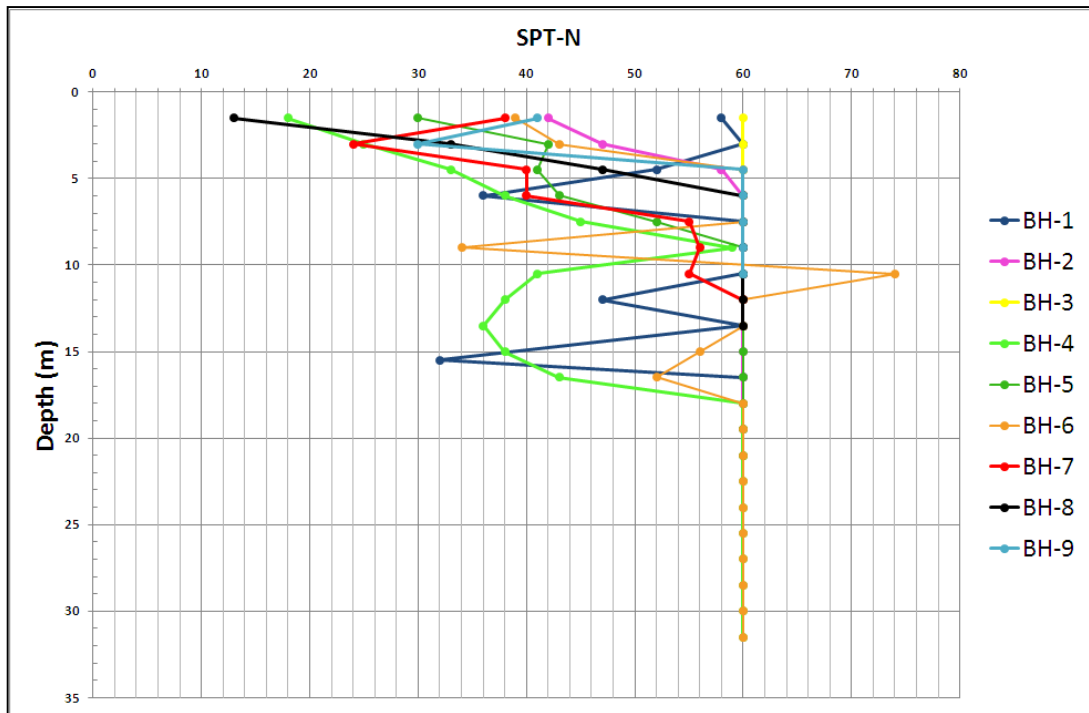


Figure 4.9 SPT N values vs. depth graph for the landslide material.

It can be seen from Figure 4.9, SPT-N values are generally increasing with depth, since there is more dense soil at deeper part of the landslide material. However, some part of the landslide material is gravelly and blocky at the surface then it has been taken high SPT-N values. Moreover, there is a relationship between the failure surface and the SPT-N values, and it can be concluded that SPT-N values decreases around the depth of failure surface.

Liquid limit of the samples taken from boreholes have a number of values. Liquid limit values vary between 24 and 48. LL values vs. depth graph for the landslide material is shown in Figure 4.10. There is no clear relationship between the depth of sliding surface and the liquid limit values.

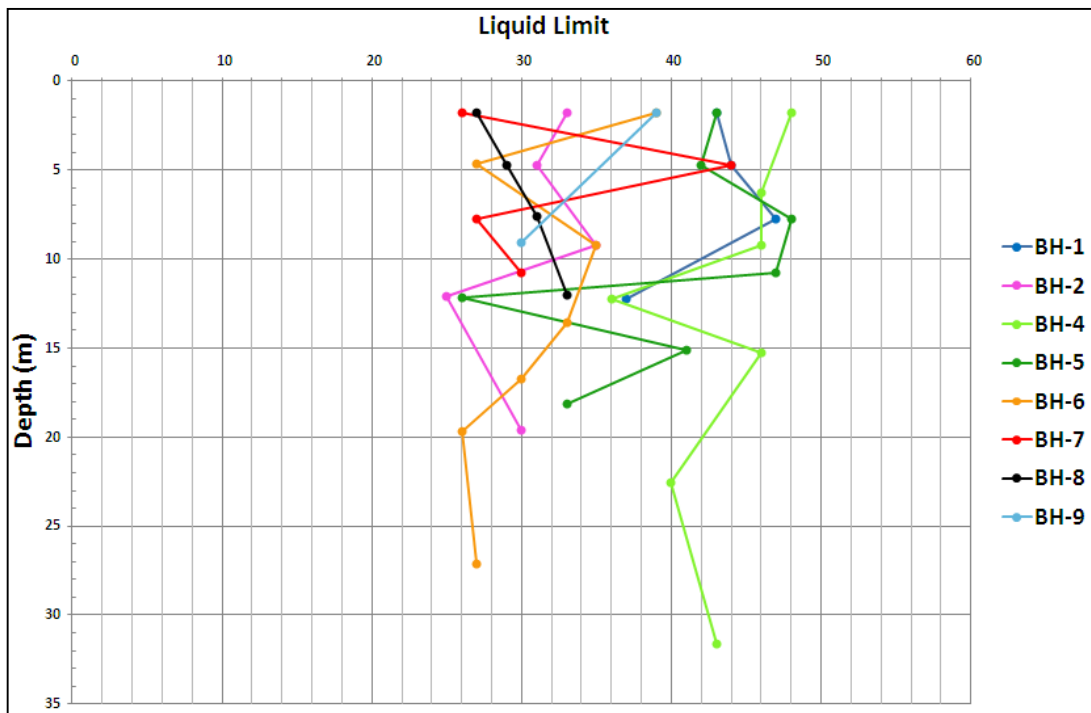


Figure 4.10 LL values vs. depth graph for the landslide material.

Particle size distribution curve for the sample soil specimen was presented in Figure 4.11. According to this curve, it is concluded that there are 43% to 56% of gravel, 22% to 26% sand and 17% clay size particles in soil specimens taken from the study area.

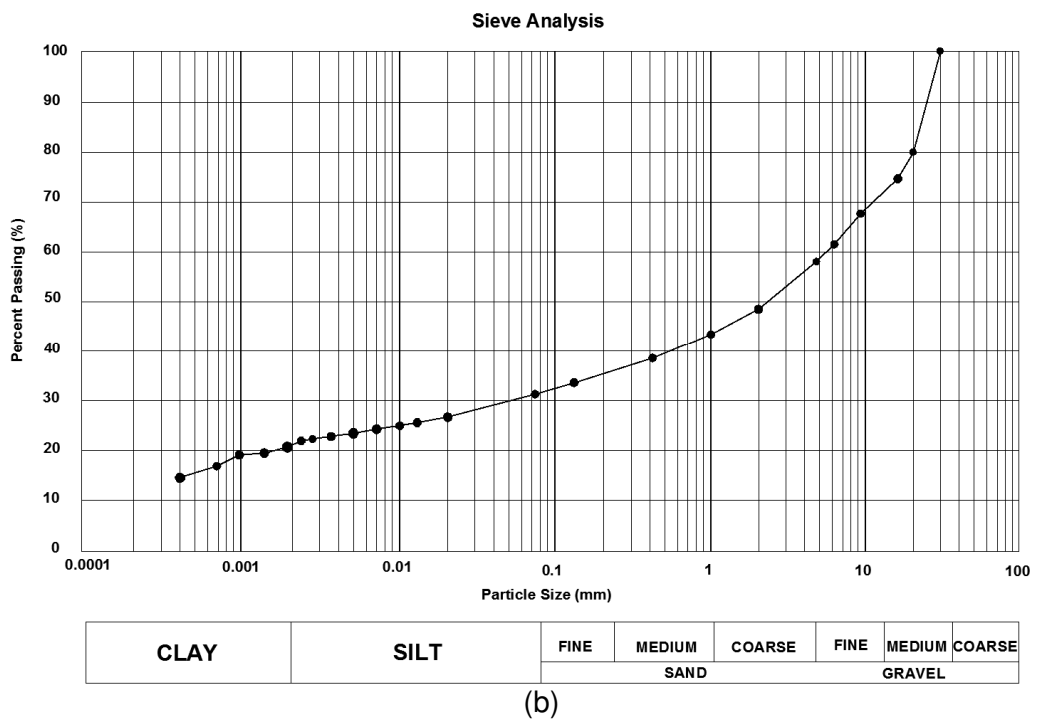
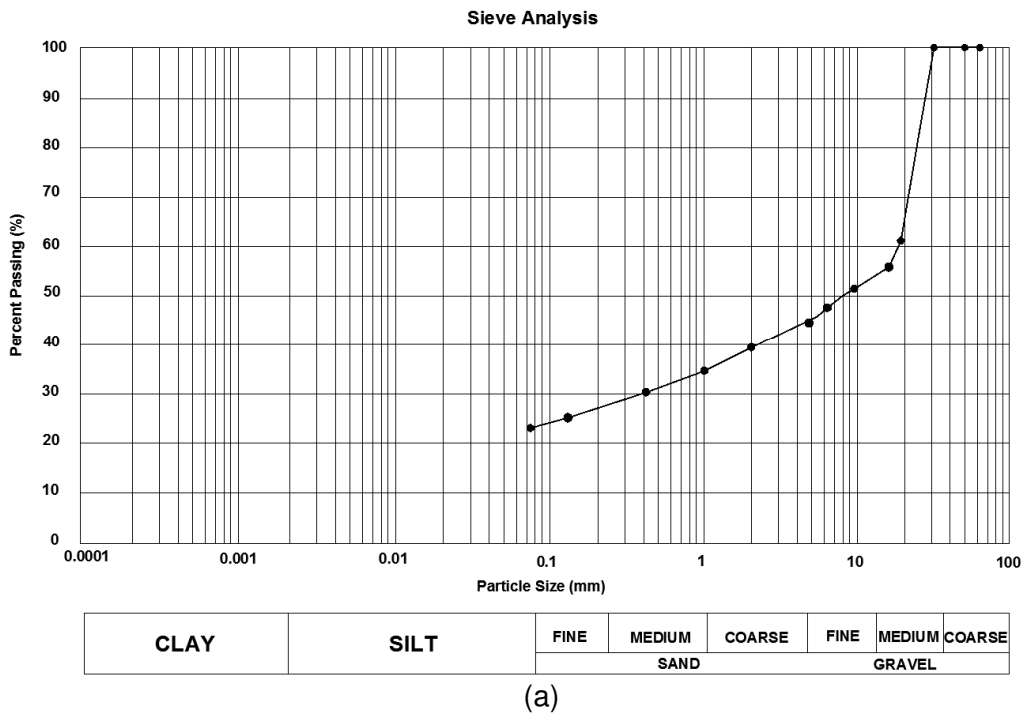


Figure 4.11 Particle size distribution of (a) SPT-15 sample taken from BH-4 (b) SPT-6 sample taken from BH-2.

Soil classification of the fine landslide material was determined by using plasticity chart which is offered for using the Atterberg limits (Figure 4.12). It is concluded that the fine soil located on the study area is clay with low plasticity.

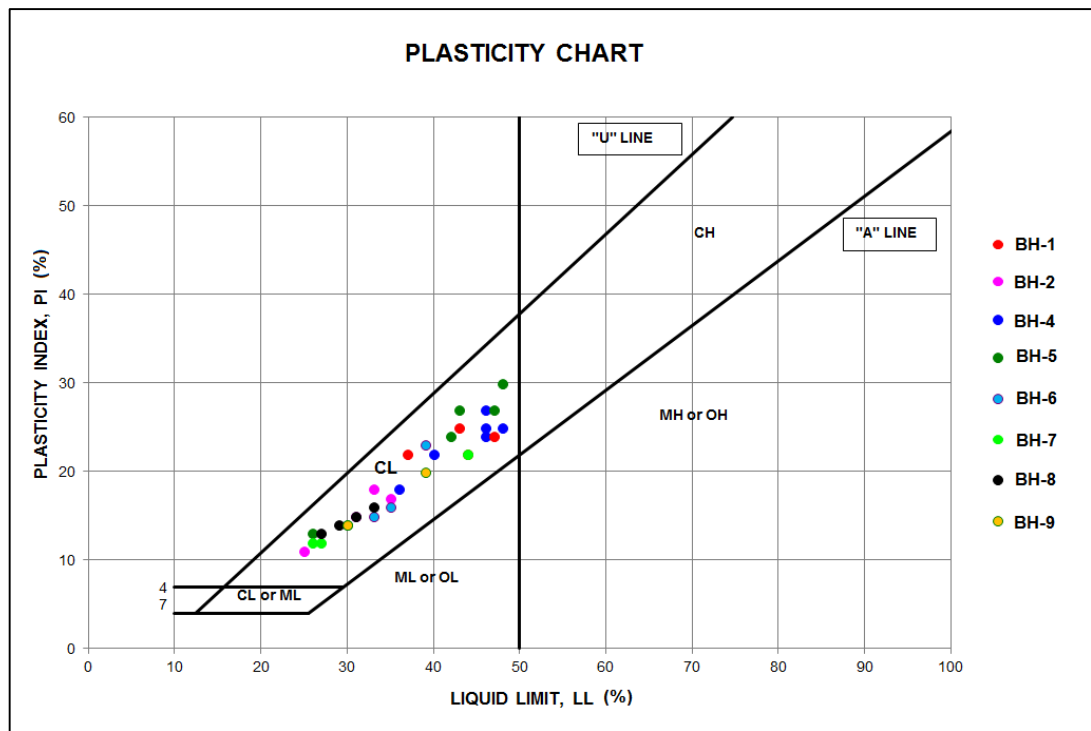


Figure 4.12 Plasticity chart for the landslide material.

Plasticity Index values vary between 12 and 30. PI values vs. depth graph for the landslide material is shown in Figure 4.13.

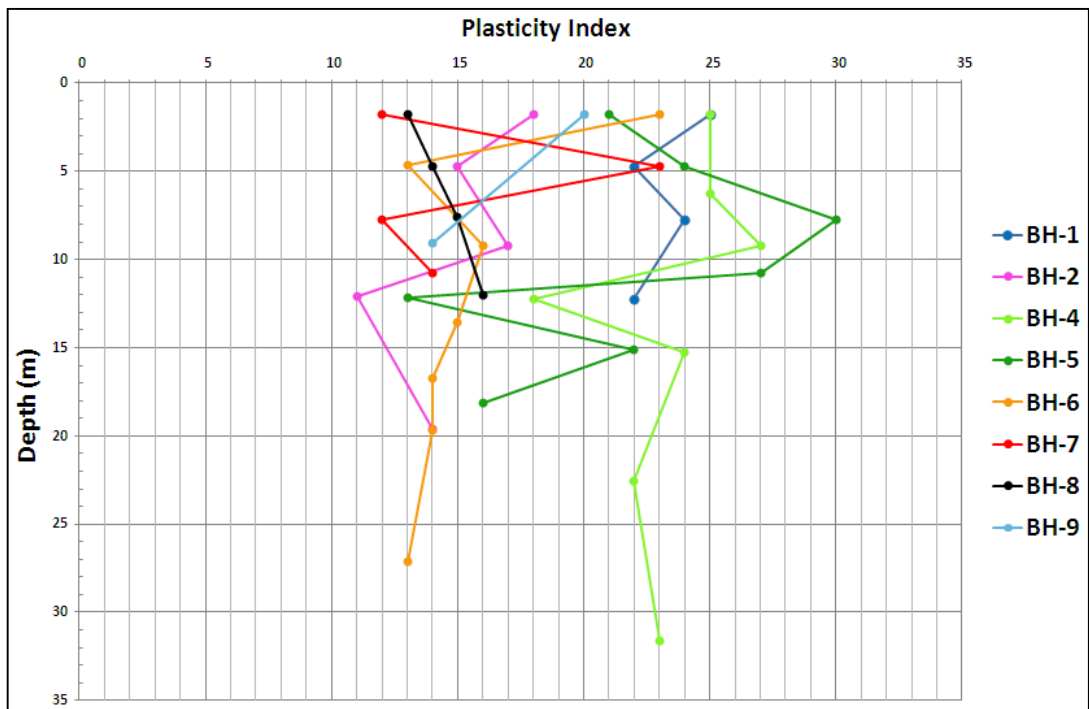


Figure 4.13 PI values vs. depth graph for the landslide material.

Range of the Liquid Limit and Plasticity Index is consistent with the range of coarse and fine soil with high and low plasticity. There is no clear relationship between the depth of sliding surface and the PI values.

Shear strength parameters along the failure surface decreases due to high water content. Thereafter, it is considered that the water content, liquid limit and plastic limit values should be shown on the same graph to see the state of soil, in other words; whether the water content is close to liquid limit or plastic limit.

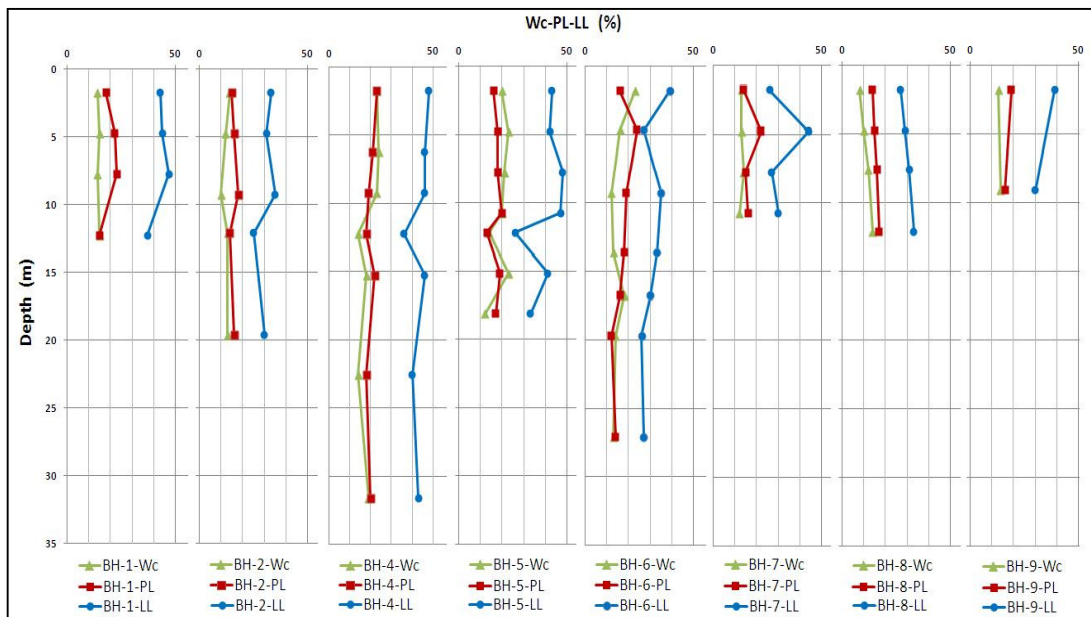


Figure 4.14 Wc-PL-LL values vs. depth graph for the landslide material

As it is seen from Figure 4.14, water content of the laboratory soil samples is lower than the liquid limit values and close to plastic limit values. The reason of this condition is that the sample has lost its water content during transportation to the laboratory or the groundwater table is low when taking the samples.

Borehole penetrates the rock at approximately 11th meter and rock core has been taken after that depth, then some rock parameters such as RQD has been determined.

RQD value vs. depth graph for the basalt and limestone under the landslide material is shown in Figure 4.15.

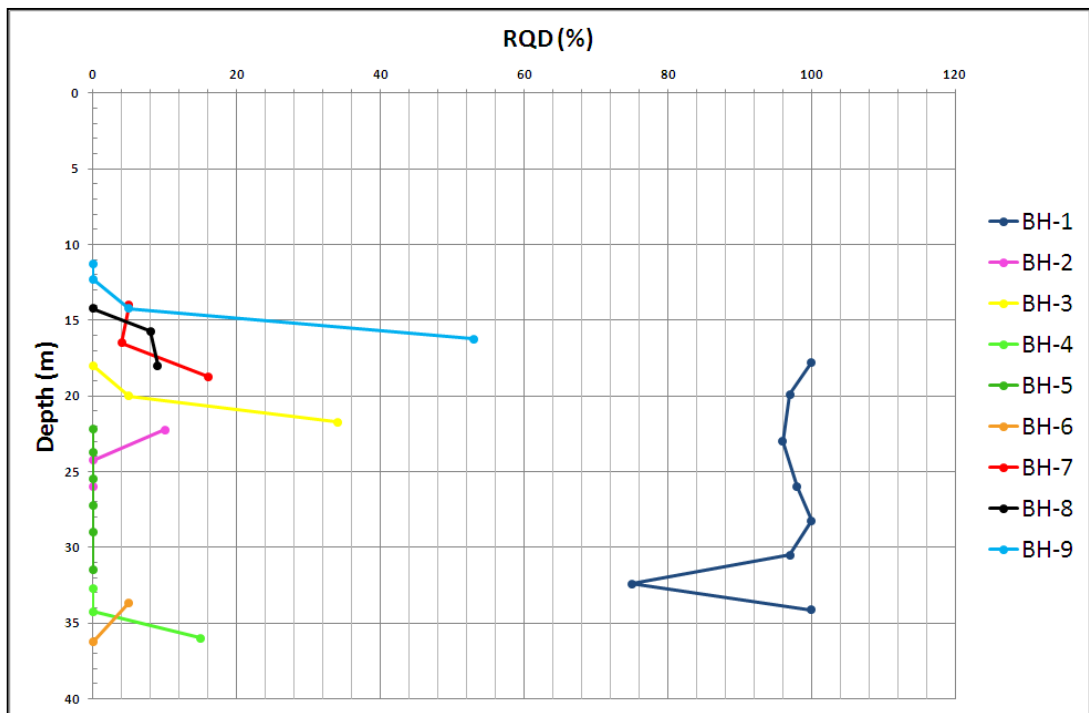


Figure 4.15 RQD value vs. depth graph for the basalt and limestone.

It can be seen from Figure 4.14 the rock materials existing in all borehole except BH-1 have a low rock mass quality. It means that they are highly fractured.

CHAPTER 5

GEOTECHNICAL ASSESSMENT OF THE LANDSLIDE

The landslide at the Artvin-Şavşat Junction - Meydancık Provincial Road Km: 12+200 occurred at the left side of the road platform under construction in April 2008 as a result of mass movement accelerating through the valley bottom.

5.1. Slope Failure Mechanism

Geological structure developed as a result of observations and research in the study area, identified marks of paleo-landslides (Figure 5.1) and the inclinometer measurement results include important information on history and active landslide generation mechanism. It is considered that paleo-landslides developed towards valley basin has formed as a result of effects such as topographic slope, seismicity, regional climate conditions etc., and movements have triggered each other by consecutively eliminating toe support of onward units. Even though paleo-landslides seems to have damped by taking their current form in time, many factors such as geomechanical strength parameters of the colluvium on slope surface, slope geometry, lithology, permeability, weathering and alteration degree, abrupt pore water pressure etc. form an environment highly suitable for generation of additional movement via deterioration of current critical equilibrium.

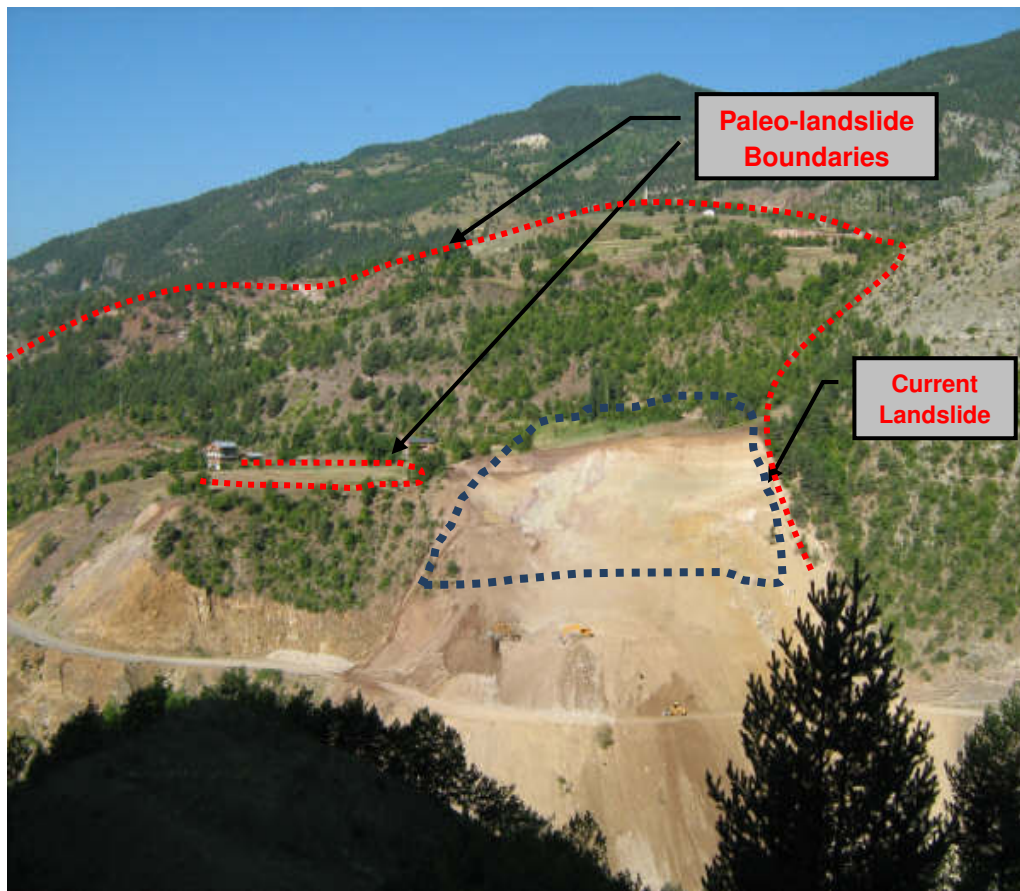


Figure 5.1 Paleo-landslide boundary observed in the study area.

Investigations on the landslide area indicate that permeable unit observed at the upper levels and generally termed as colluvium overlies limestone and basalt units. Geological units identified in the region are recharged by the surface (runoff) water depending on precipitation regime. Discharge of surface runoff from slopes and most of the groundwater principally to the landslide area both increase the slope instability that is suitable for development within the colluvium with approximately 10 to 15° angles and also forms an environment that is highly suitable for sliding at the bedrock-colluvium contact.

As can be seen from idealized geological profiles (Figures 5.2-5.4) prepared in the light of exploration boreholes and inclinometer measurements, the failure surface is located between the colluvium (20-30 m thick) and the bedrock. It is estimated that the movements are developed as a result of violating the slope stability of the paleo-

landslides with excavation of the toe region during construction activities and also due to percolation of surface water in to the colluvium unit. It is considered that the investigated area has developed as a result of triggering of final phase of consecutive movements which occur in time and which can be defined as paleo-landslide. Artvin-Şavşat Junction - Meydancık provincial road is not affected by paleo-landslide, however the current landslide adversely affected road (PETRA, 2009).

According to the geological and geotechnical data, the landslide has a length of approximately 197 m, a maximum depth of approximately 32 m and an elevation difference between the crown and toe of landslide is approximately 51 m. The mass thickness of the existing landslide material was determined between approximately 1 – 32 m along the slip surface and its mean velocity of the movement along the slip surface was measured to range from 0.02 to 1.27 mm/day at the time of measurement.

5.2. Shear Strength Characterization

The next step after the engineering geological field study, back analysis has been conducted by the help of SLIDE version 6.0 software (Rocscience, 2012) to determine the shear strength parameters of the landslide material.

5.2.1. Back Analysis

Back analysis is probably the most valuable tool available for landslide studies. It provides confidence in ensuring the reliability of remedial work and allows the practitioner to use less conservative factors of safety for landslides than for slope stability calculations where no failure has occurred (Cornforth, 2004).

The simplest back-analysis is one where average shear strength is calculated from the known slope geometry and soil unit weights. This is accomplished by assuming a friction angle of zero and calculating a value of cohesion that will produce a factor of safety of 1. This practice of calculating an average strength expressed as cohesion can, however, lead to erroneous representations of shear strength and potentially unfavorable consequences (Cooper, 1984).

The most reliable way to obtain a statistically mean value of shear strength parameters of a non-homogeneous material in an extended slope is by back-calculation. The approach is based on the following assumptions: (1) the geometry of the slope before failure is known, (2) the mechanism of land movement is known, (3) a condition of static equilibrium at the point of failure (limit equilibrium) exists at the time of failure, (4) failure of the slope occurs instantaneously when normal and shear stresses equal the tensile and shear strength of the material along the whole surface of rupture. Homogeneity and isotropy are not necessary conditions. What is obtained by back-calculation is a weighed mean value of the strength parameters along the failure surface (Sancio, 1981).

5.2.2. Shear Strength Characterization Considered In Stability of Slopes by Back Analysis

Limit equilibrium back analyses were performed to obtain the residual shear strength parameters of the landslide material. The back analysis (Sancio 1981; Chandler 1977) was applied on three cross sections, which are nearly parallel to the direction of movement, using the Janbu's corrected method with the aid of SLIDE version 6.0 software (Rocscience, 2012). The reason for using the Janbu's corrected method is that it is generally used for non-circular failure surface and gives better results. For the analysis, variation of the shear strength parameters (c' and ϕ') of the landslide material, satisfying a factor of safety (FS) of 1, which corresponds to the limit equilibrium condition, was determined for different shear strength pairs. The location and direction of the cross sections used in the analysis were given in Chapter 4. The cross sections are given in Figures 5.2 - Figure 5.4.

Slip surfaces and groundwater levels were well determined for the models in back analyses. The locations of the failure surface belonging to three cross sections were found from the inclinometer interpretations. Cross sections consisted from lithologies from bottom to the top, namely the Çağlayan formation (basalt), Ağıllar formation (limestone), and the landslide material (colluvium) that were assigned in the back analyses.

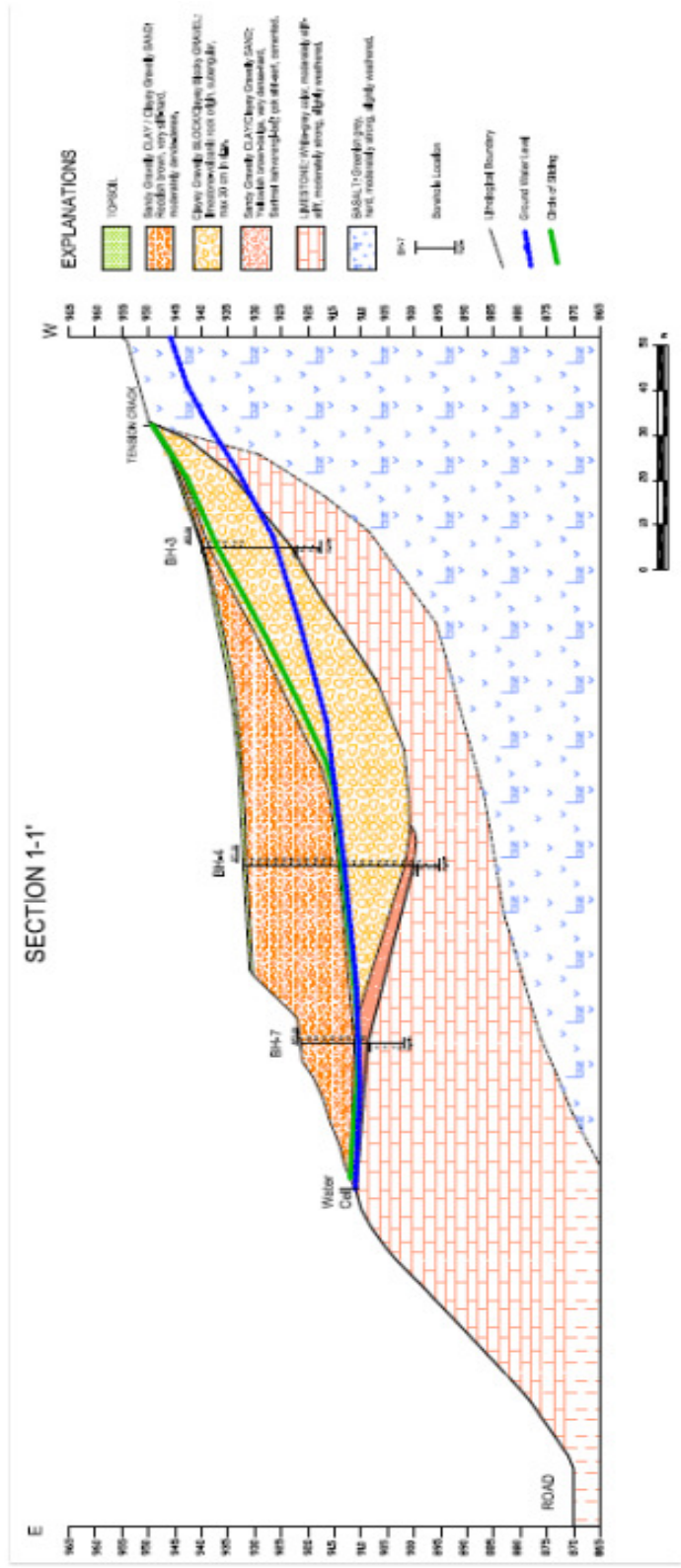


Figure 5.2 Cross-section of landslide along section line 1-1'.

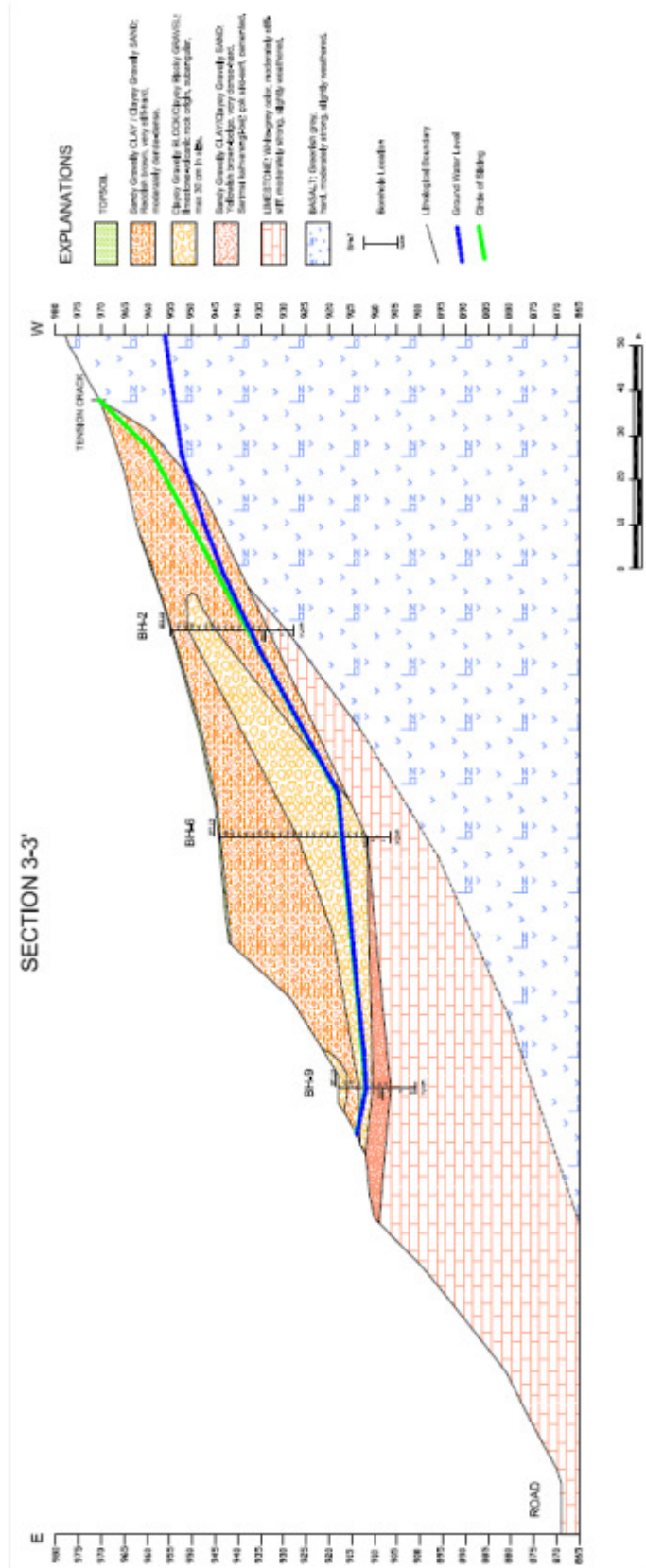


Figure 5.4 Cross-section of landslide along section line 3-3'.

The rock mass strength parameters of the Çağlayan and Ağıllar formations were determined by using the RocLab version 1.0 software (Rocscience, 2006) which uses the generalized Hoek- Brown failure criterion. In addition to the Hoek-Brown failure criterion using the other parameters (m_b , s and a), RocLab always calculates equivalent Mohr- Coulomb parameters (cohesion and friction angle) for the rock mass (Rocscience, 2006). Figure 5.5 and Figure 5.6 show the graphical relationship between the normal and shear stresses of Çağlayan and Ağıllar formations as calculated by RocLab.

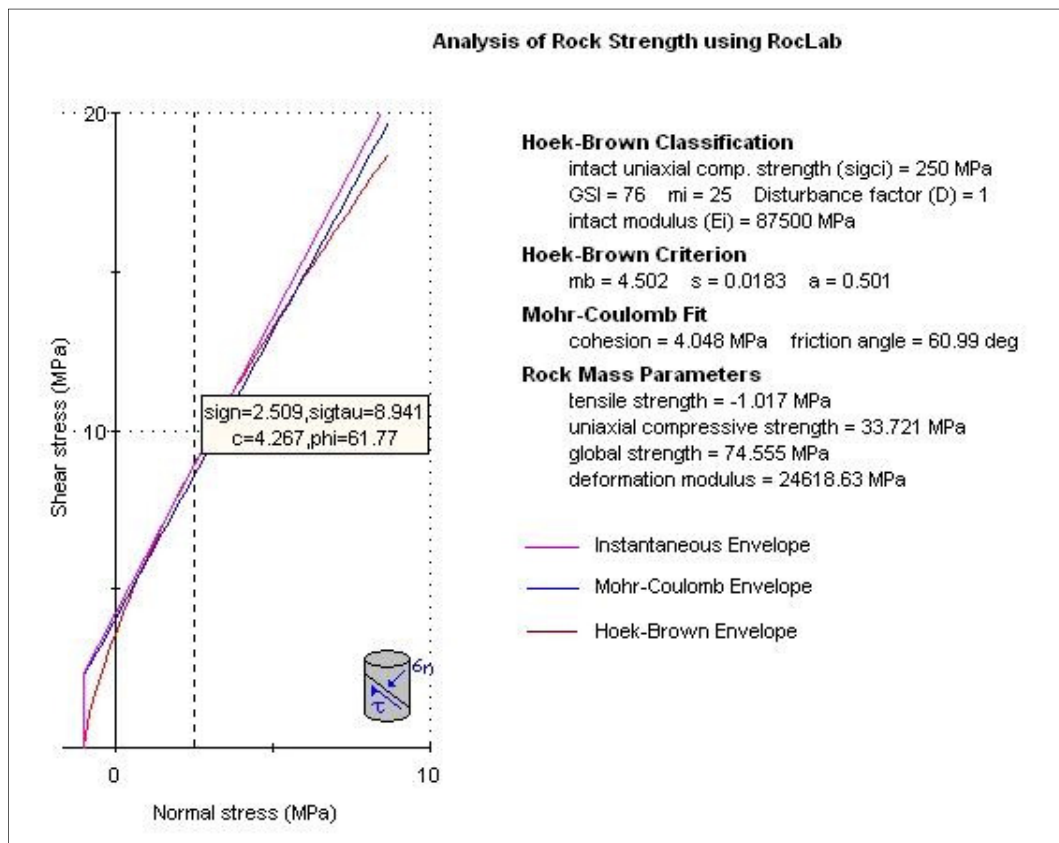


Figure 5.5 Normal stress vs. shear stress of the Çağlayan formation as calculated by RocLab 1.0.

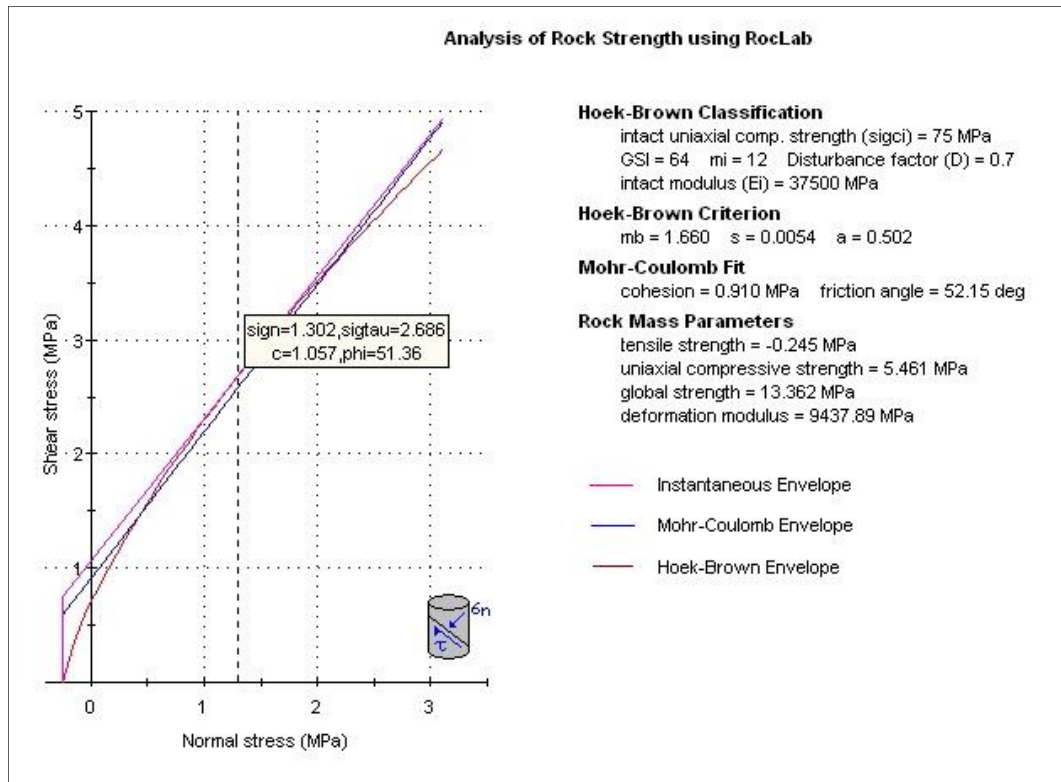


Figure 5.6 Normal stress vs. shear stress of the Ağıllar formation as calculated by RocLab 1.0.

The shear strength parameters of the Çağlayan and Ağıllar formations are $c = 17.8$ MPa - $\phi = 38^\circ$ and $c = 3.4$ MPa - $\phi = 30^\circ$, respectively.

The residual strength parameters of the landslide material were obtained from back analysis by adjusting c' and ϕ' parameters until the factor of safety is unity (FS=1.0) which is considered as a requirement for failure in a limit equilibrium analytical model. Back analysis results showing the c' - ϕ' pairs of limit equilibrium condition in the form of c' - ϕ' curves are given in Figure 5.7.

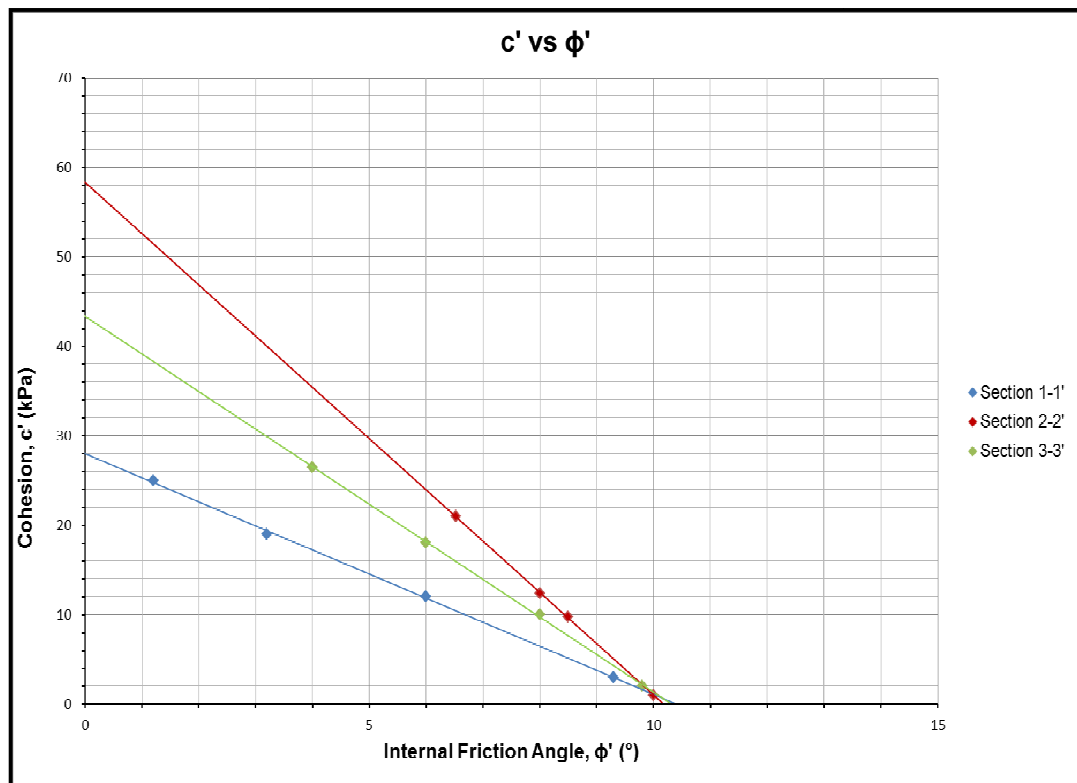


Figure 5.7 Back analysis results showing the c' - ϕ' pairs.

It can be seen from Figure 5.8, all three c' - ϕ' curves intersect at nearly one point. Soil reached the residual state under large displacement, then residual cohesion decreases and can be taken as zero (Craig, 2004). Therefore, landslide model has residual shear strength parameters of $c' = 0$ kPa due to cohesionless nature of the colluvium, $\phi' = 10^\circ$ to use landslide design.

The results of the back analysis can be checked by using the empirical relations existed in the literature (Figure 5.8 and Figure 5.9). The effective normal stress due to landslide material is about 400 kPa and the average plasticity index (I_P) of landslide material is 19 %. Then residual secant friction angle is 17 degrees according to Mesri and Shahien (2003). This value does not confirm the back analysis result, most probably because, the data used to get this empirical relation come from the case histories of slope failures in soft clays to stiff clays and clay shales.

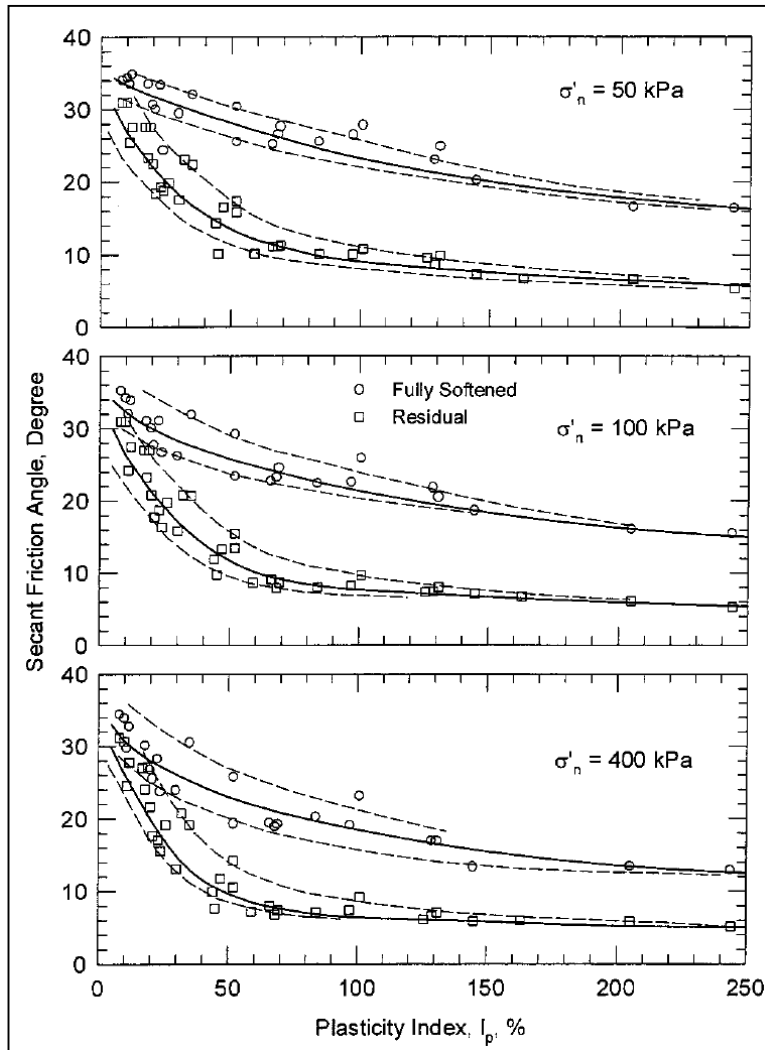


Figure 5.8 Empirical information on fully softened strength and residual strength (data from Stark and Eid 1994; Eid 1996; and Stark and Eid 1997) (Mesri and Shahien, 2003).

The average liquid limit and clay size fraction of the landslide material is 36 % and 39 %, respectively. Then secant residual friction angle is 20 degrees according to Stark et. al. (2005) for overconsolidated clays (Figure 5.9). However, the landslide material studied in this thesis is colluvium and it can be deduced that the shear strength parameters obtained from the back analysis is preferred in this study.

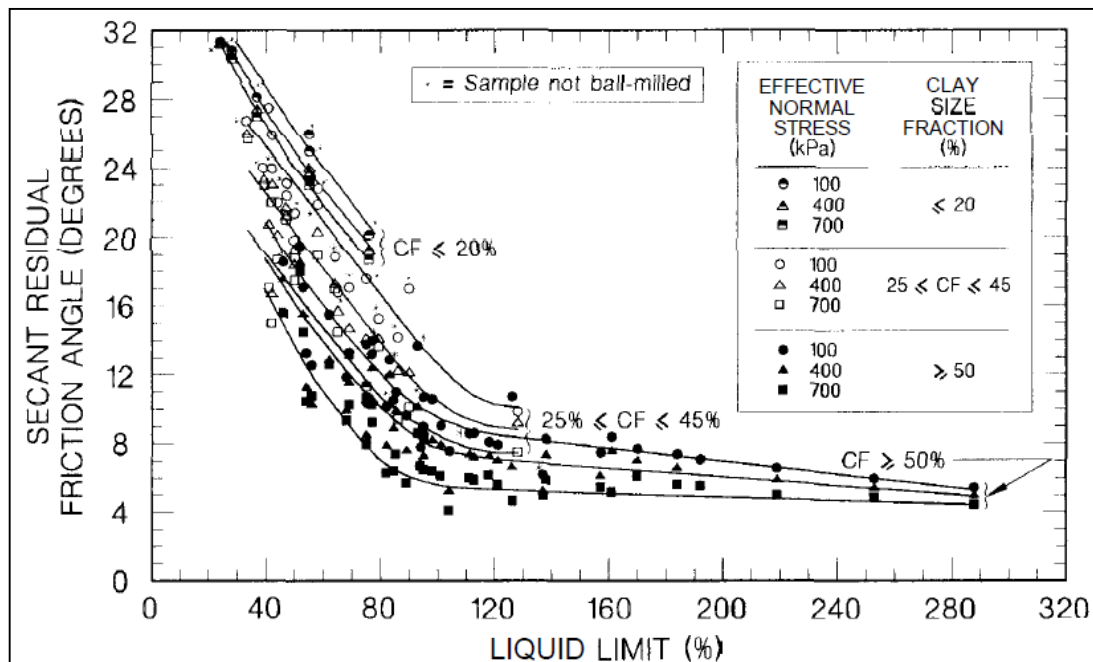


Figure 5.9 Secant residual friction angle relationships with liquid limit, clay-size fraction, and effective normal stress (Stark et. al., 2005).

5.3. Selection of the Landslide Model

The most appropriate cross section that represents the landslide area was chosen in order to model the landslide and to find the most suitable remediation technique. Cross section 2-2' was preferred for the next step in slope design, because the most extensive landslide mass, the longest slip surface and the highest number (3) of inclinometer measurements existed in this cross section. The landslide was modeled by applying limit equilibrium and finite element method analysis.

After the selection of the model, the back analysis results were applied to this model to determine factor of safety on the time of failure by using both limit equilibrium and finite element method analysis.

The groundwater level in cross section 2-2' in Figure 5.4, It was determined according to field studies and borehole data. The resulting pore water pressure distribution was directly linked into the slope stability analysis in order to perform a long term slope stability analysis. The geotechnical material parameters used in the limit equilibrium and finite element method analysis are given in Table 5.1.

Table 5.1 Material parameters used in limit equilibrium and finite element method analysis.

Material	Strength Type	Material Type	Elastic Type	Unit Weight (kN/m ³)	Cohesion, c' (kPa)	Internal Friction Angle, ϕ' (°)	Young's Modulus (MPa)	Poisson's Ratio	Tensile Strength (kPa)
Colluvium	Mohr-Coulomb	Plastic	Isotropic	18	0	10	1.26E+04 (Hunt, 1986)	0,24 (Hunt, 1986)	0
Ağllar Formation	Generalized Hoek-Brown	Elastic	Isotropic	26 (Hoek&Bray, 1977)	1057	51,4	9,40E+03	0,22 (Franklin et al., 1989)	2450
Çağlayan Formation	Generalized Hoek-Brown	Elastic	Isotropic	28,5 (Hoek&Bray, 1977)	4267	61,8	2,46E+04	0,35 (Franklin et al., 1989)	1017

Techniques for applying the Finite Element Method to slope stability analysis were mostly based on an approach that flows naturally from the definition of slope factor of safety, and is now commonly referred to as the Shear Strength Reduction (SSR) technique. By definition, the factor of safety of a slope is the “ratio of actual soil shear strength to the minimum shear strength required to prevent failure,” or the factor by which soil shear strength must be reduced to bring a slope to the verge of failure. In the SSR finite element technique elasto-plastic strength is assumed for slope materials. The material shear strengths are progressively reduced until collapse occurs (Rocscience, 2011).

Firstly, mesh was discretized with 150 numbers of six noded triangles type mesh elements and vertical rollers are used on the left and the right side of the geometry boundaries and full fixed at the bottoms of the geometry. Undeformed meshes of the slope are presented in Figure 5.10. It is clear from Figures 5.11 and 5.12 that the slope is sliding along the “toe” of the slope.

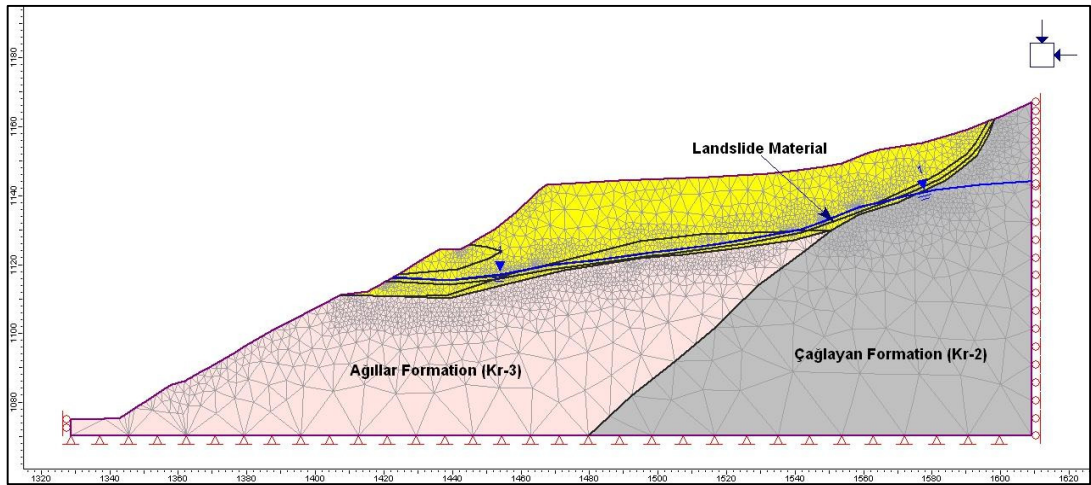


Figure 5.10 Generated mesh of the landslide model.

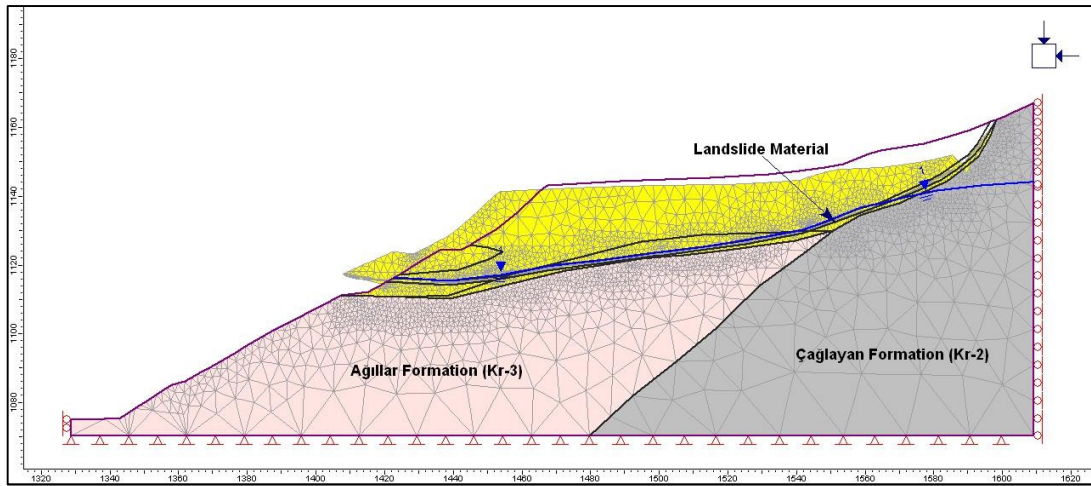


Figure 5.11 Deformed mesh of the landslide model.

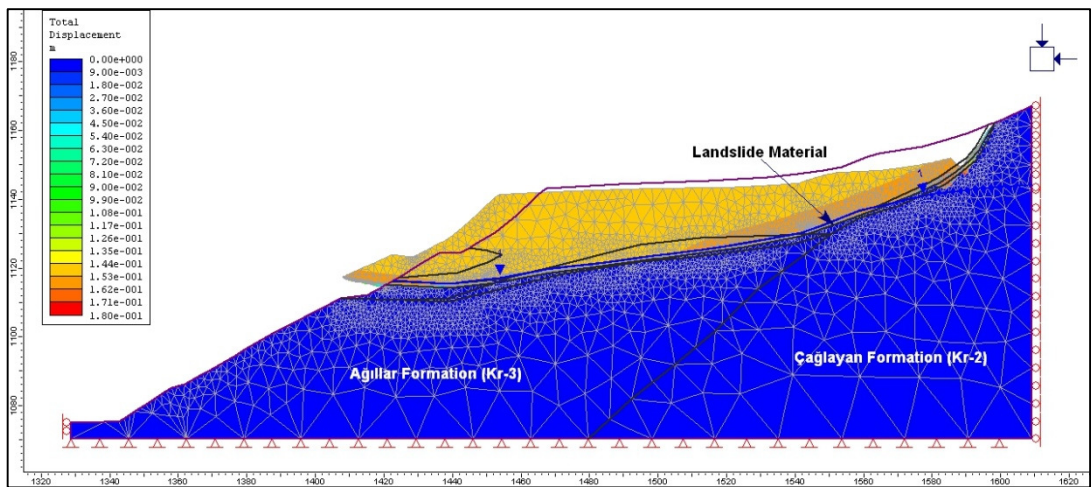


Figure 5.12 Contours of total displacement generated by Phase² v.8.

Phase² results compared well with the direction of the landslide movement.

5.4. Pseudostatic Analysis of the Landslide

When an earthquake occurs, seismic waves radiate away from the source and travel rapidly through the earth's crust. When these waves reach the ground surface, they produce shaking that may last from seconds to minutes. The strength and duration of shaking at a particular site depend on the size and location of the earthquake and on the characteristics of the site. Engineering structures are designed according to strong ground motion not to earthquakes, however, ground motions depend on the size of the earthquake, and the size of the earthquake is measured by the magnitude. The most commonly used method for estimating the ground motion is predictive relationships (in other words) attenuation relations. The attenuation relations for ground motion parameters are statistical regressions on appropriate sets of data (Kramer, 1996).

Erzurum Fault Zone (EFZ) which is left-lateral strike slip is the closest fault system to the Şavşat District in Artvin Province and the air distance is 100 km. The northern EFZ is capable of producing damaging earthquakes greater than Mw 7.1 with recurrence intervals of 1000 to 3000 years (Emre et al., 2004). Although there is no devastating earthquakes in Artvin, earthquakes may occur around this city and then ground motion may reach the surface of the study area. Therefore, this condition should be considered in analysis for selection of the slope stability methods and peak ground acceleration (PGA), the most important ground motion parameter, is estimated by attenuation relationship to use in further step of landslide design.

An earthquake with a moment magnitude of 7.1 was considered in determination of design ground motion parameters. The distance to the causal fault was estimated as a 100-km. Then, peak ground acceleration is calculated by using Abrahamson & Silva (2008) attenuation relationship (Equation 5.1).

$$\ln S_d(g) = f_1(M, R_{rup}) + a_{12}F_{RV} + a_{13}F_{NM} + a_{15}F_{AS} + f_5(PGA_{1100}, V_{S30}) + F_{HW}f_4(R_{jb}, R_{rup}, R_x, W, \delta, Z_{TOR}, M) + f_6(Z_{TOR}) + f_8(R_{rup}, M) + f_{10}(Z_{1.0}, V_{S30}) \quad \text{Eq.(5.1)}$$

The parameters in Equation 5.1 are defined in Table 5.2. Moreover, the summary of the Abrahamson and Silva (2008) attenuation relations are given in Appendix E.

The reason why Abrahamson and Silva attenuation relationship was used is that their data set includes the earthquake data from Turkey and other similar tectonic regions with shallow crustal earthquakes. Moreover, the attenuation relationships of Abrahamson and Silva (2008) were utilized to evaluate peak horizontal ground acceleration values (PGA) for the site due to their relative similarities between the geological and geotectonic characteristics of Anatolia and California (Topal and Akin, 2008).

Table 5.2 Definition of parameters used in Abrahamson & Silva (2008) attenuation relationship.

Parameter	Definition	Notes
M	Moment magnitude	
R_{rup}	Rupture distance (km)	
R_{jb}	Joyner-Boore distance (km)	
R_x	Horizontal distance (km) from top edge of rupture	Measured perpendicular to the fault strike
Z_{TOR}	Depth-to-top of rupture (km)	
F_{RV}	Flag for reverse faulting earthquakes	1 for reverse and reverse/oblique earthquakes defined by rake angles between 30 and 150 degrees, 0 otherwise
F_{NM}	Flag for normal faulting earthquakes	1 for normal faulting earthquakes defined by rake angles between -60 and -120 degrees, 0 otherwise
F_{AS}	Flag for aftershocks	1 for aftershocks, 0 for mainshocks, foreshocks, swarms
F_{HW}	Flag for hanging wall sites	1 for sites on the hanging wall side of the wall, 0 otherwise.
δ	Fault dip in degrees	
V_{S30}	Shear-wave velocity over the top 30 m (m/s)	
$Z_{1.0}$	Depth to $V_S=1.0$ km/s at the site (m)	
PGA_{1100}	Median peak acceleration (g) for $V_{S30}=1100$ m/s	
W	Down-dip rupture width (km)	

According to the ICC (International Code Council, 2006), stiff soil profile has the soil shear wave velocity between 180 m/s and 360 m/s. Then, for the study area shear-wave velocity over the top 30 m was selected as 200 m/s.

Width of the Erzurum fault zone is varying between 5 km and 10 km (Barka and Kadinsky, 1988) and for the study area the width is assumed as 10 km.

Median peak acceleration for V_{S30} -1100 m/s was calculated by inserting 1100 m/s into V_{S30} in equation 5.1, and then it is obtained as 0.0288 g.

The values of all parameters used in the attenuation relationship to calculate PGA for study area are given in Table 5.3.

Table 5.3 Values of all parameters used in the attenuation relationship.

M	R_{rup}	R_{jb}	R_x	Z_{TOR}
7.1	100 km	0	0	2 km
F_{RV}	F_{NM}	F_{AS}	F_{HW}	δ
0	0	0	0	90°
V_{S30}	Z_{1.0}	PGA₁₁₀₀	W	f₁
200 m/s	1 km	0.0288 g	10 km	-3.44
f₅	f₆	a₁₂	a₁₃	a₁₅
0.586	0	0	-0.06	-0.35

Utilizing the Abrahamson and Silva (2008) attenuation relationship, the expected PGA is determined to be 0.07 g. This PGA value utilizes in the step of specifying the remediation techniques as a potential seismic loading.

CHAPTER 6

STABILIZATION OF THE LANDSLIDE

The main objective of this study is to determine the most suitable remediation method. This chapter is about particular stabilization methods for the landslide at the Artvin-Şavşat Junction - Meydancık Provincial Road Km: 12+200.

In agreement with regulations of engineering structures along highways of General Directorate of Highways, $FS \geq 1.5$ is required for the static condition and $FS \geq 1.125$ is required for the earthquake condition in landslide investigation (General Directorate of Highways, 2012). To be on the safe side $FS \geq 1.2$ was taken into consideration to design the slope under earthquake condition. Surface drainage, excavation of the landslide material, rock buttress, and pre-stressed anchorage are selected as a stabilization technique in both static and pseudo-static conditions (with a seismic coefficient of 0.07g). Pre-stressed anchorage is presented as an alternative remediation instead of rock buttressing.

The surface drainage system is satisfied by surface drainage canal which is used when shallow groundwater is encountered and collects the rainwater before reaching the underground. Figure 6.1 shows the surface drainage canal layout in the landslide area.

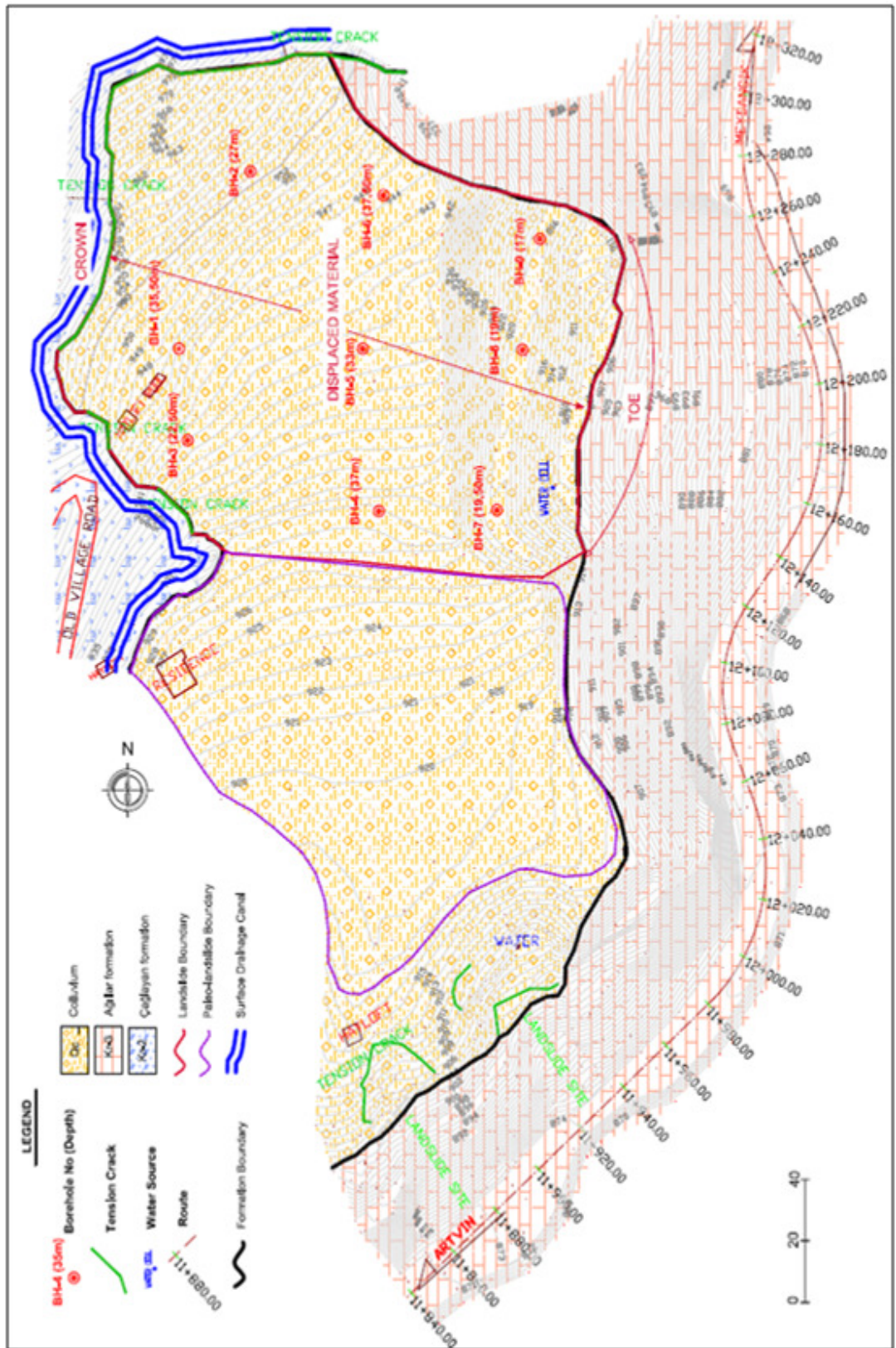


Figure 6.1 Surface drainage canal layout in the landslide area.

The best quality of rock-fill is produced by a hard rock quarry where the rock is blasted into fragments (shot rock) and subsequently processed to different gradations. The rock material by weight passing the No. 4 sieve should be limited to about 30% (or even 25%). This criterion is needed to ensure point-to-point contact between the coarser rock fragments. It should be mentioned that 30% by weight has the appearance of a higher percent when seen on a site. In a rock-fill stockpile with 30% by weight of gravel-size (or larger) pieces, the sand fraction will appear to cover about one half of the surface of the stockpile (Cornforth, 2005).

Basalt existing around the study area can be used for rock-fill material while rock buttressing remediation. It has a 28.5-kN/m^3 -unit weight and the unit weight of its particles be used in buttress has a 23-kN/m^3 -unit weight when considering 25 % porosity.

Janbu's corrected and Spencer analysis methods are used in the stabilizing techniques of the slope to compare the results of these methods. Rock buttressing geometry is designed by using the non-circular block search analysis along observed failure surface. Moreover, the non-circular path search analysis is used to see whether there are another failure surfaces or not.

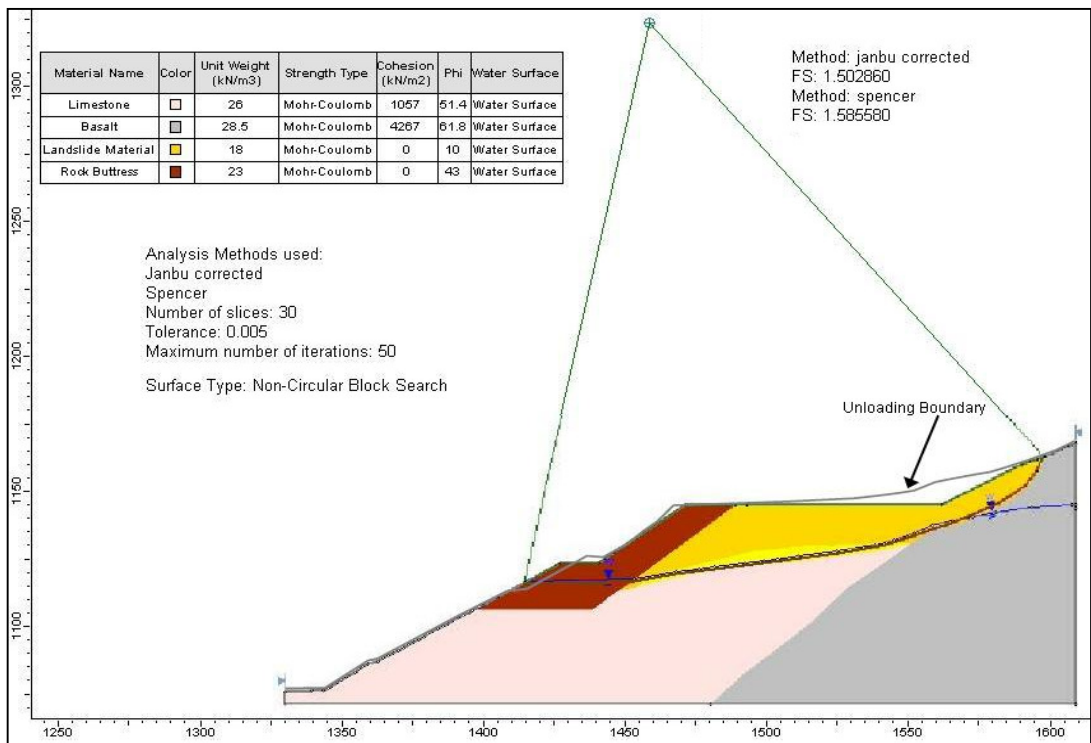


Figure 6.2 Rock buttressing with static condition.

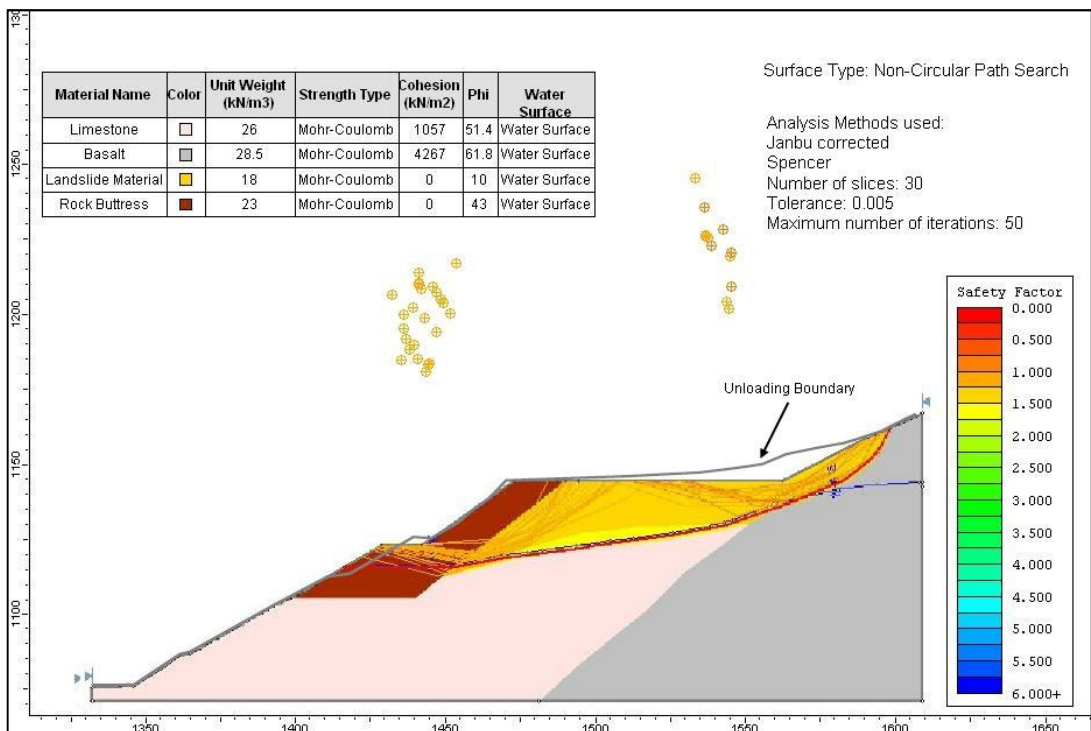


Figure 6.3 Searching the most critical failure surface in rock buttressing with static condition.

Figure 6.2 shows the results of the model for static condition in the rock buttressing remediation. Figure 6.3 presents the non-circular path search analysis result for the rock buttressing. As it can be seen from the figures, some of these failure surfaces are not realistic. Therefore, it is decided that it is sufficient to provide safety along the observed failure surfaces.

Figure 6.4 shows the block search result of rock buttressing with pseudo-static condition and Figure 6.5 shows the result of the non-circular path search analysis result for the rock buttressing with pseudo-static condition.

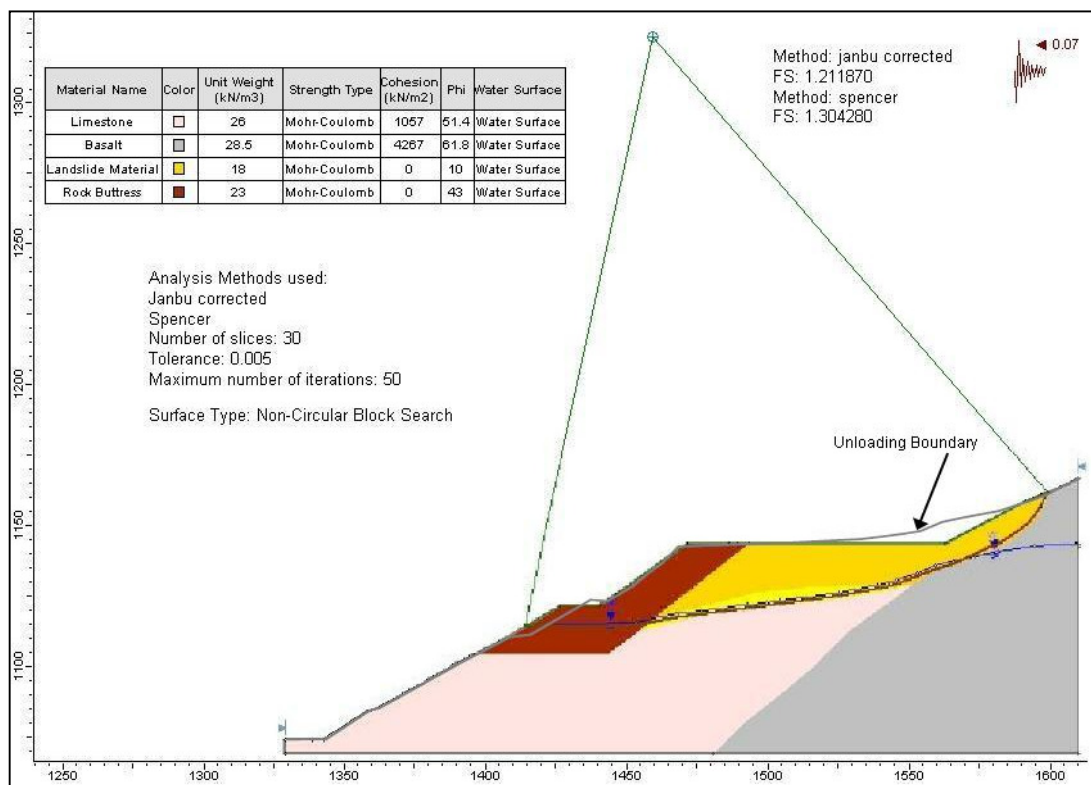


Figure 6.4 Rock buttressing with pseudo-static condition.

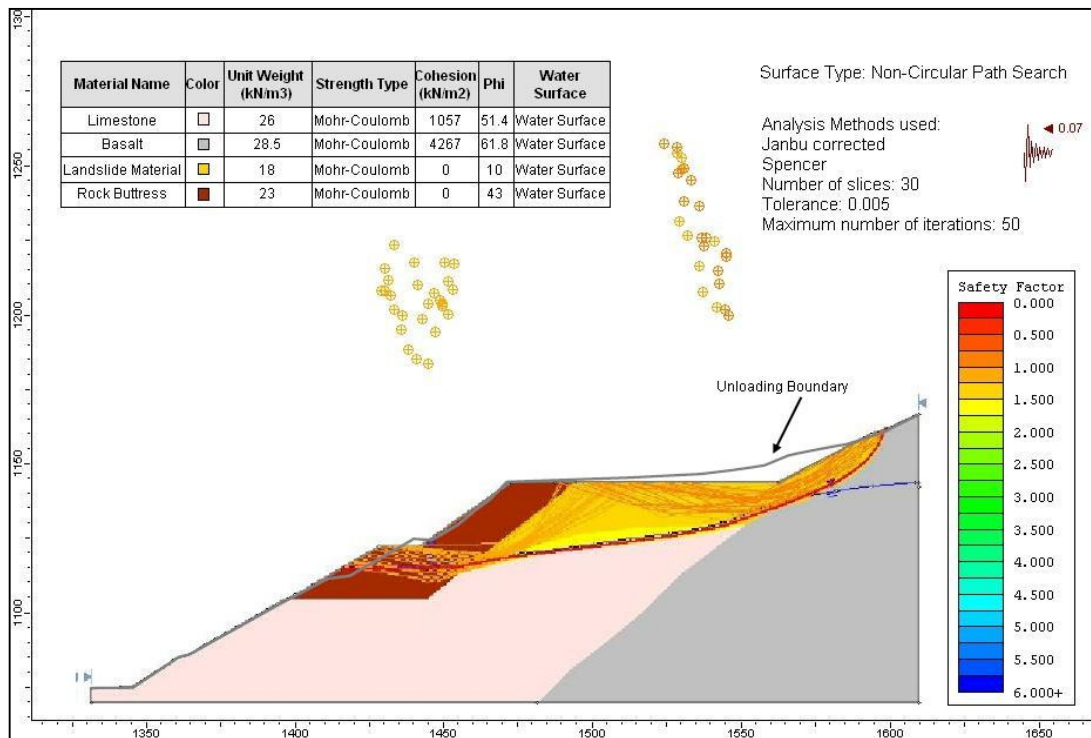


Figure 6.5 Searching the most critical failure surface in rock buttressing with pseudo-static condition.

List of the factor of safeties obtained from two different methods for static and pseudo-static conditions in rock buttressing are given in Table 6.1.

Table 6.1 List of the factor of safeties for the rock buttressing technique.

FS	Rock Buttressing Remediation Technique	
	Non-circular Block Search	
	Static	Pseudo-static
Janbu's Corrected	1,50	1,21
Spencer	1,59	1,31

Although the buttressing is one of the alternatives, it is not practical due to requirement of approximately 32-m-height and 150 000.0-m³-volume excavation. Then the second method, anchoring, is evaluated.

An inclined anchor provides a dual benefit of: (i) pullback resistance, and (ii) incremental shear strength improvement to slope stability (Cornforth, 2005). The application of anchorage remediation method is tested by using SLIDE version 6.0 software (Rocscience, 2012) and pressure-grouted tieback was selected as a support type. Bond strength is specified from Table 2.6 presented in Chapter 2 as a 1330 kN/m.

To satisfy safety factor of 1.50 in static condition and 1.20 in pseudostatic condition, various values assigned to the capacity and the angle to the landslide boundary of the pressure-grouted tieback. The variations of these values are given in Figure 6.6.

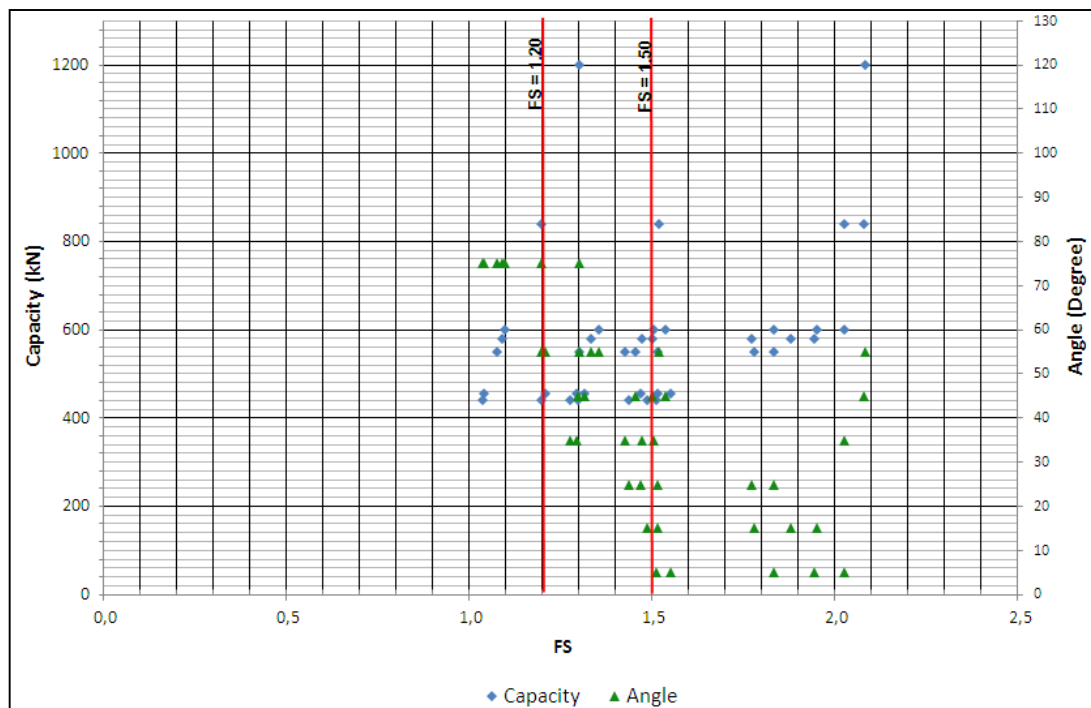


Figure 6.6 Angle and capacity variations of pressure-grouted tieback for the landslide.

As the angle of pressure-grouted tiebacks decreases, the length of the anchor increases. There is clearly a trade-off between the increased resistance to sliding and the extra construction cost of longer anchors (Cornforth, 2005). Since construction cost for anchors is not directly related to length, the optimum angle with

regard to construction cost is likely to fall between these 15° and 30° limits with considering both length and capacity.

The angle of pressure-grouted tiebacks is selected as 30 degrees from the horizontal and pre-stressed anchor capacity was determined by using the non-circular block search analysis. Figure 6.7 (with FS=1.507) and in Figure 6.8 (with FS=1.205) shows the results of the model for static and pseudo-static conditions in the anchoring remediation, respectively.

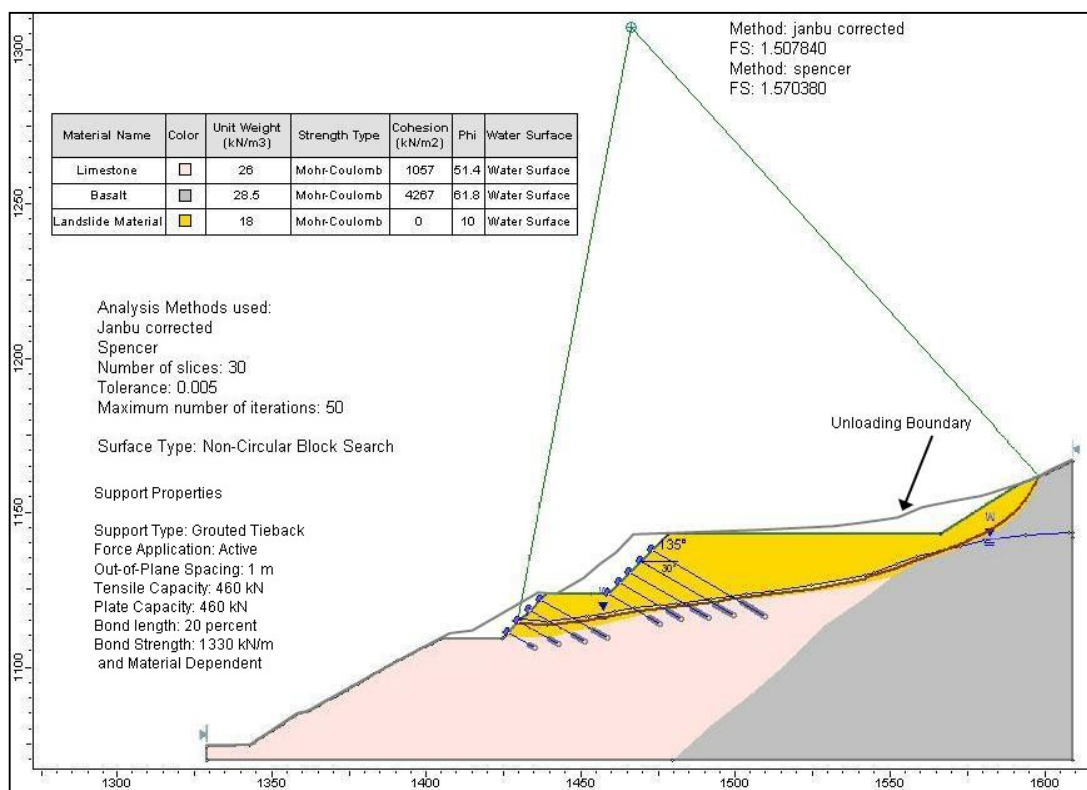


Figure 6.7 Pre-stressed anchors with static condition.

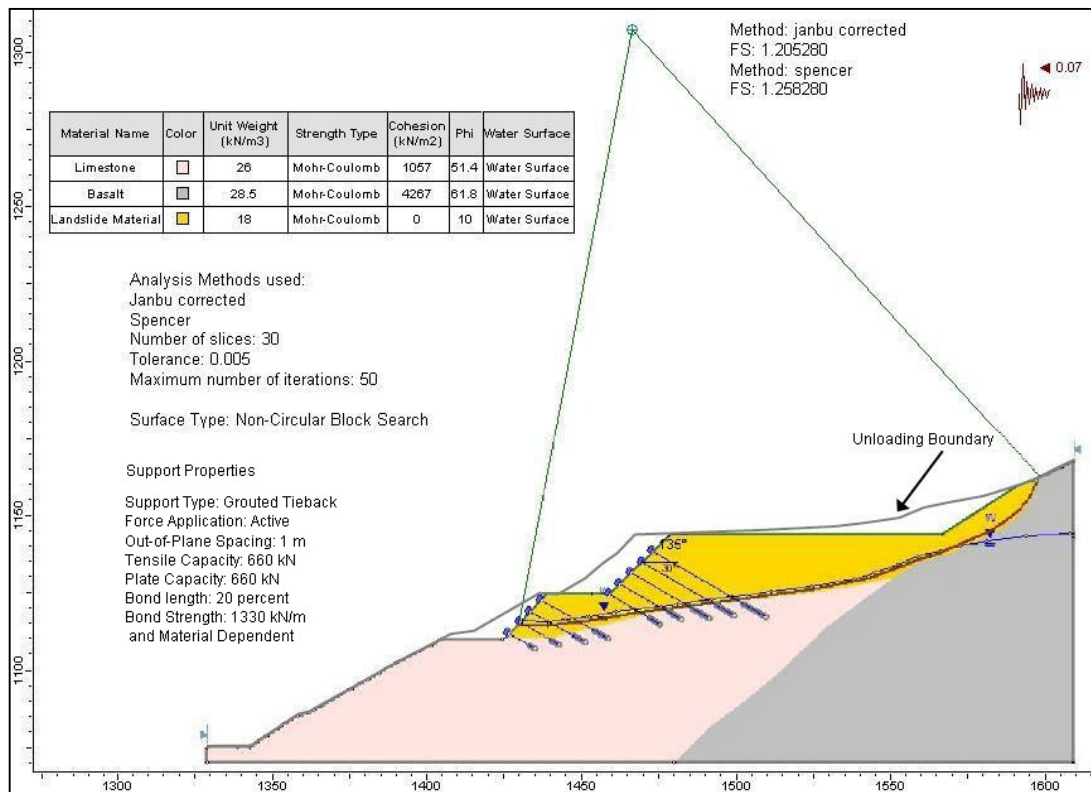


Figure 6.8 Pre-stressed anchors with pseudostatic condition.

List of the factor of safeties obtained from two different methods for static and pseudo-static conditions in pre-stressed anchoring are given in Table 6.2.

Table 6.2 List of factor of safeties for the pre-stressed anchoring technique.

FS	Pre-stressed Anchor Remediation Technique	
	Non-circular Block Search	
	Static	Pseudo-static
Janbu's Corrected	1,51	1,21
Spencer	1,57	1,26

The slope remediation method for the static analysis presented in Figure 6.7 which covers unloading of the landslide material and the application of pre-stressed anchors leads to a FS of 1.51 which is sufficient for the stability of the slope according to Regulations of engineering structures along highways of General Directorate of Highways (2012). The slope stability model for the pseudostatic analysis given in Figure 6.8 by which unloading of the landslide material and the application of pre-stressed anchors for a seismic coefficient of 0.07 g brings to a FS of 1.21 which is also sufficient for the stability of the slope according to Regulations of engineering structures along highways of General Directorate of Highways (2012).

CHAPTER 7

CONCLUSIONS AND RECOMMENDATIONS

The landslide at the Artvin-Şavşat Junction - Meydancık Provincial Road Km: 12+200 occurred at the left side of the road platform under construction in April 2008 as a result of mass movement accelerating through the valley bottom. Geological material of the landslide area is colluvium, mainly composed of gravel, clayey sand and clay. Groundwater has been observed in landslide area and its level is varying between 6.2 and 27.2 m.

30 to 40 cm wide and 180-240 cm long tension cracks formed approximately 145 m behind the face of the slope, and deformations have been observed to progress towards the toe of the landslide. The landslide has a length of approximately 197 m, a depth of approximately 32 m and complex type of the landslide has been observed. The soil and groundwater conditions together with the geotechnical properties have been considered to suggest appropriate stabilization techniques for landslide.

First, residual parameters of the landslide material were determined by back analyses of the landslide geometry along three profiles. According to the back analyses results, shear strength parameters were specified as $c = 0$ kPa and $\phi = 10^\circ$ for the landslide material. Then, the study area was modeled along the most representative profile of the study area and the most suitable remediation technique was determined by considering the landslide mechanism, parameters determined from the geotechnical investigations, the size of the landslide and location of the slip circle. Furthermore, since the study area is located in a third degree earthquake hazard region, pseudostatic stability analyses using the Slide software was performed for the earthquake potential and the most suitable stabilization technique

was determined. For both static and pseudostatic analyses the most appropriate remediation techniques are surface and subsurface drainage by surface drainage canal, unloading the landslide material and application of pre-stressed anchoring.

Basalt existing around the study area may be used for rock-fill material while rock buttressing remediation. However, it requires huge amount of excavation, then anchoring was evaluated as an alternative technique and type of support is pressure-grouted tieback.

By applying the pre-stressed anchoring remediation method, the unstable material in the area may be prevented to slide. It is noticed that the length of the anchorage have been determined approximately according to idealized soil profile of the area and available data, therefore; predicted anchorage length should be reevaluated before implementation. The application length of the anchorage will be determined in-situ by considering that the minimum % 20-bond length in the fresh part of the limestone.

REFERENCES

- Abrahamson, N. A., Silva, W. J., 2008, "Abrahamson & Silva NGA ground motion relations for the geometric mean horizontal component of peak and spectral ground motion parameters", Pacific Earthquake Engineering Research Center, 67-97 pp.
- Abramson, L. W., Lee, T., S., Sharma, S., Boyce, G., M., 2001, "Slope Stability and Stabilization Methods", John Wiley & Sons, Inc., New York, 712 pp.
- ASTM. D 1586-08a, 2000 , "Standard Test Method for Standard Penetration Test (SPT) and Split-Barrel Sampling of Soils", West Conshohocken, PA: ASTM International.
- Barka, A., A., Kadinsky K., 1988, "Strike-slip Fault Geometry in Turkey and its influence on Earthquake Activity", *Tectonics*, Vol.7, No.3, 663-684 pp.
- Bromhead, E. N., 1992, "The Stability of Slopes", 2nd ed., Glasgow, Scotland: Blackie Academic and Professional, 411 pp.
- CANMET, 1977, "Pit Slope Manual: Chapter 8-Monitoring", Canmet Report No. 77-115, 25 pp.
- Chandler, R. J., 1977, "Back analysis techniques for slope stabilization works: a case record", *Geotechnique* 27(4), 479–495 pp.
- Cheng, Y. M., Lansivaara, T., Wei, W. B., 2006, "Two-dimensional slope stability analysis by limit equilibrium and strength reduction methods", *Journal of Computers and Geotechnics*, Vol.34, 137-150 pp.
- Chowdhury, R. N., 1981, "Discussion of Stability Analysis of Embankments and Slopes", *Journal of Geotechnical Engineering Division, ASCE*, Vol. 107, No.GT-5, May, 691-693 pp.
- Chowdhury, R., 2010, "Geotechnical Slope Analysis", Taylor & Francis Group, London, UK, 737 pp.

Clough, R. W., Woodward, R. J., 1967, “ Analysis of Embankment Stresses and Deformations”, Journal of Geotechnical Division, ASCE, July, 529-549 pp.

Cooper, M. R., 1984, “The application of back-analysis to the design of remedial works for failed slopes”, Proceedings of the 4th International Symposium on Landslides, Toronto, Vol. 2, 387–392 pp.

Cornforth, D. H., 2005, “Landslides in Practice”, John Wiley & Sons, Inc., New York, 495 pp.

Corps of Engineers, 1982, “Slope Stability Manual EM-1110-2-1902”, Washington, DC: Department of the Army, Office of the Chief of Engineers, Washington, D.C.

Craig, R.F., 2004, “Soil Mechanics”, Spon Press, London. 435 pp.

Duncan, J.M., 1996, “State of The Art: Limit Equilibrium and Finite-Element Analysis of Slopes”, Journal of the Geotechnical Engineering, Vol. 122, No 7, 577-596 pp.

Duncan, J.M., Wright, S.G., 2005, “Soil Strength and Slope Stability”, John Wiley & Sons, Inc, New York, 293 pp.

Emre, Omer, Koehler, Richard D., Hengesh, James V., Duman, Tamer Y., Akyuz, Serdar, Altunel, Erhan, Barka, Aykut, 2004, “Late Holocene Activity Of Erzurum Fault Zone In Eastern Anatolia, Turkey”, Geological Society of America Abstracts with Programs, Vol. 36, No. 5, 148 pp.

Franklin, J. A., M. B. Dusseault, 1989, “Rock Engineering”, New York: McGraw-Hill, 301 pp.

General Directorate of Disaster Affairs, Earthquake Research Center, 2012, Updated: 1993, Accessed: 26.April.2012
<http://www.deprem.gov.tr/SarbisEng/Shared/ DepremHaritalari.aspx> (in Turkish)

General Directorate of Highways, 2012,” Karayolu Yolboyu Mühendislik Yapıları İçin Teknik Şartname”, 105 pp (in Turkish).

Gökçe, O., Özden, Ş., Demir, A., 2008, "General Directorate of Disaster Affairs, Department of Disaster Survey and Damage Assessment", Türkiye'de afetlerin mekansal ve İstatistiksel dağılımı afet bilgileri envanteri. Ankara, 26 pp.

Griffiths, D. V., Lane, P.A., 1999, "Slope stability analysis by finite elements", Journal of Geotechnique, Vol.49, No. 3, 387-403 pp.

Güven, İ. H., Nalbantoğlu, A.K. , Takaoğlu, S., 1993, MTA Genel Müdürlüğü 1/100 000 ölçekli açın-sama nitelikli Türkiye Jeolojisi haritaları serisi, Trabzon F42 ve G42 Paftaları, Ankara.

Hausmann, M. R., 1992, "Engineering Principles of Ground Modification", McGraw-Hill, New York, 632 pp.

Hunt, R. E., 1986,"Geotechnical Engineering Analysis and Evaluation", McGraw-Hill: USA, 5-134 pp.

Hoek, E, Bray, J.W., 1977, "Rock slope engineering", Stephen Austin and Sons Ltd, Hertford, 402 pp.

Hynes-Griffin, M. E., Franklin, A. G., 1984, "Rationalizing the Seismic Coefficient Method", Miscellaneous Paper No. G.I., 84-13, U.S. Army Engineer Waterways Experiment Station, Vicksburg, Mississippi.

ICC 2006, International Code Council, 2006. "International Building Code, Structural and Fire-And Life-Safety Provisions Covering Seismic, Wind, Accessibility, Egress, Occupancy and Roofs Codes", 672 pp.

Koçyiğit, A., 1991. Changing stress orientation in progressive intercontinental deformation as indicated by the neotectonics of Ankara Region, NW Central Anatolia. TAPG Bulletin, Ankara, vol. 31, pp.43–55

Kramer, S.L., 1996, "Geotechnical Earthquake Engineering", Prentice-Hall, Inc, New Jersey, 653 pp.

Makdisi, F. I., Seed, H. B., 1978, "Simplified Procedure for Estimating Dam and Embankment Earthquake Induced Deformations", Journal of the Geotechnical Engineering Division, ASCE, Vol. 104, No. GT7, 849-867 pp.

Marcuson, W.F., Franklin, A. G., 1983, "Seismic Design, Analysis and Remedial Measures to Improve the Stability of Existing Earth Dams – Corps of Engineers Approach", Seismic Design of Embankments and Caverns, T.R. Howard, Ed., New York: ASCE.

Mesri, G., Shahien, M., 2003, "Residual Shear Strength Mobilized in First-Time Slope Failures", Journal of Geotechnical and Geoenvironmental Engineering, ASCE, Vol. 129, No. 1, 12-31 pp.

Meteoroloji Genel Müdürlüğü (Turkish State Meteorological Service, TSMS), 2012, "Resmi İstatistikler", Updated: 01.January.2012, Accessed: 25.April.2012, <http://www.mgm.gov.tr/veridegerlendirme/il-ve-ilceler-istatistik.aspx> (in Turkish).

Morgenstern, N. R., Price, V. E., 1965, " The Analysis of the Stability of General Slip Surfaces", Geotechnique, Vol. 15, No.1, 77-93 pp.

MTA, 1998, Artvin 1:100.000 Ölçekli Jeoloji Haritası.

Newmark, N. M., 1965, "Effects of Earthquakes on Dams and Embankments", Geotechnique, Vol. 15, No. 2, 129-160 pp.

PETRA Engineering and Consulting Company, 2009, "Artvin-Şavşat Junction - Meydancık Provincial Road KM:12+200 Heyelanı Jeolojik-Jeoteknik Etüt ve Geoteknik Proje Raporu", Ankara, 50 pp.

Rahardjo, H., Hritzuk, K. J., Leong, E. C., Rezaur, R. B., 2003, "Effectiveness of horizontal drains for slope stability", Engineering Geology, 2154, 1–14 pp.

Rocscience, 2006, "RocLab User's Guide", Rocscience Inc., Toronto, 25 pp.

Rocscience (2012) SLIDE 6.0 - 2D slope stability analysis for soil and rock slopes. Rocscience Inc., Toronto

Rocscience, 2011, "A New Era in Slope Stability Analysis: Shear Strength Reduction Finite Element Technique", Rocscience Inc., Toronto, 10 pp.

Sabatini, P.J., Pass, D.G., Bachus, R.C., 1999, "Ground Anchors and Anchored Systems", Geotechnical Engineering Circular No.4, FHWA-IF, 99-015, 176 pp.

Sancio, R. T., 1981, "The use of back-calculations to obtain shear and tensile strength of weathered rocks", Proceedings of the international symposium on weak rock, Tokyo, 647–652 pp.

Sayısal Grafik, 2012, "Türkiye Deprem Haritası", Updated: 21.April.2012, Accessed: 21.April.2012, http://www.sayisalgrafik.com.tr /deprem/tr_frames.htm (in Turkish).

Seed, H.B., 1979, "Considerations in the Earthquake-Resistant Design of Earth and Rockfill Dams", Geotechnique, Vol. 29, No. 3, 215-263 pp.

Spencer, E., 1967, "A Method of Analysis of the Stability of Embankments Assuming Parallel Inter-Slice Forces", Geotechnique, Vol. 17, 11-26 pp.

Stark, T., D., Choi, H., McCone, S., 2005, "Drained Shear Strength Parameters for Analysis of Landslides", Journal of Geotechnical and Geoenvironmental Engineering, ASCE, Vol. 131, No. 5, 575-588 pp.

Topal, T., Akın, M., 2008, "Geotechnical assessment of a landslide along a natural gas pipeline for possible remediations (Karacabey-Turkey)", Environ Geol (2008) 57, 611–620 pp.

TS 1900-1, 2006, "İnşaat mühendisliğinde zemin laboratuvar deneyleri-Bölüm 1: Fiziksel özelliklerin tayini", Türk Standartları Enstitüsü, Ankara, 93 pp. (in Turkish)

TS 1900-2, 2006, "İnşaat mühendisliğinde zemin laboratuvar deneyleri-Bölüm 2: Mekanik özelliklerin tayini", Türk Standartları Enstitüsü, Ankara, 12 pp. (in Turkish)

Yılmaz, B. S., Gülibrahimoğlu, İ., Yazıcı, N. E., Yaprak, S., Saraloğlu, A., Konak, O., Köse, Z., Çuvalcı, F., Tosun, C. Y., 1998, "Artvin İlinin Çevre Jeolojisi ve Doğal Kaynakları", M.T.A. Derleme Raporu No 98-21 E, 8-30 pp (in Turkish)

Xanthakos, P. P., Bruce, D.A., Abramson, L.W., 1994, "Ground Control and Improvement", John Wiley & Sons Inc: UK, 936 pp.

APPENDIX A

BOREHOLE LOGS

PETRA Müh.Müş.ve İnş.Ltd.Şti. SONDAJ LOGU / BORING LOG				SONDAJ NO Borehole No BH-1	SAYFA Page 1 / 3										
PROJE ADI/Project Name : (ARTYIN-ŞAYŞAT) JUNCTION - MEVDANCIK PROVINCIAL ROAD			DELİK ÇAP/Hole Diameter : 114 mm												
SONDAJ YERİ/Boring Location : LANDSLIDE			YERALTI SUYU/Groundwater : 16.2 m												
KİLOMETRE/Chainage : 12+200			MUH.BOR.DER./Casing Depth : -												
SONDAJ DER./Boring Depth : 35,50 m.			BAŞ.-BIT.TARİHİ/Start-Finish Date : 10/11/2008 -- 16/11/2008												
SONDAJ KOTU/Elevation : 946			KOORDİNATI/Coordinate(Northing) : 4581001												
SON. MAK.&VÖNT./D.Rig & Mot. : MOBILE DRILL B-53			KOORDİNATI/Coordinate(Easting) : 523875												
DAYANIMLIK/Strength		AYRIĞMA/Weathering		İNCE DANELİ/Fine Grained											
I ÇOK DAYANIMLI II ORTA III ZAYIF IV ÇOK ZAYIF	Serong M Strong NEWeak V Weak VI Weak	I TAZE II AZ AYRIĞMIŞ III ORTA D. AYIL IV ÇOK AYIL V TÜMÜLE AYIL	Fresh Slightly W. Mod. Wash. Highly W. Comp. W.	N: 0-2 ÇOK YUMUŞAK N: 3-4 YUMUŞAK N: 5-8 ORTA KATI N: 9-15 KATI N: 16-20 ÇOK KATI N: >20 SERT	Very Soft Soft Moderately stiff Stiff Very stiff Hard										
IRI DANELİ/Coarse Grained		IRI DANELİ/Coarse Grained		IRI DANELİ/Coarse Grained											
N: 0-4 ÇOK GEVGEK N: 5-10 GEVGEK N: 11-30 ORTA SIKI N: 31-50 SIKI N: >50 ÇOK SIKI		N: 0-4 ÇOK GEVGEK N: 5-10 GEVGEK N: 11-30 ORTA SIKI N: 31-50 SIKI N: >50 ÇOK SIKI		N: 0-4 ÇOK GEVGEK N: 5-10 GEVGEK N: 11-30 ORTA SIKI N: 31-50 SIKI N: >50 ÇOK SIKI											
Very Loose		Very Loose		Very Loose											
Loose		Loose		Loose											
Moderately Dense		Moderately Dense		Moderately Dense											
Dense		Dense		Dense											
Very Dense		Very Dense		Very Dense											
KAYA KALİTESİ TANIMI/ROD		KIRIKLAR-30 cm/Fractures		ORANLAR/Proportions											
% 0-25 ÇOK ZAYIF % 25-50 ZAYIF % 50-75 ORTA % 75-90 İYİ % 90-100 ÇOK İYİ	Very Poor Poor Fair Good Excellent	I SEYREK II ORTA III SIK IV ÇOK SIK V PARÇALI	Wdly (W) Moderate (M) Close (C) Intense (I) Crushed (Cr)	% 5 PEK AZ % 5-15 AZ % 15-35 ÇOK	Slightly Little Very										
SPT STANDART PENETRASYON TESTİ Standard Penetration Test		UD ORSELENMEMİŞ NUMUNE Undersized Sample		P PRESİYOMETRE DENEYİ Pressuremeter Test											
D ORSELENMİŞ NUMUNE Described Sample		K KAROT NUMUNESİ Core Sample		R REFU Retained (N30, 60)											
Boring Depth (m) SONDAJ DERİNLİĞİ	NUMUNE ÇİNSİ Sample Type	STANDART PENETRASYON DENEYİ Standard Penetration Test				JEOTEKNİK TANIMLAMA Geotechnical Description	ZEMİN SINIFI Soil Classification	PROFİL Profile	DAYANIMLIK/Strength	AYRIĞMA/Weathering	KIRIKLAR/Fracture (30 cm)	KAROT % (TC) (YT) Core R.	FOD %	KAROT % (D) (Y) (S) Core R.	ÇİNEREK NO / Sample No.
		DARBE SAYISI Num. of Blows	GRAFİK Graph												
	MAKNE VİDEO Run	0 - 15 cm 15 - 30 cm 30 - 45 cm	N	10 20 30 40 50 60											
0.0															
1.0															
2.0	SPT1	16 / 29 / 29	58					SC							
3.0	SPT2	33 / 38 / 27	60												
4.0															
5.0	SPT3	19 / 26 / 26	52					SC							
6.0	SPT4	25 / 15 / 21	36												
7.0															
8.0	SPT5	33 / 39 / 49	86					SC							
9.0	SPT6	44 / 50/2	R												
SONDÖR / Driller			SONDAJ MÜHENDİSİ / Drilling Engineer			TARİH / Date			İMZA / Sign						
Kamil YAMALI			MURAT DOĞAN			16/11/2008									

Figure A.1 Borehole No.1 (Page 1)

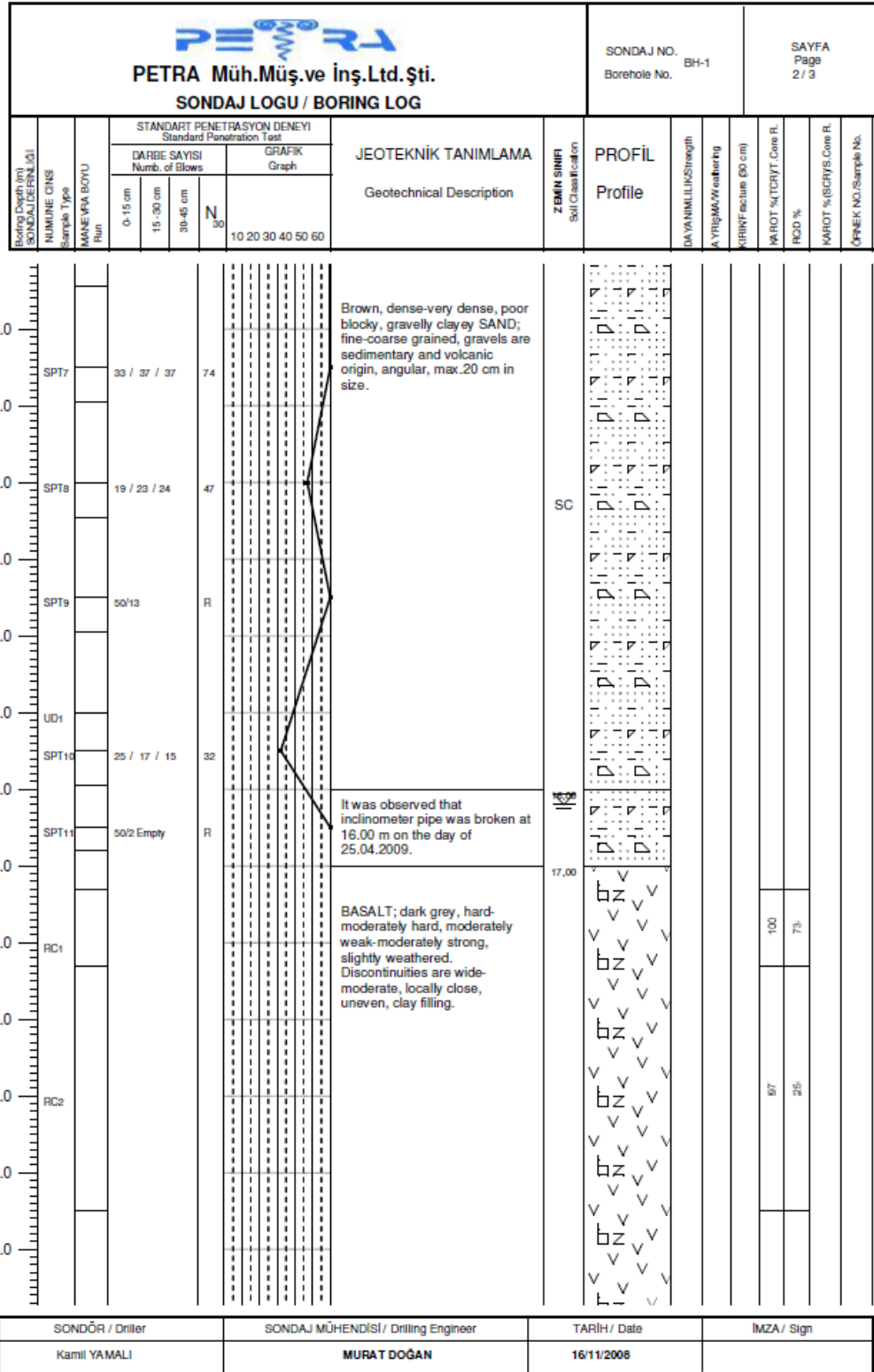

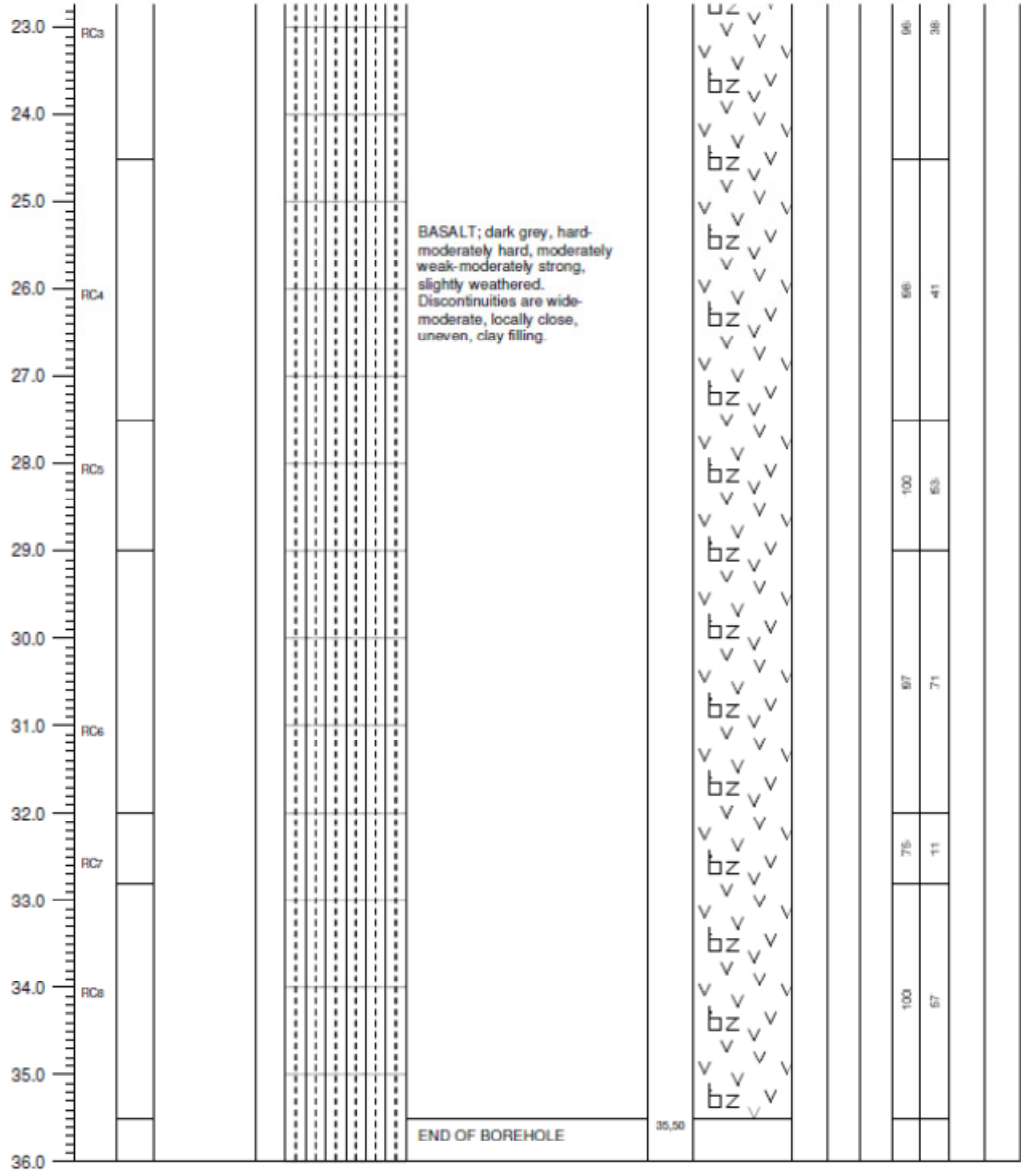


Figure A.2 Borehole No.1 (Page 2)

 PETRA Müh.Müş.ve İnş.Ltd.Şti. SONDAJ LOGU / BORING LOG				SONDAJ NO. Borehole No. BH-1		SAYFA Page 3 / 3										
Boring Depth (m) SONDAJ DERİNLİĞİ	NUMUNE ÖNSİ Sample Type	KARNE İFA BOYU Flut	STANDART PENETRASYON DENEYİ Standard Penetration Test				JEOTEKNİK TANIMLAMA Geotechnical Description	ZEMİN SINIFI Soil Classification	PROFİL Profile	DAYANIMLILIK Strength	A YIĞILMAK Weathering	KIRINTI Fracture (cm)	KAROT NİÇLİKTİ Core R.	RQD %	KAROT NİÇLİKTİ Core R.	ÖRNEK NO./Sample No.
			DARBE SAYISI Numb. of Blows		GRAFİK Graph											
			0-15 cm	15-30 cm	30-45 cm	N ₃₀	10 20 30 40 50 60									



SONDÖR / Driller	SONDAJ MÜHENDİSİ / Drilling Engineer	TARİH / Date	İMZA / Sign
Kamil YAMALI	MURAT DOĞAN	16/11/2008	

Figure A.3 Borehole No.1 (Page 3)

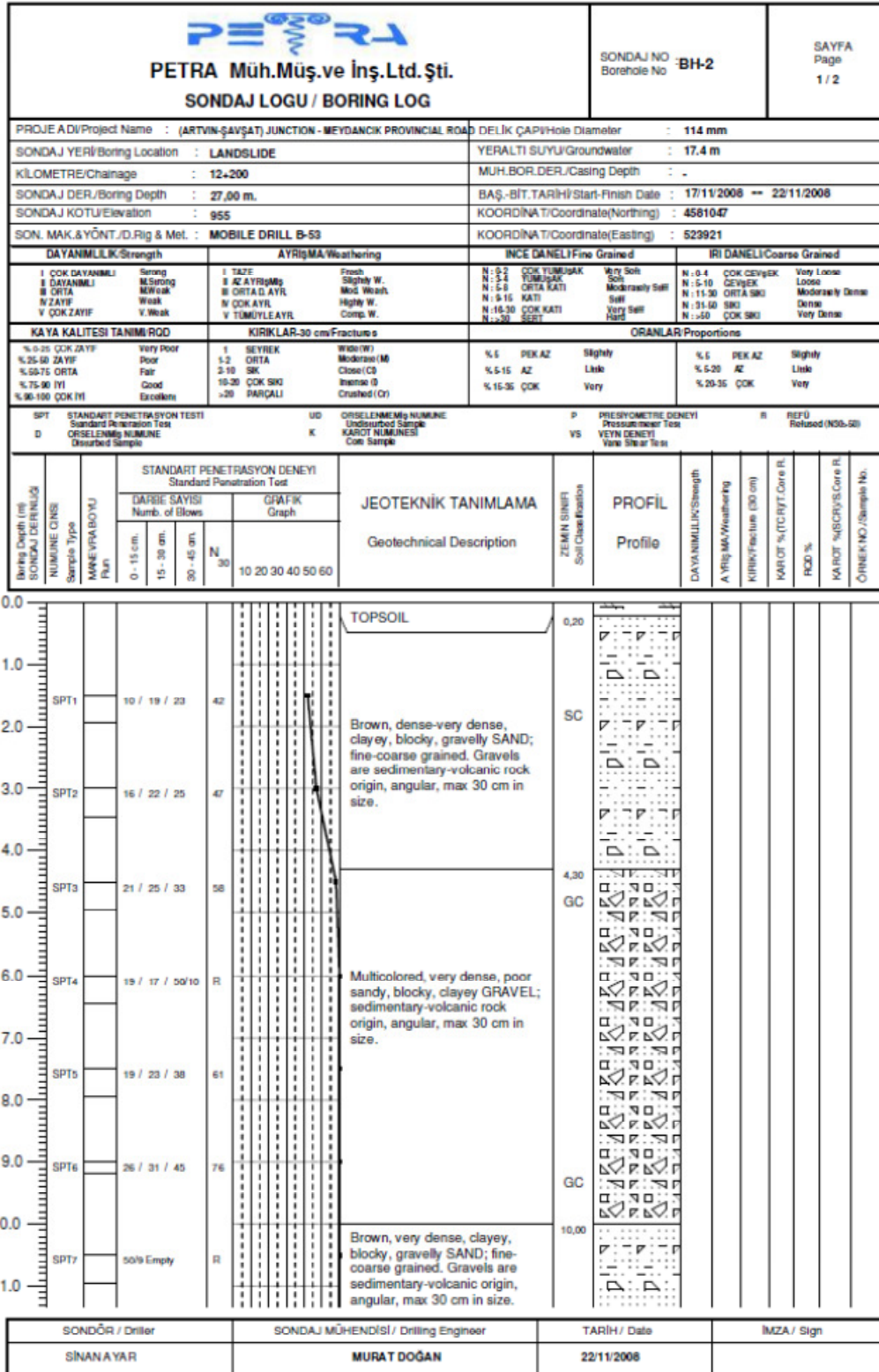


Figure A.4 Borehole No.2 (Page 1)

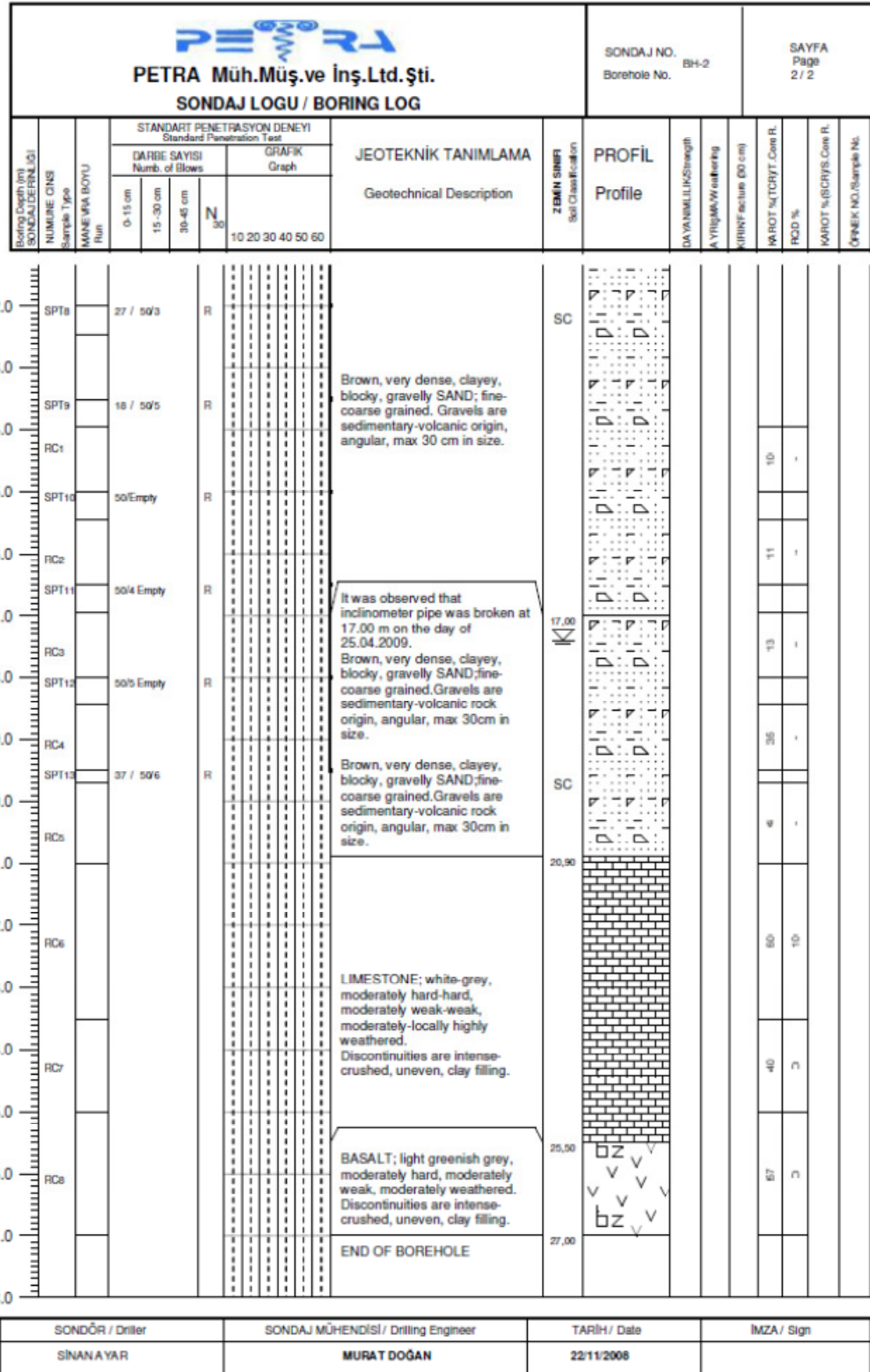


Figure A.5 Borehole No.2 (Page 2)

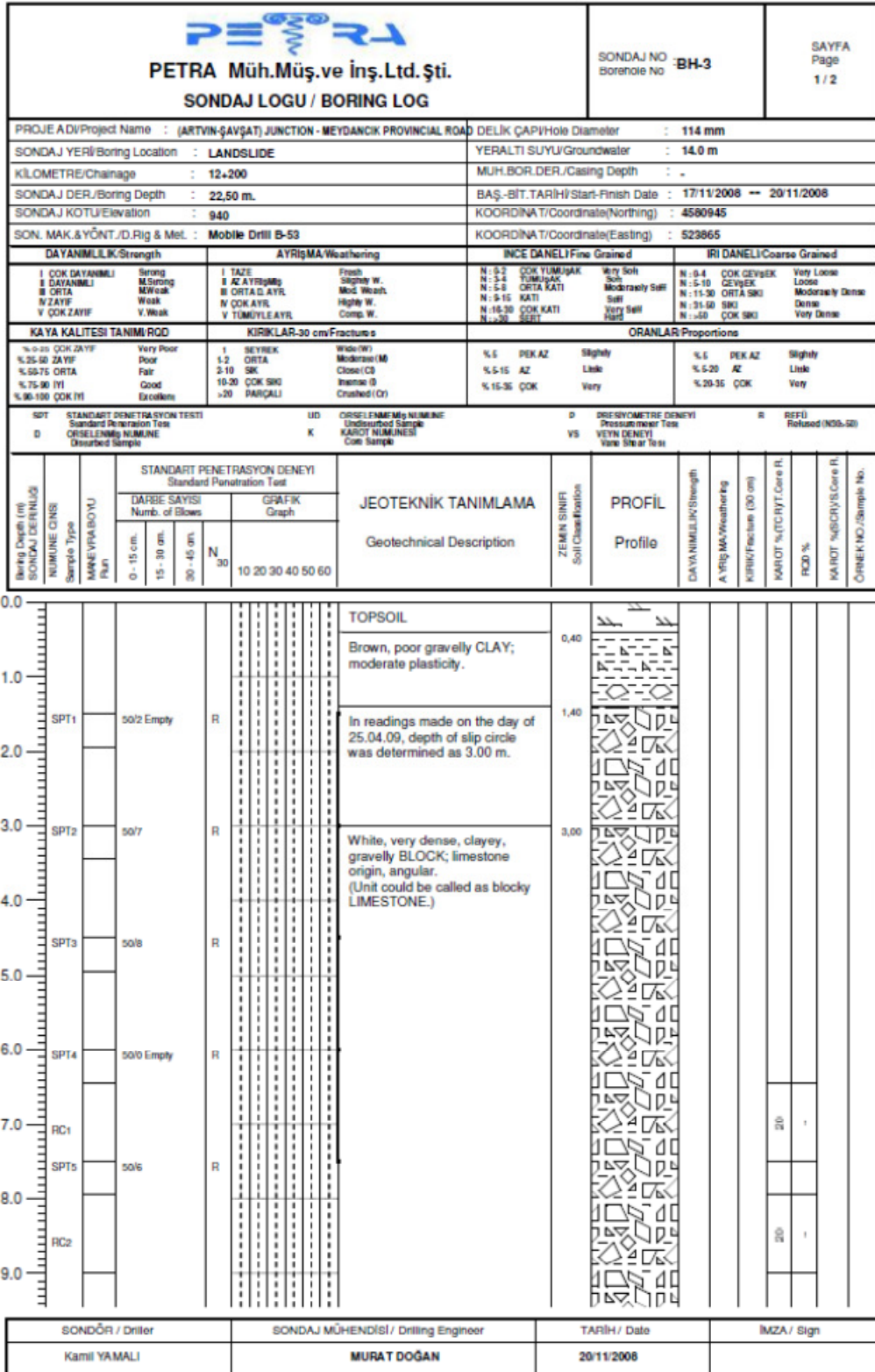

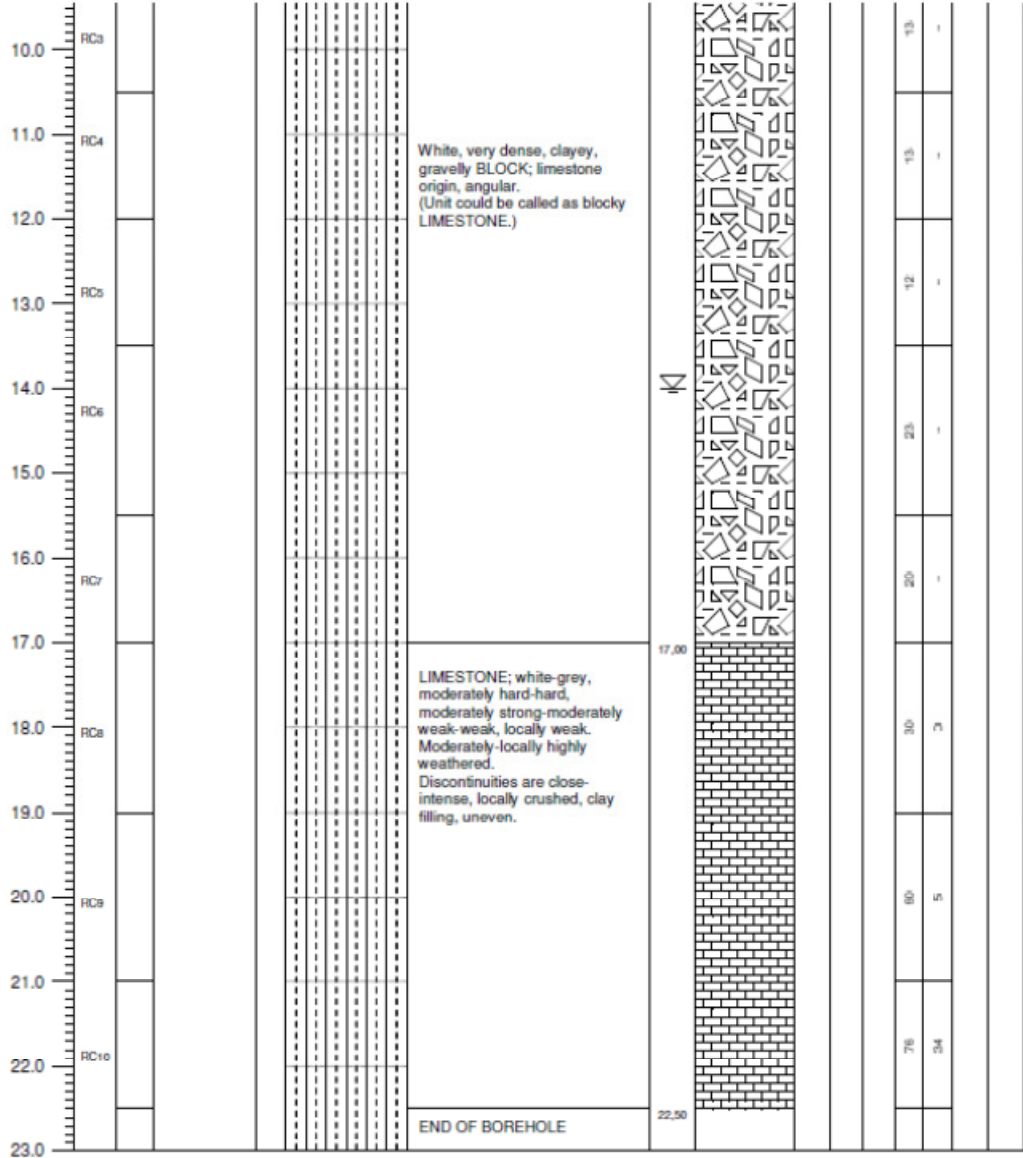


Figure A.6 Borehole No.3 (Page 1)

 PETRA Müh.Müş.ve İnş.Ltd.Şti. SONDAJ LOGU / BORING LOG				SONDAJ NO. Borehole No. BH-3	SAYFA Page 2 / 2								
Boring Depth (m) SONDAJ DERİNLİĞİ	NUMUNE ÖLÇÜSÜ Sample Type	MAMNE İPİNİN BOYU Pipe	STANDART PENETRASYON DENEYİ Standard Penetration Test		JEOTEKNİK TANIMLAMA Geotechnical Description	ZEMİN SINIFI Soil Classification	PROFİL Profile	DA YA NİMLİLİK Strength	AYRIĞI Weathering	ZARARLI FAKTÖR Core R.	RİZİT % Core R.	SARTI % Core R.	ÖRNEK NO. Sample No.
			DARBE SAYISI Num. of Blows	GRAFİK Graph									
			0-15 cm 15-30 cm 30-45 cm	N ₃₀	10 20 30 40 50 60								



SONDÖR / Driller	SONDAJ MÜHENDİSİ / Drilling Engineer	TARİH / Date	İMZA / Sign
Kamil YAMALI	MURAT DOĞAN	20/11/2008	

Figure A.7 Borehole No.3 (Page 2)

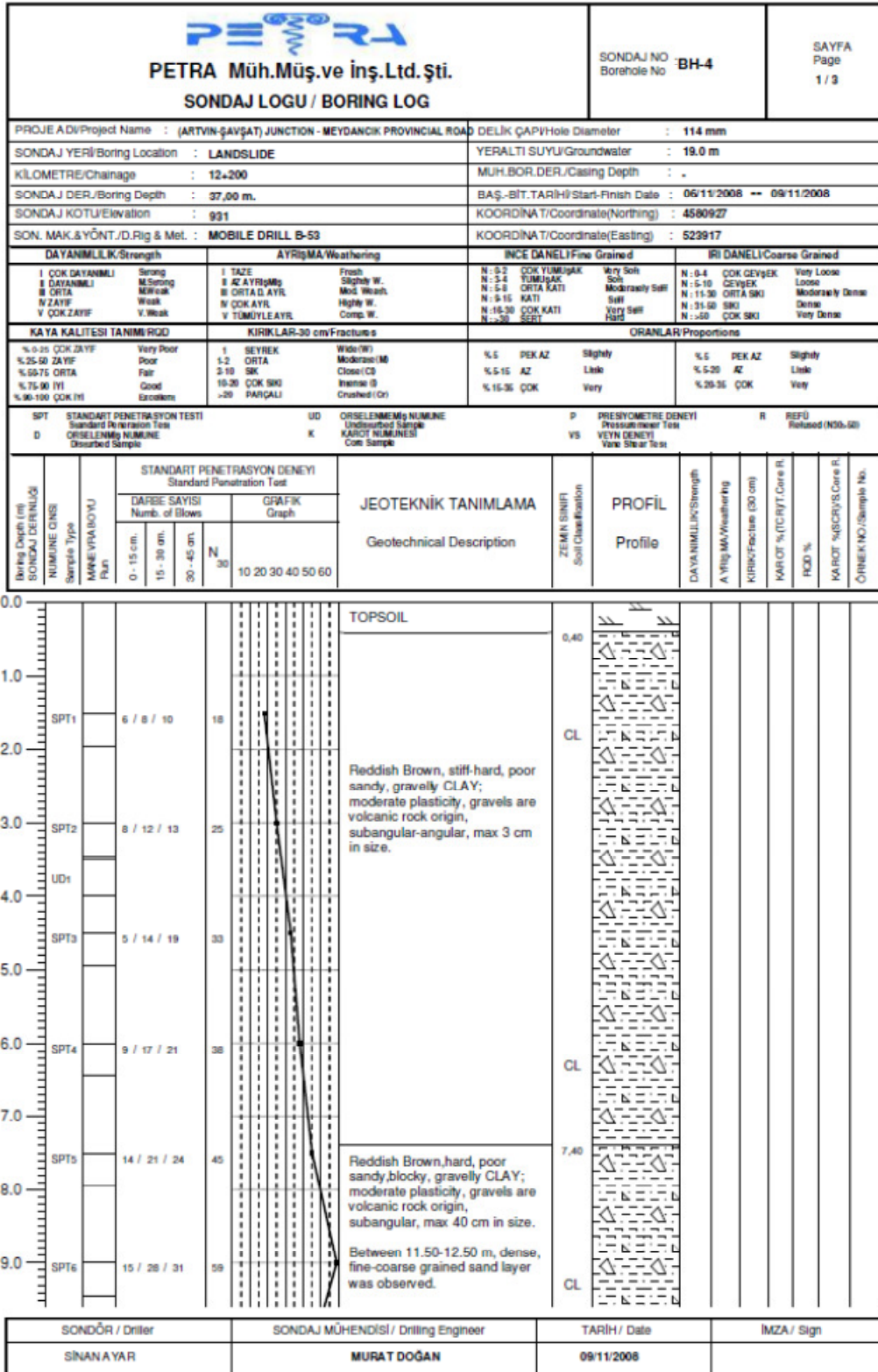


Figure A.8 Borehole No.4 (Page 1)

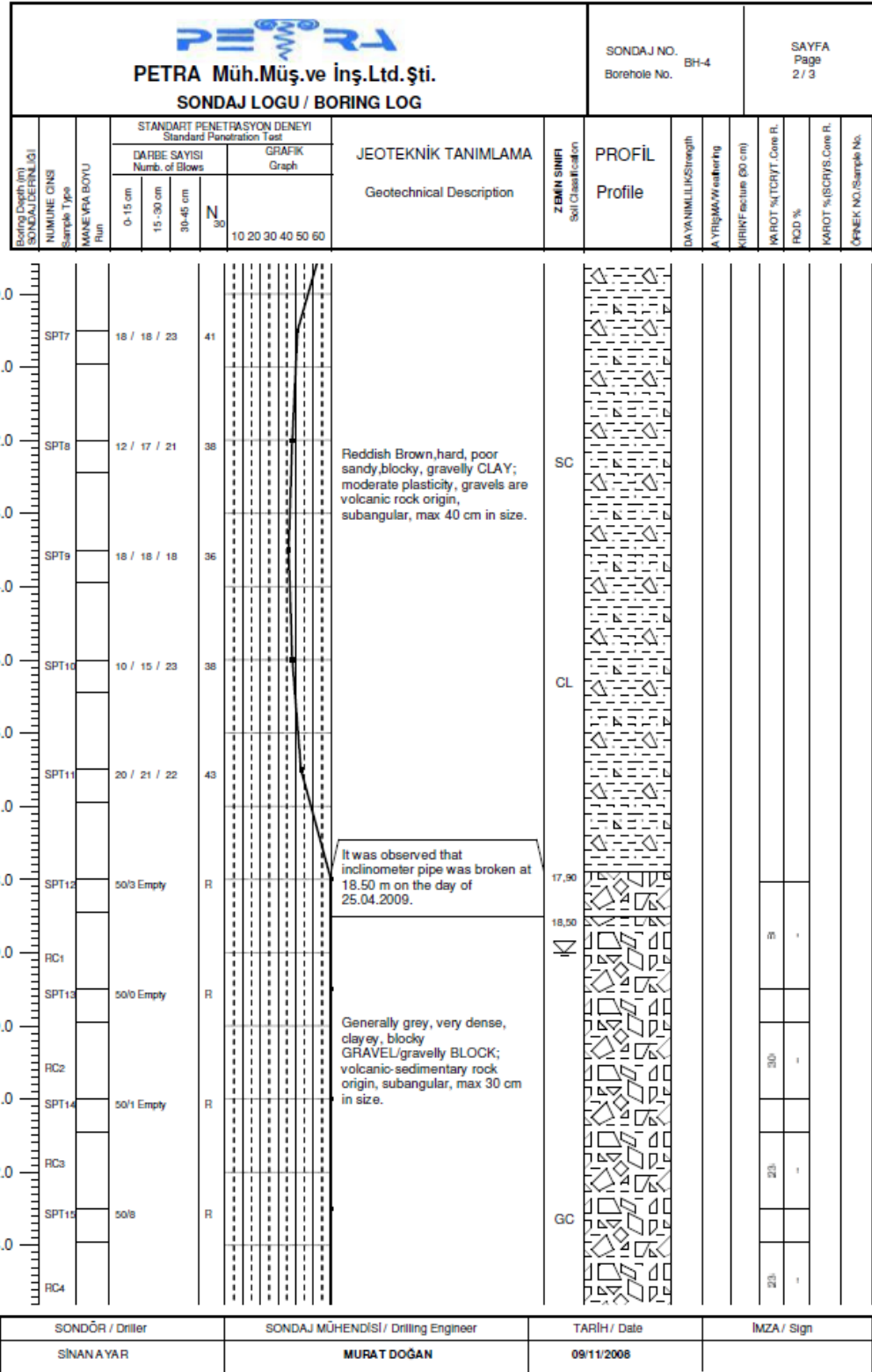


Figure A.9 Borehole No.4 (Page 2)


 PETRA Müh.Müş.ve İnş.Ltd.Şti. SONDAJ LOGU / BORING LOG				SONDAJ NO. Borehole No. BH-4		SAYFA Page 3 / 3												
Kuyu Derinliği (m) SONDAJ DERİNLİĞİ	NUMUNE ÖLÇÜSÜ Sample Type	MANİFRA BOYU Flut	STANDART PENETRASYON DENEYİ Standard Penetration Test				JEOTEKNİK TANIMLAMA Geotechnical Description	ZEMİN SINIFI Soil Classification	PROFİL Profile	DAYANIMLILIK Strength	AYRILMA Weathering	SİBRİT Settlement (90 cm)	% RÖT % RCTRYT	% RÖT % RCTRYT	% RÖT % RCTRYT	% RÖT % RCTRYT	% RÖT % RCTRYT	
			DARBE SAYISI Numb. of Blows		GRAFİK Graph													
			0-15 cm	15-30 cm	30-45 cm	N ₃₀	10 20 30 40 50 60											
24.0	SPT16	50/2 Empty	R															
25.0	RC5																	
26.0	SPT17	50/6 Empty	R															
27.0	RC6																	
27.0	SPT18	50/3 Empty	R															
28.0	RC7																	
29.0	SPT19	50/0 Empty	R															
29.0	RC8																	
30.0	SPT20	29 / 50/8	R															
31.0	RC9																	
32.0	SPT21	31 / 50/10	R															
32.0	RC10																	
33.0	RC11																	
34.0	RC12																	
35.0	RC13																	
36.0																		
37.0																		
38.0																		
SONDÖR / Driller			SONDAJ MÜHENDİSİ / Drilling Engineer			TARİH / Date			İMZA / Sign									
SİNAN AYAR			MURAT DOĞAN			09/11/2008												

Figure A.10 Borehole No.4 (Page 2)

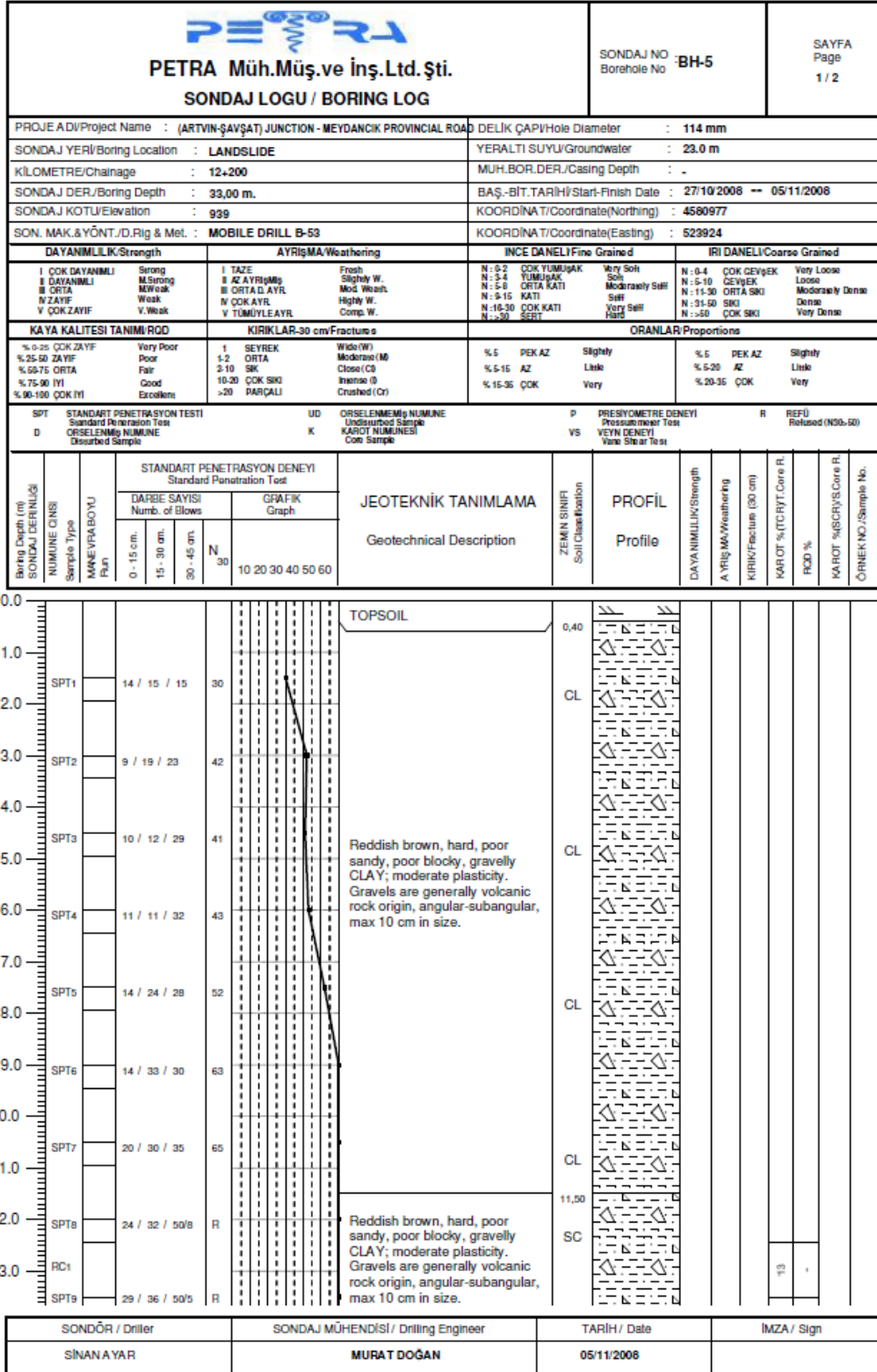


Figure A.11 Borehole No.5 (Page 1)

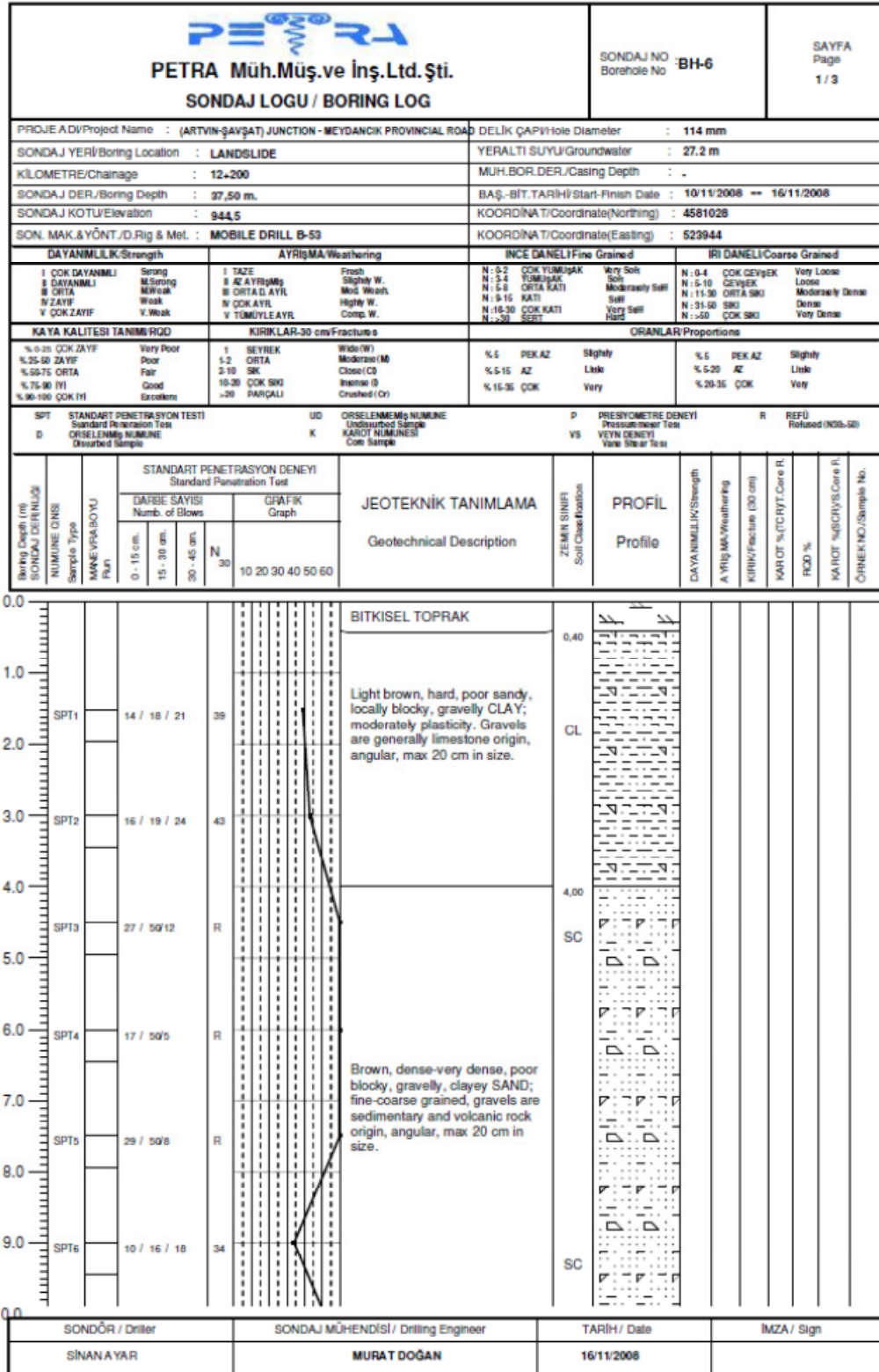


Figure A.13 Borehole No.6 (Page 1)

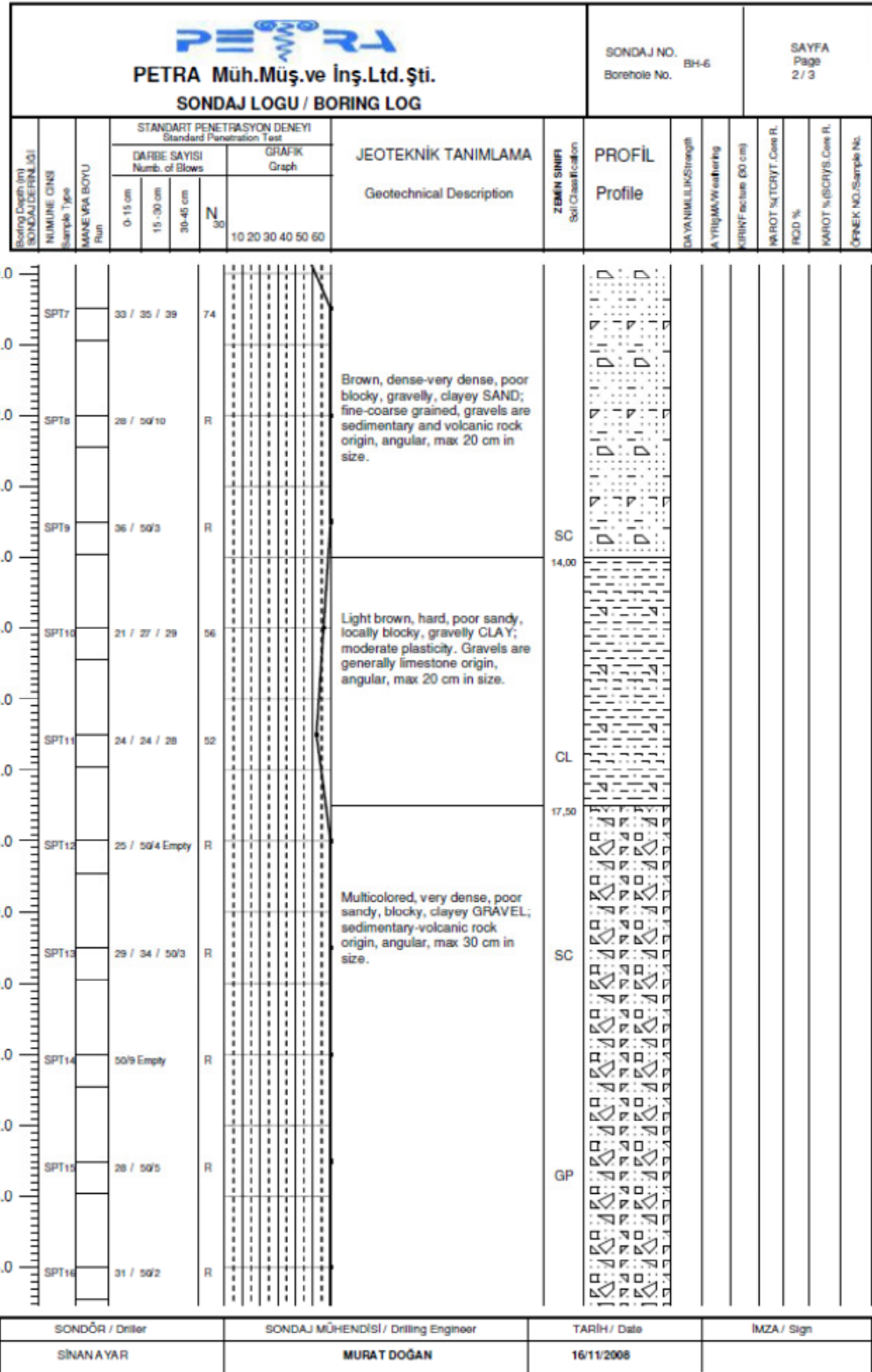

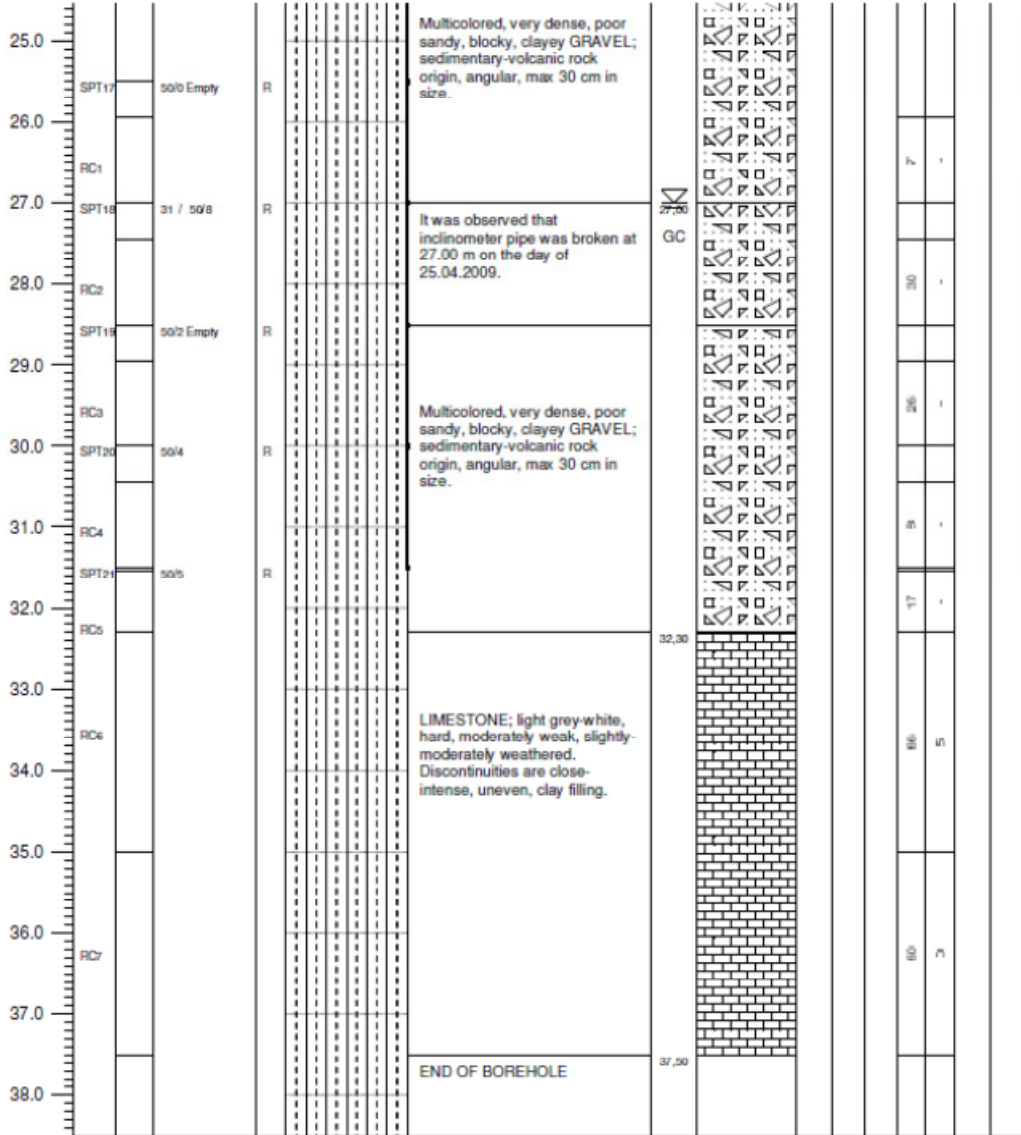


Figure A.14 Borehole No.6 (Page 2)

 PETRA Müh.Müş.ve İnş.Ltd.Şti. SONDAJ LOGU / BORING LOG				SONDAJ NO. BH-6 Borehole No.		SAYFA Page 3 / 3						
Boring Depth (m) SONDAJ DERİNLİĞİ NUMARALI ÇUKUR Sample Type	STANDART PENETRASYON DENEYİ Standard Penetration Test	DARBE SAYISI Numb. of Blows		GRAFIK Graph	JEOTEKNİK TANIMLAMA Geotechnical Description	ZEMİN SINIFI Soil Classification	PROFİL Profile	DAYANIMLI İNŞİTİRENG A YERİNEK/Weathering	KIRINTI ÇUKUR (30 cm) KIRINTI ÇUKURU (30 cm)	KIRINTI ÇUKURU (%) KIRINTI ÇUKURU (%)	KIRINTI ÇUKURU (%) KIRINTI ÇUKURU (%)	ÇİPNEK NO./Sample No.
		0-15 cm 15-30 cm 30-45 cm N 10 20 30 40 50 60										



SONDÖR / Driller	SONDAJ MÜHENDİSİ / Drilling Engineer	TARİH / Date	İMZA / Sign
SINAN AYAR	MURAT DOĞAN	16/11/2008	

Figure A.15 Borehole No.6 (Page 3)

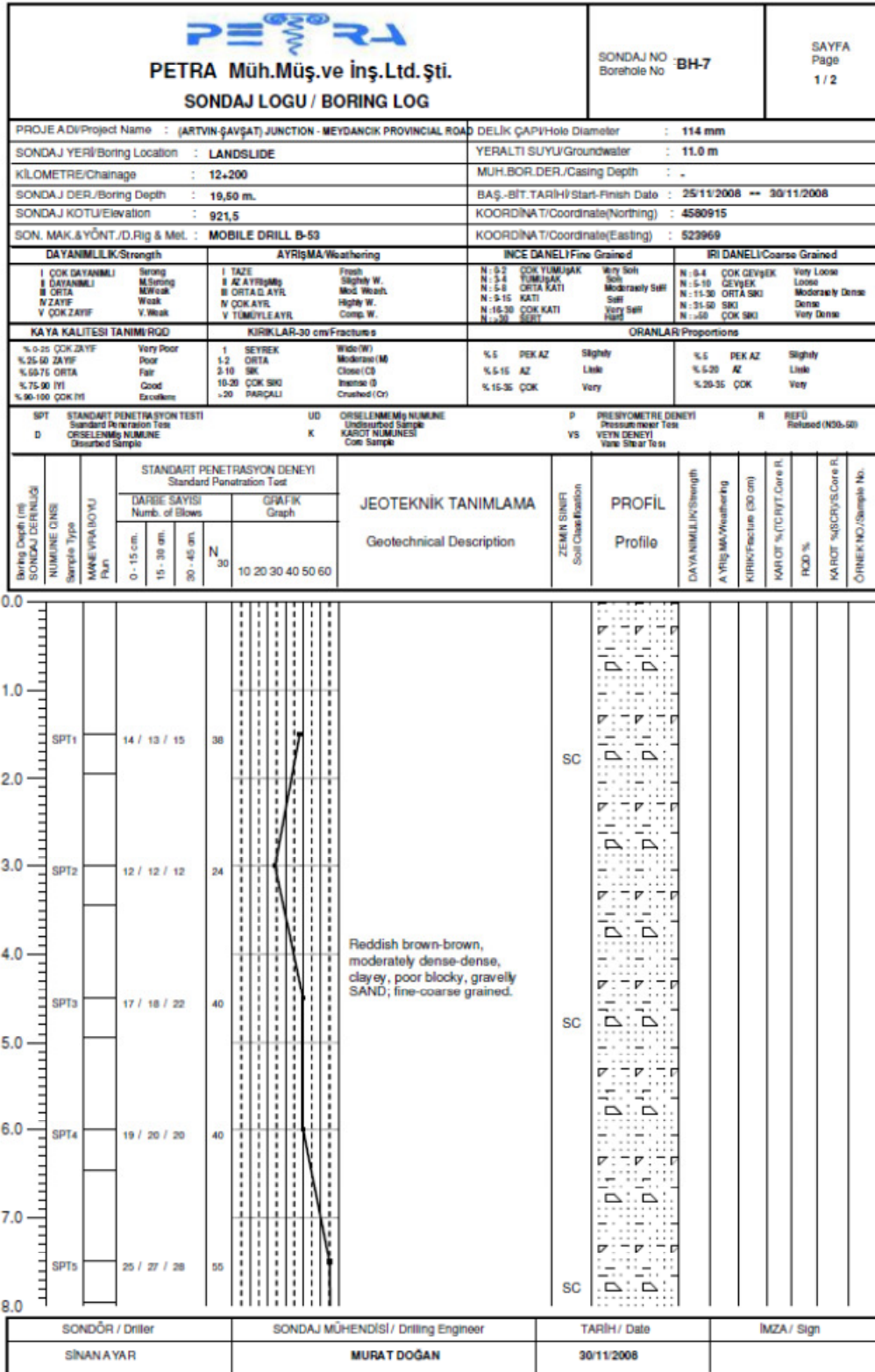

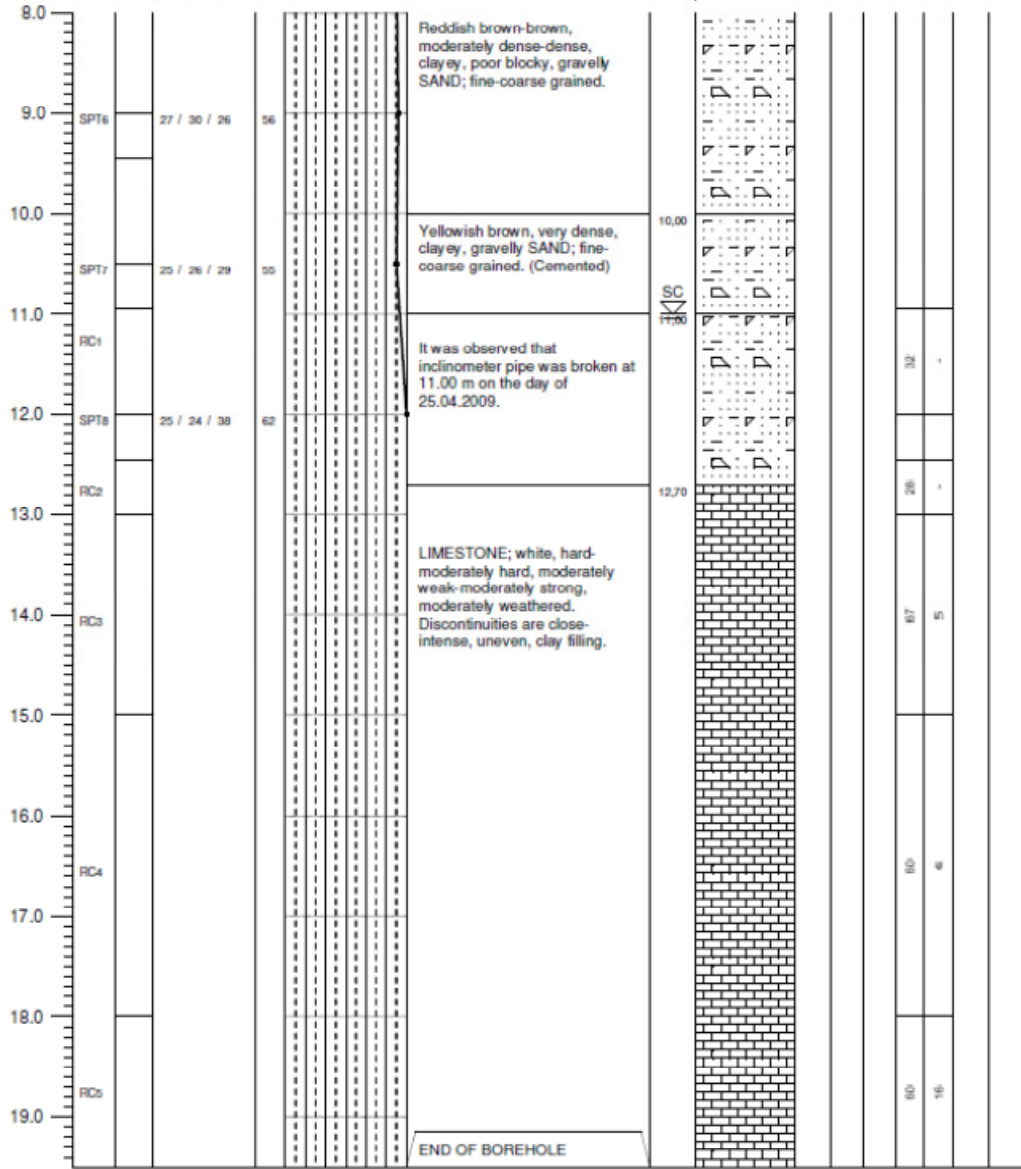


Figure A.16 Borehole No.7 (Page 1)

 PETRA Müh.Müş.ve İnş.Ltd.Şti. SONDAJ LOGU / BORING LOG				SONDAJ NO. BH-7 Borehole No.		SAYFA Page 2 / 2								
Boring Depth (m) SONDAJ DERİNLİĞİ	NUMARALI ÖRNEK Sample Type	MAMULETİNİN BOYU Run	STANDART PENETRASYON DENEYİ Standard Penetration Test		JEOTEKNİK TANIMLAMA Geotechnical Description	ZEMİN SINIFI Soil Classification	PROFİL Profile	DAVANIMLIK GÜCÜ Strength	AYRILMA VE YERLEŞİM Weathering	KIRILMA DERİNLİĞİ (cm) Fracture Depth (cm)	KAROT % (TCRYT) Core R.	HGD %	KAROT % (SCHRYS) Core R.	ÖRNEK NO./Sample No.
			DARBE SAYISI Numb. of Blows	GRAFIK Graph										
			0-15 cm	15-30 cm	30-45 cm	N ₃₀	10 20 30 40 50 60							



SONDÖR / Driller	SONDAJ MÜHENDİSİ / Drilling Engineer	TARİH / Date	İMZA / Sign
SİNAN AYAR	MURAT DOĞAN	30/11/2008	

Figure A.17 Borehole No.7 (Page 2)

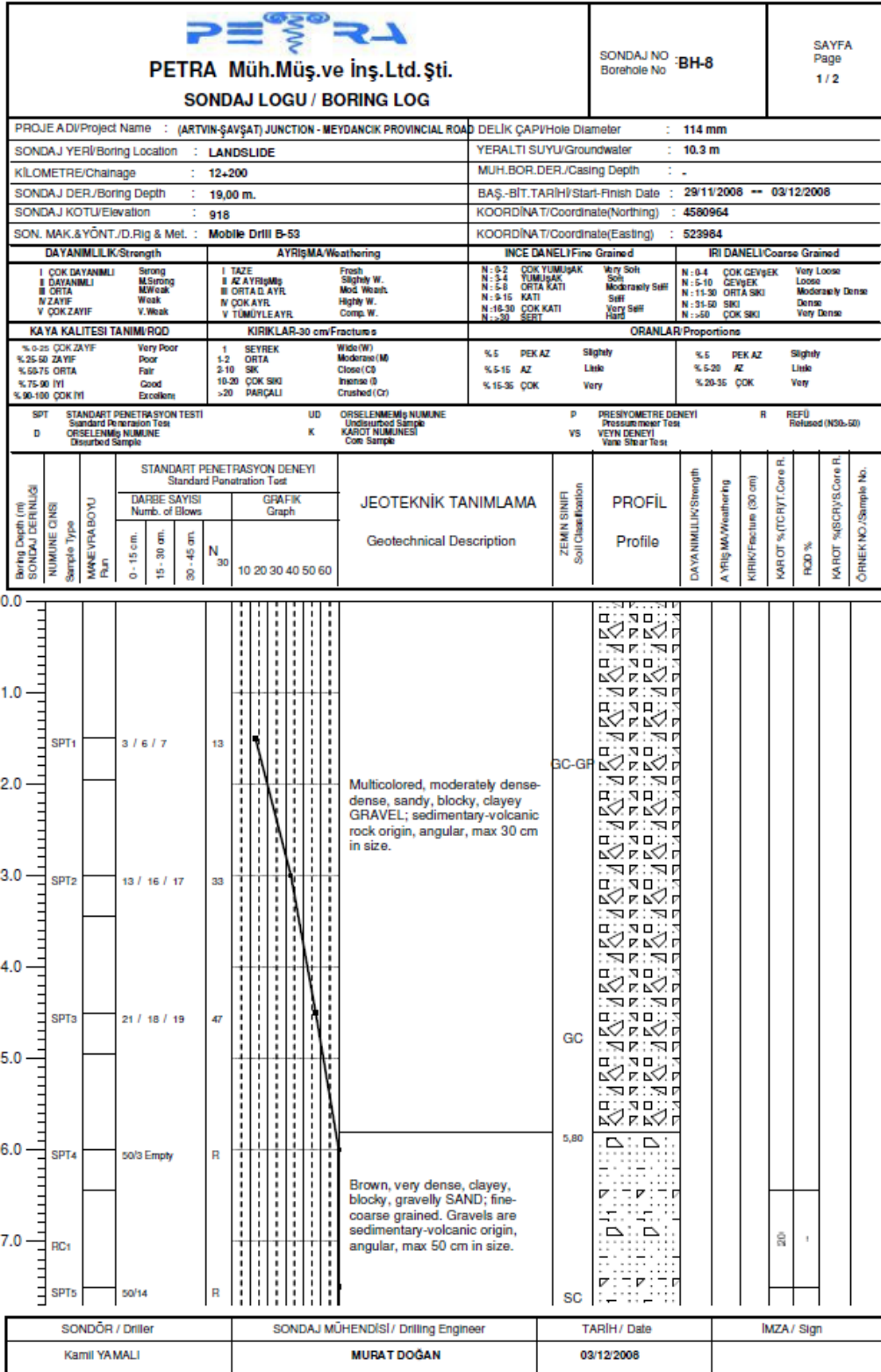


Figure A.18 Borehole No.8 (Page 1)

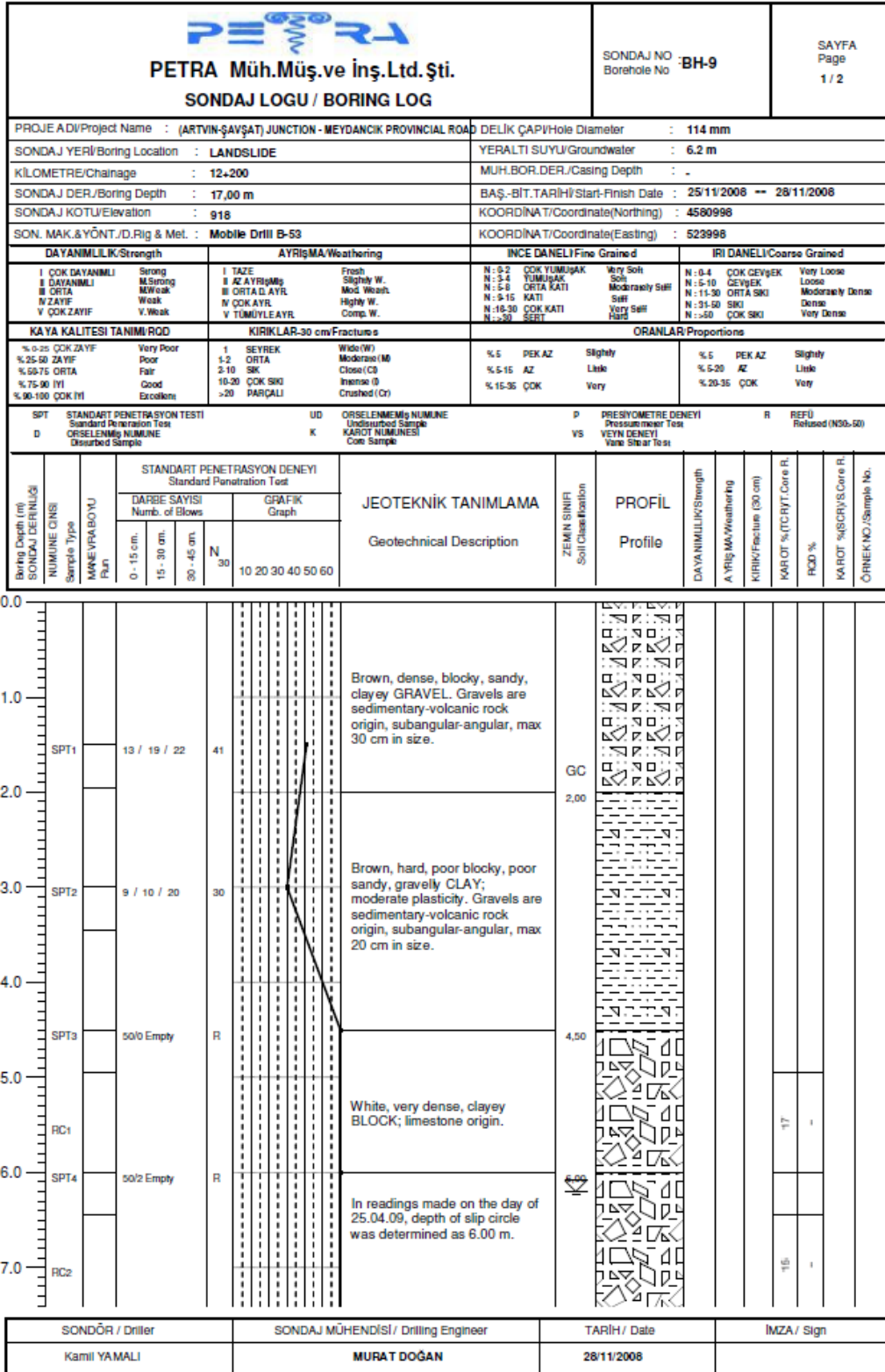
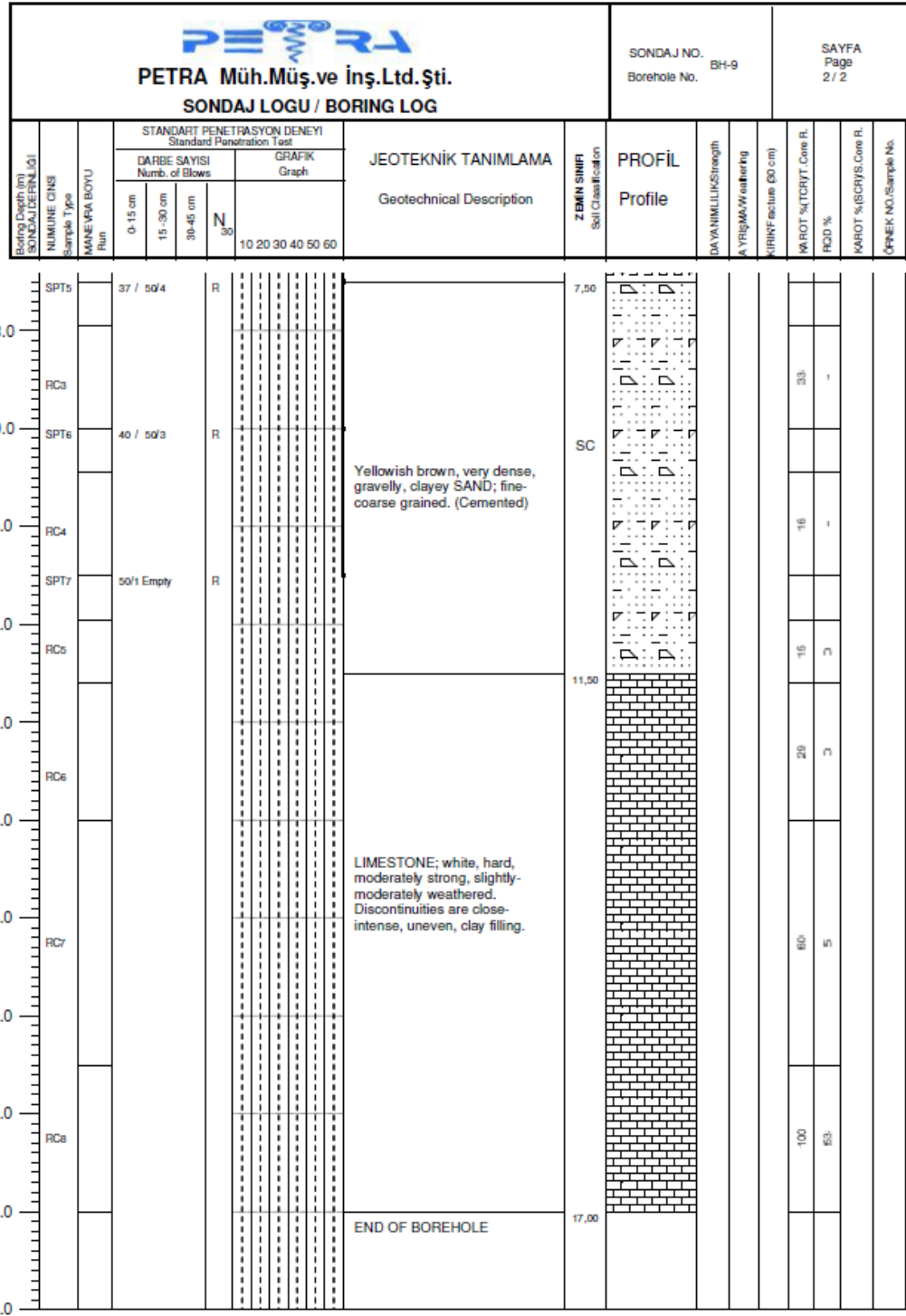


Figure A.20 Borehole No.9 (Page 1)



SONDÖR / Driller	SONDAJ MÜHENDİSİ / Drilling Engineer	TARİH / Date	İMZA / Sign
Kamil YAMALI	MURAT DOĞAN	28/11/2008	

Figure A.21 Borehole No.9 (Page 2)

APPENDIX B

CORE BOX PHOTOS



Figure B.1 BH-1, core box no: 1/4

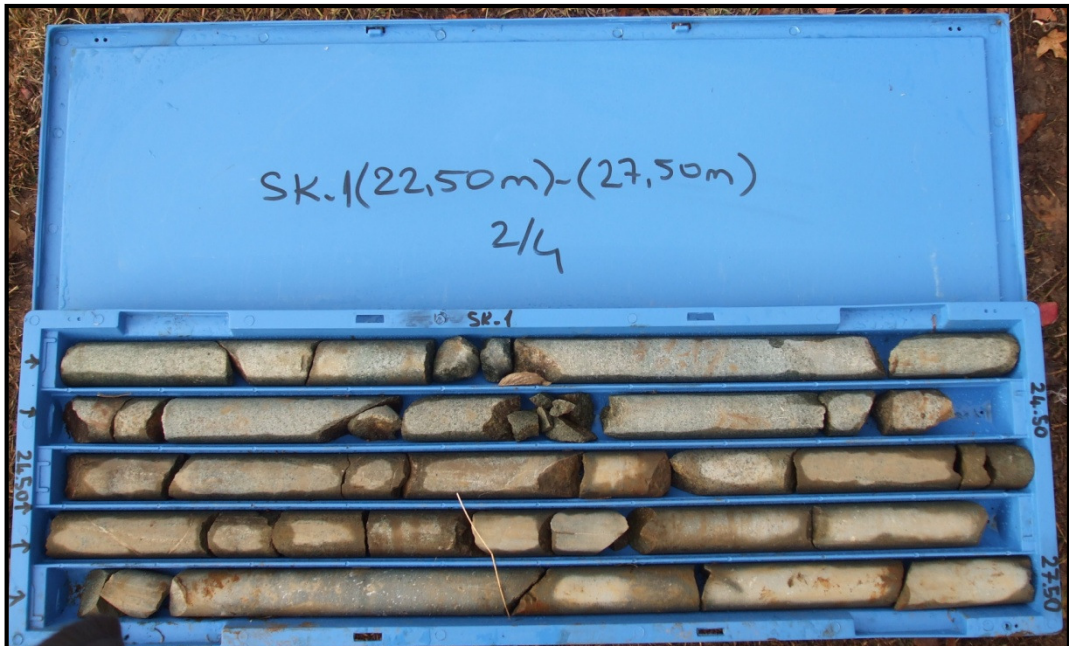


Figure B.2 BH-1, core box no: 2/4



Figure B.3 BH-1, core box no: 3/4



Figure B.4 BH-1, core box no: 4/4

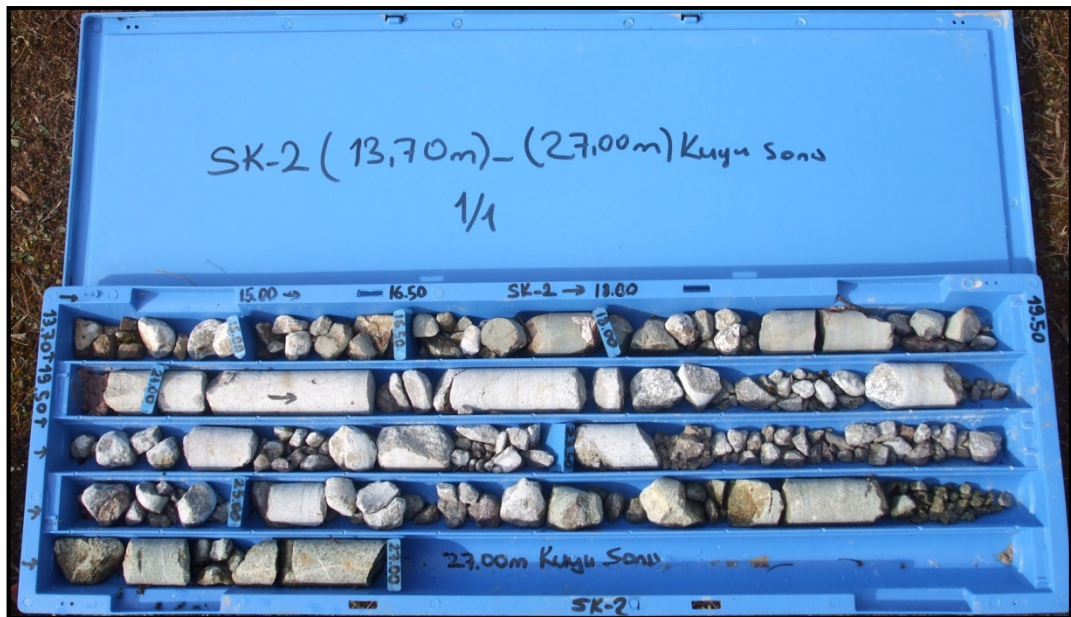


Figure B.5 BH-2, core box no: 1/1

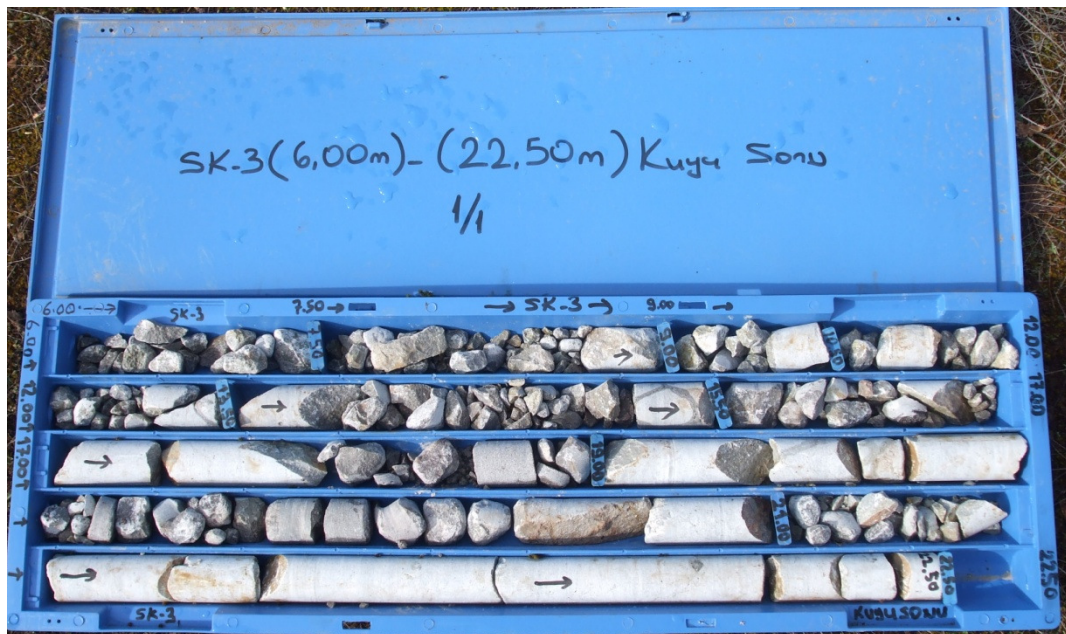


Figure B.6 BH-3, core box no: 1/1



Figure B.7 BH-4, core box no: 1/2

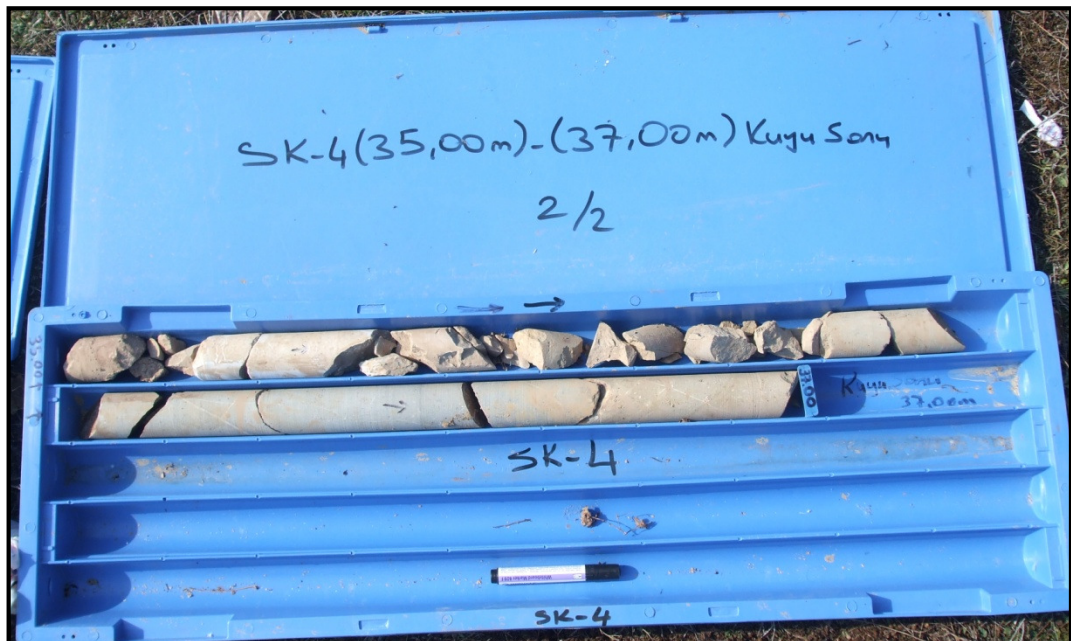


Figure B.8 BH-4 core box no: 2/2

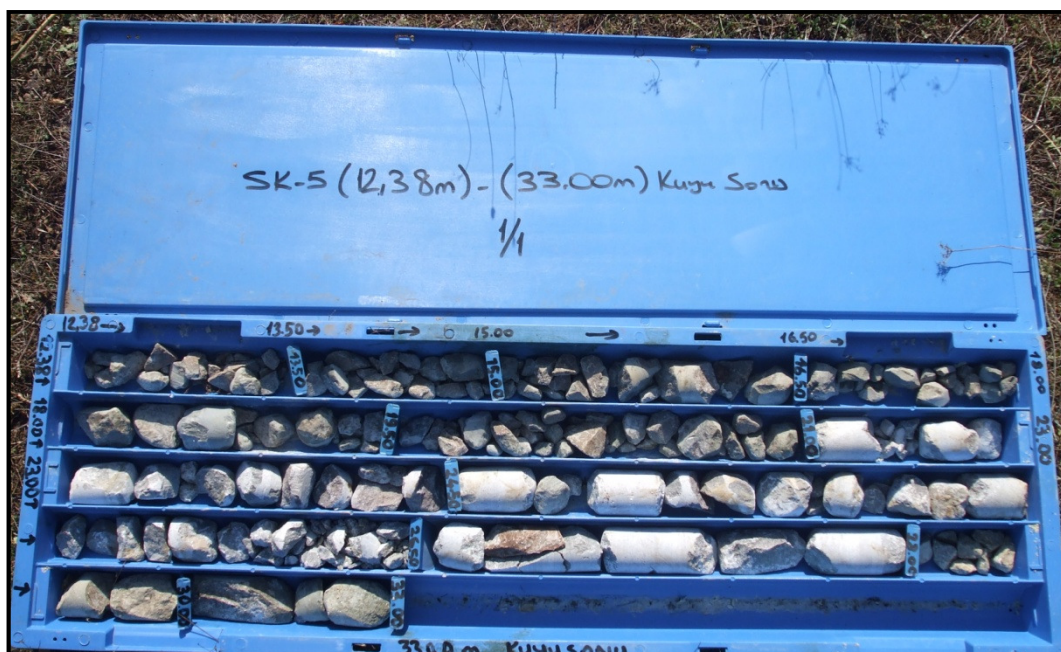


Figure B.9 BH-5, core box no: 1/1



Figure B.10 BH-6, core box no: 1/1



Figure B.11 BH-7, core box no: 1/1



Figure B.12 BH-8, core box no: 1/1

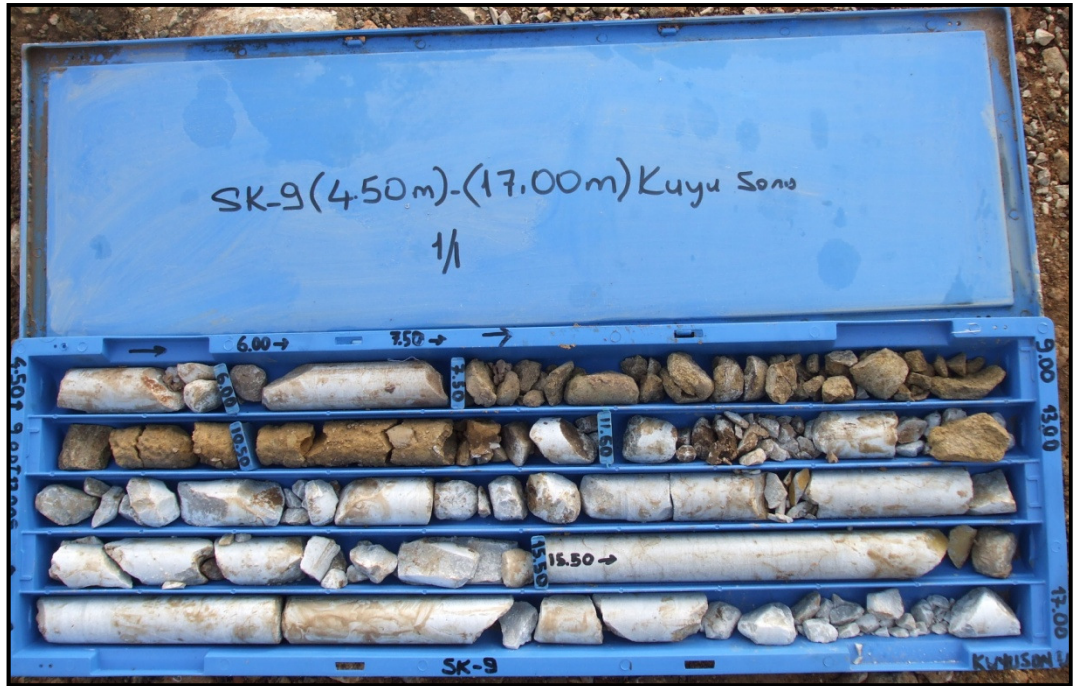


Figure B.13 BH-9, core box no: 1/1

APPENDIX C

SOIL LABORATORY TEST RESULTS

EF EFOL JEOTEKNİK HİZMETLER TİCARET LİMİTED ŞTİ. Çarşamba Sokakı No: 47, 54, 101, 102, Çarşamba Tel: (0312) 341 01 15 Fax: (0312) 341 01 52		RAPOR NO : NUMUNE GELİŞ TARİHİ:		TARİH DENEY TA																				
DENEY YAPILIRAN KURULUŞ : PETRA MİN. MÜŞ. LİD. ŞİRKETİ		Ek : sayfa deney sonucu raporu of test results		03.02.2010																				
DENEY SONUÇLARI ÖZET TABLOSU / LABORATORY TEST RESULTS TABLE																								
Kuyu No / BH No	Derinlik / Depth	Elek Analizi / Sieve Analysis			Atterberg Limit / Limits			USCS Bölgeleşme Zemin Sınıfı / Unified Soil Classification System	Su Oranı / Water Content	Doğal B.A. / Natural U.W.	Kuru B.A. / Dry U.W.	% Boy Kısalmaları / % Deformation	Deney Tipi / Test Type	c	Ø	Derece / Degree	Konsolidasyon / Consolidation		Hidrometri / Hydrometer	Prokter / Proctor Test		Nokta Yükleme İnd / Point Load Index		
		#4	#10	#40	#200	LL	PL										PI	Oran / Void Ratio		Oran / Natural Void Ratio	% Ağırlık Kaybı / % Weight Loss		0-076	0-002
BH-1	SPT-1 1,50-1,95	90	83	62	40	43	18	25	SC	14									40	22				
	SPT-3 4,50-4,95	87	80	62	44	44	22	22	SC	15									44	32				
	SPT-5 7,50-7,95	76	69	58	49	47	23	24	SC	14									49	30				
	SPT-8 12,00-12,45	65	60	52	44	37	15	22	SC	15														
	UD-1 15,00-15,50	88	67	40	31	32	16	15	SC	14	17,91													
BH-2	SPT-1 1,50-1,95	88	77	60	45	33	15	18	SC	14										45	31			
	SPT-3 4,50-4,95	56	51	42	33	31	16	15	GC	12										33	22			
	SPT-6 9,00-9,45	57	48	38	31	35	18	17	GC	10										31	20			
	SPT-8 12,00-12,18	69	53	36	24	25	14	11	SC	13														
	SPT-13 19,50-19,71	69	60	40	27	30	16	14	SC	13														

Laboratuvarımız Bayındırlık ve İskan Bakanlığı Yapı İşleri Genel Müdürlüğü tarafından verilen 11 numaralı "Laboratuvar İçin Belgeleme Sahipleri" / Our Laboratory is having the Permission Certificate given by Ministry of Prosperity and Settlement. Yapılan deneylerde TS 1900-1 ve TS 1900-2 standartları kullanılmaktadır / TS - 1900-1 & 2 are used in tests carried out in our laboratory. Laboratuvarımız örnek alımı ve taşımasından kaynaklanabilecek hatalardan sorumlu değildir. / Laboratory is not responsible from the errors caused by sampling and transportation. Bu deney sonuçları yalnızca test edilen örnek için geçerlidir. / These test results are valid only for the tested sample. Bu deney sonuç tablosu Laboratuvarımız izni olmadan kısmen kopyalanamaz, değiştirilemez. / This test result sheet can not be partially copied or changed without permission of Laboratory.

TESTED BY : Anıl ÖĞRETİM

APPROVEN BY: O. Faruk ÖZTÜRK
Lab. Denetçi Müh.
Belge No: 3654

Figure C.1 Laboratory test results of BH-1 and BH-2

APPENDIX D

INCLINOMETER RESULTS

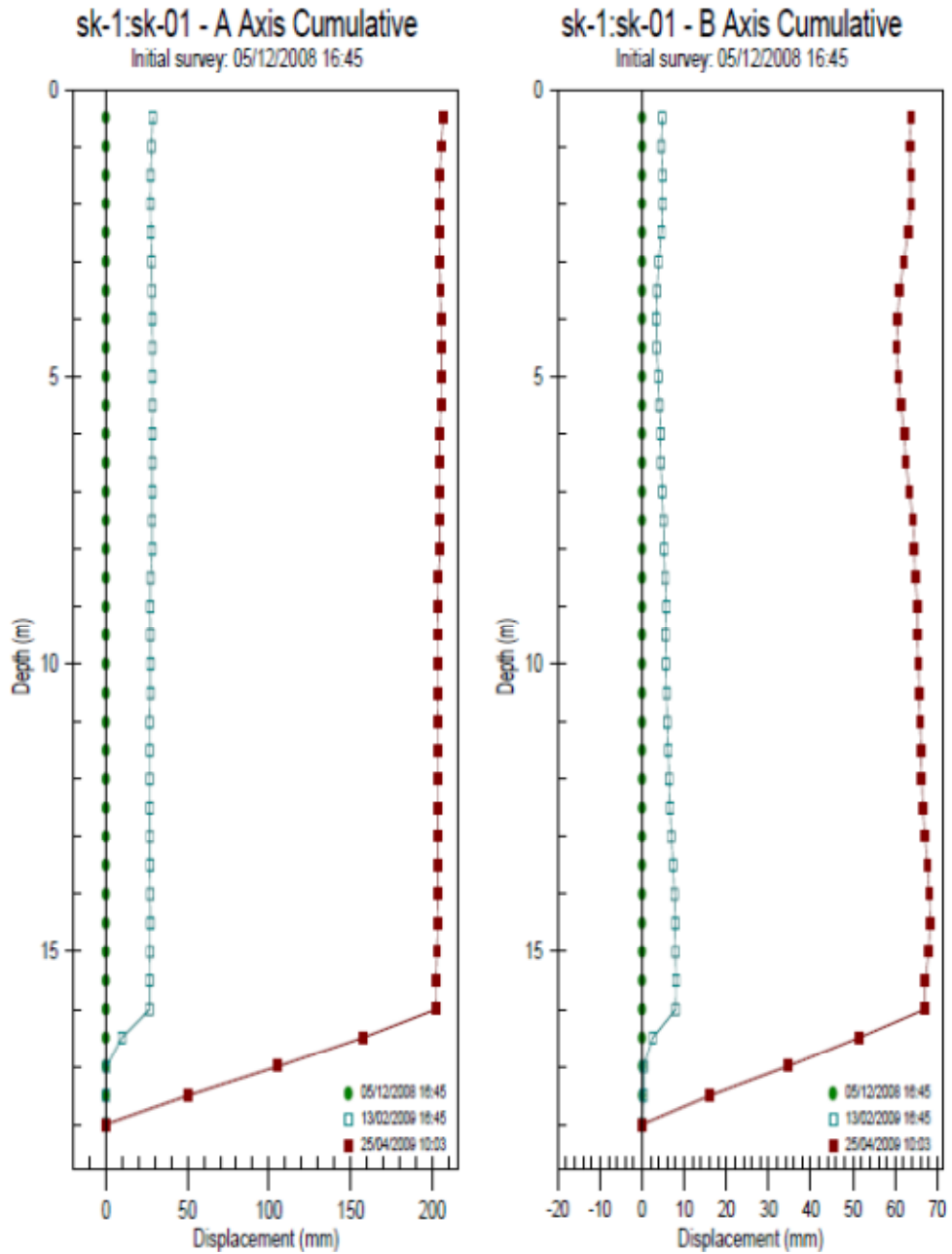


Figure D.1 Cumulative displacement of BH-1

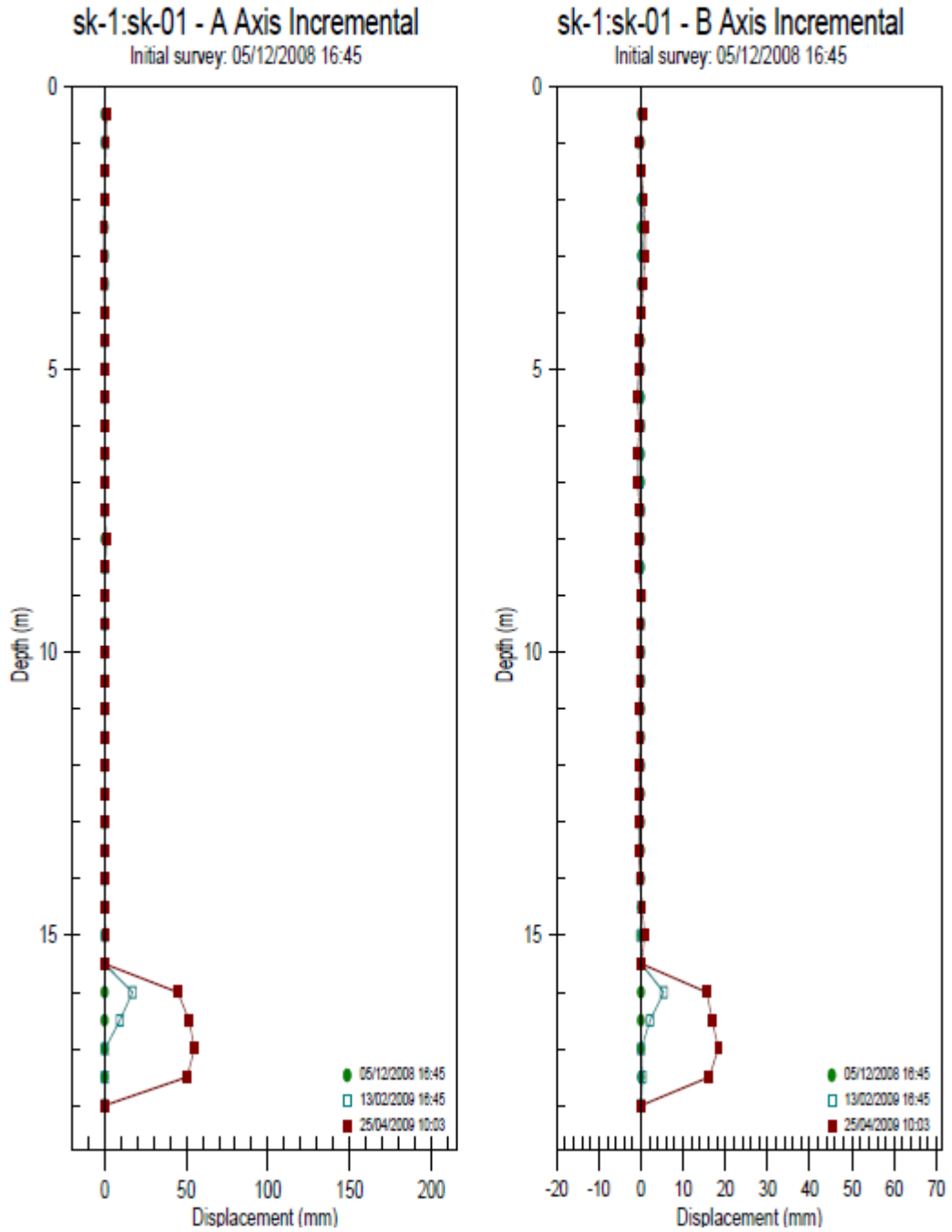


Figure D.2 Incremental displacement of BH-1

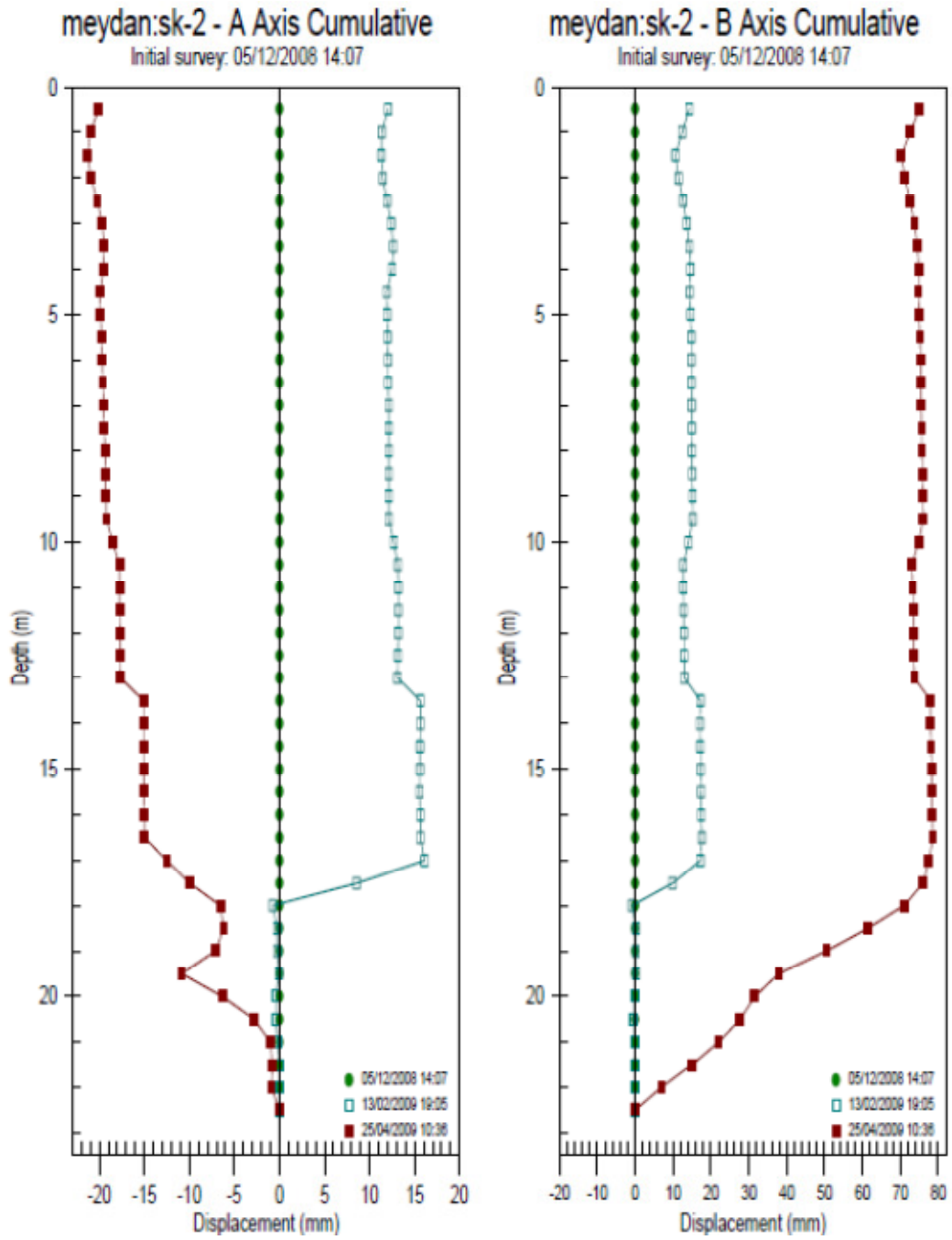


Figure D.3 Cumulative displacement of BH-2

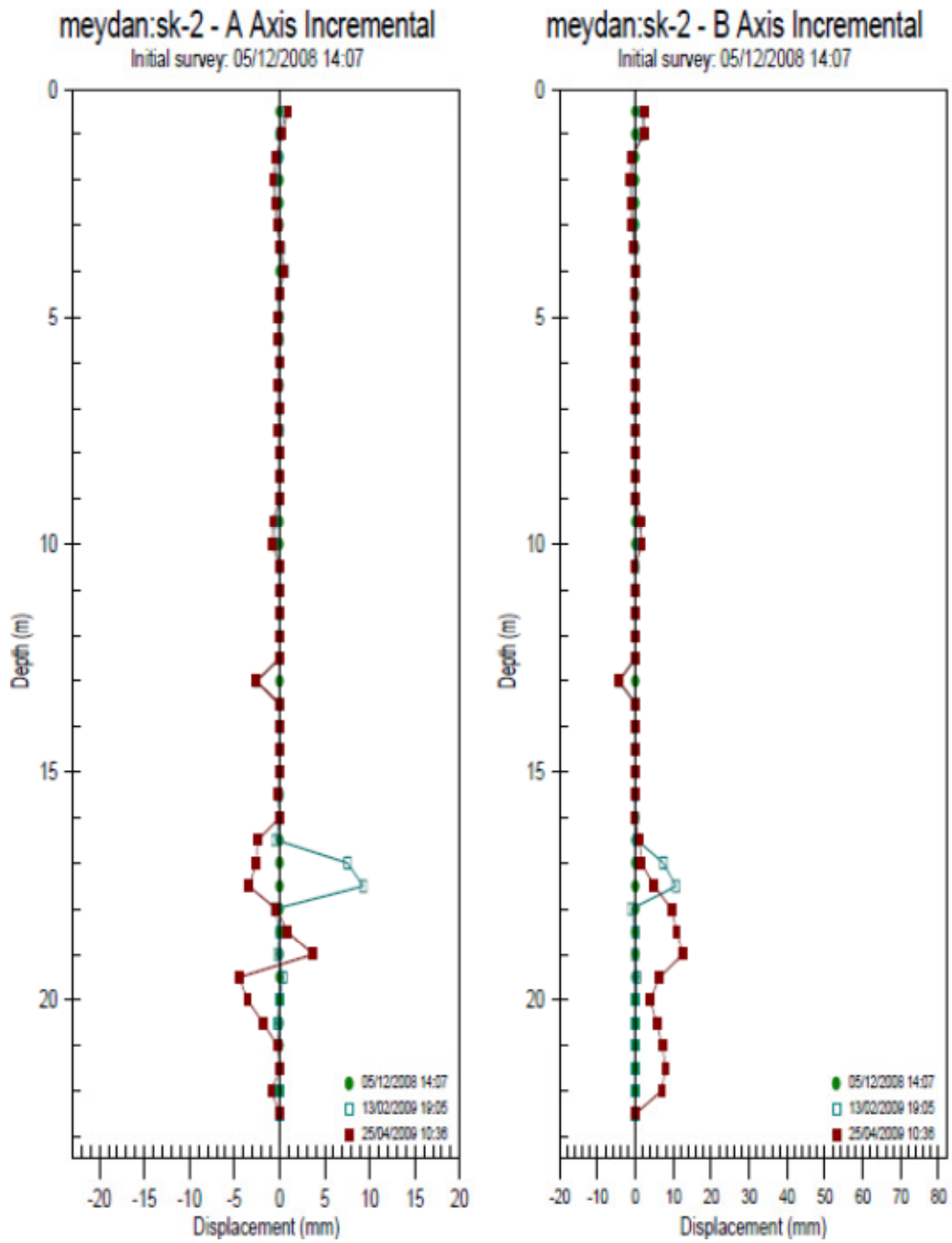


Figure D.4 Incremental displacement of BH-2

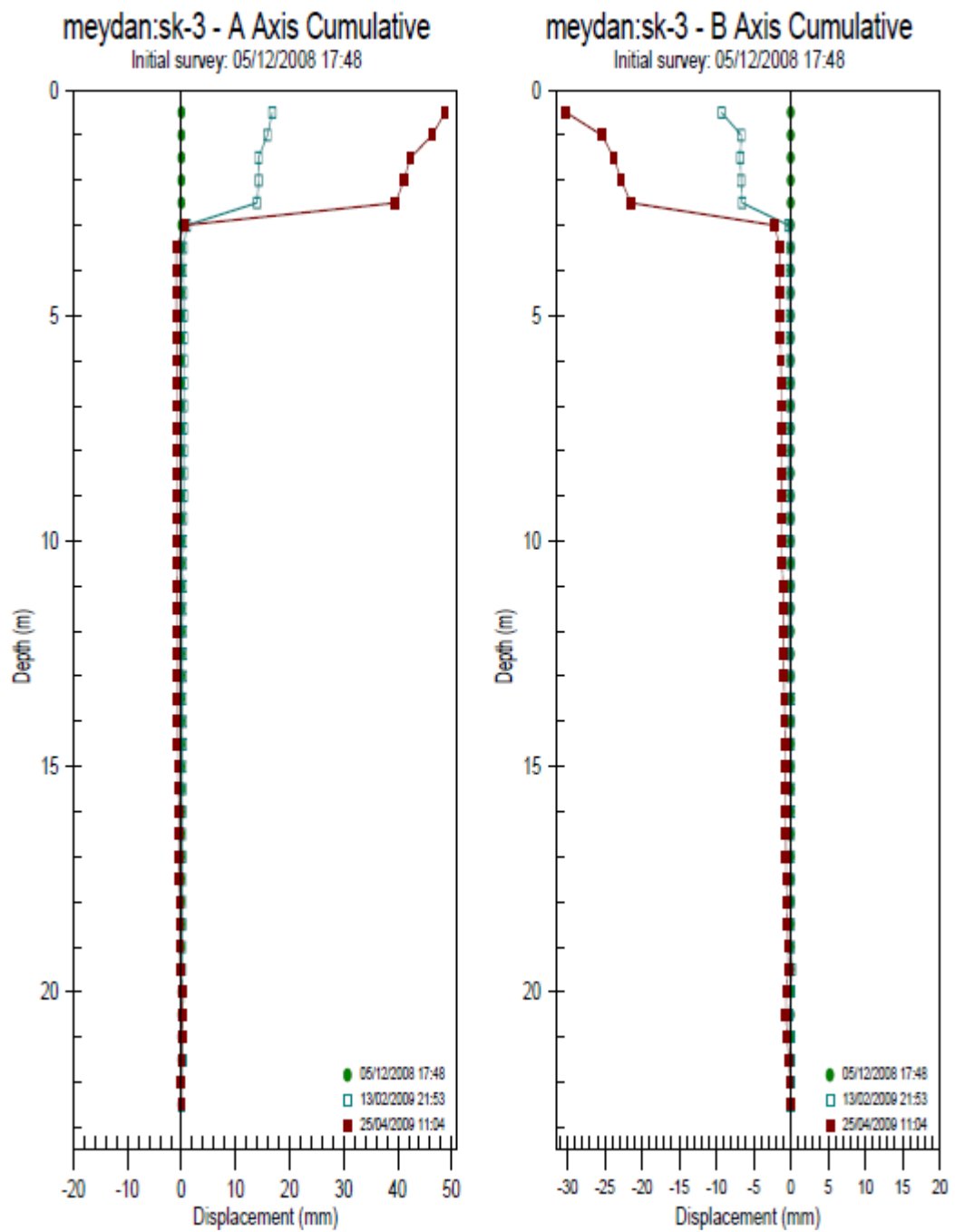


Figure D.5 Cumulative displacement of BH-3

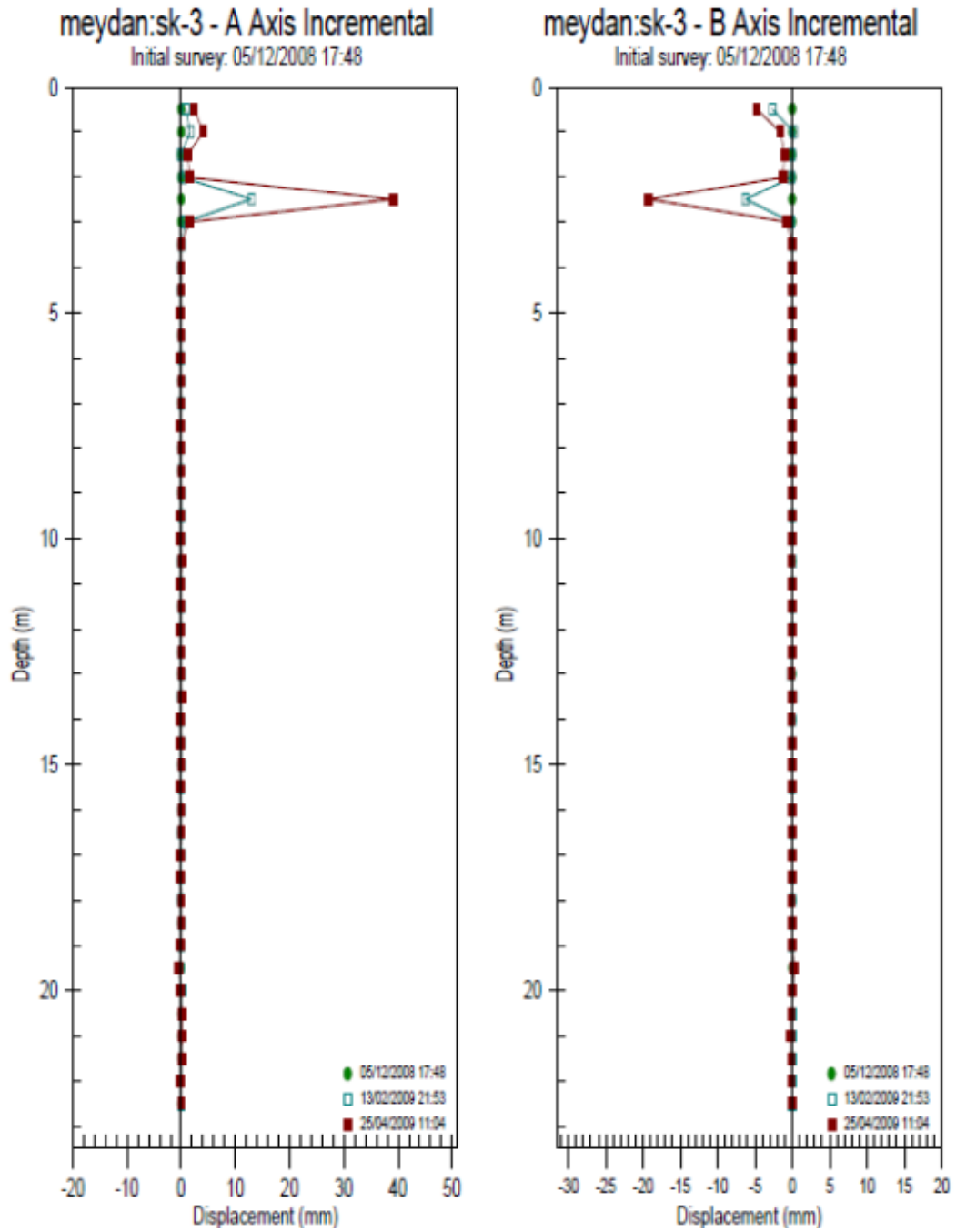


Figure D.6 Incremental displacement of BH-3

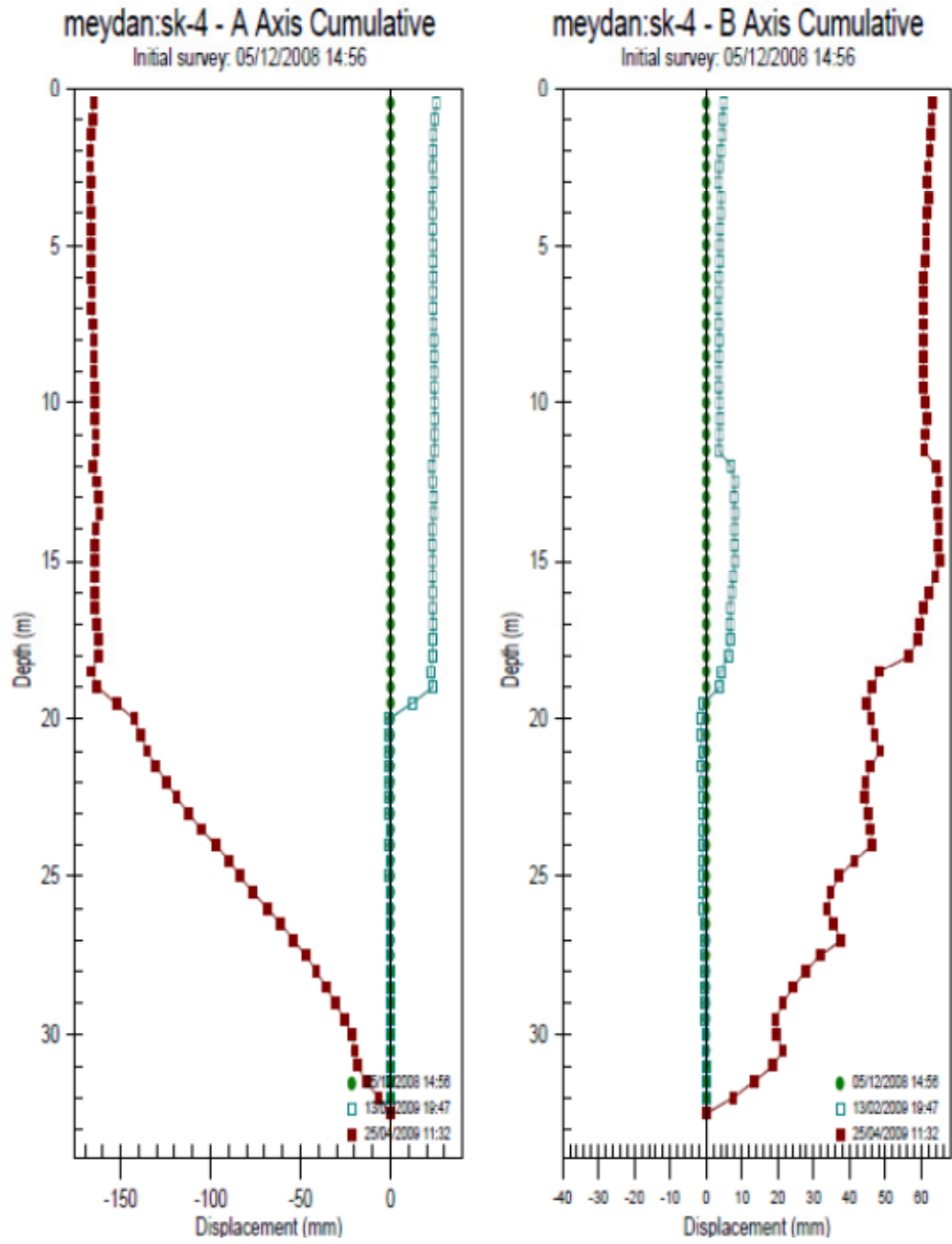


Figure D.7 Cumulative displacement of BH-4

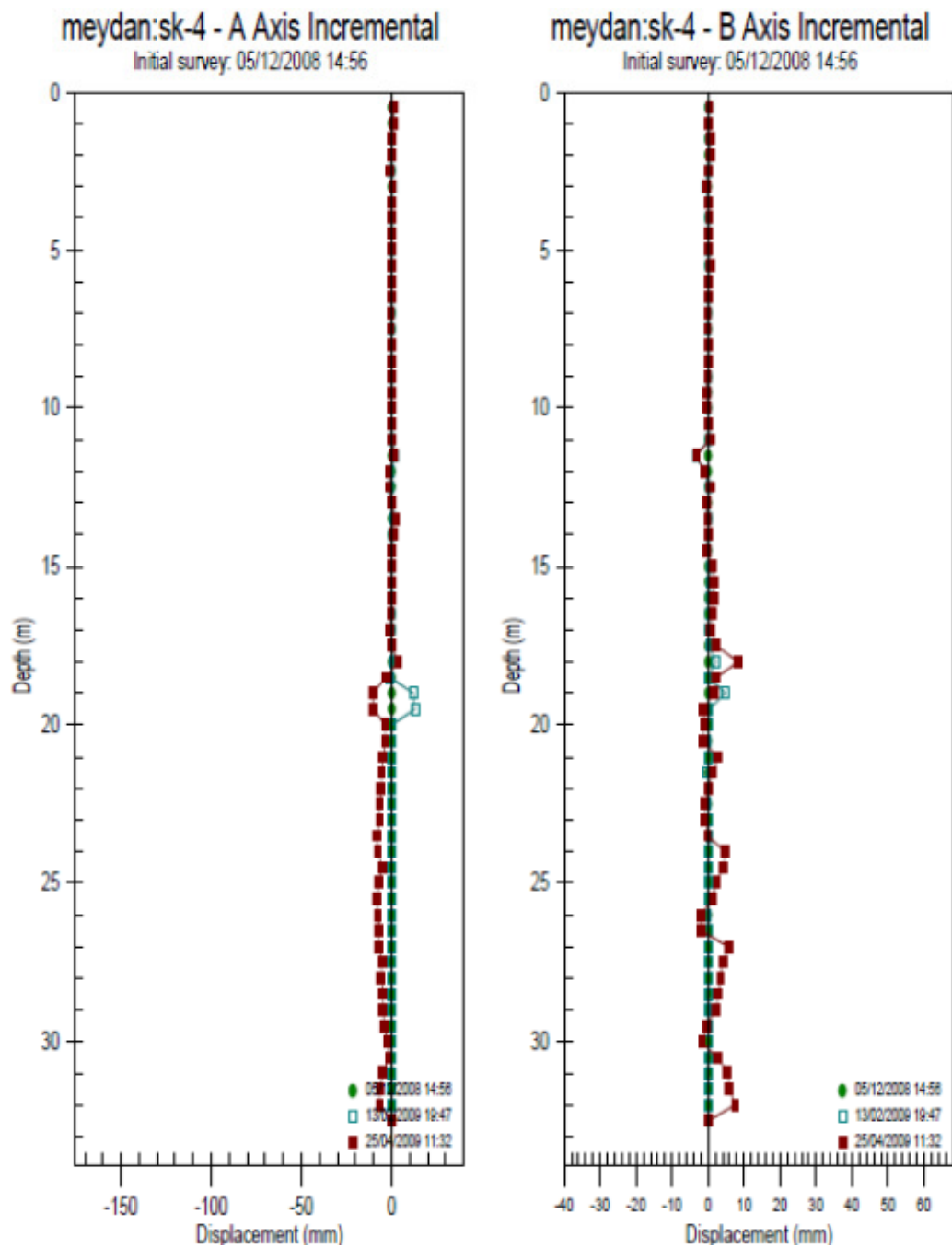


Figure D.8 Incremental displacement of BH-4

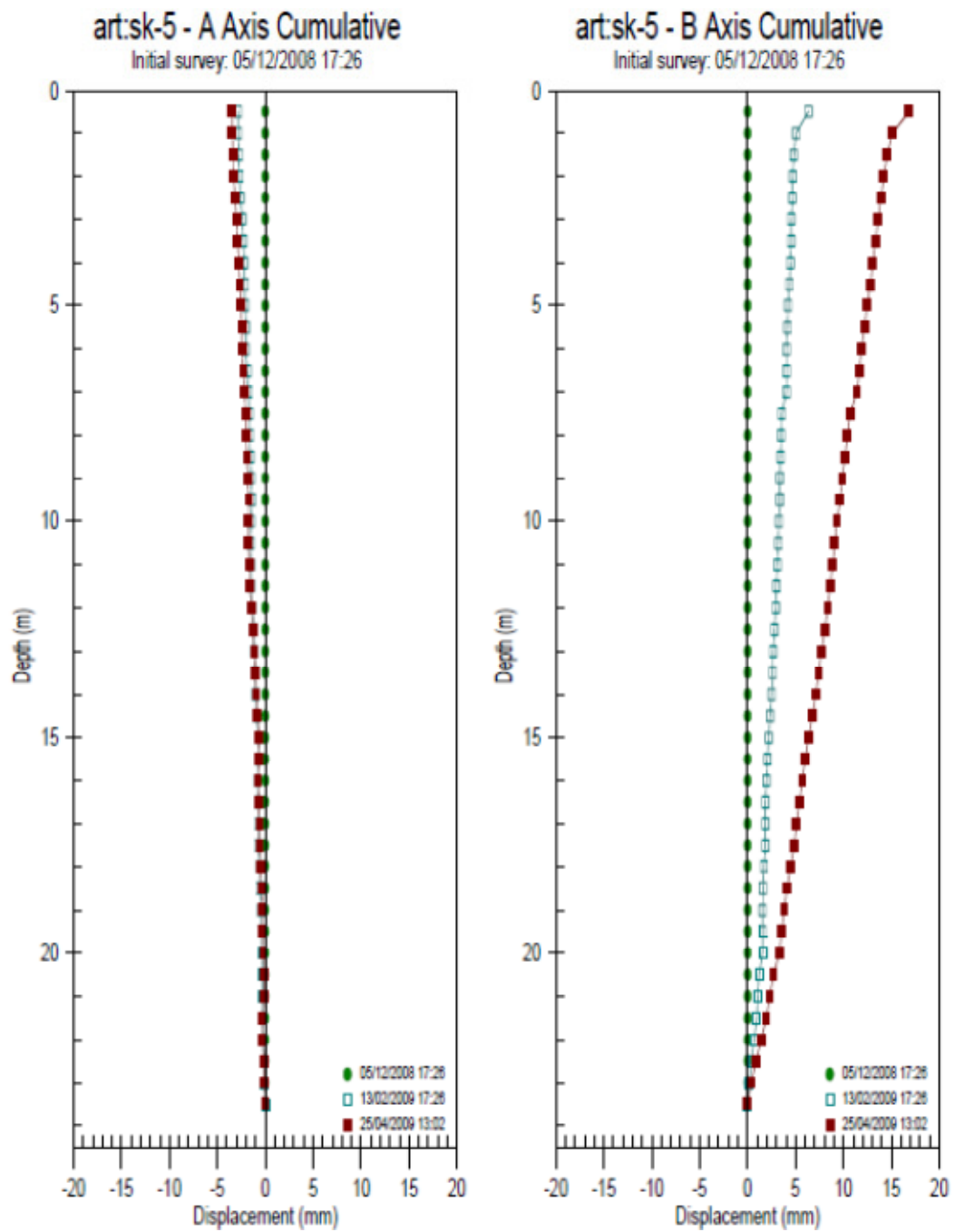


Figure D.9 Cumulative displacement of BH-5

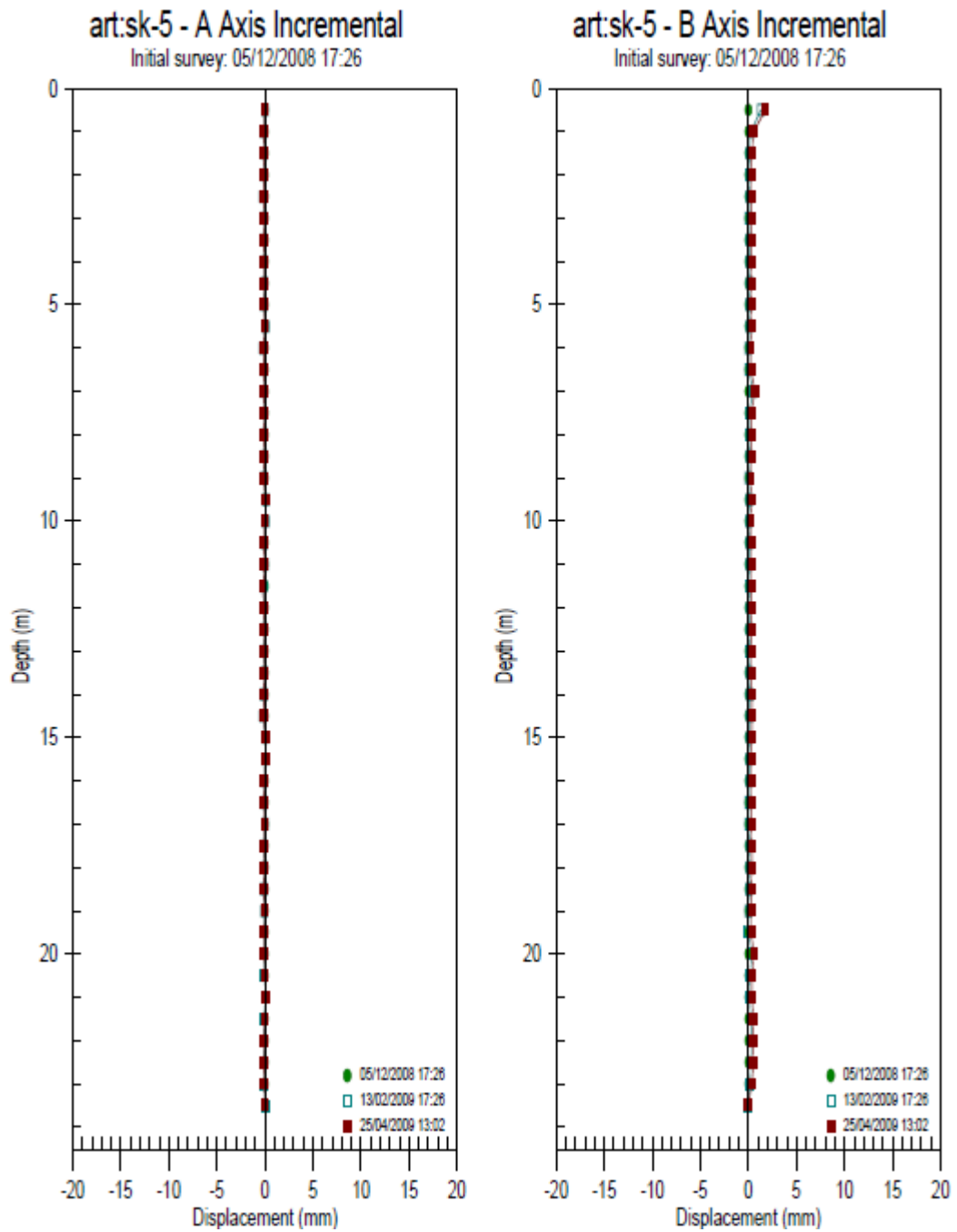


Figure D.10 Incremental displacement of BH-5

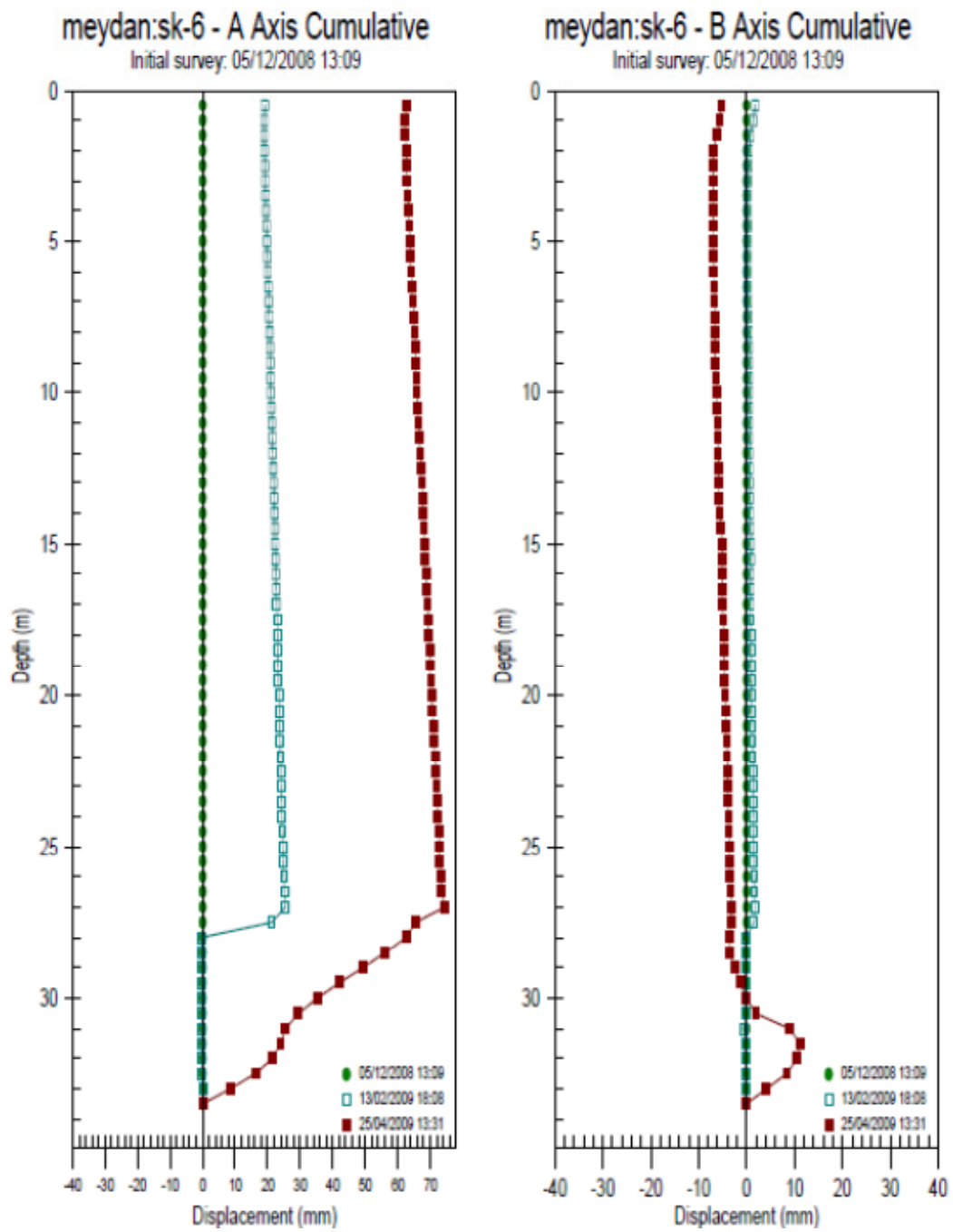


Figure D.11 Cumulative displacement of BH-6

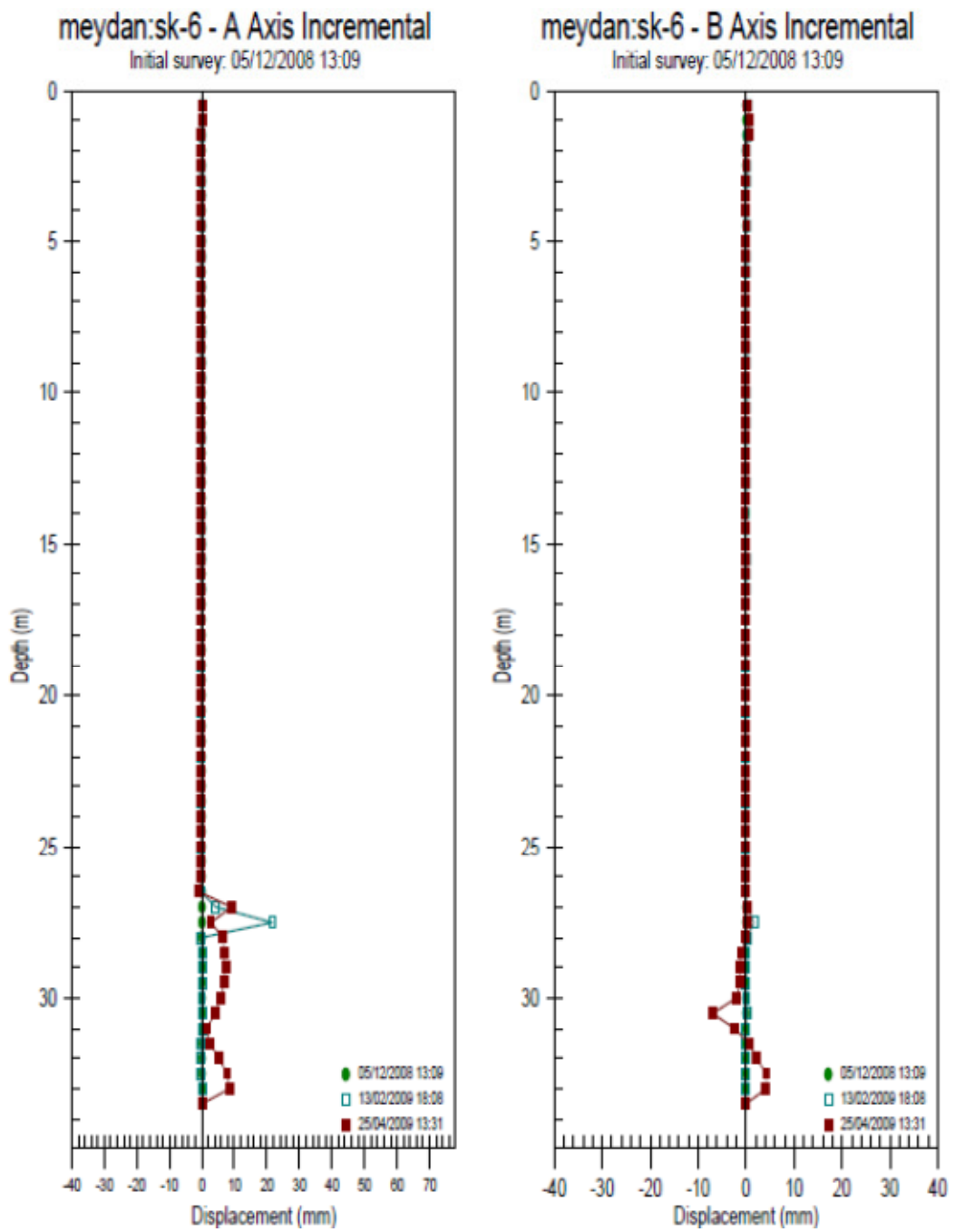


Figure D.12 Incremental displacement of BH-6

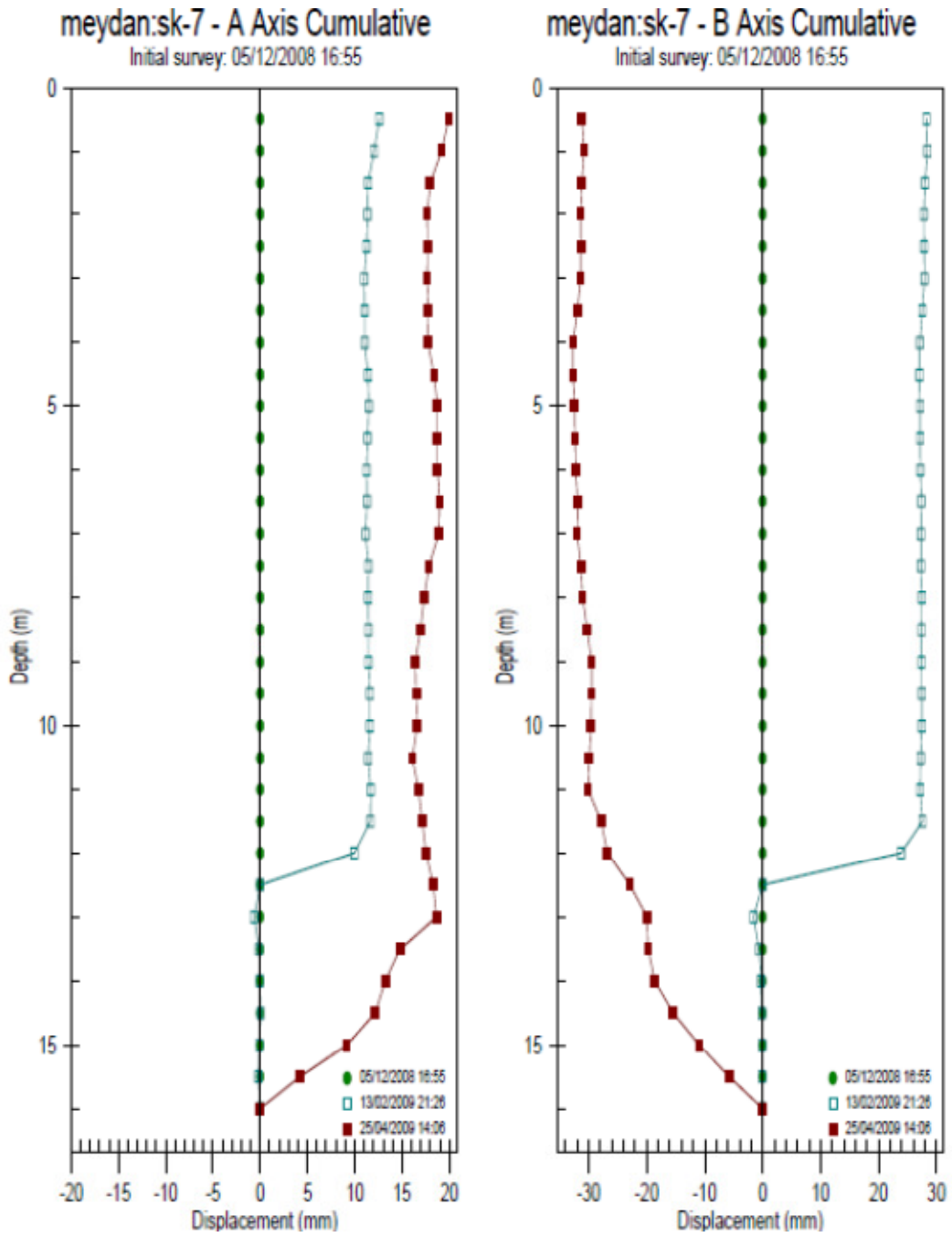


Figure D.13 Cumulative displacement of BH-7

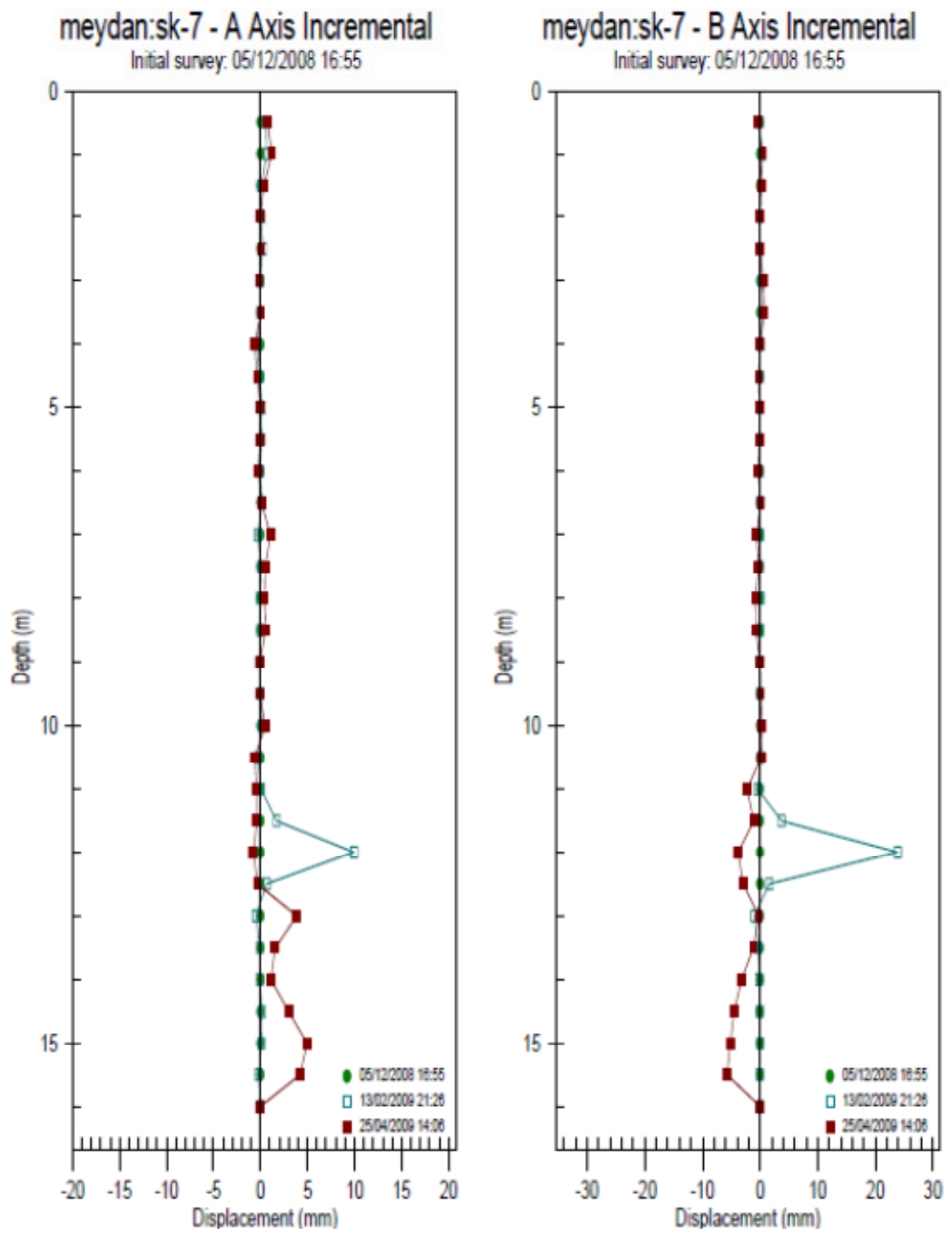


Figure D.14 Incremental displacement of BH-7

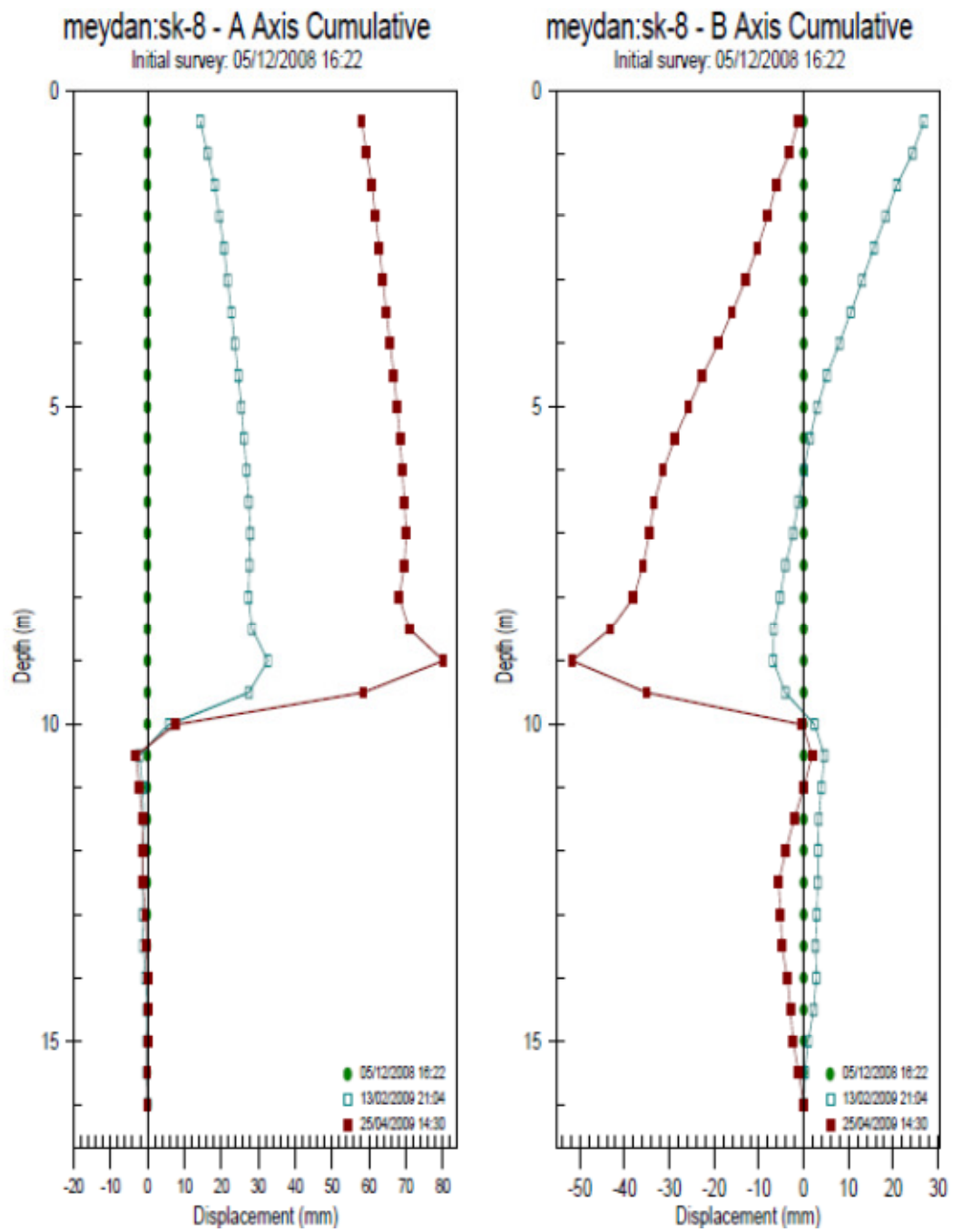


Figure D.15 Cumulative displacement of BH-8

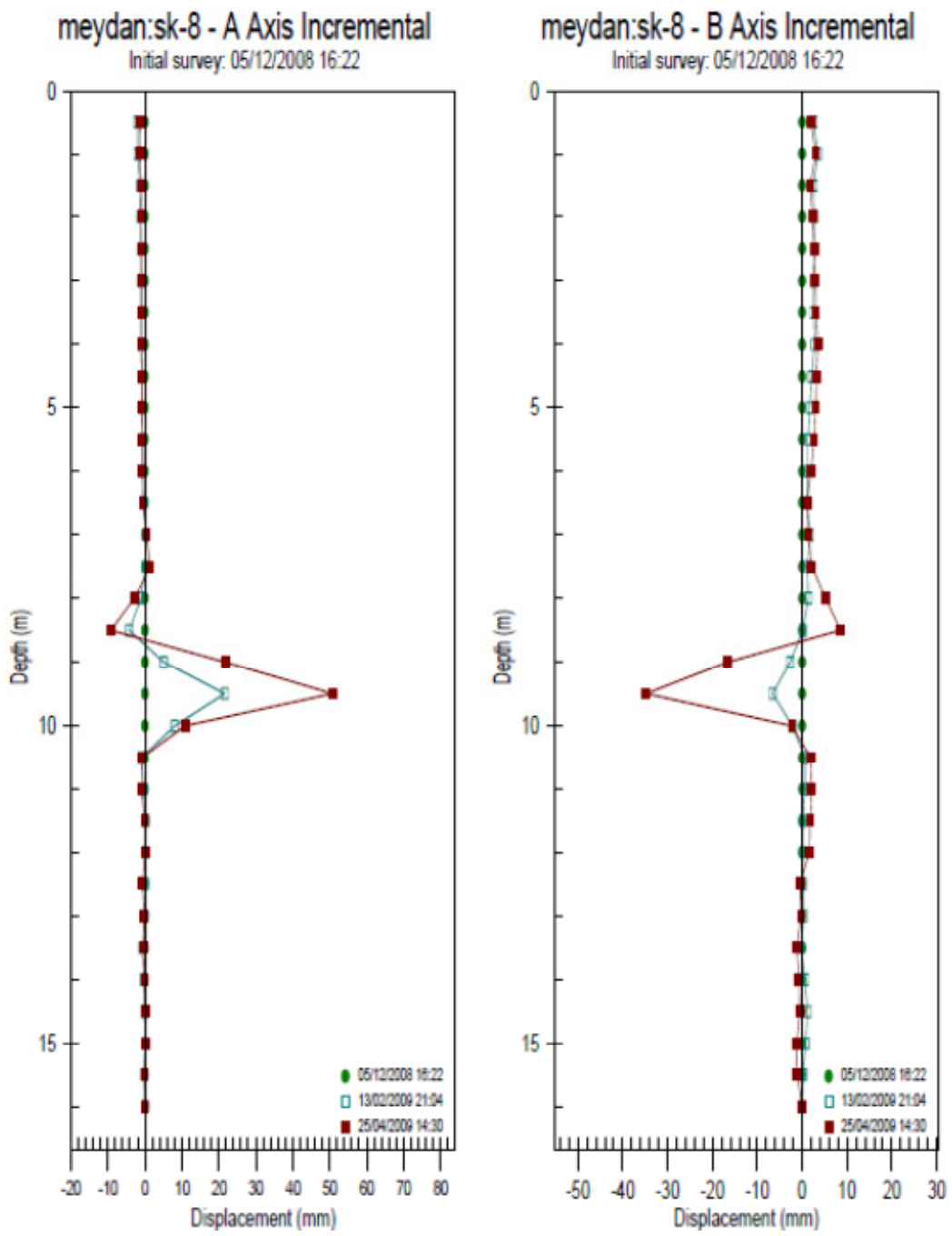


Figure D.16 Incremental displacement of BH-8

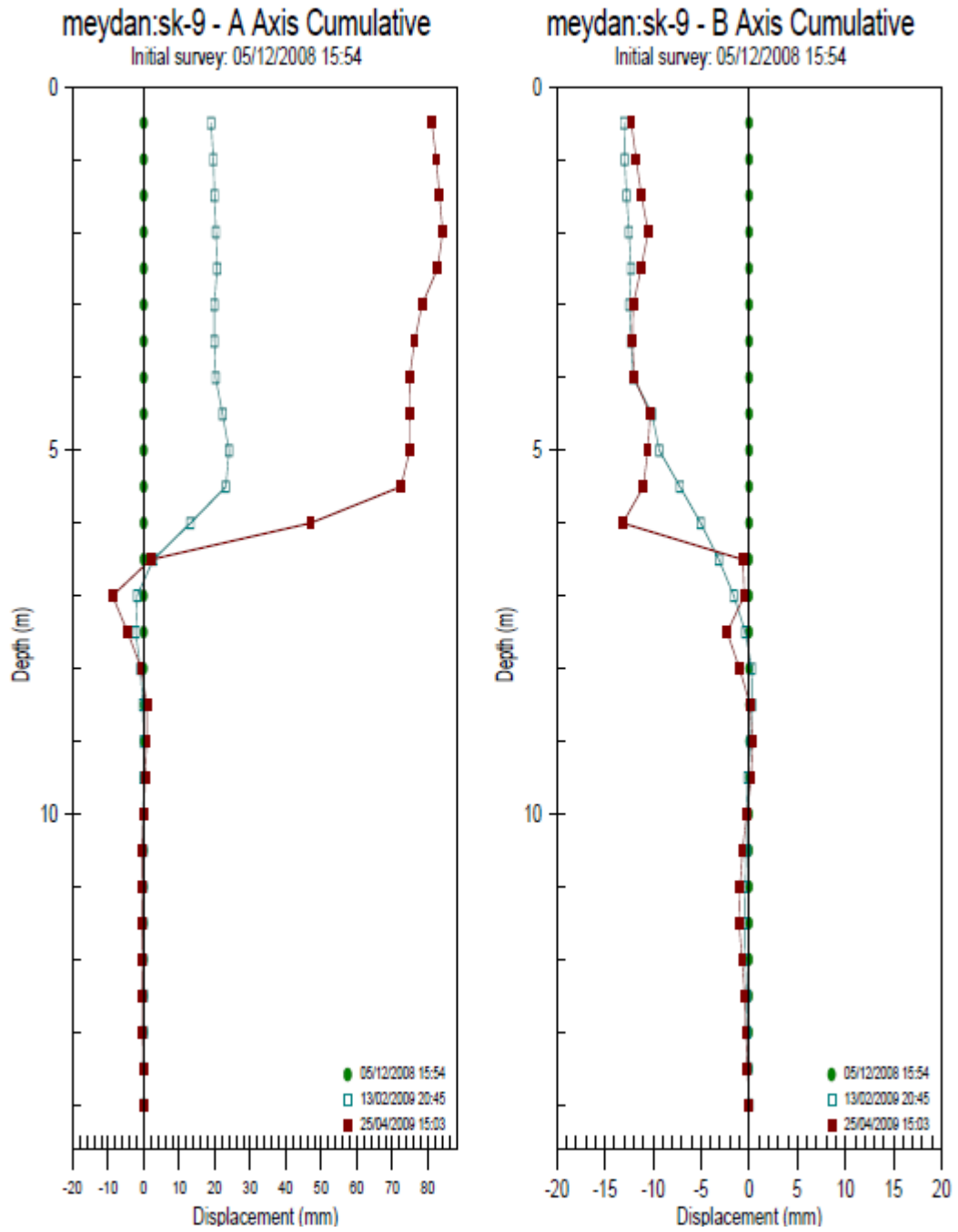


Figure D.17 Cumulative displacement of BH-9

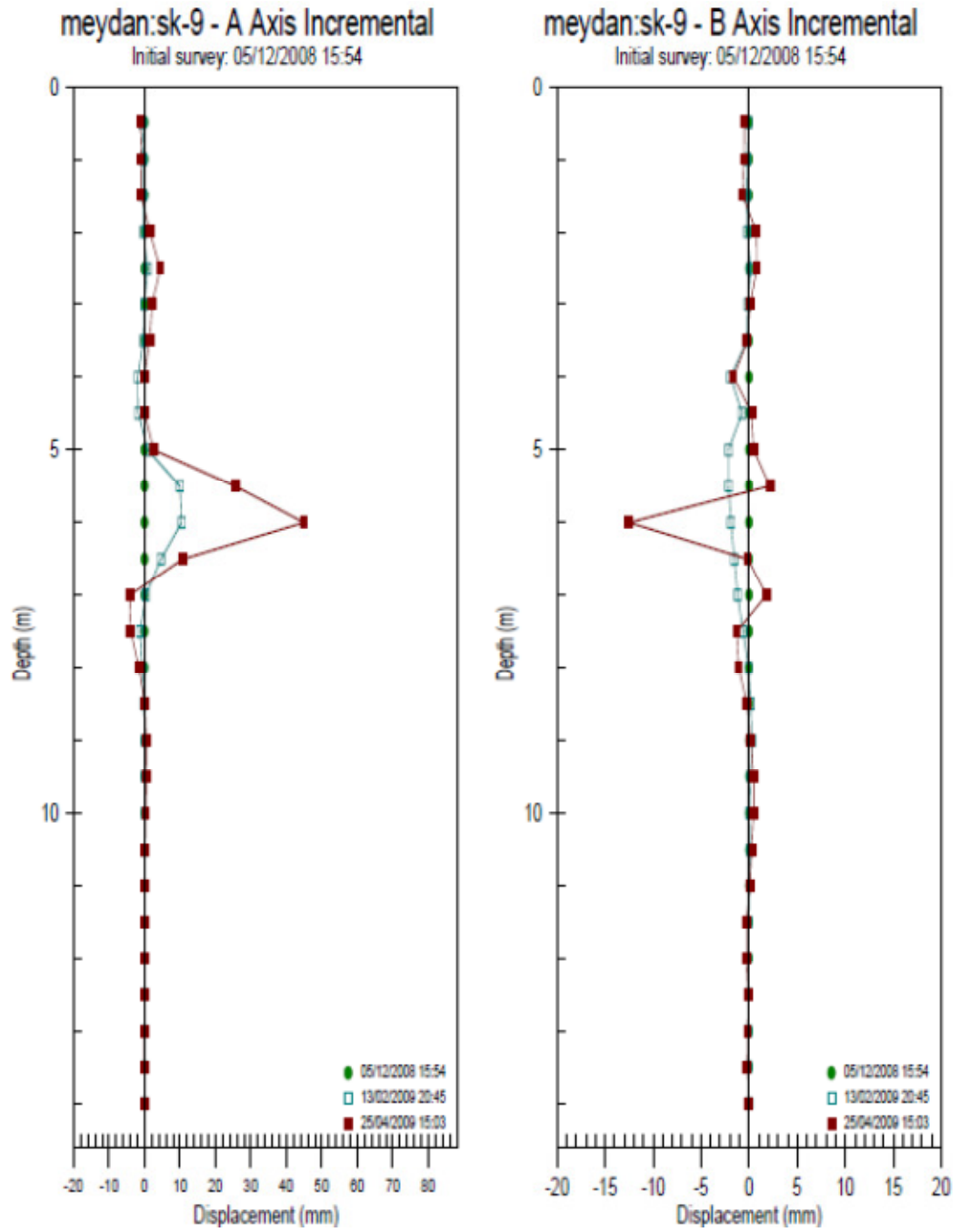


Figure D.18 Incremental displacement of BH-9

APPENDIX E

SUMMARY OF THE ABRAHAMSON AND SILVA (2008) GROUND-MOTION RELATIONS

Equations for the Median Ground Motion

The model for the median ground motion is given by:

$$\ln S_a(g) = f_1(M, R_{rup}) + a_{12}F_{RV} + a_{13}F_{NM} + a_{15}F_{AS} + f_5(PGA_{1100}, V_{S30}) + F_{HW}f_4(R_{jb}, R_{rup}, R_x, W, \delta, Z_{TOR}, M) + f_6(Z_{TOR}) + f_8(R_{rup}, M) + f_{10}(Z_{1.0}, V_{S30}) \text{ Eq.(E.1)}$$

The functional forms for f_1 , f_4 , f_5 , f_6 , f_7 , f_8 , and f_{10} are given below.

Base Model

The base form of the magnitude and distance dependence for strike-slip earthquakes is the same as our 1997 model and is given by:

$$f_1(M, R_{rup}) = \begin{cases} a_1 + a_4(M - c_1) + a_8(8.5 - M)^2 + [a_2 + a_3(M - c_1)] \ln(R) & \text{for } M \leq c_1 \\ a_1 + a_5(M - c_1) + a_8(8.5 - M)^2 + [a_2 + a_3(M - c_1)] \ln(R) & \text{for } M > c_1 \end{cases} \text{ Eq.(E.2)}$$

where

$$R = \sqrt{R_{rup}^2 + c_4^2} \text{ Eq.(E.3)}$$

Site Response Model

The site is characterized by V_{S30} , so the nonlinear soil model was modified to incorporate V_{S30} dependence. A shear-wave velocity, V_{LIN} , was defined above which the site response is linear. The model for the nonlinear site response was selected so that it becomes proportional to $\ln(V_{S30})$ as the input motion (PGA_{1100}) becomes small and as the V_{S30} approaches to V_{LIN} . We define a second shear-wave velocity, V_1 , above which there is no scaling with V_{S30} . For $V_{S30} > V_{LIN}$, there is no dependence on the PGA_{1100} ; for $V_{S30} > V_1$, there is no dependence on V_{S30} .

It was adopted the form of the nonlinear site response developed by Walling et al. (2008):

$$f_5(PGA_{1100}, V_{S30}^*) = \begin{cases} a_{10} \ln\left(\frac{V_{S30}^*}{V_{LIN}}\right) - b \ln(PGA_{1100} + c) \\ + b \ln\left(PGA_{1100} + c \left(\frac{V_{S30}^*}{V_{LIN}}\right)^n\right) & \text{for } V_{S30} < V_{LIN} \\ (a_{10} + bn) \ln\left(\frac{V_{S30}^*}{V_{LIN}}\right) & \text{for } V_{S30} \geq V_{LIN} \end{cases} \quad \text{Eq.(E.4)}$$

where

$$V_{S30}^* = \begin{cases} V_{S30} & \text{for } V_{S30} < V_1 \\ V_1 & \text{for } V_{S30} \geq V_1 \end{cases} \quad \text{Eq.(E.5)}$$

and

$$V_1 = \begin{cases} 1500 \text{ m/s} & \text{for } T \leq 0.50 \text{ sec} \\ \exp[8.0 - 0.795 \ln(T/0.21)] & \text{for } 0.50 \text{ sec} < T \leq 1 \text{ sec} \\ \exp[6.76 - 0.297 \ln(T)] & \text{for } 1 \text{ sec} < T < 2 \text{ sec} \\ 700 \text{ m/s} & \text{for } T \geq 2 \text{ sec} \\ 862 \text{ m/s} & \text{for } PGV \end{cases} \quad \text{Eq.(E.6)}$$

The nonlinear site response terms (b, c, n, V_{LIN}) were constrained by the results of the 1-D analytical site response model using the Peninsula Range soil model (Walling et al. 2008). Only the a_{10} term was estimated in the regression analysis.

Hanging-Wall Model

1997 model included a hanging wall (HW) factor, but the model lead to jumps in the HW scaling for some cases and it was not clear how to apply the model for steeply dipping faults. To avoid these shortcomings, the new model includes five tapers to produce a smoothly varying HW effect. The model for the HW effect is given by:

$$f_4(R_{jb}, R_{rup}, \delta, Z_{TOR}, M, W) = a_{14} T_1(R_{jb}) T_2(R_X, W, \delta) T_3(R_X, Z_{TOR}) T_4(M) T_5(\delta) \quad \text{Eq.(E.7)}$$

where

$$T_1(R_{jb}) = \begin{cases} 1 - \frac{R_{jb}}{30} & \text{for } R_{jb} < 30 \text{ km} \\ 0 & \text{for } R_{jb} \geq 30 \text{ km} \end{cases} \quad \text{Eq.(E.8)}$$

$$T_2(R_x, W, \delta) = \begin{cases} 0.5 + \frac{R_x}{2W \cos(\delta)} & \text{for } R_x \leq W \cos(\delta) \\ 1 & \text{for } R_x > W \cos(\delta), \text{ or } \delta = 90 \end{cases} \quad \text{Eq.(E.9)}$$

$$T_3(R_x, Z_{TOR}) = \begin{cases} 1 & \text{for } R_x \geq Z_{TOR} \\ \frac{R_x}{Z_{TOR}} & \text{for } R_x < Z_{TOR} \end{cases} \quad \text{Eq.(E.10)}$$

$$T_4(M) = \begin{cases} 0 & \text{for } M \leq 6 \\ M - 6 & \text{for } 6 < M < 7 \\ 1 & \text{for } M \geq 7 \end{cases} \quad \text{Eq.(E.11)}$$

$$T_5(\delta) = \begin{cases} 1 - \frac{\delta - 70}{20} & \text{for } \delta \geq 70 \\ 1 & \text{for } \delta < 70 \end{cases} \quad \text{Eq.(E.12)}$$

The first three tapers (T_1 , T_2 , and T_3) were constrained by the 1-D rock simulations and by the data from the Chi-Chi mainshock. The last two tapers (T_4 and T_5) were constrained by the events with well-recorded HW effects. Only the a_{14} term was estimated in the regression analysis.

Depth-to-Top of Rupture Model

A key issue for incorporating a depth-to-top of rupture dependence is that there is a correlation of magnitude and depth to-top of rupture: large earthquakes tend to rupture to the surface, whereas small earthquakes tend to be at depth.

$$f_6(Z_{TOR}) = \begin{cases} \frac{a_{16} Z_{TOR}}{10} & \text{for } Z_{TOR} < 10 \text{ km} \\ a_{16} & \text{for } Z_{TOR} \geq 10 \text{ km} \end{cases} \quad \text{Eq.(E.13)}$$

Large Distance Model

The NGA data set does not contain many recordings from small magnitude (M4-M5) earthquakes at large distances ($R_{rup} > 100$ km). As a result, the distance attenuation is not well constrained for moderate magnitudes.

$$f_s(R_{rup}, M) = \begin{cases} 0 & \text{for } R_{rup} < 100 \text{ km} \\ a_{18}(R_{rup} - 100)T_6(M) & \text{for } R_{rup} \geq 100 \text{ km} \end{cases} \quad \text{Eq.(E.14)}$$

where

$$T_6(M) = \begin{cases} 1 & \text{for } M < 5.5 \\ 0.5(6.5 - M) + 0.5 & \text{for } 5.5 \leq M \leq 6.5 \\ 0.5 & \text{for } M > 6.5 \end{cases} \quad \text{Eq.(E.15)}$$

Soil Depth Model

A key difficulty has been that the soil depths have not been well determined for the strong motion data set. The NGA data set contains estimates of the depth of the soil (e.g., $Z_{1.0}$) for about 1/4 of the data, but some significant inconsistencies between the V_{S30} and soil depths indicate that this parameter is not well constrained.

The analytical models show a strong dependence of the long-period ground motion on the soil depth. We consider many of the $Z_{1.0}$ estimates in the flat-file to be unreliable, but we believe that there should be soil-depth dependence for long periods. Therefore, the soil-depth scaling was completely constrained by the analytical site response models. The 1-D site response results (Silva, 2005) were used to constrain the scaling with soil depth for shallow soil sites ($Z_{1.0} < 200$ m) and the 3-D basin response modeling results (Day et al., 2006) were used to constrain the scaling with soil depth for deep soil sites ($Z_{1.0} > 200$ m). The model for the scaling with soil depth is given by:

$$f_{10}(Z_{1.0}, V_{S30}) = a_{21} \ln\left(\frac{Z_{1.0} + c_2}{Z_{1.0}(V_{S30} + c_2)}\right) + \begin{cases} a_{22} \ln\left(\frac{Z_{1.0}}{200}\right) & \text{for } Z_{1.0} \geq 200 \\ 0 & \text{for } Z_{1.0} < 200 \end{cases} \quad \text{Eq.(E.16)}$$

where $Z_{1.0}(V_{S30})$ is the median $Z_{1.0}$ (in m) given by:

$$\ln(Z_{1.0}(V_{S30})) = \begin{cases} 6.745 & \text{for } V_{S30} < 180 \text{ m/s} \\ 6.745 - 1.35 \ln\left(\frac{V_{S30}}{180}\right) & \text{for } 180 \leq V_{S30} \leq 500 \text{ m/s} \\ 5.394 - 4.48 \ln\left(\frac{V_{S30}}{500}\right) & \text{for } V_{S30} > 500 \text{ m/s} \end{cases} \quad \text{Eq.(E.17)}$$

$$a_{21} = \begin{cases} 0 & \text{for } V_{S30} \geq 1000 \\ \frac{-(a_{10} + bn) \ln\left(\frac{V_{S30}^*}{\min(V_1, 1000)}\right)}{\ln\left(\frac{Z_{1.0} + c_2}{Z_{1.0} + c_2}\right)} & \text{for } (a_{10} + bn) \ln\left(\frac{V_{S30}^*}{\min(V_1, 1000)}\right) \\ & + e_2 \ln\left(\frac{Z_{1.0} + c_2}{Z_{1.0} + c_2}\right) < 0 \\ e_2 & \text{otherwise} \end{cases} \quad \text{Eq.(E.18)}$$

$$e_2 = \begin{cases} 0 & \text{for } T < 0.35 \text{ sec or } V_{S30} > 1000 \\ -0.25 \ln\left(\frac{V_{S30}}{1000}\right) \ln\left(\frac{T}{0.35}\right) & \text{for } 0.35 \leq T \leq 2 \text{ sec} \\ -0.25 \ln\left(\frac{V_{S30}}{1000}\right) \ln\left(\frac{2}{0.35}\right) & \text{for } T > 2 \text{ sec} \end{cases} \quad \text{Eq.(E.19)}$$

and

$$a_{22} = \begin{cases} 0 & \text{for } T < 2 \text{ sec} \\ 0.0625(T - 2) & \text{for } T \geq 2 \text{ sec} \end{cases} \quad \text{Eq.(E.20)}$$

For PGV, the a_{21} and a_{22} values are computed using $T=1$ sec in Equation 18 and Equation 20. A constraint on the model is that the ground motion for shallow soil sites does not fall below the ground motion for $V_{S30}=1000$ m/ s.

Regression Results

Table E.1 Coefficients for the median ground motion

Parameter	VLIN	b	a ₁	a ₂	a ₈	a ₁₀	a ₁₂	a ₁₃
PGA	865.1	-1.186	0.804	-0.9679	-0.0372	0.9445	0.0000	-0.0600
Sa(T=0.010)	865.1	-1.186	0.811	-0.9679	-0.0372	0.9445	0.0000	-0.0600
Sa(T=0.020)	865.1	-1.219	0.855	-0.9774	-0.0372	0.9834	0.0000	-0.0600
Sa(T=0.030)	907.8	-1.273	0.962	-10.024	-0.0372	10.471	0.0000	-0.0600
Sa(T=0.040)	994.5	-1.308	1.037	-10.289	-0.0315	10.884	0.0000	-0.0600
Sa(T=0.050)	1053.5	-1.346	1.133	-10.508	-0.0271	11.333	0.0000	-0.0600
Sa(T=0.075)	1085.7	-1.471	1.375	-10.810	-0.0191	12.808	0.0000	-0.0600
Sa(T=0.10)	1032.5	-1.624	1.563	-10.833	-0.0166	14.613	0.0000	-0.0600
Sa(T=0.15)	877.6	-1.931	1.716	-10.357	-0.0254	18.071	0.0181	-0.0600
Sa(T=0.20)	748.2	-2.188	1.687	-0.9700	-0.0396	20.773	0.0309	-0.0600
Sa(T=0.25)	654.3	-2.381	1.646	-0.9202	-0.0539	22.794	0.0409	-0.0600
Sa(T=0.30)	587.1	-2.518	1.601	-0.8974	-0.0656	24.201	0.0491	-0.0600
Sa(T=0.40)	503.0	-2.657	1.511	-0.8677	-0.0807	25.510	0.0619	-0.0600
Sa(T=0.50)	456.6	-2.669	1.397	-0.8475	-0.0924	25.395	0.0719	-0.0600
Sa(T=0.75)	410.5	-2.401	1.137	-0.8206	-0.1137	21.493	0.0800	-0.0600
Sa(T=1.0)	400.0	-1.955	0.915	-0.8088	-0.1289	15.705	0.0800	-0.0600
Sa(T=1.5)	400.0	-1.025	0.510	-0.7995	-0.1534	0.3991	0.0800	-0.0600
Sa(T=2.0)	400.0	-0.299	0.192	-0.7960	-0.1708	-0.6072	0.0800	-0.0600
Sa(T=3.0)	400.0	0.000	-0.280	-0.7960	-0.1954	-0.9600	0.0800	-0.0600
Sa(T=4.0)	400.0	0.000	-0.639	-0.7960	-0.2128	-0.9600	0.0800	-0.0600
Sa(T=5.0)	400.0	0.000	-0.936	-0.7960	-0.2263	-0.9208	0.0800	-0.0600
Sa(T=7.5)	400.0	0.000	-1.527	-0.7960	-0.2509	-0.7700	0.0800	-0.0600
Sa(T=10.0)	400.0	0.000	-1.993	-0.7960	-0.2683	-0.6630	0.0800	-0.0600
PGV	400.0	-1.955	57.578	-0.9046	-0.1200	15.390	0.0800	-0.0600

Table E.1 (Continued) Coefficients for the median ground motion

Parameter	a₁₄	a₁₅	a₁₆	a₁₈
PGA	10.800	-0.3500	0.9000	-0.0067
Sa(T=0.010)	10.800	-0.3500	0.9000	-0.0067
Sa(T=0.020)	10.800	-0.3500	0.9000	-0.0067
Sa(T=0.030)	11.331	-0.3500	0.9000	-0.0067
Sa(T=0.040)	11.708	-0.3500	0.9000	-0.0067
Sa(T=0.050)	12.000	-0.3500	0.9000	-0.0076
Sa(T=0.075)	12.000	-0.3500	0.9000	-0.0093
Sa(T=0.10)	12.000	-0.3500	0.9000	-0.0093
Sa(T=0.15)	11.683	-0.3500	0.9000	-0.0093
Sa(T=0.20)	11.274	-0.3500	0.9000	-0.0083
Sa(T=0.25)	10.956	-0.3500	0.9000	-0.0069
Sa(T=0.30)	10.697	-0.3500	0.9000	-0.0057
Sa(T=0.40)	10.288	-0.3500	0.8423	-0.0039
Sa(T=0.50)	0.9971	-0.3191	0.7458	-0.0025
Sa(T=0.75)	0.9395	-0.2629	0.5704	0.0000
Sa(T=1.0)	0.8985	-0.2230	0.4460	0.0000
Sa(T=1.5)	0.8409	-0.1668	0.2707	0.0000
Sa(T=2.0)	0.8000	-0.1270	0.1463	0.0000
Sa(T=3.0)	0.4793	-0.0708	-0.0291	0.0000
Sa(T=4.0)	0.2518	-0.0309	-0.1535	0.0000
Sa(T=5.0)	0.0754	0.0000	-0.2500	0.0000
Sa(T=7.5)	0.0000	0.0000	-0.2500	0.0000
Sa(T=10.0)	0.0000	0.0000	-0.2500	0.0000
PGV	0.7000	-0.3900	0.6300	0.0000